

A Thesis Submitted for the Degree of PhD at the University of Warwick

Permanent WRAP URL:

<http://wrap.warwick.ac.uk/111277>

Copyright and reuse:

This thesis is made available online and is protected by original copyright.

Please scroll down to view the document itself.

Please refer to the repository record for this item for information to help you to cite it.

Our policy information is available from the repository home page.

For more information, please contact the WRAP Team at: wrap@warwick.ac.uk

**Theoretical and physical models of a pressure pulse
propagation in the spinal system**

Karim Berkouk

B.Sc., M.Sc.

submitted for the degree of Ph.D. at

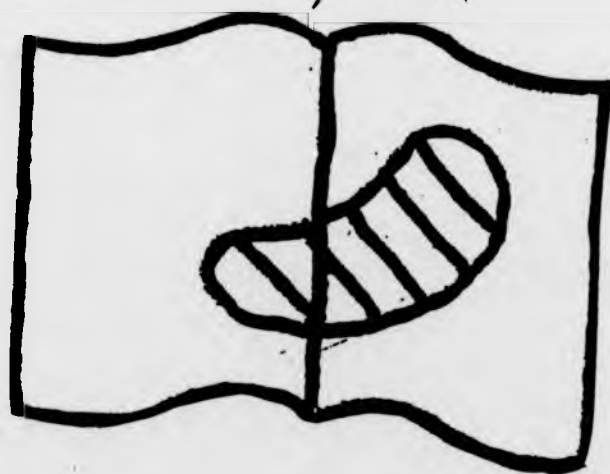
The University of Warwick

School of Engineering

November 1999

Best Copy Available

*poor quality on some of the
Figures.*



Abstract

This work is motivated by an attempt to explain the origins of *syringomyelia*. This serious disease is characterized by the appearance of cavities, called *syrinxes*, in the central canal of the spinal cord resulting in partial or complete paralysis. The causes of syringomyelia are unknown but pressure propagation is probably implicated. Pressure pulses, caused by coughing, sneezing and similar activities, propagate up the cerebrospinal fluid (CSF) in the spinal subarachnoid space. Williams (1990) suggested a possible cause of syrinx formation is that when such pressure pulses encounter a partial or total blockage a large pressure rise would be generated in the spinal central canal. Our theoretical model modeling was undertaken to investigate Williams' hypothesis.

Essentially, we model the spinal system as a channel separated into two parts by a flexible diaphragm representing the spinal cord. The upper part (A) represents the subarachnoid space while the lower part (B), which has a much smaller cross-sectional area, represents the central canal. A theory for pressure wave propagation in such a two-chamber system is described. It has been used to study the wave characteristics of the two-chamber system. In this way it has been found that the leading edge of a pressure pulse/wall bulge tends to steepen into a shock-like wave or elastic jump. When such a pressure pulse is incident on a blockage in the subarachnoid space, a large pressure rise is generated in its vicinity. We showed that this pressure rise could be momentary or permanent depending on whether the pressure pulse bulge is positive or negative. This provides a possible mechanism for the formation of the syrinxes.

An experimental rig has also been built in order to qualitatively confirm some theoretical results. The experimental wave speed agreed with the wave speed defined in the theoretical model. We were also able to confirm that the reflection of a pressure pulse from a blockage placed in the upper part A (subarachnoid space) leads to high pressure in the vicinity of the blockage.

Contents

1	Introduction	1
	1.1 Historical concept of biological flows	1
	1.2 About syringomyelia	3
2	Cerebrospinal system	7
	2.1 Introduction	7
	2.2 Structure and functions of the spinal cord	7
	2.2.1 Anatomy of the spinal cord	8
	2.2.2 Principal elements and their functions (spinal cord)	9
	2.3 Principal elements of the brain and their functions	11
	2.4 Peculiar features of the nervous system	13
	2.4.1 Main sites of secretion and absorption of CSF	14
	2.4.2 Spaces or cavities in the cerebrospinal system	15
	2.5 Cerebrospinal fluid (CSF)	19
	2.5.1 Properties of CSF	19
	2.5.2 Cycle of CSF	20
	2.5.2.1 Secretion of CSF	20
	2.5.2.1.1 Site of formation of CSF	20
	2.5.2.1.2 Mechanisms of formation of CSF	22
	2.5.2.2 Route of CSF	24
	2.5.2.3 Absorption of CSF	24

2.5.3 Mechanism for transmission of vascular pressure	26
2.5.3.1 Effect of artery alone	26
2.5.3.2 Effect of outflow through a valve	26
2.5.3.3 Effect of veins	27
2.5.3.4 Effects of removing CSF on the CSF	28
2.5.3.5 CSF pulsation	28
2.6 Measurements of pressure	31
2.6.1 Pressure measurement	31
2.6.2 Dynamics of intracranial pressure (ICP)	31
2.6.3 Posture affects ICP	33
2.6.4 Coughing	34
3 About syringomyelia	37
3.1 Definition	37
3.2 Historical concept	39
3.3 Causes of syringomyelia	40
3.4 Forms of syringomyelia	41
3.5 Symptoms of syringomyelia	42
3.6 Diagnosis and treatments	45
3.6.1 Diagnosis	45
3.6.2 Treatments	47
3.7 Pathogenesis	49
3.7.1 The hydrodynamic forces	49

	3.7.2 Suck mechanism	50
	3.7.3 The communicating hypothesis	51
	3.7.4 The slosh mechanism	52
	3.7.5 Transmural pressure gradient	53
	3.8 State of research	54
	3.9 Summary of research initiatives	57
4	Flows through collapsible tubes	60
	4.1 Definition and applications	61
	4.2 The Starling resistor	62
	4.3 The mechanics of the tube wall: tube law	64
	4.4 Wave speed	73
	4.5 The elastic jump	74
5	Pressure wave propagation in a coaxial tube model	79
	5.1 Introduction	79
	5.2 Coaxial tubes model	80
	5.2.1 Assumptions of the model	80
	5.2.2 Governing equations	81
	5.3 Wave speed definition	83
	5.3.1 Linear case.....	83
	5.3.1 Non-linear case.....	85
	5.4 Tube law (Pressure-area relation)	87

5.5 Elastic jump phenomenon	88
5.5.1 Variations of the wave speed	88
5.5.2 Nonlinear effects on the wave speed: constant total cross-sectional area	89
5.5.3 Nonlinear effects on the wave speed: gradual changes in the total cross-sectional area	91
5.5.3.1 Increase of the total cross-sectional area	91
5.5.3.2 Decrease of the total cross-sectional area	92
5.6 Summary of the nonlinear effects on the wave speed	93
6 Solving the equations	94
6.1 Introduction	94
6.2 Direct method (linear case)	94
6.2.1 Type of solution	94
6.2.2 Examples	95
6.2.2.1 Piston in harmonic motion	95
6.2.2.1 Other cases: with compliance, resistance	98
6.2.3 Analysis	100
6.3 Method of characteristics	102
6.3.1 Introduction.	102
6.3.2 Governing equations.	103
6.3.3 Characteristic lines and compatibility equations	104
6.3.3.1 Linear case	104

6.3.3.2 Nonlinear case	107
6.3.3.2 Weakly nonlinear case	108
6.3.4 Numerical integration procedure	110
6.3.4.1 Numerical procedure for the linear case	111
6.3.4.2 Numerical procedure for the nonlinear case	112
6.3.4.2.1 Finite difference equations	112
6.3.4.2.2 Numerical strategy	112
6.3.5 Numerical analysis	114
6.3.5.1 Linear case	114
6.3.5.2 Full nonlinear case	117
7 Propagation of pressure pulses in a two-coaxial tube model	120
7.1 Introduction	120
7.2 Governing equations	121
7.2.1 Notation	121
7.2.2 Governing equations	122
7.3 Tube law (pressure-area relation)	123
7.4 Small perturbation theory for elastic jumps	124
7.4.1 Estimate of the shock-like wave speed	124
7.4.2 Elastic jump reflection	126
7.4.2.1 Effect of the incident wave	127
7.4.2.2 Effect of the reflected wave	127

7.4.2.3 Analysis of the transmitted wave	130
7.5 Numerical solution	131
7.5.1 Incident wave analysis	132
7.5.2 Reflected wave analysis	133
7.6 Examples	135
7.6.1 Relations before-after the elastic jump	136
7.6.2 Reflection of an elastic jump	137
7.6.3 Comparison between the small perturbation theory and the numerical results	138
7.7 Propagation of a pressure pulse	139
7.7.1 Introduction	139
7.7.2 Propagation and reflection of a pulse with pressure difference drop	140
7.7.2 Propagation and reflection of a pulse with pressure difference rise	141
8 Physical model of the spinal CSF system	143
8.1 Experimental apparatus	143
8.1.1 Overview of the measurements	143
8.1.2 Description of the apparatus	144
8.1.3 Measurement instruments	145
8.2 Measurement of the wave speed	146
8.3 Reflection of a pressure wave	147

9	Pressure pulse propagation in the spinal CSF system:	
	syrinx formation	150
	9.1 Introduction	150
	9.2 Analysis of the propagation and reflection of a pulse with pressure difference drop	151
	9.3 Analysis of the propagation and reflection of a pulse with pressure difference rise	153
	9.4 Possible mechanism for syrinx formation in syringomyelia	155
	9.4.1 Porosity effects on syrinx formation	156
	9.4.2 Syrinx expansion	157
	9.4.2 Conclusion	158
10	Conclusions and recommendations for further work	160
	References	170
A	Tables	182
	A.1 Tables of chapter 2	182
	A.2 Tables of chapter 3	183
	A.3 Tables of chapter 6	185
	A.4 Tables of chapter 7	188
	A.5 Tables of chapter 9	192
B	Figures	192
	B.1 Figures of chapter 2	192
	B.2 Figures of chapter 3	213

B.3	Figures of chapter 4	225
B.4	Figures of chapter 5	230
B.5	Figures of chapter 6	233
B.6	Figures of chapter 7	243
B.7	Figures of chapter 8	252
B.8	Figures of chapter 9	256
	Appendix A: Method of characteristics	266
	Appendix B: About the elastic jump	276
C	Glossary	284
D	Diagram of the experimental apparatus (format A3)	291

Acknowledgments

This work is dedicated to the memory of Bernard Williams: when a personal passion serves the general interest.

I also would like to thank Peter Carpenter for his guidance and Tony Lucey for adding an extra-academic aspect to this Ph. D.

Finally I would like to thank my family and friends for their continuous support.

Declaration

This thesis was prepared by myself.

CHAPTER 1

INTRODUCTION

1.1 HISTORICAL CONCEPT OF BIOLOGICAL FLOWS

The field of biological flows is vast. The main topics are the cardiovascular system, the air-flow in lungs, and more recently, the cerebrospinal fluid (CSF) system, particularly in the head. It is believed to originate in ancient Egypt with observations concerning pulse wave propagation in arteries. The Edwin Smith Papyrus (about 3000 BC) records that pulsations originating in the heart were observed on trephining the skull. Later, in ancient Greece, Erasistrathos (280 BC) is said to have taught that the arterial pulse originates at the heart and arrives at peripheral locations a short time later. However, it is common to start with Gallen (130-200 AD) who recognised the structures of the heart and that the vessels contained blood.

We will now cite the most famous contributors to the field, with an extremely brief description of their contribution. Harvey (1578-1657) was the first to discover that the blood path was a circle. However, there is no evidence to the effect that Harvey, or any of his contemporaries, were aware of observations on the circulation made about 400 years earlier by Ibn an Nafis (979-1037). Nevertheless, it was Harvey who introduced the modern scientific method into biology. Galileo (1564-1642) showed that mathematics was the essential key to science, without which nature could not be properly understood. This outlook inspired Descartes (1596-1650) to work on physiology. This proved to be a failure because of his lack of knowledge in physiology. This shows us that a specialist of

one single field does not have a sufficient knowledge to properly understand the complexity of the phenomena involved in biological flows. Borelli (1608-1679, mathematics) and Malpighi (1628-1694, medicine) understood that a collaboration was necessary in order to understand physiology. Borelli would seem to be the first to apply the laws of mechanics to living matter and is thus often called the founder of medical physics. Malpighi discovered the passages in the lung substance predicted by Harvey (the lung capillary blood vessels), with a simple microscope. What would have happened if Descartes had had a Malpighi close to him?

However, collaboration between science and biology was not stillborn. Most of the following contributors to the field (like the earlier ones) had both a science and medical background. In the eighteen century, Hales (1677-1761) measured the hydrostatic pressure in the arteries and veins of living animals. Bernoulli (1700-1782) renowned for his equation on pressure changes with the inter-conversion of kinetic and potential energy, made his inaugural lecture on the mechanics of breathing. Euler (1707-1783) wrote the equations of motion which lead to description of wave propagation in arteries. Young (1773-1829) was the first to correctly estimate the arterial pulse wave velocity (5 m/s). At the same time Poiseuille (1797-1867) was a physician interested in blood-flow. He invented the mercury manometer to measure the blood pressure in the aorta of a dog while he was a medical student, and discovered Poiseuille's law of viscous flow upon graduation. Von Helmholtz (1821-1894) is often seen as the "father of bioengineering". He was the first to determine the velocity of the nerve pulse, giving rate of 30 m/s and made many other discoveries. E. H. Weber (1795-1878) and his brother W. E. Weber (1804-1891) established many of the properties of propagated and reflected waves in arteries.

Fick (1829-1901) who is renowned for Fick's law on diffusion, proposed a method for the measurement of cardiac output. In this century, McDonald (1917-1973) and Womersley (1907-1958) had a productive collaboration. They clarified the arterial fluid dynamics and catalysed a great expansion of interest in the field.

From an engineering point of view, research in biological flows has been mostly devoted to cardiovascular and respiratory problems. In contrast cerebrospinal fluid (CSF) movements in the cerebrospinal system have mainly been studied by physiologists. This is probably the reason why few theoretical models have been developed compared with the cardiovascular system. The existing models tend to use the compartmental model theory which in rough terms involves exchanges between compartments, ignoring what is happening within the compartment itself. This approach is not useful if one wants to understand the variations of certain quantities (CSF pressure and velocities for instance) within a compartment. For example, if one were interested in understanding what happens when a pressure wave propagating along the spinal CSF system encounters a blockage to its path.

1.2 ABOUT SYRINGOMYELIA

Syringomyelia is a serious disease of the spinal cord. It is characterised by the appearance of longitudinal cavities (see figure 3.1) within the spinal cord (Williams 1990a, 1993, Gjerris and Børgesen 1992). These cavities are termed syrinxes and in severe cases can be large and extensive, destroying the nervous tissue of the spinal cord and resulting in partial or complete paralysis. The causes of syringomyelia are unknown but pressure propagation is probably implicated (Williams, 1990b). Pressure pulses,

caused by coughing, sneezing and similar activities, propagate up the CSF in the spinal subarachnoid space. Williams has proposed two possible mechanisms involving such pressure pulses for the formation of syrinxes which he has called *suck* and *slosh* (see chapter 3). The *suck* mechanism is relatively easy to understand. Many cases of syringomyelia involve a structural lesion at the foramen magnum, leading to the descent of a hindbrain tonsil into the spinal subarachnoid space (see figure 3.2). The tonsil is envisaged as acting as a one-way valve, lifting to allow a pressure pulse to drive CSF into the head, thereby raising the pressure there. This pressure rise would subsequently act to drive the CSF back into the spinal subarachnoid space but for the one-way action of the hindbrain tonsil. Accordingly a new return path is sought and the CSF is driven into the central canal of the spinal cord, thereby creating a syrinx. This hypothesised mechanism is plausible and can be roughly modelled theoretically, but it cannot explain the formation of non-communicating syrinxes. The alternative, more vague, *slosh* mechanism was proposed to explain these. For *slosh*, a high resistance in the form of a partial or complete blockage to the flow of CSF in the spinal subarachnoid is still required. In this case, though, the pressure pulses generated by coughing or sneezing, are thought to be communicated to the spinal central canal and intensified through interaction with the blockage thereby causing syrinxes to form. The aim of this PhD research project is to develop theoretical models to help us to understand how and why these cavities form. A particular attention will be paid to the *slosh* mechanism.

In order to understand the problem raised by syringomyelia well, we describe the cerebrospinal system in chapter 2. By the end of chapter two, enough anatomical knowledge of the cerebrospinal system will have been provided to understand what is

syringomyelia, which is described in detail in chapter 3. In this chapter we will expose most of the concepts linked with syringomyelia; causes and forms of syringomyelia, symptoms, treatments available, and the state of research. Williams (1976) carries out pressure measurements of the CSF in the lumbar and cisternal (top of the neck) regions of human subjects during and following coughing. These results suggested that the pressure propagation process is similar to the propagation of longitudinal waves in elastic tubes and channels (see Lighthill, 1978). This is the reason why we started developing a theoretical model for wave propagation in the spinal system. Therefore, in chapter 4, we review flows through collapsible tubes, demonstrating some peculiar phenomena involved with collapsible tubes: for example, tube law, wave propagation, elastic jump, etc. We will then adapt the classical collapsible tube theory to our case of coaxial tubes system, where the inner tube is compliant. In chapter 5, after having derived the governing equations for this system, we will define the wave speed. A simple analysis of the wave speed will lead us to the possibility of an elastic jump (a phenomenon akin to the shock wave or hydraulic jump which usually involves a large pressure jump). In chapter 6 we will solve the linearized governing equations using a "direct method". However, we will need another method to solve the full non-linear equations: the method of characteristics. This will concern the final part of chapter 6. As with collapsible tubes, we will derive the characteristic lines (lines along which a perturbation propagates) and the compatible equations (which governs how the quantities change along these characteristic lines). In this chapter, we will confirm the possibility of the creation of an elastic jump through the convergence of the characteristic lines. In chapter 9, we will analyse what happens to the fluid properties across these lines when they join together to

form an elastic jump or a shock-like wave. We will then use this analysis of elastic jumps combined with the results of the characteristics method to analyse the propagation and reflection of a pressure pulse, especially when it encounters a blockage. We also carried out experiments in an attempt to confirm some of the theoretical results. Chapter 8 will describe the experimental rig and results. In the final chapter (chapter 9), we will apply this theory to the spinal system. Indeed, we will propose a possible mechanism for the formation of syrinx in syringomyelia.

Note that a glossary is available at the end of the thesis (appendix E) which may be useful for the non-specialists of the cerebrospinal system, especially for chapters 2 and 3. It includes technical words like *theca* or *anencephalus* as well as more common words like *hernia* or *capillary* which are well-known words, but a brief definition was thought to be helpful.

CHAPTER 2

CEREBROSPINAL SYSTEM

2.1 INTRODUCTION

In order to well understand the problem raised by syringomyelia, it is essential to describe the surrounding of the spinal cord: the cerebrospinal system. This brief description will only show the important features of the system, necessary to understand the overall problem, especially to non-specialists of the cerebrospinal system. The anatomy of the spinal cord is the concern of section 2.2, including functions of the important elements. The spinal cord system being continuous with the cerebral system, section 2.3 is devoted to the description of the brain. Some particular attention is then paid to some peculiar features of the cerebrospinal system (section 2.4). We will then concentrate on the cerebrospinal fluid: its path, its secretion and absorption (section 2.5). In the same section, we will also review some mechanisms involved with the cerebrospinal fluid. Finally, we will focus our attention on the intracranial pressure (ICP), especially when sudden pressure changes due to cough or posture occur (sections 2.6).

Let us recall that a glossary is available at the end of the thesis (appendix C).

2.2 STRUCTURE AND FUNCTIONS OF THE SPINAL CORD

The aim of this section is to give a brief description of the spinal cord for the non-specialists. A particular attention is given to the meninges, the grey and white matter and the central canal.

2.2.1 Anatomy of the spinal cord

The spinal cord can be divided into cervical, thoracic, sacral and coccygeal regions according to the parts of the body its nerves supply (figure 2.1). Each of these can be further subdivided into segments, each giving rise to a pair of spinal nerves i.e. eight cervicals (C1-C8), 12 thoracic (T1-T12), five lumbar (L1-L5), five sacral (S1-S5) and one coccygeal. The spinal cord lies in the vertebral canal and is continuous with the medulla oblongata (see figure 2.2). Distally it tapers into the conus medullaris which ends at a variable level between the twelve thoracic vertebrae (T12) and the disc between the first and second vertebrae (L1-L2). The cord is surrounded and protected by all three layers of the meninges and by the cerebrospinal fluid, all of these are continuous with those around the brain. A longitudinal groove, the anterior or (ventral) median fissure, runs the entire length of the cord. Although there is no fissure posteriorly, a posterior (dorsal) median septum is seen in cross-section.

In cross-section (figure 2.3), the spinal cord consists of an external layer of white matter and an inner core of grey matter, within which there is a minute central canal continuous with the fourth ventricle of the brain. The grey matter is shaped like a butterfly with the wings on each side being the anterior (ventral) and posterior (dorsal) horns. The anterior horn is motor in function, the posterior horn is sensory and the lateral horn is sympathetic.

As it can be seen in figure 2.1, the diameter varies along the spine. Even though it has the same structure throughout the spine, the arrangement of grey matter is modified locally as indicated in figure 2.3. This is the result of differences in the numbers and type of its

contained neurons. Thus the grey matter of cervical and lumbo-sacral regions is more abundant because these regions supply the limbs. That of thoracic and upper lumbar segments is relatively scanty because it supplies only the trunk. The white matter differs but little in its fundamental arrangement throughout the spinal cord, being contained within three funiculi on each side. A large part of white matter is composed of spinospinalor propriospinal fibres , i.e. the ones arising and terminating within the spinal cord, thereby linking various levels and providing for coordinated activity. They are of short and long types. The short ones interconnect levels within a given region, such as from one cervical segment to another. The long ones pass from one region to another, i.e. from cervical to lumbar.

2.2.2. Principal elements and their functions (spinal cord)

In this section we will focus on some parts of the spinal cord (some of them are continuous with the cerebral part) which are particularly relevant to our research.

The meninges

The brain and spinal cord are protected by three layers of non-nervous tissue collectively called meninges. The outmost is the dura mater, the middle one is the arachnoid mater, and the inner one close to the nervous tissue is the pia mater (figure 2.4). These layers have a protective function; they enclose the central nervous system and anchor it against sudden movements. They also enclose the cerebrospinal fluid, which forms a fluid cushion to protect the brain from trauma and is an intermediary in the exchange of substances between the brain and rest of the body.

The cranial dura mater is a double layer of tough connective tissue (figure 2.5). Its outer layer adheres to the bones of the skull. Its inner layer, the true dura mater, lines the skull and forms sheets of tissue which dip between the cerebral hemispheres (falx cerebri), between the cerebellar hemispheres (falx cerebelli), and between the cerebellum and the cerebrum (tentorium cerebelli). The dura mater forms a pathway for the cranial venous sinuses. In the spinal cord, only the true dura mater is present.

The arachnoid mater is an important component of the blood-brain barrier by means of which an optimal environment is created and maintained for the cells of the central nervous system. In the region of the superior sagittal sinus the arachnoid mater projects through small openings in the dura mater. These projections resemble granules (arachnoid granulations). Their function is to return cerebrospinal fluid to the blood in the superior sagittal sinus in the process of cerebrospinal fluid circulation. The arachnoid mater is composed of connective tissue with flat interdigitating cells on its surface.

The pia mater is very thin and rich in capillaries. It is attached to the brain, closely following the contours of its folds (gyri) and fissures (sulci). It is also closely bound to the spinal cord. It is thicker, stronger and less vascular along the spinal cord. Additionally the spinal pia mater forms an anchoring sheet, the denticulate ligament. Within the brain, the tela choroidea are thin areas in the roof of the third and fourth ventricles and the wall of the lateral ventricle. They consist of an adherent layer of pia mater and ependyma and give rise to the choroid plexus.

Grey matter (figure 2.6)

The grey matter (cortex) covering the surface of the hemispheres is composed of neural cell bodies, their proximal neurites, blood vessels and supporting neuroglial cells. The neurons are of various type and some areas contain a concentration of certain types of multipolar neurons.

White matter (figure 2.6)

The white matter consists of myelinated nerve fibres (axons) embedded in neuroglia. The nerve fibres in the white matter form nerve tracts which connect different areas of the same hemisphere (short and long association fibres) or connect one hemisphere with the other hemisphere (commissural fibres) or are afferent and efferent fibres (projection fibres) which pass from and to the brainstem or spinal cord, sometimes via masses of grey matter buried inside the cerebral hemisphere.

Central canal

It extends from lower extremity of fourth ventricle to within a few millimetres of the commencement of the filum terminale, being about 500 mm long. It is lined with a variable thickness of ependyma. The canal is scarcely visible to naked eye, about 0.1 mm of diameter. Frequently occluded, it may exhibit forking. Beyond the point where the coccygeal nerve leaves the cord, the central canal dilutes to form the terminal (fifth) ventricle: an expanded sac which ends bluntly just above the filum terminale.

2.3 PRINCIPAL ELEMENTS OF THE BRAIN AND THEIR FUNCTIONS

In the same way as section 2.2, we give a brief description of the cerebral system. The elements described are: the cerebral hemispheres, the cerebellum, the brainstem and the falx cerebelli.

Cerebral hemispheres

The two cerebral hemispheres are the largest part of the brain and cover many other structures. The right and left cerebral hemispheres are connected to one another inferiorly by a band of transversely running white fibres called the corpus callosum (figure 2.7). Each hemisphere has four lobes named after their position in the skull, i.e. frontal, parietal, temporal and occipital. Inside, each cerebral hemisphere has a C-shaped lateral ventricle. In the floor and medial walls of the hemispheres are collections of grey matter, and nerve fibres.

The surface of each hemisphere is covered by broad folds of grey matter (gyri) and spaces or furrows (sulci) between the gyri.

Cerebellum

The cerebellum is the largest part of the hindbrain (see figure 2.8). It consists of two cerebellar hemispheres united by a central, median vermis. The surface of the cerebellum is deeply folded. Major folds, the fissures, subdivide the cerebellum into superior and inferior halves, and demarcate subdivisions, the anterior, posterior and flocculonodular lobes within each hemispheres. The cerebellum is similar in structure to the cerebral

hemisphere: the cerebral cortex (grey matter) forms folds (folia) on the surface and surrounds the white matter, within which are embedded the intracerebellar or deep nuclei.

The brainstem

The brainstem consists of the midbrain, the pons and the medulla (see figure 2.9). All of these are midline structures which are overgrown by the cerebral hemispheres during development. Therefore, most parts of the brainstem can only be seen when the brain is viewed from below or in section. Rostrally the brainstem is continuous with the diencephalon. Caudally it blends with the first cervical segment of the spinal cord. Dorsally it is connected to the cerebellum by the superior, middle and inferior cerebellar peduncles. The white matter of the brainstem is arranged in bundles or tracts. These may be local connections within the brainstem itself or projection fibres linking brainstem structures to other parts of the central nervous system, often as part of functional systems.

The falx cerebri

A prominent longitudinal fissure partially divides the cerebrum into two hemispheres (figure 2.10). The fissure is occupied by a downward projection or fold of dura mater: the falx cerebri (figure 2.11). When the arachnoid and pia mater are removed, it is seen that the hemispheres are folded or convoluted. The convolutions are called gyri, the depressions or intervals between gyri, sulci.

2.4 PECULIAR FEATURES OF THE NERVOUS SYSTEM

In this part we will focus our attention on some features of the system which are particularly essential in order to understand the formation, the path and the absorption of the cerebrospinal fluid. It is subdivided in two parts: the elements responsible for the secretion and absorption of cerebrospinal fluid (respectively choroid plexuses and arachnoid villi), and the spaces that the fluid uses to circulate (subarachnoid and subdural spaces, cisterna, ventricles, interventricular foramen, median and lateral apertures and the perivascular spaces; see figure 2.12).

2.4.1 Main sites of secretion and absorption of CSF

Choroid plexuses

Choroid plexuses are peculiar structures which project into ventricular cavities (lateral, third and fourth ventricles). These ventricles are lined with a thin epithelial membrane: the ependyma. Epithelium is an animal tissue consisting of one or more layers of closely packed cells covering the external and internal surfaces of the body (figure 2.13). The cells vary in structure according to their function, which maybe protective, secretory or absorptive. In certain region of these ventricles , the ependymal cells, together with blood vessels and pia mater, form the choroid plexuses. The bulk of the evidence suggests that the cerebrospinal fluid source is primarily secreted in the choroid plexuses, although there may be some contribution by diffusion across the remaining ventricular ependyma. When a substance, such as glucose, is injected into blood, it escapes rapidly into surrounding tissue. However, it is much longer before it appears in the cerebrospinal fluid. This

implies that there is a blood-cerebrospinal fluid barrier which is probably chiefly in the choroid plexuses.

Arachnoid villi and granulations

The villi are simple projections of tissue through dural wall of venous sinuses (figure 2.14), and are covered by an endothelium continuous with that lining the sinus. It is generally accepted that their function relates with the absorption of cerebrospinal fluid from subarachnoid space into venous system. The distribution of the villi correspond to that of the granulations. Within the cranial cavity, they tend to be aggregated around the points where veins enter to venous sinuses. The commonest sites are the superior sagittal sinus (figure 2.15) and the transverse sinus. In the spinal canal arachnoid villi occur in relation to the menigeal cuffs around the emerging nerve roots, where they pierce the dura to lie within the lumen of the large venous sinuses surrounding the nerve roots.

However, it is possible that arachnoid villi form in the spinal veins. Welch and Pollay (1963) have described the spinal venous plexuses and associated arachnoid in monkeys. The villus shown as C appears sufficiently similar microscopically to those in cranial dura to justify the hypothesis that it constitutes a pathway from spinal subarachnoid space to blood. But it is not certain how important this route is since only in 5 out of 32 roots studied by Welch and Pollay (1963) were arachnoid tissue found in direct relation to a vein. Rexed and Wennstrom (1959) have described invasion of the spinal dura mater by arachnoid tissue in man.

2.4.2 Spaces or cavities in the cerebrospinal system

The cerebrospinal system contains many spaces or cavities which play an important role, particularly for the circulation of the cerebrospinal fluid. The main ones are the subarachnoid and subdural spaces, cisterna, the ventricles and some apertures (figures 2.12 and 2.15).

The subdural space

A narrow potential space, the subdural space, lies between the arachnoid and the dura mater. It contains only a little serous lubricant fluid.

The subarachnoid space

A wider space, the subarachnoid space, separates the arachnoid from the pia mater. It is crossed by connections, the arachnoid trabeculations, which run between the arachnoid mater and the pia mater. It contains the arteries and veins of the brain and spinal cord and the cerebrospinal fluid. The subarachnoid space is sealed off by the interdigitations and tight junctions between the cells on the arachnoid surface known as mesothelial cells.

Cisterna (figure 2.16)

Areas where the arachnoid and pia mater are widely separated are referred to as cisterns or cisternae. The major cisterns are the cerebellomedullaris (cisterna magna); the interpeduncular; the pontine; and the chiasmatic. The cisterna magna is a region where the arachnoid is reflected from the inferior surface of the cerebellar hemispheres and the dorsum of the medulla. It is continuous with the subarachnoid space of the vertebral

column through the foramen magnum. The cisterna interpeduncularis is the space where the arachnoid crosses between the two temporal lobes, enclosing the cerebral peduncles and the interpeduncular fossa. It is continuous rostrally with the chiasmatic cistern and caudally with the pontine cisterna.

Three others cisterns are also recognised: the bilateral cisterna fossa cerebri lateralis, where the arachnoid bridges the lateral fissures; and the cisterna venae magnae cerebri, a single space lying between the splenium of the corpus callosum and the superior surface of the cerebellum.

Ventricles

Deep inside the forebrain, midbrain and hindbrain, is a series of connecting chambers (ventricles) lined with epithelium called ependyma (figures 2.16 and 2.17). There are two large lateral ventricles inside the cerebral hemispheres (forebrain), each of which connects in the midline through the interventricular foramen (of Monro) which leads into the midline third ventricle. This connects through the narrow cerebral aqueduct (of Sylvius) in the midbrain to the midline fourth ventricle in the pons and medulla oblongata (hindbrain).

The fifth (terminal) ventricle lies at the bottom of the spinal cord and is only separated by ependyma and a thin layer of nervous tissue from the posterior surface of the conus medullaris. It is 8-10 mm long and 0.4 to 1 mm in diameter. After the age of 40, the terminal ventricle narrows but is still patent even in extreme old age.

The foramen magnum

The junction between the medulla oblongata and the spinal cord lies in the foramen magnum. The vertebral arteries and the spinal portion of the accessory nerve also pass through the foramen magnum.

The interventricular foramen (of Monro)

Each side of the lateral ventricle communicates with the third ventricle through a short wide canal: the interventricular foramen (figure 2.12). The two foramina do not join together to make a transversal canal. The roof of the third ventricle projects between the points where the two foramina open into the lateral ventricular walls.

Median aperture (of Magendie)

The foramen of Magendie is often seen as an aperture of varying dimensions at, or some way forward from, the apex of the calamus scriptorius (figures 2.18a and 2.12). The cavity of the fourth ventricle is thus freely open to the subarachnoid space.

Lateral apertures (of Luschka)

The lateral recesses of the fourth ventricle pass laterally and ventrally round the medulla from the lateral extremities of the ventricle. Normally the end of the recess is open and the plexus floats out into the subarachnoid space through the lateral apertures (figures 2.18b and 2.12)

According to Strong, Green and Oliverio* (1926), the lateral recesses are narrow and somewhat tortuous, but in the normal brain, always open into the subarachnoid space.

The perivascular spaces

In the past the true perivascular space has been confused with the artifact space of Held which lies external to it (figure 2.19). This misunderstanding led to the concept of the neuron being bathed by a fluid continuous with the cerebrospinal fluid. Such a system would make the existence of separate blood-brain and blood-cerebrospinal fluid barriers difficult to understand since substances could pass directly from the neurons to the cerebrospinal fluid and vice versa (Woollam and Millen, 1955). The perivascular spaces appear to be in reality 'backwaters in which there is a gentle eddy in both directions rather a constant flow in one' (Woollam and Millen, 1954). As such they must obviously be excluded from any role either in the production or in the absorption of the cerebrospinal fluid and probably act as protective cushions between vessels and nerve cells (Schaltenbrand and Bailey*, 1928).

2.5 CEREBROSPINAL FLUID SYSTEM (CSF)

2.5.1 Properties of the CSF

Composition

The cerebrospinal fluid is a clear, colourless, slightly heavier than water. It is not a simple filtrate or dialysate of blood plasma. It has a higher concentration in Na, Cl and Mg ion

* as cited in Woollam & Millen (1962)

* as cited in Woollam & Millen (1962)

concentrations, whereas concentration of K, Ca, urea and glucose are lower (see table 2.1). The main differences are that the cerebrospinal fluid contains only a very small amount of protein, that it contains less sugar, and that chloride is present in greater concentration than in plasma. Composition of cerebrospinal fluid varies somewhat according to the location (see table 2.2). More protein is present in fluid withdrawn from cisterna magna and from the lumbar cistern than in that from the ventricles.

Quantity

The rate of formation of cerebrospinal fluid has been reported to be 0.4 ml/min in adults (Rubin et al, 1966) and measured in children to be 0.35 ml/min, or 500 ml/day (Cutler et al, 1968). Cerebrospinal fluid is therefore renewed four or five times a day. The rate of formation has also been shown to be virtually independent of short-term changes in lumbar cerebrospinal fluid pressure and hence, from previous studies to remain unaffected by age throughout most of adult life (Rubin et al, 1966).

In the adult the total amount of the cerebrospinal fluid is about 140 ml, with a range between 110 ml and 160 ml. According to Weston* (1921), the spinal subarachnoid space contains 30 ml and the ventricles plus the cranial subarachnoid space around 110 ml. Lups and Haan* (1954) split it up such as: each of lateral ventricle, 15 ml; the third, fourth and aqueduct, 5 ml; cerebral subarachnoid spaces and cisterns, 25 ml; spinal subarachnoid space, 75 ml.

* as cited in Woollam & Millen (1962)

2.5.2 Cycle of CSF

2.5.2.1 Secretion of cerebrospinal fluid

2.5.2.1.1 Site of formation of cerebrospinal fluid

The weight of evidence is that cerebrospinal fluid is a secretion principally formed in the ventricular choroid plexuses as concluded by Davson (1956).

However, many investigators have performed experiments trying to prove that the cerebrospinal fluid could be secreted elsewhere than in the choroid plexuses. Some of those believed that some cerebrospinal fluid is secreted by the brain: Cserr and Jang (1975), Pollay and Curl (1967). Others believed that some cerebrospinal fluid is secreted in the spinal system. Here we report the main investigators and a brief description of their experiments.

Extra secretion of cerebrospinal fluid in the brain

Weed^{*} believed that cerebrospinal fluid was produced in the perivascular spaces, but the perineuronal spaces are artifacts and the perivascular spaces do not communicate with extracellular spaces in the nervous system. Cserr and Jang (1975) made some experiment study of spread of radio-ionated human serum albumen and blue dextran injected into caudate nucleus of rats, and found that ¹³¹I disappeared from brain simultaneously about 0.4 to 0.5% of it appeared in cisternal cerebrospinal fluid. This suggests that some small fraction of cerebrospinal fluid is produced by the brain. This is consistent with measurements of cerebrospinal fluid production in isolated region of the fluid cavities,

^{*} as cited in Davson (1962)

devoid of choroid plexuses tissue, and in animal experiments as reviewed by Cserr (1971). Pollay and Curl (1967 and 1968) postulated for an extrachoroidal source of ventricular cerebrospinal fluid across ventricular ependyma. Best evidence comes from aqueduct perfusions carried out in rabbits by Pollay and Curl (1967). Against a significant contribution from the brain is the observed distribution of extracellular markers in brain after perfusions through ventricles. According to Rall (1968), an observable distortion of diffusion profiles ought to be detected if a quarter of cerebrospinal fluid formed come from the brain. That distortion of the diffusion profile has not been found.

Extra secretion of cerebrospinal fluid in the spinal system

Experiments on injected ^{24}Na suggest that the lumbar region of the subarachnoid space comes into equilibrium with plasma more rapidly than cervical region. But this does not prove that cerebrospinal fluid is secreted in the lumbar region. It seems likely that the cerebrospinal fluid comes into equilibrium with plasma chiefly by diffusion through the spinal nervous system. Experiments by Riser' (1929) in which spinal subarachnoid space was separated from the cranial by the application of a ligature to a dog, suggest that there is no cerebrospinal fluid formation in the spinal system. He found that the spinal subarachnoid space of the dog contained about 5 ml. of cerebrospinal fluid when this was separated from cranial subarachnoid, in 9 hours only 5 ml. could be withdrawn by lumbar puncture. Definitive study was made by Coben and Smith (1969). They perfused the spinal subarachnoid space in isolation from the rest of the system and found no

acceleration of fluid in their perfusate. Davson (1956) showed that if cerebrospinal fluid is generated in subarachnoid space, capillaries should exist there, but no capillaries have ever been found there, only arteries and veins. In order for cerebrospinal fluid to be formed from the vessels they would need to possess permeability characteristics not found in vessels of similar character elsewhere in the body.

We will end this discussion by saying that cerebrospinal fluid is chiefly secreted in the choroid plexuses and that if other sites of cerebrospinal fluid secretions exist (as it has not been clearly proved up to now), their production must be very little compared with the choroid plexuses contribution.

2.5.2.1.2 Mechanisms of formation of cerebrospinal fluid

The cerebrospinal fluid may be formed in different ways: (i) Under hydrostatic pressure in the thin-walled, highly convoluted wall of the choroid plexuses (figures 2.20). (ii) By secretory mechanism inherent in the epithelial cells overlying the vessels of the plexuses. (iii) A combination of both. There is also some evidence that a small amount of cerebrospinal fluid is derived from the nervous tissue of the brain itself, passing outward into the subarachnoid space through the perivascular channels which occur along the penetrating blood vessels or by ependymal secretion in the central canal of the spinal cord.

* as cited in Woollam & Millen (1962)

Evidence against mechanism being filtration

They are two main pieces of evidence that tend to prove that filtration is not the mechanism of secretion of CSF. The first evidence is that the chemical composition of cerebrospinal fluid is markedly different from plasma (see table 2.1) with most the protein filtered out. The second one is the fact that the pressure difference across the capillary wall would need to be around 84 mmHg (3630 Pa) to exceed the osmotic pressure by a comfortable margin: this is well in excess of the capillary pressure.

Active transport as mechanism of secretion

How could the marked differences in chemical composition between cerebrospinal fluid and plasma arise? Suppose that cerebrospinal fluid and plasma were separated by a membrane which promoted active transport of Na^+ ions for instance, so that the number of Na^+ ions crossing the membrane at first exceeds the number of Cl^- ions, therefore establishing a potential difference across the membrane. As a result of this potential difference, the Cl^- ions are accelerated and Na^+ decelerated and given time, equal numbers of Na^+ and Cl^- ions will cross the membrane. It seems quite likely that a system operates across the choroidal epithelium, in which the Na^+ and Cl^- ions, and possibly other ions, are actively transported to the ventricles, thereby giving rise to a localised difference in osmotic pressure that forces in water in order to maintain approximate osmotic equality between plasma and secreted fluid.

2.5.2.2 Route of cerebrospinal fluid

The typical route of the cerebrospinal fluid is now described (figure 2.21). The cerebrospinal fluid forms in the choroid plexuses of the lateral ventricles and passes to the third ventricle through the interventricular foramina (of Monro). There, additional cerebrospinal fluid is generated from the choroid plexuses. Using the cerebral aqueduct, it goes to the fourth ventricle where further augmented by cerebrospinal fluid produced by choroid plexuses and by some cerebrospinal fluid ascending from the central canal of the spinal cord. Through the foramina of Magendie and of Luschka, it leaves the ventricular system to enter the subarachnoid space. Then it flows down and around the spinal cord and up its ventral side to basal part of the brain. Then dorsally over the hemispheres where it enters the arachnoid villi and is discharged through them into the venous system of the superior sagittus sinus or its lacunae. During the whole process, a small amount of cerebrospinal fluid returns to blood circulation as seen in figure 2.22.

2.5.2.3 Absorption of cerebrospinal fluid

It is generally accepted that major escape route of the cerebrospinal fluid is through the arachnoid villi, which are essentially evaginations of the subarachnoid space into the lumen of the large dural sinuses. Other drainage sites have been suggested, e. g. from spinal subarachnoid space into large spinal veins associated with emerging nerve routes, but these are, at most, subsidiary pathways.

According to Davson et al (1970), two mechanisms for absorption had been proposed:

(1) Flow due to difference in pressure between subarachnoid space and dural sinus (ΔP):

$$Q = \frac{\Delta P}{R} \quad \text{where R is the resistance, and Q the flow rate.}$$

(2) Flow due to difference of colloid osmotic pressure between virtually protein free cerebrospinal fluid and plasma (Mortensen and Weed*, 1934; Weed*, 1935).

Davson et al (1970) found that resistance to flow was not affected by the colloid osmotic pressure of an artificial cerebrospinal fluid infused into the ventriculo-subarachnoid system. Thus, they concluded that drainage channels allow an unrestricted passage of protein through their pores, thereby eliminating the second mechanism.

Absorption from the spinal subarachnoid space and the central canal

Chronic adhesive arachnoiditis caused by introduction of irritant into cisterna magna leads, not only to hydrocephalus, but also to dilatation of central canal as found by Becker et al (1972). In experiments on cats, they also found, in three out of six cases, communication between the fourth ventricle and the spinal subarachnoid space via the central canal. It was known from Coben and Smith (1969) that there is capacity for absorption from spinal subarachnoid space. Absorption of fluid from the spinal subarachnoid space may also play an important role in compensation during human hydrocephalus, as suggested by study of Paraicz et al (1972). They found that during cisternography in presence of tentorial block the radiopharmaceutical material was absorbed into the blood while scintigrams showed radioactivity confined to the spinal and basal regions.

* as cited in Davson (1967)

2.5.3 Mechanism for transmission of vascular pressure

Davson (1967) cleared up many misconception with the following exposition.

2.5.3.1 Effect of artery alone

Suppose walls of artery are rigid and inextensible (figure 2.23a). Then the cerebrospinal fluid pressure cannot be influenced by the arterial pressure, whatever its value is. Suppose now that the arterial walls are somewhat extensible, so that as the pressure is raised from 0 to 80 mmHg (0 to 3.5 kPa), the arterial wall will tend to expand. But this will reduce the volume of cerebrospinal fluid. If the cerebrospinal fluid is incompressible and the chamber (dura) is inextensible, then the expansion of the arterial walls must be held in check by the cerebrospinal fluid pressure and $P_F = P_A$. The artery has transmitted its own pressure completely to the cerebrospinal fluid.

2.5.3.2 Effect of outflow through a valve

If we now consider figure 2.23b, a valve is inserted in our control volume. When the fluid pressure rises beyond a certain value, some of the fluid can leak away through the valve, at A, which opens, say, when the pressure is 20 mmHg (850 Pa). As the arterial pressure is raised, the walls will tend to expand, thus transmitting a pressure to the surrounding fluid; but this expansion is prevented by the incompressibility and the inextensibility of the system until the fluid pressure has been raised to 20 mmHg (850 Pa). At this point, expansion becomes possible because fluid can escape, and the walls will continue to expand until the elastic tension in the arterial wall, together with the opposing fluid pressure, just balance the arterial pressure. Once again, then, the fluid pressure is created

by the arterial pressure, but this time its value is determined by the valve, i.e. by the critical pressure above which fluid is allowed to escape. If the arterial pressure is raised very quickly, and the fluid can only escape through the valve slowly, there will be certain transitory changes that will not be observed if the arterial pressure is raised only very slowly; the system will tend to behave like the incompressible and inexpandible system considered earlier, that is, the sudden rise in arterial pressure will be reflected in a sudden rise in fluid pressure, which will only subside when sufficient fluid has leaked away to provide a state of balance, with the fluid pressure equal to the critical pressure at which the valve opens. Rapid fluctuations in arterial pressure, such as those caused by the cardiac pulse, will thus be reflected in transitory changes in the fluid pressure, if the valve offers some resistance to outflow of fluid. The rise and fall in arterial pressure during transmission of the fluid will be considerably damped by the presence of an outflow mechanism, but it will be clear that, other things being equal, the greater the resistance to outflow, the greater will be the pressure pulse within the fluid.

2.5.3.3 Effect of veins

Let us consider figure 2.23c where P_f is only slightly greater than P_v , which is a lot smaller than P_A . The walls of the veins being highly distensible compared with arteries, the veins are capable of considerable expansion when P_v exceeds P_f . Under these circumstances P_f is largely determined by P_v (analogous to outflow pressure). Rapid fluctuation in P_A will be transmitted to P_f (as described above), but only during the time required for the venous system to adjust itself by partial collapse of its walls, associated

with expulsion of blood out of the system. So the system will show arterial pulse, but highly damped. The level of damping depends on the outflow resistance to venous blood.

2.5.3.4 Effects of removing cerebrospinal fluid on the cerebrospinal fluid

Ignoring contribution due to arteries: $P_F = P_V$ - (elastic component). If cerebrospinal fluid is withdrawn, the magnitude of the elastic component rises because vein dilates: P_F falls.

2.5.3.5 Cerebrospinal fluid pulsation

Bering's (1955) experiments showed that the choroid plexuses of the cerebral ventricles are the chief sites for the transfer of the arterial pulsation to the cerebrospinal fluid. The venous pressure variation has a secondary effect. Each pulse sets up a pressure gradient through the cerebrospinal fluid system which tends to force cerebrospinal fluid out of the cerebral ventricles. This acts as an unvalved pulse pump, imparting to-and-fro motion to the cerebrospinal fluid, the net flow depending on the amount removed from the subarachnoid pathways. The cerebrospinal fluid pulsation contributes a small increment to the intracranial pressure. Under certain pathological conditions, such as hypertrophy or tumours of the choroid plexus, it may become the major source of the increased intracranial pressure.

Effect of damping

The normal cerebrospinal fluid pulse can be damped by volume increase. The effect of damping was illustrated by Bering by measuring the pulse pressure in one ventricle and

an open-bare manometer attached to a needle in the opposite ventricle. The cerebrospinal fluid pulse was recorded with the manometer open and closed. The patient (a hydrocephalic child) had a pulse pressure of 50 $\text{mm H}_2\text{O}$ (160 Pa) with manometer closed which dropped to 28 $\text{mm H}_2\text{O}$ (90 Pa) with manometer open.

Mechanism of circulation

According to Bering (1955) the pumping action of the choroid plexuses is not vital for cerebrospinal fluid circulation since there are many adults who have had choroid plexectomy without apparent ill effect.

In contradiction to Bering, Hamit et al (1965) describe a series of experiment on dogs that show that: (1) arterial blood pressure is an important factor in maintaining the static (i.e. the average) pressure of the cerebrospinal fluid; (2) the pulsations of cerebrospinal fluid correspond both temporally and conform to the venous pulse, whether it is normal or abnormal. Furthermore, the cerebrospinal fluid pulsations continue in characteristic form and amplitude when arterial pulsations to the brain are obliterated.

Sepp^{*} (1929) regarded vascular contractions as a major factor in circulation of cerebrospinal fluid. He also made the clinical observation on the formation of pouches along the course of the major cerebral arteries in case of localised obstructions of the subarachnoid space.

^{*} as cited in Davson (1967)

^{*} as cited in Woollam & Millen (1962)

O'Connell* (1943) has drawn the attention to significance of the cardiac and respiratory pulses in the cerebrospinal fluid pressure in relation to the movements of the cranial and spinal fluids.

Riser* (1929) pointed out that the movement of the cerebrospinal fluid is considerably affected by changes in posture and by coughing.

Sachs et al* (1930) state that it seems probable that the flow is a slow wave-like progression rather than an actual streaming. That was confirmed by Mortensen and Weed** (1934).

The Cushing response

Cushing** (1902) postulated that the increase in systemic blood pressure which often coincides with marked cranial hypertension was a compensatory mechanism designed to keep blood pressure above intracranial pressure, thereby maintaining perfusion of the vital centres of the brain. Cushing's experiments were carried out on animals in which the intracranial pressure was increased either by an expanding intracranial balloon or by perfusion of the subarachnoid space with saline.

* as cited in Woolam & Millen (1962)

** as cited in Davson (1967)

2.6 MEASUREMENTS OF PRESSURE

2.6.1 Pressure measurement

The unit used to measure the cerebrospinal fluid is the mm of saline (almost water) or sometimes, mm of mercury: $1 \text{ mmHg} = 13.5 \text{ mm saline (or csf)} = 43.2 \text{ Pa or } N/m^2$.

In figure 2.24, a frequency distribution amongst 1033 apparently normal human beings is plotted. Persons are considered normal when the intracranial pressure is less than 180 mm saline (580 Pa). Between the pressures of 180 and 200 mm saline (respectively 580 and 640 Pa), the persons are critical. Above 200 mm saline (640 Pa), they are definitely hypertensive.

2.6.2 Dynamics of intracranial pressure (ICP)

The adult cranium contains approximately 1500 ml of brain substance, and 120 ml of both blood and cerebrospinal fluid. Normal intracranial gauge pressure is considered to be in the range 7-10 mmHg (300-430 Pa). The reason why the intracranial pressure is above the atmospheric pressure lies in the relationship between formation and reabsorption of cerebrospinal fluid. Cerebrospinal fluid is derived from blood mainly in the networks of small blood vessels, called choroid plexuses, in the ventricles and the brain. It is formed largely in the lateral ventricles from where it progresses to the subarachnoid space. During its journey it is added to by choroid plexus in the third and fourth ventricles. It is then reabsorbed into the venous circulation through a series of small, pressure sensitive, one-way valves: the arachnoid villi. Cutler et al (1968) showed that there is a linear relationship between the rate of absorption of cerebrospinal fluid and

the intraventricular pressure over a range of at least 5 to 18 mmHg (220 to 780 Pa; see figure 2.25). Reabsorption ceased at 5 mmHg (220 Pa) and it was suggested that this value may approximate the pressure in the superior sagittal sinus. Studies have been made of relationship between the pressure of the cerebrospinal fluid and the sagittal sinus in both normal and pathological conditions (Shulman et al, 1964). Several workers have developed techniques for clinically assessing rates of cerebrospinal fluid formation and absorption as a function of pressure.

Normal cerebrospinal fluid pressure is not a steady pressure, but contains dynamic components which result primarily from the arterial blood pressure wave and from the respiration: the cerebrospinal fluid pressure falling during inspiration and rising during expiration (McDowall, 1975; Dunbar et al, 1966; Dardenne et al, 1969). The dynamic components are shown clearly in figure 2.24, but the respiratory pulsations are inverted because the recording was taken from a patient who was artificially ventilated using intermittent positive pressure ventilation. The mean level of the pressure in this example is also slightly above normal. The pulsations increase in amplitude when the mean cerebrospinal fluid pressure increases (Bradley, 1970). If, however, intracranial pressure is raised by increasing the venous pressure through, for example, anaesthesia or heart failure, venous components can become apparent on the cerebrospinal fluid pulsations (Dardenne et al, 1969).

The arterial pressure wave is believed to be transmitted to the cerebrospinal fluid partly through pulsation of the intracranial arteries, in particular those at the base of the brain, and partly by the pulsatile volume changes in the choroid plexuses (Bering, 1955 and 1965). The arterial pulsations increase in amplitude when the mean cerebrospinal fluid

pressure is elevated. In their study of the cerebrospinal fluid pulse waves, Dunbar et al (1966) demonstrated that in the lumbar subarachnoid space the arterial cerebrospinal fluid pulsations are derived from the local arterial supply to the spinal cord. These pulsations lag slightly behind the intracranial pulsations (by 1/25 to 2/25 sec) which reflects the delay between the arterial supply reaching the brain and reaching the lumbar spinal cord. The dynamic components due to respiration appear to follow changes in intrathoracic venous pressure, hence the fall during the inspiration and rise during expiration. Transmission of the intrathoracic pressure changes to the cerebrospinal fluid is likely to be via the jugular and intracranial veins through the changes in intracranial blood volume, and probably to a lesser extent via changes in systemic arterial pressure which occur during respiration. Since large increases in intrathoracic venous pressure result from coughing and straining, therefore, large increases in intracranial pressure are possible with a corresponding reduction in cerebral blood flow. Fortunately such changes are usually of short duration.

2.6.3 Posture affects ICP

The posture of a patient changes the intracranial pressure (Bradley, 1970), although the mechanisms by which the effects occur have been subject to debate and some confusion (McDowall, 1974). Indeed, it has been noticed that the fluid pressure in the lumbar sac is greater in the sitting than in the recumbent posture. If a subject is placed in a recumbent position, the pressure measured in the lumbar sac is about 150 mm saline (480 Pa) on average. The subject is now tilted into the vertical position. The pressure rises but the increase will not be equal to the increase in hydrostatic pressure due to the height.

Masserman^{*} in 1935 evaluated that the pressure increase actually read was 40 % of the theoretically possible increase. This consideration led Weed (series of papers) to postulate the existence of an elastic component within the system. This elastic component would operate to damp down the large fluctuations in pressure that would otherwise occur during postural changes.

For patient management it is generally accepted that a slight elevation of the patient's head above the horizontal plane will reduce cerebral venous and intracranial pressures. Equally important, however, are the effects of changes in the position of the head and neck which can alter thereby the intracranial pressure (Shapiro, 1975; Hulme and Cooper, 1976).

2.6.4 Coughing

Coughing produces a short sharp pressure rise within the major body cavities of the thorax and abdomen. The diaphragm is relaxed and the glottis closed, the intra-abdominal pressure is then raised by contraction of the trunk muscles and pressure is raised until the glottis relaxes, releasing air from the lungs whereafter the pressure drops to atmospheric and the cough is over (figure 2.26). Coughs studied by Lockey et al (1975) were those of the order of 0.9 second duration, pressure in the abdomen rises to around 75-100 mmHg (3240-4320 Pa; see figures 2.27, 2.28).

As seen in part 2.2, the spine is made up of vertebrae, a series of bones and tough ligaments which are enveloped by muscles. It forms part of the body wall which surrounds the abdominal and thoracic cavities. The spinal canal runs through the bone

^{*} as cited in Davson (1967)

and is protected from the direct action of muscles. It is within the protection of this spinal canal that the spinal cord lies, surrounded by cerebrospinal fluid, arachnoid and dural membranes giving off a pair of nerves for each vertebra. Outside the dura there is a little fat and a plexus of epidural veins which lie chiefly on the front of the cord as two vertical channels which are crosslinked and supplies with anastomoses (connecting channels which allow flow in either direction) to the veins from bones of the spines, the veins within the surrounding muscles and to the veins of the abdominal cavities. The anastomotic veins occur at each segment level. There are thirty vertebrae, each of them corresponding to a segment throughout the spine. All but the topmost seven (cervical) vertebrae are intimately connected to the thoracic or abdominal cavities by veins (figure 2.26).

As the pressure in the thorax and abdomen rise during coughing, or any similar manoeuvre, the veins within the major body cavities are subject to a high pressure and blood moves into the epidural veins transmitting most of that rise in pressure (figure 2.29). The increase in pressure is normally transmissible across the membrane forming the wall of the veins and across the dura and arachnoid to the cerebrospinal fluid.

Queckenstedt has shown in 1830 that slow pressure changes are normally transmitted along the spinal canal with little attenuation. His test produces a movement of cerebrospinal fluid downwards initially followed by an upward rebound, but coughing produces a pulse in the opposite direction, that is it travels from the lumbar region to the cisternal. The cough impulse provides a much sharper rise in pressure of higher amplitude and also provides a quick fall instead of a plateau.

CHAPTER 3

ABOUT SYRINGOMYELIA

For a better understanding of the origins of syringomyelia, we have first described the cerebrospinal system in the previous section. In this section, we will give an overview of the main features linked with syringomyelia and the state of research in the field. We will first answer some basic questions like:

What is syringomyelia?

What are the different causes and forms of syringomyelia?

What are the symptoms?

How can it be diagnosed?

What are the treatments available?

What is the pathology?

This will be followed by a summary of the knowledge about the origins of the disease, including an interesting aspect of the CSF dynamics in the spinal cord.

3.1 DEFINITION

The name syringomyelia comes from the Greek syrix: pipe or flute and myelo: marrow. Thus, it means syringes or cavities in the spine. It is a condition of longitudinal cavities within the spinal cord extending over several segments (Greenfield 1963). This abnormal fluid-filled cyst (syrinx) in the spinal cord causes progressive neurologic symptoms as it expands (figure 3.1). Syringomyelia may be congenital or acquired. It most commonly

occurs in the cervical segments of the spinal cord but can involve the entire length of the spinal cord and occasionally extends to the brainstem (syringobulbia: dysfunction of the lower cranial nerves). There are three types of syringomyelia: (1) hindbrain herniation of Chiari Type 1 (associated with syrinx formation); (2) hindbrain herniation of Chiari Type 2 (associated with syrinx formation); (3) post-traumatic syringomyelia. The hindbrain herniation of Chiari Type 1 (or Arnold-Chiari Deformity) is characterized by the descent of the tonsil through the foramen magnum (figures 3.2 & 3.3). The term Arnold-Chiari deformity is sometimes used to describe the severe deformities of the hindbrain and upper cord found in association with spina bifida and hydrocephalus. This is sometimes called Chiari type 2. It is not possible to delineate the two conditions precisely and many intermediate forms may be found. The aetiology of both types is likely to be pressure differences (Williams 1975). The first two cases involving hindbrain herniation are characterized primarily by crowding and compression of craniospinal spaces. Post-traumatic syringomyelia is characterized primarily by scarring of the arachnoid membrane surrounding the spinal cord and tethering or extensive attachment of the cord itself to the spinal canal (figure 3.4). Studies have found that a syrinx that forms after a spinal cord injury almost always appears at the site of the original injury. The syrinx may also extend several spinal segments above or below the level of injury.

The shape of cavities is variable. There may be one oblong cavity, or a large cavity may have several oblong compartments that are connected, or several separate cavities that have nerve tissue between them (figure 3.5). The ends of the cavities may have a round, bulb-like shape or may stretch down to a thin strand.

3.2 HISTORICAL CONCEPTS

Ollivier* (1827), who named syringomyelia in 1827, understood that cavitation followed the weaknesses along which fluid tracked through the grey matter of the spinal cord. He carried out air injection to support this notion. The idea later became prevalent that the disease was due to degenerative changes in glia. The cavities become surrounded by gliosis, but Greenfield (1963), pointed out that the cavities appeared to be due to tearing of tissues by the spread of fluid. Studies on human cadaver, subsequent to that of Ollivier, and also by injections of saline or CSF into the grey matter of living animals produced cavities mimicking syringomyelia. Kaolin (an irritant) induced hydrocephalus is a reliable animal model but the relevance to the human condition is limited (Williams 1986a).

The relationship between abnormalities of the base of the brain which cause pressure differences between the head and the spinal subarachnoid space was noted by Gardner (1973). He suggested that the majority of cases have a communication from the fourth ventricle to the syrinx in the initial stages of syringomyelia.

Gardner showed that operative craniovertebral decompression was often accompanied by improvement in the patient's clinical state. He produced a theory which attempted to explain spina bifida, anencephalus, iniencephalus, Dandy-Walker cysts and syringomyelia on the basis of failure of the fourth ventricle roof to perforate during embryogenesis. This concept seems unsound, but has been of value in stimulating subsequent workers.

* as cited in Williams (1993)

3.3 CAUSES OF SYRINGOMYELIA

As we have discussed earlier, CSF normally flows around the spinal cord and brain for two main reasons: to transport nutrients and waste products and to serve to cushion the brain and the spinal cord. A number of medical conditions can cause an obstruction in the normal flow of CSF, redirecting it into the spinal cord itself. For reasons that are not totally clear, this results in syrinx formation. To understand the underlying causes of syringomyelia, it is necessary to understand the structure and physiology of the normal spinal cord and CSF, as well as the structure and mechanisms of expansion of the syrinx. The early theories of Gardner and Williams assume that the CSF is being driven or sucked down from the fourth ventricle into the central canal. The central canal is now understood to act like a sink draining CSF. Experimental studies in animals have indicated that horseradish peroxidase molecules or red blood cells injected into the spinal interstitial spaces can pass into the lumen of the central canal through the open gap junctions of its ependymal cell lining. The central canal accumulates such products (as well as normal abnormalities or products of disease) and carries them rostrally towards the fourth ventricle. Drainage is probably assisted by vascular pulsations transmitted to this fluid-filled tube.

An experimental model of acquired syringomyelia has been created in animals by injecting an irritating substance (Kaolin) into the CSF or into the spinal cord. An inflammatory response with ependymitis and occlusion of the subarachnoid space or partial occlusion of the central canal outflow pathway resulted, depending on where the

Kaolin was injected. Subsequently, cavitation and dilatation of the central canal occurred with the histopathologic features characteristic of syringomyelia.

3.4 FORMS OF SYRINGOMYELIA

Generally, there are three forms of syringomyelia: the Chiari 1 malformation, the Chiari 2 malformation and the complication of trauma, meningitis, hemorrhage, a tumour or arachnoiditis. In the first form, the malformation occurs during the development of the foetus and causes the lower part of the cerebellum to protrude from its normal location in the back of the head into the cervical or neck portion of the spinal canal (figure 3.2). A syrinx may then develop in the cervical region of the spinal canal. Because of the relationship that was once thought to exist between the brain and the spinal cord in this type of syringomyelia, physicians sometimes refer to it as "communicating syringomyelia". Here, symptoms usually begin between the ages of 25 and 40 and may worsen with straining or any activity that causes CSF pressure to fluctuate. Some patients, however, may have long periods of stability. Some patients with this form of the disorder also have hydrocephalus, in which CSF accumulates in the skull, or a condition called arachnoiditis, in which the arachnoid membrane (the covering membrane of the spinal cord) is inflamed. The second form of syringomyelia is similar to the Chiari 1 malformation but an additional displacement of the brainstem outside the foramen magnum occurs (instead of a displacement of only the cerebellar tonsils, which occurs in the Chiari 1 malformation). The third major form of syringomyelia occurs as a complication of trauma, meningitis, hemorrhage, a tumour or arachnoiditis. Here the syrinx develops in a segment of the spinal cord damaged by one of these conditions. The

syrinx then starts to expand. This is sometimes referred to as "noncommunicating syringomyelia". Symptoms may appear months or even years after the initial injury, at the location of the injury.

Some rare cases of syringomyelia are familial. Zakeri et al (1995) made a review of the world literature on familial syringomyelia. They identified 16 reported families with syringomyelia since the beginning of the century. Chatel et al (1979) suggested the incidence of inherited syringomyelia is approximately 2%. In these rare cases, a genetic predisposition is the primary factor in the development of familial syringomyelia.

In addition, one form of the disorder involves a part of brain called the brainstem (which controls many of our vital functions, such as respiration and heartbeat). When syrinxes affect the brainstem, the condition is called syringobulbia.

3.5 SYMPTOMS OF SYRINGOMYELIA

Destruction of nervous tissues of the spinal cord and elevation of pressures in the skull are the primary consequences of syringomyelia. Consequently, the main symptoms of syringomyelia are: strong headaches; stiffness, weakness or pain in the back, shoulders, arms or legs; loss of the ability to feel extremes hot or cold, especially in the hands. Here we give some details of these symptoms, separating the hindbrain herniation from the spinal cord case.

Hindbrain-related syringomyelia symptoms (see table 3.1)

The symptoms of hindbrain herniation related syringomyelia include intracranial symptoms, pain, medullary symptoms such as vertigo, oscillopsia, or any complaint of

lower cranial nerve involvement. The symptoms related to the medulla are often thought of as "syringobulbia".

Strain-related headache is a characteristic presentation. The pain is usually nuchal and bilateral, radiating into the occiput or vertex. It may be strictly unilateral. It is commonly brought on by suddenly rising from the lying or sitting position, by coughing, straining, lifting, shouting and only rarely by emotional tension (Nightingale & Williams, 1987). It is characteristically pounding and patients may be able to draw a graph of the pain which they experience after blowing in a sphygmomanometer to raise the mercury to a height of 40 mm (1700 Pa) for 5 seconds, or of the similar pain produced after an individual event such as a sneeze. This type of headache is the same as that found when patients have a hindbrain hernia due to brain tumour, always the first consideration in cases presenting this way.

Cord symptoms

Any manifestation of spinal cord disorder may be the first symptom, including scoliosis, trophic, sensory or motor features (Barnet et al, 1973; Gurr et al, 1988; Williams, 1979). Sensory changes present in the majority in the upper limbs, but stiffness in the legs was the commonest symptom reported by Barnet et al (1973), and presentation with leg symptoms alone is not uncommon. Pain occurs in the majority of patients and many present to an orthopaedic surgeon before seeing a neurologist or neurosurgeon (Williams, 1979). Pain may be associated with slosh (see CSF dynamics section), for instance sudden pain in the trunk or limbs after coughing or sneezing.

Scoliosis is present in more than half the patient with hindbrain-related syringomyelia (Gurr et al, 1988; Williams, 1979). It is correlated with early onset, and usually precedes other neurological features. The side and level of the cord cavity are not related to the curve (Gurr et al, 1988). Paraplegia during correction of scoliosis may be the first declaration of syringomyelia. The history is paramount. To take the birth history in adult life is not common, since most birth-related injuries are diagnosed in paediatric practice. Syringomyelia (like hydrocephalus and epilepsy) are causes of late neurological presentation. Difficult birth is related to over half the cases of adult syringomyelia and of those who have no other cause detectable, and it is probable that the majority are birth-related (Williams 1977a).

Similarly, complaints like giddiness, syncope, drop attacks sweating changes, transient double vision, swallowing difficulties, hypersalivation, stiffness of the legs may not be linked by the patient to their presenting complaint if that is a different type of symptom, such as pain or scoliosis. The characteristic dissociated sensory loss is often not present in the early stages, but inquiry may include asking if the an underarm deodorant feels the same on the two sides, and asking women if their hair rollers burn the backs of their necks.

On examination, scoliosis, hemiatrophy, asymmetries of the face and upper limbs, wasting, Charcot's joints, trophic changes often with severe finger involvement, are all late manifestations. Slight trophic changes, such as burns and ulceration from brassiere straps, may precede the patients' noticing that they have dissociated loss. Tendon jerks are commonly lost early in the arms and brisk in the legs, abdominal reflexes tend to be lost. Wasting and fasciculation may be present in the arms.

3.6 DIAGNOSIS AND TREATMENT

3.6.1 Diagnosis

There are no world-wide ways of syringomyelia investigation. However, there are some techniques that should be applied depending on the condition of the patient. Williams (1990b) suggested a pattern of investigation which is summarised in figure 3.6. This pattern of investigation consists in radiological assessment. There are four types of radiology that can be used to diagnosed syringomyelia: plain radiographs, computerized tomography, myelography with water-soluble contrast, magnetic resonance imaging (MRI).

Plain radiographs

In hindbrain-related cases the radiographs may be interesting and variable. Plain radiographs of the lateral skull may show effects hydrocephalus, platybasia, or basilar invagination (Williams 1979). They are only associated anomalies, however, and probably have a common cause. They may be segmentation abnormalities of the skull base with fusion of the occiput and atlas or fusion of cervical vertebrae.

The concept of primary osseous dysplasia as suggested by Shady at al (1987) is not necessarily supported by the frequent finding of a small posterior fossa (Williams 1975 & 1977b). In spinal post-arachnoid adhesion cases, plain radiographs show only the changes of the paraplegia or associated disease. Some tumour patients may have had syringomyelia for sufficiently long, or at an early enough age, for it to have affected the growth of the bones. The certain diagnosis of syringomyelia from enlargement of the

vertebral canal is not possible because intraspinal tumours and neurofibromatosis also cause it. If the anteroposterior diameter of the canal and body at C5 (cervical 5) are measured, there is a 25% chance of pathology if the canal is more than 4 mm bigger than the body, and a 98% chance of pathology if it is more than 6 mm bigger than the body (Williams 1979)

Computerized tomography

The ventricles should be scanned in most cases. In around one third of cases of syringomyelia, there is some ventricle enlargement (West & Williams 1980). Posterior fossa, midbrain, and even supratentorial tumours are uncommon causes of syringomyelia, but tumours at the foramen magnum are more common and are sometimes missed on computerized tomography. The tumour may form the hindbrain hernia. Head pouches are related to hindbrain arachnoiditis and, therefore, also to birth injury (Williams 1986b).

Myelography with water soluble contrast

Water-soluble myelography is a valuable technique. The flexibility of the cord and its susceptibility to slosh (see CSF dynamics) are demonstrable on screening. In mysterious neurologic cases the contrast material should be run up to the cisterna magna and the position of the tonsils and the fourth ventricle checked.

Post-myelography computerized tomography scanning is of value in showing hindbrain compression and tonsillar descent. It may show typical deformities such as are associated with syringobulbia (figure 3.7). Convenient times for computerized tomography scanning

are 1, 6 and 24 hours after the myelogram (figure 3.8). The syrinx cavity may opacify, commonly at 6 hours or at 24 hours.

These investigations have largely been supplanted by magnetic resonance imaging (MRI). One area in which myelogram is more useful than MRI is in establishing the readiness of communication between compartments. Moreover, MRI is not good at showing arachnoiditis.

Magnetic resonance imaging (MRI)

Magnetic resonance imaging shows the ventricles, including the third and fourth, hindbrain descent, and the spinal cord (Barkovich et al, 1986; Duddy and Williams, 1991; Grant et al, 1987 for instance). Scanning scoliotic patients may be difficult, and skill is required in interpretation. Myelography and computerized tomography scanning may be dispensed with provided that the whole brain is imaged, but plain radiographs remain useful because the bones do not show well (figures 3.7, 3.9, 3.10, 3.11).

The investigation is especially useful during outpatient surveillance. It is possible, with the T2-weighted image, to see flow void in the CSF pathways (figure 3.12), and to confirm patency of the pathways to arterial pulsation.

3.6.2 Treatment

The treatment of syringomyelia falls into two parts. The first is the correction, so far as it is possible, of the filling mechanism which causes the fluid to be forced into the syrinx and to lead to progression along site of grey matter. The second is the prevention of the persistence of the cavity by drainage. When the cavity is empty it can be expected to

negate the continuation of mechanism of slosh. It may be expedient, or even necessary, to treat using both principles in some cases. In cases where there is proteinous fluid and an obvious structural lesion, such as an intrinsic or extrinsic tumour of the spine, then removal or attempted removal of the lesion is the obvious first line of treatment.

In practice, the progression of syringomyelia being often slow, many of the patients have become accustomed to their disabilities and fear operation. It is obviously necessary to advise them carefully and not to minimize the difficulties. The younger the patients are, the better they do. The smaller the tumour, the better it does. As with the hindbrain-related cases, the sooner after development of post-traumatic paraplegia an operation is carried out the more likely it is that the resultant cavities will be limited. Early operation is, thus, ideal.

There are three main operations to consider: syrinx drainage, ventricular drainage, and attempted correction of the likely filling mechanism by operation on the site of presumed or proved pressure dissociation. Williams (1990b) suggested a sort of guide. He attempts to demonstrate decisions that may be necessary (figure 3.13). The peculiar "may be" in a decision tree proves the difficulty to decide in some cases. The decision to operate on a syrinx that may be drainable often cannot be made until the surgeon tries to insert a tube, and the decision is greatly influenced by things such as leg function. If the patient is already wheelchair-bound, there is much less to lose in attempts to save hand or bulbar function.

We have just outlined treatments for syringomyelia. For a more detailed review of the techniques of operation, refer to Williams (1990b).

3.7 PATHOGENESIS

The pathogenesis of syringomyelia is not understood. Theoretical concepts abound but surgery is currently practised based upon an empirical or pragmatic background rather than a certain knowledge of causation.

The observation of its occurrence in association with the disorders shown in table 3.2 almost certainly indicates a causative connection between the syringomyelia and the other structural abnormalities; or that both are due to a common cause. Most patients who have syringomyelia secondary to post-traumatic paraplegia for instance, had a normal central nervous system in all respects prior to the injury. In the pathology associated with hindbrain-related cases, the factor which links them seems not so much something protruding through the foramen magnum or even forming a valvular configuration there, but more the absence of cisterna magna.

We now consider the forces which are brought to play on the tissues of the neuraxis through the CSF.

3.7.1 The hydrodynamic forces

The CSF within the neuraxis is in continual movement. Cardiac pulsation in the capillary bed of the brain is constant throughout the nervous system. Of greater significance and power are the effects of venous plexuses (see section 2.5.3.3). These have free connection through valveless veins present at each vertebra of the neuraxis and up to the head. Any increase in pressure in the abdominal and thoracic cavities is transmitted into the spine. Compression of the dura by venous distension of the epidural plexuses produces rapid

movements of CSF with associated pressure changes. Williams (1976) found that the pressures produced by a cough may exceed the pressures produced by cardiac pulsation by a hundred times. The energy imposed upon the tissues of the neuraxis affects the formation and the maintenance of syringomyelia (Williams 1981).

3.7.2 Suck mechanism

The first mechanism is the creation of pressure differences between CSF compartments by venous pulsation. If the patient has a spinal tumour, for example, energetic coughing will force fluid upwards past the tumour more efficiently than it can run back down again (figure 3.14). This leads to a collapsed theca below the tumour with a high protein content and a low pressure -Froin's syndrome. If fluid can find its way into the cord at the site of the obstruction, then, this may be the mechanism which gives rise to a syrinx. Tumours outside the cord, fracture, Pott's disease or other partial blockage of the subarachnoid spaces caused by the formation of pathological arachnoid adhesions are the common causes.

When measurements are made at rest in the majority of adults with hindbrain-related syringomyelia, or even patients with well-developed herniation due to tumour, pressures are substantially equal in the head and the spine.

When coughing and sneezing, the pressure in the lumbar sac rises higher and more quickly than it does in the head. In the majority of patients with hindbrain hernia, however, the CSF is delayed in its return downwards past the foramen magnum (Williams 1975, 1976, 1980 & 1981). In normal cases, the half-life of the return of pressure differences to normal, i.e. equal in the spine and the head, is less than 1/10th of a

second. With hindbrain herniation, the equalisation of pressure may be delayed, sometimes with a half-life of over 30 seconds. During a post-Valsalva rebound after straining, the pressure differences may be high across the foramen magnum and may remain high for a significant period. Pressure differences across the foramen may be called craniospinal pressure dissociation, but with pressure differences across the site of any obstruction lower in the neuraxis, may be conveniently described as "suck" (figure 3.15). This exerts a force which continues to mould the hindbrain hernia as well as sometimes being concerned with the pathogenesis of syringomyelia. Correction of the hindbrain hernia will commonly produce radiological and clinical improvement in hindbrain problems and also in syringomyelia (many investigators).

3.7.3 The communicating hypothesis

Gardner's idea, that the embryological communication between the fourth ventricle and the central canal was usually the means by which the syrinx filled, had immediate appeal once the nature and severity of the suck mechanism between the head and the spine was measurable. Widespread acceptance of this idea led to a following for the operative step of blockage of the site of presumed communication, as advocated by Gardner (1973). The search for such communication in life was, however, often fruitless. West and Williams (1980) reported seventy ventriculograms with either water-soluble or oily contrast media. They found the communication in only seven cases. This figure of about 10% of cases of detectable communications in "communicating syringomyelia" accords well with other estimates. The objection that there was no communication demonstrable might be met, for some cases, by proposing that there had been a communication in the past which had

been closed, perhaps partially by the compression of tissues in the foramen magnum in the hindbrain-related cases. There seems however to be a proportion of cases in which the communication could never have been present. These include hindbrain tumour cases and also cases where the top of the syrinx is well away from the hindbrain (figures 3.3, 3.7, 3.11 & 3.16).

The communicating hypothesis may not be dead, but it is not adequate as a universal explanation for the association between hindbrain abnormalities and the syrinx.

3.7.4 The slosh mechanism

Energy imposition upon the spine by manoeuvres which raise the intra-thoracic and the intra-abdominal pressure is probably a usual mechanism in syringomyelia. If the cord contains fluid, it is likely that the fluid within will move more readily than that outside, because of the greater impediments to movement outside the cord from the dura, the pia, dentate ligaments, arachnoid strands, blood vessels and nerve roots as well as the narrowing of the subarachnoid space. Fluid surging on the inside can stress the walls of the cord and lead to tearing of the tissues in the same way as injection of fluid. Pathological preparations showing the collapsed cord are misleading. Most syrinx cavities in life are at least partially filled. It was stressed by Williams (1974), after creation of an analogue model, that cord fluctuation could be violent and the fluid inside is free to surge upwards and downwards in an indulating manner imposing ballistic distending stresses. The phenomenon of surging, impulsive intracord fluid movements is tersely called "slosh". If a cavity is being maintained by slosh, then it is likely that the natural shape of the cavity will be kept in existence by the diffusion of fluid through the

walls of the cord. Septations within the syrinx cavity, sometimes called haustreae, are of interest (figure 3.17). They probably represent nodes or no flow areas in the cord. The slosh occurs in limited zones and the walls may tend to heal or else not break down at the site of septation. Their existence naturally leads to the contemplation of wave phenomena and the existence of standing waves as part of pathology, as illustrated in figures 3.17 to 3.19. These septae may be surgically important because they make it difficult for the surgeon to pass a drainage catheter and sometimes lead to persistence of short section of syrinx after other parts of the cavity have been drained.

3.7.5 Transmural pressure gradients

It may be simplistic to think of "filling mechanisms" as applicable to this class of problem. Syringes are not necessarily in a state of active filling at all times. It may be more reasonable to seek an analogy with the Starling equations describing the behaviour of tissue fluid as being a state of balance representing the equilibrium point of several interacting forces. The cord is a porous structure. There are no tight junctions in the gliotic lining of the syrinx cavity and fluid can enter readily, as may be observed by looking at the behaviour of water-soluble contrast material in post-myelography computerized tomography scans.

Ball and Dayan (1972) in a critique of "communicating " hypothesis, drew attention to the porous state of the cord, particularly to the sizeable spaces alongside the vessels which are sometimes called the Virchow-Robin spaces. They suggested that the fluid was driven into the syrinx by the nature of the blockage at the foramen magnum. This seems at first an unlikely suggestion. Why should it be that the obstruction of the subarachnoid

pathways should force the fluid into the solid structure? Imagining the cord as being completely porous and passive suggests only that the cord would flap slightly if the fluid outside it should slosh up and down the spine. The Ball and Dayan hypothesis deserves close consideration, however, although the reasons that they gave themselves do not seem to be the best. They remarked that the pressure differences between the head and the spine were insufficient to cause filling along a tiny communication. The pressure differences are enormous however, as Williams (1981) recorded pressures of over 100 mm Hg (4300 Pa) between the head and the spine.

Fluid is unlikely to track along the proposed communication in a majority of cases, however, for the reason that there is no communication. The behaviour of water-soluble contrast which enters the cord cavities easily as shown in post-myelography computerized tomography, illustrates the likelihood that the cord is acting in a porous way, perhaps as suggested as Williams (1993) in figure 3.19.

3.8 STATE OF RESEARCH

In 1994, a workshop on syringomyelia was organized. Small and Sheridan (1994) reported the event. Here are the main elements that came out, in terms of physical understanding of syringomyelia pathogenesis.

Gordon McComb¹ spoke about the physiology of bulk CSF flow. He described two types of syrinxes: communicating and noncommunicating, which are differentiated by the composition of the cavity fluid. The majority of CSF is produced by the choroid plexus, with the remaining portion originating from the parenchyma (check on formation of csf).

A threefold turnover of CSF occurs daily, a very active process. The hydrostatic pressure differential between the newly formed CSF and the site of drainage in the ventricles and the parenchyma causes CSF to circulate. Other factors contributing to CSF circulation include pulsations of the brain, arterial tree respiration variations, changes in body position, and ciliary action. There is normally an ongoing process of communication between CSF in the subarachnoid space and fluid in the spinal cord parenchyma. In syringomyelia associated with hindbrain malformation, there is also a process of communication between the syrinx and the subarachnoid space. The therapeutic goal should be to alter this dynamic process to either prevent or collapse the syrinx.

Bernard Williams^{*} talked about his research concerning pressures in CSF and their relationship to syringomyelia. The presence of syringomyelia suggests a balance of forces such that at some time during the patient's activity in some part of the spinal cord, the pressure on the outside is lower than the pressure on the inside. Otherwise the syrinx would collapse spontaneously. He then described the slosh mechanism to support this supposition.

The human neuraxis has a large rostral capacitance (the compressibility of the veins and the compressibility of the vascular bed), but only a small caudal capacitance. The caudal capacitance is affected by the external veins and by the elasticity of the dura. Valsava's maneuver begins a fluid wave at the caudal end, which moves rostrally until it encounters a blockage. It may rebound to produce an area of consternation, diffuse chaotic flow, which may be responsible for syrinx filling. Considering the pressure-volume fluid curve,

^{*} as cited in Small & Sheridan (1996)

^{*} as cited in Small & Sheridan (1996)

reducing the volume of CSF will reduce the efficiency with which Valsava's manoeuvre will expand the syrinx. This has been the rationale for the surgical placement of a valve to lower the CSF pressure.

Edward Oldfield^{*} spoke of the pathophysiology of syringomyelia and the implications for diagnosis and treatment. There is no consensus on the pathophysiology of syringomyelia, particularly in Chiari 1 malformations. There is a great diversity in the surgical approaches that are currently being used. Detection of the pathophysiology preoperatively or during surgery may provide the basis for choosing the least invasive therapy. The use of MRI scans, pre- and postoperatively, allows for observation of the syrinx and dynamic changes that occur in the CSF and syrinx fluid during the cardiac cycle. Use of intraoperative ultrasound allows monitoring of the anatomy of the spinal cord, the syrinx and the cerebellar tonsils during surgery. In patients with Chiari 1 malformation, there is an occlusion of the subarachnoid space at the foramen magnum. In one operative study, images were obtained before and after the dura was opened. Before the dura was opened, the tonsils moved abruptly downward and the cervical portion of the syrinx constricted with each systole. After the dura was opened, but with the arachnoid still intact, there was no longer pulsatile motion of the spinal cord, and downward movement of the tonsils ceased. Patients were treated only by decompression of the foramen magnum and dural grafting, without opening the arachnoid. All patients had resolution of syringomyelia within 3 to 6 months of surgery. The results of this study imply that the mechanism of syringomyelia is external to the cord and that the transmission of a pulsatile systolic

^{*} as cited in Small & Sheridan (1996)

pressure wave in the subarachnoid space underlies the development and progression of syringomyelia.

3.9 SUMMARY OF RESEARCH INITIATIVES

A number of areas of research need to be addressed for a better understanding of, and to provide optimal treatment for, syringomyelia. The first need is a consensus on the terminology. More specific descriptions of the various types of syringomyelia are needed in the literature, so that the treatments can be described in the context of the physical defect. The outcome of research is often listed as "the symptoms improved or did not progress" or "the syrinx was reduced". Consistent modifiers are needed to quantify the changes, so that the results of various studies can be used in an integrated manner. Common terminology is of vital importance if there is to be pooling of information and collaborative efforts aimed at determining the most appropriate treatments for various types of syringomyelia.

Basic studies need to be done to learn more about spinal cord structure and function. Anatomic features and chemical composition could be compared between normal spinal cord and syringomyelia spinal cord. Metabolic, pharmacological, and physiological studies would also be informative.

A laboratory model of syringomyelia that stimulates the pathophysiology occurring in humans is needed. New animal models could be developed, or they could be expansion of research on existing models. This would allow for accumulation of data on syrinx formation and the identification of factors that aggravate the syrinx. Studies could also determine the effectiveness of various treatments. Although the laboratory model would

not be a replacement for studies of human subjects, a wealth of information would be obtained that would provide additional insights.

Improvement in imaging techniques may facilitate the understanding of how syrinxes form and what mechanisms are involved in expansion. Studies need to be aimed at determining the normal physiology of the cord, normal bulk flow in the cord, and normal physiology of CSF motion in the cord. Another emphasis would be on real-time imaging to obtain pulse pressure information noninvasively. Armed with such information, it would be possible to intervene early in the disease process by identifying those persons at risk of developing syringomyelia.

Because the pathophysiology of syringomyelia is controversial, a variety of surgical techniques are used for treatment. Research is needed to establish the pathophysiology of the ongoing progression of the various forms of syringomyelia. Currently, there is a disagreement about the use of shunts, shunt materials, and shunt locations. Clinical studies should include outcome data over a number of years, so that the various treatment options can be evaluated effectively. The goals of all treatments are reduction in the size of the syrinx and neurologic improvements. Syrinxes can be detected by MRI before the development of neurologic symptoms. Should the surgery be performed at an early stage to prevent any damage from developing, or should the patient be closely monitored, since in many cases the syrinx may never expand or problems may never arise? The ultimate goal should be for the most minimally invasive surgery for each patient to eliminate the mechanism(s) of maintenance and progression of syringomyelia.

Even when surgery successfully reduces the syrinx and improves neurologic functions, there is often no relief from chronic pain. Finding more effective treatments for chronic pain will require further studies.

There should be a wider educational outreach to medical professionals to expedite diagnosis and treatment of syringomyelia. The primary care physician is often the first consulted, and many months may pass before the patient is either diagnosed or referred to a neurologist. This allows the condition to worsen when earlier treatment may have prevented progression. In addition, there must be evaluations as to the psychological, social, and vocational adjustments necessary for these patients.

We will conclude this chapter by stressing the importance of understanding the dynamics of CSF in order to elucidate syringomyelia. This thesis is devoted to this aspect. An important point is to model pressure wave propagation in coaxial tubes where the main unknown is the pressure difference between the subarachnoid space and the central canal. This will allow us to understand the formation of syrinxes.

CHAPTER 4

FLOWS THROUGH COLLAPSIBLE TUBES

We have described the cerebrospinal system and the anomalies due to syringomyelia. We now assess the theories and techniques available for a better understanding of the movement of cerebrospinal fluid in the spinal cord.

A number of theoretical models of the intracranial cerebrospinal fluid (CSF) system have been developed. Most of them are based on compartmental models which ignore the spinal part of the system (Agarwal et al 1969, Karni et al 1987, Sorek et al 1988a,b and 1989, and Hoffmann 1987). Elements of continuum modeling have been developed by Hakim et al (1976). A continuum mathematical model of the cerebrospinal fluid system in the vertebral canal has been developed by Lockey et al (1975). Williams (1974) constructed an analogue model of the ventricular and intraspinal cerebrospinal fluid system which incorporated selected features of the real system.

However, we came to realize that compartmental models suffered fundamental deficiency for modeling many features (e.g. slosh, continuous wave propagation). Indeed, compartmental modeling is incapable of dealing with pressure propagation (for instance to understand what happens in terms of pressure propagation along the spinal subarachnoid space and along the central canal when a patient coughs) because it is based on the assumption that the pressure is uniform instantaneously over a given compartment. One way to tackle this problem would be to divide the spinal compartment in many sub-

compartments in order to achieve the pressure changes in this compartment. However this would constitute another daunting task.

A better approach to reach this aim is to follow the analysis of flows through collapsible tubes, and adapt it to the spinal cord system. That is the reason why we first describe some interesting features linked with collapsible vessels.

4.1 DEFINITION AND APPLICATIONS

Collapsible tubes have received great attention in the last forty years because of the wide range of applications, especially in physiological flows. By collapsible tubes (or vessels), one means the ability of a tube to change its cross-sectional area and shape according to the transmural pressure applied to the compliant wall of the tube. In the body, all fluid-carrying conduits are elastic and hence prone to collapse. Sometimes, the collapse of a vessel occurs as a normal and useful course of events. The best known example is the return flow of blood to the right side of the heart. In this case the feature of collapsible tube exhibited is the flow limitation (Guyton, 1963).

An extensive variety of physiological phenomena and medical diagnostic or therapeutic applications are described as examples of flow in collapsible tubes. Here is a list of these applications, but for a more accurate documentation on these applications, see Shapiro (1977a). We can distinguish three categories: (1) Physiological examples: veins, arteries, the pulmonary circulation, autoregulation, the pulmonary airways, the urethra, the eustachian tube, the vocal cords; (2) Diagnostic and therapeutic devices: Korotkoff sounds, vascular diagnosis by pressurising cuffs, intermittent external compression of the legs as prophylaxis against the occurrence of deep vein thrombosis, intra-aortic balloon

counterpulsation as an aid to the failing heart, external counterpulsation of the legs as an aid to the failing heart, prosthetic heart devices, vein cannulation for withdrawal of blood, prosthetic vocal cords; and (3) Engineering devices: amplifiers, switches, logic units.

These collapsible tube flows exhibit all the phenomena associated with flows in distended tubes, but, in addition, they offer a wealth of other interesting characteristics. These include autoregulation, flow limitation, and flow-induced flutter for instance.

In this section, the literature will be presented (which follows the survey made by Kamm, 1987), as well as some features of collapsible tubes that are particularly interesting for our model (which is described in the following chapters). We will start with the analysis of the Starling resistor, followed by some mechanics of the tube wall. We will then make some comments on the wave speed. We will finish this section by discussing the elastic jump phenomenon.

4.2 THE STARLING RESISTOR

In order to well understand the behavior of flows through collapsible tubes, so important for physiological flows, an analysis of the Starling resistor is crucial. The earliest literature by Knowlton and Starling (1912), Holt (1944, 1953, 1959), Rodbard and Saiki (1953), Rodbard (1952, 1955, 1966), Rodbard and Takacs (1966), and Bradley (1963) (as cited in Kamm, 1987) describes experimental results of hydraulic tests on the so-called "Starling resistor", used for purported simulation of certain physiological phenomena.

The device consists of a compliant tube segment mounted between two rigid tubes and surrounded by a rigid enclosure that can be pressurised (see figure 4.1). One rigid tube is connected to an open supply reservoir filled with water to an adjustable level, which

determines the inlet pressure, P_1 . The exit tube is connected to a discharge reservoir at an adjustable lower level, which determines the outlet pressure, P_2 . The enclosing chamber contains air or water at an adjustable external pressure P_e . The various experimental results reported by Holt (1944, 1953, 1959), Conrad (1969), Katz et al (1969) and Brower and Noordergraaf (1973) (as cited in Kamm, 1987) suffer from a variety of deficiencies that make interpretation of results difficult, for instance:

- (a) A "black box" view of the device, which is considered to be a resistor (often treated as though linear) characterized by a driving pressure drop from inlet to exit, $P_1 - P_2$, that produces the flow rate, Q .
- (b) The confusing presence of additional flow-resisting valves in the rigid tubes.
- (c) A misconception that there are three controlling pressure variables (P_1, P_2, P_e), rather than two controlling pressure differences ($P_1 - P_2$, and $P_2 - P_e$, for instance) with the consequence that the variables are not controlled in an appropriately systematic manner.
- (d) Failure to perceive that the end effects exhibited in figure 4.2 are dominant when $P_2 - P_e$ becomes substantially negative.

Clarification of the foregoing item (c) was provided by Brower and Noordergraaf (1973), but with no further elucidation from a fluid mechanical point of view.

We finish this brief description of the Starling resistor with three remarks:

- (a) Since the flow limitation behaviour appears to occur at both very low and very high Reynolds numbers, it seems reasonable to suppose that it applies over the entire range of Reynolds numbers.

(b) The flow limitation behaviour appears here independently of any consideration of a wave-speed type of limitation. Can there be wholly different and physically independent sources of flow limitation? Probably not. The analysis here ignores the question of whether the sequence of states through which the flow must pass is possible.

(c) Oscillations of a Starling resistor have been studied by various investigators (Conrad, 1969; Brower and Scholten, 1975; Griffiths, 1977). It has been shown, however, that the character of these oscillations is governed largely by the properties of the system downstream of the device (Conrad, 1978; Bertram and Pedley, 1982) and is also likely to be influenced by the non-physiological attachment between the compliant and rigid tubes at the downstream end.

Note that Kamm (1987) made a more detailed description of the Starling resistor.

4.3 THE MECHANICS OF THE TUBE WALL: TUBE LAW

Virtually all the literature on flow in collapsible tubes contains the assumption that there exists a 'local tube law', namely a unique relationship between the local cross-sectional area and the local transmural pressure: $A = A(P - P_e)$, where P and P_e are the internal and external pressures, respectively. This is valid when stiffness against area change resides solely in circumferential bending or tension; or, equivalently, when the structural stiffness due to longitudinal tension and bending are both negligible. But such is the case only if longitudinal area variations are of sufficiently long wavelength. Thus the hypothesis of a local tube law is equivalent to the assumption of infinite wavelength in area variation.

Although all vessels found in physiological systems are imbedded in other tissues, we will at first neglect the influence of external tethering. Furthermore we will assume, for now, that the vessel is being subjected to a uniform transmural pressure, which does not vary in either the circumferential or axial direction, and that the tube circumference remains of constant length despite changes in cross-sectional area. The tube wall will be treated as a homogenous, isotropic structure, the walls of which are subject to both tensile and bending stresses. The response of the tube to changes in transmural pressure has been treated by several investigators as Kresh and Noordergraaf (1972), Kresh (1979), Flaherty et al (1972), each using different analytical and numerical techniques. Here we follow Flaherty et al (1972) to write the structural equations for a small element of the tube wall at a circumferential position s (figure 4.3):

$$\begin{aligned}\sum F_n &= \frac{dN}{ds} - TK + P = 0 \\ \sum F_t &= \frac{dT}{ds} - NK = 0 \\ \sum M &= \frac{dM}{ds} + N = 0\end{aligned}\tag{4.1}$$

where $N(s)$ and $T(s)$ are dimensionless components of force in the outward normal and tangential directions, respectively, and $M(s)$ is the local dimensionless bending moment. s is the circumferential position and P is the dimensionless transmural pressure:

$$P = \frac{p - p_e}{K_p} \quad \text{with} \quad K_p = \frac{Eh^3}{12R^3(1 - \sigma^2)}$$

where h is the wall thickness, E is the Young's modulus, and σ is the Poisson ratio.

If we assume that the bending moment is proportional to the difference between the curvature of a circular tube and the actual curvature, and we call k the local curvature, we can reduce equations 4.1 to the following differential equation:

$$k'' + 1/2k^3 - (T + 1/2k^2)k^3 + P = 0 \quad (4.2)$$

The numerical solution of equation 4.2 was obtained in three different regimes:

- (1) Before the two opposing walls come into contact
- (2) When contact occurs at a single point (or line in a uniformly pressurised tube)
- (3) When a line of contact exists between the two opposing surfaces.

The resulting relationship between transmural pressure and cross-sectional area are given in figure 4.4 from Shapiro (1977b). Four different cross-sectional tube shapes can be seen from this figure:

- (a) In positive transmural pressure difference (inflated tube), the shape of the cross-section is circular, and the pressure difference is supported by hoop tension.
- (b) In the range of negative transmural pressure ($0.27 < \alpha < 1$ where $\alpha = A/A_0$), the tube is partially collapsed, and the pressure difference is supported by the bending stiffness of the tube wall.
- (c) When $0.21 < \alpha < 0.27$, a contact point occurs.
- (d) When $\alpha < 0.21$, a line contact occurs. The tube is in the form of two parallel conduits.

No reasonably simple analytic relation $P(\alpha)$ can fit the experimental data over the entire range $\alpha < 1$. Nevertheless, Flaherty et al (1972) proposed:

$$P = -\alpha^{-n} \quad (4.3)$$

where $n = 3/2$ for the thin-walled latex tube used in figure 4.4.

In order to match better the point $\alpha = 1$, Shapiro (1977b) proposed the following tube law:

$$P = 1 - \alpha^{-n} \quad \text{where } n = 3/2 \quad (4.4)$$

Physiological vessels (e.g. veins, arteries, the urethra, the trachea) are usually surrounded by or connected to large tissue masses, and they may not even be axisymmetric. The results presented above are valid for thin-walled elastic tubes, but can be expected to be only broadly indicative of the behaviour of physiological vessels. Nevertheless, simple mechanical considerations suggest that the tube law for physiological vessels conforms generally to the experimental curve of figure 4.4. Because of the difficulty in obtaining similar experimental measurements on physiological vessels, only qualitative and rough quantitative comparisons can be made. However, it seems highly likely that the phenomena later described may or do occur physiologically.

Thus far it has been assumed that both the tube law and the transmural pressure difference are uniform along the length of the tube. Physiologically and in laboratory model experiments as well, this is not always true. When longitudinal nonuniformities exist, the combination of a longitudinal tension, T per unit perimeter, in the tube wall, together with a curvature, $1/R_L$, in the longitudinal plane, produces a strong loading roughly equivalent to a transmural pressure difference with an order of magnitude of $-T/R_L$. If T/R_L is negligibly small compare to $p - p_e$, then the local tube law described above is essentially applicable at each longitudinal section x . But if T/R_L is not comparatively negligible, the local area and cross-section shape depend not only on the local transmural pressure difference and local tube properties (e.g. rest radius, wall thickness and modulus

of elasticity), but also on the shape of the tube and the longitudinal tethering along its entire length. McClurken et al (1981) go further by including the bending forces. Indeed, a more accurate pressure-area relation was developed. Focusing on the range where $0.3 < \alpha < 0.8$ (the shape of the tube is elliptic see figure 4.4), they postulate that the three stiffnesses (longitudinal tension and bending, and the circumferential bending) are separable and act additively to support the transmural pressure. The modified tube law is written as:

$$p - p_e = K_r P(\alpha) + \Delta P_t + \Delta P_b \quad (4.5)$$

Here ΔP_t and ΔP_b represent the stiffness of the tube against collapse due to the effects of axial tension and bending, respectively.

Circumferential bending. In the geometry of figure 4.5, the circumferential bending stiffness would be physically due to the forces required to bend the semicircular end regions to a new radius of curvature. However in applying the local tube law defined by Flaherty (equation 4.3), we make the assumption that the circumferential stiffness $P(\alpha)$ is the same as that determined for the actual tube under longitudinally uniform conditions.

Axial tension. An estimate of the tension stiffness ΔP_t considered as the transverse displacements of the straight segments of the wall is (McClurken et al, 1981):

$$\Delta P_t = -\frac{T}{R} \cong -\frac{T/D_o}{4} \left[\frac{1}{(1-\alpha)^{1/2}} \frac{\partial^2 \alpha}{\partial \xi^2} + \frac{1}{2(1-\alpha)^{3/2}} \left(\frac{\partial \alpha}{\partial \xi} \right)^2 \right] \quad (4.6)$$

where D_o is the diameter of the circle in figure 4.5, and $T = \varepsilon_x Eh$ is the axial force per unit perimeter resulting from the axial strain ε_x , R is the longitudinal radius of curvature defined as: $\frac{1}{R} = \frac{\partial^2 y}{\partial x^2}$, h is the wall thickness, E is the modulus of elasticity, $\xi \equiv x / D_o$ is the normalised longitudinal co-ordinate and y is expressed in terms of α .

Note:

- (a) It has been assumed for the above equation that $\partial y / \partial x$ is small.
- (b) The ratio of the second to the first term within the square brackets is very small in general. However, in elastic jumps (analogous to shock waves), the ratio is about unity, hence, except for when considering elastic jumps, we will neglect the second term within the square brackets to give:

$$\Delta P_i \equiv -\frac{T / D_o}{4} \left[\frac{1}{(1-\alpha)^{1/2}} \frac{\partial^2 \alpha}{\partial \xi^2} \right] \quad (4.7)$$

- (c) It can be seen from equation (4.7) that the estimate of the tension stiffness blows up when $\alpha \rightarrow 1$. This is not surprising since the geometry considered here is elliptical and the estimate of the tension stiffness is not valid anymore when it becomes circular, i.e. when α is close to unity.

- (d) Even though T is a function of axial distance because of skin friction forces, experimental results show that it can be taken as a constant.

Longitudinal bending. The stiffness against bending of the two parallel surfaces of figure 4.5 is given by:

$$\Delta P_b = EI \frac{\partial^4 y}{\partial x^4} = \frac{K_p}{32(1-\alpha)^{1/2}} \frac{\partial^4 \alpha}{\partial \xi^4} \quad (4.8)$$

where I is the second moment of area equal to $h^3 / [12(1-\nu^2)]$ and ν is the Poisson ratio.

As for the estimate of the axial tension, only the linear term is retained when y is expressed in terms of α . The four non-linear terms neglected are in fact small compared with the surviving linear term of equation 4.8, except in elastic jumps. And, as with the tension term, the model leading to equation 4.8 loses validity as $\alpha \rightarrow 1$.

From the above considerations and considering equation 4.5, we can write the modified tube law as:

$$\frac{p-p_c}{K_p} = P(\alpha) + \frac{1}{32(1-\alpha)^{1/2}} \frac{\partial^4 \alpha}{\partial \xi^4} - \frac{T/K_p D_o}{4(1-\alpha)^{1/2}} \frac{\partial^2 \alpha}{\partial \xi^2} \quad (4.9)$$

Evaluation of the modified tube law.

(a) The assumption that circumferential bending and longitudinal tension and bending act independently, and are thus additively superposable, is clearly incorrect for large deformations with compound curvature (e.g. a corrugated sheet is stiffer in bending than flat sheet). Because of the tube collapse, the circumferential curvature is normally very much larger than the longitudinal curvature. The effect of compound curvature is to increase the effective bending stiffness constant, K_p . This may be quite pronounced with respect to stiffness in longitudinal bending. Considering the two correction terms of the local tube law, the formulation for ΔP_b is therefore of much weaker validity than the formulation of ΔP_t .

(b) One aspect of the coupling between the different stiffnesses is that, owing to longitudinal tension, the effective transmural loading on the wall is variable around the perimeter, whereas the experimental function $P(\alpha)$ is necessarily measured with uniform transmural loading. The non-uniform loading produced by longitudinal tension in fact changes the shape of the cross-section and thus indirectly affects the function $P(\alpha)$.

(c) Perhaps the most difficult assumption to justify is that longitudinal bending and tension stresses, as modeled on the straight upper and lower surfaces, are representative of those acting on the entire perimeter. If we neglect axial bending forces over the axial tension forces (as the experiment of McClurken et al (1981) has confirmed) and we consider a local area minimum $\partial^2 \alpha / \partial \xi^2$ positive, we can see from equation 4.9 that tension acts like a decrease in external pressure and tends to pull the upper and lower walls of figure 4.5 further apart, thereby increasing the area. Over much of the side walls, however, tension pulls the surfaces inward, seeming to counteract the anticipated increase. There is no contradiction, however, since both displacements are consistent with an increase of area for a tube of fixed perimeter, i.e. both forces tend to produce a more rounded shape. Thus the net effect of tension on the entire perimeter is, with regard to cross-sectional area, at least consistent with the direction of change given by the model. Let us recall that the model is no longer valid when $\alpha \rightarrow 1$.

(d) Further complications arise when modeling unsteady flows. To account for unsteadiness in the tube law would require, in addition to those already included, wall inertia and viscoelasticity terms.

Although the modified tube law seems crude, it suffices for a qualitative correct determination of those physical events that are due to longitudinal tension and bending, particularly for small-amplitude, long-wavelength phenomena. Moreover, the numerical results of the modified tube law are in a good agreement with the experimental results performed by McClurken et al (1981).

Cowley (1982) developed a "tube law" for the case of a circular elastic tube, following the static balance equations derived by Flugge (1973). He separated two cases: a tethered and an untethered tube. In the case of a longitudinal tethered tube, he found that the tube law recovered in the form of a pressure-area relation independent of time, confirming the results of McClurken et al (1981) for a collapsed tube. However, in the case of untethered tube, a time-dependent tube law was recovered, even though the physical properties of the tube did not vary in time. He emphasised that there was no reason why the tube law should take the form of a pressure-area relation for unsteady deformations, such as those observed in the experiment of Conrad (1969). He suggested the use of the tube law directly from experiment rather than the predicted one, even for steady flow (for spatially slowly varying untethered collapsed tubes).

Several attempts to model a realistic tube law by including viscoelasticity, head loss, wall inertia and viscous effects were made by many investigators (Cancelli & Pedley, 1985; Bertram & Pedley, 1983 for instance). Even though the tube law model was not completely satisfactory, it elucidated other problems concerning collapsible flow such as flow separation, oscillations.

The author's point of view is that it is appropriate to use an analytic tube law to obtain crucial information about some flow phenomena.

For instance, for non-linear elastic behaviour, one should always separate the inflated tube (positive transmural pressure) from the collapsed tube (negative transmural pressure) as:

$$p - p_e = K_{r1}(\alpha^{n_1} - 1) \quad \text{for inflated tube}$$

$$p - p_e = K_{r2}(1 - \alpha^{-n_2}) \quad \text{for collapsed tube}$$

To avoid discontinuity in derivatives and difficulties in numerical calculations, Shapiro et al (1987) proposed:

$$P \equiv \frac{p - p_e}{K_p} = (\alpha^{n_1} - \alpha^{-n_2}) \quad (4.10)$$

Equation 4.10 should be used as a qualitative tool, and if some more accurate information are needed, it should always be compared with experimental results.

4.4 WAVE SPEED

The importance of the tube law comes from the fact that the velocity of long area waves are directly derived from it (Lightill 1975, chapter 12):

$$C = \left(\frac{\alpha}{\rho} \frac{dP}{d\alpha} \right)^{1/2} \quad (4.11)$$

Because of the non-linear behaviour of the tube law, the wave speed, as derived from experimental data using equation 4.11 can be seen to vary considerably as the tube collapses from a circular state (figure 4.6). The abrupt jump in C at a value of α of about 0.27 corresponds to walls of the tube coming into contact, with a consequent increase of the tube stiffness.

In the partially collapsed state, and assuming that the effects of circumferential bending and longitudinal tension could be superimposed for waves of small amplitudes, McClurken et al (1981) obtained the following dispersion relationship:

$$C^2 = C_\infty^2 + \frac{\pi^2 T D_o \bar{\alpha}}{\rho \lambda^2 (1 - \bar{\alpha})^{1/2}} + \frac{\pi^4 K_p D_o^4 \bar{\alpha}}{2 \rho \lambda^2 (1 - \bar{\alpha})^{1/2}} \quad (4.12)$$

where C_∞ is given by equation 4.11, T is the axial tension, $D_o = (A_o / \pi)^{1/2}$, λ is the wavelength and $\bar{\alpha}$ is the mean area ratio. Good agreement was obtained between the theory (when the third term on the right in equation 4.12 was neglected) and the experimental measurement (obtained from the precursor waves preceding stationary jumps, see section 4.5), as indicated in figure 4.7.

4.5 THE ELASTIC JUMP

Studies on the wave speed show that a compression wave can steepen and eventually create an elastic jump or a shock wave. We define an elastic jump as a big discontinuity propagating into a fluid through which the properties (pressure, velocity, cross-sectional area) change suddenly.

If a sub- to supercritical flow transition is possible, is it also possible to decelerate the flow from a super- to subcritical state? The theory draws no distinction between sub- to supercritical transitions and super- to subcritical transitions. Therefore we have no reason to believe that either is possible. Unlike transitions of the former type, however, experiments have not yet been able to demonstrate the existence of a smooth super- to subcritical transition. Instead, the flow tends to decelerate to subcritical speed by means of an elastic jump, across which the fluid properties undergo an abrupt change (over a

distance of several tube diameters) while the speed index goes from greater than one to less than one. The close analogy between an elastic jump and either a shock wave in gas-dynamic duct flow or a hydraulic jump in free surface flow can readily be seen.

Figure 4.8 depicts an elastic jump as it occurs in a collapsible latex tube suspended in water. We generally refer to the region of rapid area expansion (b to c) as the jump, although the train of waves seen standing upstream (a to b) originate at the jump and are closely associated with it.

The jump (b to c) has a length of from one to five tube diameters depending on its strength and the imposed longitudinal tension. As in the gas-dynamic shock, energy is dissipated by the elastic jump. This occurs by several mechanisms, including viscous dissipation and the release of energy in the form of a stationary wave train propagating upstream from the jump. These "precursor waves" appear to be stationary because their phase speed equals the local fluid velocity. They are able to propagate upstream because their group velocity exceeds the local flow speed.

Several analyses have appeared in the literature to predict the nature of the transition across the elastic jump (Shapiro, 1977b; Oates, 1975; Beam, 1968; Cowley, 1982). To model the jump realistically, however, proves to be an extremely difficult task owing to several complicating factors, including: (1) the essential coupling between the pressure distribution created by the flow and the geometry of the tube wall, (2) the importance of the three-dimensional aspects of the jump, and (3) the flow separation that occurs in the region of rapid area expansion. For all these reasons, an analysis must rely on various simplifying assumptions and can therefore be thought of as only approximate models of the true elastic jump. One of the most rigorous analysis is that of Cowley (1982), who has

examined two cases: (1) a jump with internal dissipation (associated, for instance, with turbulence) but negligible wall shear stress, and (2) a jump with no internal dissipation.

Let us consider the former case. Denoting the area, velocity and internal pressure by A , U , p , respectively, at the upstream (b) and downstream (c) locations, Cowley obtains, from conservation of mass and momentum:

$$A_b U_b = A_c U_c = Q \quad (4.13)$$

$$\rho A_b U_b^2 - \rho A_c U_c^2 = p_c A_c - p_b A_b + \int_{S_{b-c}} p \mathbf{n} \cdot \mathbf{z} dS \quad (4.14)$$

where S_{b-c} is the internal surface area between points b and c , and \mathbf{n} and \mathbf{z} are unit vectors normal to the tube wall and pointing in the axial direction respectively.

If one assumes that there exist points upstream and downstream of the shock at which the tube area is uniform, then the area and transmural pressure are uniquely related there by the tube law. Cowley goes on to show that if the external pressure is uniform and the shock is quasi-steady, then:

$$\int_{S_{b-c}} p \mathbf{n} \cdot \mathbf{z} dS = - \int_{A_b}^{A_c} P(A) dA \quad (4.15)$$

This expression is valid whether or not the tube law is strictly satisfied at all points along the tube. Combining equations 4.13 to 4.15, one obtains the following relationship between conditions upstream and downstream of the shock:

$$\Phi(A_b) = \Phi(A_c) \quad (4.16)$$

where

$$\Phi(A) = \frac{Q^2}{A} + \int_A \frac{A}{\rho} \frac{d(p - p_e)}{dA} dA \quad (4.17)$$

This is the same result obtained by Beam (1968) and Oates (1975), but Cowley's analysis is less restrictive in that it does not need to assume that the tube law is valid throughout the shock. Cowley does assume, however, that the tube wall has no curvature at points *b* and *c* (upstream and downstream the jump), and that wall shear stress is negligible within the control volume. These assumptions prove to be difficult to satisfy under typical experimental conditions and probably account for some differences between the theoretical predictions and the experimental results reported next.

Griffiths (1971, 1975) was probably the first to demonstrate experimentally the existence of a stationary elastic jump, although the lack of precise measurement capabilities prevented him from proving that the transition was indeed from a super- to subcritical flow state. Later experiments (Kececioglu et al, 1981; McClurken et al, 1981; Elliott and Dawson, 1979) were able to demonstrate clearly the existence of the jump and to characterize it in terms of upstream and downstream conditions. McClurken et al (1981) were able to determine the flow velocity, cross-sectional area and pressure upstream and downstream of the shock and compared their measurements with several theoretical predictions. They found that the dimensionless pressure recovery coefficient generally fell between the two limiting curves of a jump free of viscous dissipation and of one with total loss of dynamic head in the jump (figure 4.9). In those jumps for which the pressure recovery fell below the lower curve (generally for very long jumps), it was thought that wall shear stress played a dominant role. The analysis of Oates (and also of Cowley) represented an improvement over either of these extreme cases, but still failed to yield a good prediction.

The lack of close agreement between theory and experiment can probably be attributed to the two assumptions identified above. For very long shocks, wall shear stress clearly plays an important role, causing the pressure recovery to fall below the prediction based on a total loss of kinetic energy. For shorter shocks, it is not possible to identify a point just upstream of the shock where the wall curvature is zero or insignificant as required by Cowley. Therefore the neglect of the effects of tension at point *b* and *c* is often not justified.

McClurken et al (1981) also predicted the length of the jump by using the simple notion that the jump was merely the first wave in the train of waves propagating upstream. A predication of wavelength including the effects of longitudinal tension is in reasonably good agreement with the measured lengths of the jump.

We have discussed some features of collapsible tubes. In the following chapters, we will adapt this collapsible tube theory to the spinal system. We will also discuss a few interesting features developed in this chapter.

CHAPTER 5

PRESSURE WAVE PROPAGATION IN A COAXIAL TUBES MODEL

5.1 INTRODUCTION

Many years ago, Williams (1976; see also section 2.6.4) carried out pressure measurements of the CSF in the lumbar and cisternal (top of the neck) regions of human subjects during and following coughing. Both normal subjects and those suffering from syringomyelia were studied. The most striking outcome of the study is the fact that for normal subjects the shape of the pressure signals obtained at the two locations did not differ greatly, whereas with syringomyelia the cisternal pressure is extremely weak and attenuated compared with the lumbar one (see figures 2.27 and 2.28). This suggests that the pressure propagation process is almost nondispersive (in the sense that the pressure amplitude is roughly conserved at both locations). In other words, it is similar to sound propagation or, more particular, to the propagation of longitudinal waves in elastic tubes and channels (see Lighthill, 1978). That is the reason why we developed a wave propagation model for the spinal CSF system.

The research done in the domain of wave propagation typically either concerns a single stiff tube (e.g. metal pipe) or a single elastic tube (collapsible tube). The definition of the wave speed is the same in both cases, but an additional tube law equation (pressure-area relation) is needed in the case of an elastic tube in order to fully describe the behaviour of

the elastic wall. However, our case is a mix of these two theories, since it consists of coaxial tubes where the outer tube is stiff and the inner is elastic (figure 5.1).

5.2 COAXIAL TUBES MODEL

5.2.1 Assumptions of the model

The spinal CSF is modeled crudely as rigid-walled channel of constant cross-section which is divided into two unequal parts by a longitudinal flexible diaphragm (see figure 5.1a). The diaphragm represents the spinal cord. The upper (*A*) and lower (*B*) parts of the channel represent respectively the subarachnoid space and the central canal. The cross-sectional area of *B* is very much smaller than *A*. It should be noted that in healthy adult humans the spinal central canal is barely 100 μm wide. Mathematically this arrangement is equivalent to concentric annular channels separated by an annular diaphragm (see figure 5.1b).

The assumptions of the model are the following:

- (1) The CSF is inviscid and we ignore other possible sources of resistance to flow in the spinal subarachnoid space. In fact, the viscosity of CSF is similar to that of water and the subarachnoid space contains structures, such as trabeculae, which create a certain amount of resistance to flow.
- (2) The flow is 'stationary' (i.e. there is no mean flow). Indeed, the CSF is fully replaced about 7 times every 24 hours. This corresponds to a maximum undisturbed flow speed in the spinal system no more than 0.1 mm/s which is minute compared with the wave speed

(about 5 m/s, from Williams' pressure records, 1976). However, the analysis will be modified into the next chapters to take into account a steady flow speed.

(3) That the tube law (pressure-area relation) is linear.

(4) The effects of wall inertia are negligible.

(5) The diaphragm is non porous.

(6) The problem is one-dimensional.

5.2.2 Governing equations

The theory of longitudinal waves is based on the concept that variation of excess pressure P_e is negligible over a cross section: $P_e = P - P_o$, where P_o is the undisturbed pressure including the hydrostatic component, so it is the excess pressure which produces fluid acceleration (Lighthill, 1978). The motions produced by longitudinal gradients of P_e can be large compared with those forced by transverse gradients only if P_e varies negligibly over each cross-section. Considering the flow as one-dimensional, incompressible and inviscid, Lighthill (1978) showed that the wave speed in a single elastic tube was defined as (when the convective terms are neglected):

$$\frac{1}{C^2} = \rho \left(\frac{1}{\rho} \frac{d\rho}{dP_e} + \frac{1}{A_o} \frac{dA}{dP_e} \right)_{P_e=0} = \rho(K + D) \quad (5.1)$$

where C is the wave speed, A is the cross-sectional area and ρ is the density. A_o is the cross-sectional area in the undisturbed conditions.

$K = \left(\frac{1}{\rho} \frac{d\rho}{dP_e} \right)_{P_e=0}$ is called the compressibility, and $D = \left(\frac{1}{A_o} \frac{dA}{dP_e} \right)_{P_e=0}$ is the distensibility.

The sum $(K+D)$ is the effective compressibility of the fluid.

However, since we treat the problem of water in a thin-walled flexible tube, we can neglect the effects of compressibility, and the variations of the wave speeds will only be due to distensibility D . We can thus write the definition of the wave speed in a elastic tube as:

$$\frac{1}{C^2} = \frac{\rho}{A_0} \left. \frac{dA}{dP} \right|_{P_0=0} \quad (5.2)$$

Equation (5.2) is the speed at which waves propagate along a single flexible tube filled with water, provided that the compressibility of water is neglected.

Coaxial tubes

Adapting the theory to the coaxial tube model defined in section 5.2.1, we can write:

$$\text{Continuity equation in chamber A: } \frac{\partial A_A}{\partial t} + \frac{\partial(A_A U_A)}{\partial x} = 0 \quad (5.3)$$

$$\text{Continuity equation in chamber B: } \frac{\partial A_B}{\partial t} + \frac{\partial(A_B U_B)}{\partial x} = 0 \quad (5.4)$$

where $A_{A,B}$ and $U_{A,B}$ are respectively the cross-sectional areas and the fluid velocities in chamber A or B and ρ is the fluid density.

$$\text{Momentum equation in chamber A: } A_A \frac{\partial P_A}{\partial x} + \rho \frac{\partial(A_A U_A)}{\partial t} + \rho \frac{\partial(A_A U_A^2)}{\partial t} = 0$$

$$\text{Momentum equation in chamber B: } A_B \frac{\partial P_B}{\partial x} + \rho \frac{\partial(A_B U_B)}{\partial t} + \rho \frac{\partial(A_B U_B^2)}{\partial t} = 0$$

where $P_{A,B}$ is the fluid pressure in channel A and B.

We neglect the convective terms (the third term in the left hand side) in the momentum equations:

$$A_A \frac{\partial P_A}{\partial x} + \rho \frac{\partial(A_A U_A)}{\partial t} = 0 \quad (5.5)$$

$$A_B \frac{\partial P_B}{\partial x} + \rho \frac{\partial(A_B U_B)}{\partial t} = 0 \quad (5.6)$$

Equations 5.3 to 5.6 are the governing equations of our system.

If we linearize around A_{Ao} the above equations (A_{Ao} is the outer cross-sectional area at equilibrium), the driving equations become:

$$\text{Continuity in the outer channel A: } \frac{\partial A_A}{\partial t} = -A_{Ao} \frac{\partial U_A}{\partial x} \quad (5.7)$$

$$\text{Continuity in the inner channel B: } \frac{\partial(A_T - A_A)}{\partial t} = -(A_T - A_{Ao}) \frac{\partial U_B}{\partial x} \quad (5.8)$$

$$\text{Momentum in the outer channel A: } \rho \frac{\partial U_A}{\partial t} = -\frac{\partial P_A}{\partial x} \quad (5.9)$$

$$\text{Momentum in the inner channel B: } \rho \frac{\partial U_B}{\partial t} = -\frac{\partial P_B}{\partial x} \quad (5.10)$$

where the subscripts A, B respectively denote quantities in the outer and inner chamber.

$A_T = A_A + A_B$ is the total cross-sectional area and is taken constant in the first place.

Equations 5.3 to 5.6 are the governing equations for the general case whereas equations 5.7 to 5.10 are the governing equations for the linear case.

5.3 WAVE SPEED DEFINITION

5.3.1 Linear case

We differentiate with respect to t the continuity equations 5.7 and 5.8, respectively:

$$\frac{\partial^2 U_A}{\partial x \partial t} = -\frac{\partial}{\partial t} \left(\frac{1}{A_{Ao}} \frac{\partial A_A}{\partial t} \right) = -\frac{1}{A_{Ao}} \frac{\partial^2 A_A}{\partial t^2}$$

$$\frac{\partial^2 U_B}{\partial x \partial t} = -\frac{\partial}{\partial t} \left(\frac{1}{(A_T - A_{Ao})} \frac{\partial(A_T - A_A)}{\partial t} \right) = -\frac{1}{(A_T - A_{Ao})} \frac{\partial^2(A_T - A_A)}{\partial t^2}$$

We differentiate with respect to x the momentum equations 5.9 and 5.10, respectively:

$$\frac{\partial^2 U_A}{\partial t \partial x} = -\frac{1}{\rho} \frac{\partial}{\partial x} \left(\frac{\partial P_A}{\partial x} \right) = -\frac{1}{\rho} \frac{\partial^2 P_A}{\partial x^2}$$

$$\frac{\partial^2 U_B}{\partial t \partial x} = -\frac{1}{\rho} \frac{\partial}{\partial x} \left(\frac{\partial P_B}{\partial x} \right) = -\frac{1}{\rho} \frac{\partial^2 P_B}{\partial x^2}$$

Assuming that U_A and U_B are continuously differentiable, we can write:

$$\frac{\partial^2 U_{A,B}}{\partial t \partial x} = \frac{\partial^2 U_{A,B}}{\partial x \partial t}$$

and thus we can deduce that:
$$\frac{\partial^2 P_A}{\partial x^2} = \frac{\rho}{A_{Ao}} \frac{\partial^2 A_A}{\partial t^2}$$

Noting that A_T is not a function of time, we similarly obtain:

$$\frac{\partial^2 P_B}{\partial x^2} = -\frac{\rho}{(A_T - A_{Ao})} \frac{\partial^2 A_A}{\partial t^2}$$

We take A_A as a function of ΔP ($\Delta P = P_A - P_B$) only, we can therefore write:

$$\frac{\partial^2 A_A}{\partial t^2} = \left(\frac{dA_A}{d\Delta P} \Big|_{\Delta P=0} \right) \frac{\partial^2 \Delta P}{\partial t^2}$$

We can finally write that:

$$\frac{\partial^2 \Delta P}{\partial x^2} = \left(\rho \left(\frac{1}{A_{Ao}} + \frac{1}{A_T - A_{Ao}} \right) \frac{dA_A}{d\Delta P} \Big|_{\Delta P=0} \right) \frac{\partial^2 \Delta P}{\partial t^2} \quad (5.11)$$

Equation 5.11 expresses the fact that small amplitude disturbances can propagate along the channel in either direction at speed C_o defined as follow:

$$\frac{1}{C_o^2} = \frac{\rho A_T}{A_{Ao} (A_T - A_{Ao})} \frac{dA_A}{d\Delta P} \Big|_{\Delta P=0} \quad (5.12)$$

The general solution of equation (5.11) is well known:

$$\Delta P = f(x - C_o t) + g(x + C_o t) \quad (5.13)$$

where f and g are arbitrary functions.

Note that from the two continuity equations 5.7 and 5.8, we can link fluid velocities in both tubes with the relation:

$$-\alpha_o \frac{\partial U_A}{\partial x} = (1 - \alpha_o) \frac{\partial U_B}{\partial x} \quad (5.14)$$

where $\alpha_o = A_{Ao} / A_T$.

We have now determined the wave speed in our coaxial tubes model for the linear case.

5.3.2 Non-linear case

We differentiate equation 5.3 with respect to x and equation 5.5 with respect to t .

Assuming that the product function $(A_A U_A)$ is continuously differentiable, we readily obtain:

$$\frac{\partial^2 P_A}{\partial x^2} = \frac{\rho}{A_A} \frac{\partial^2 A_A}{\partial t^2} - \frac{1}{A_A} \left(\frac{\partial A_A}{\partial x} \right) \left(\frac{\partial P_A}{\partial x} \right)$$

We manipulate in the same way the continuity and momentum equations for chamber B , recalling that $A_B = A_T - A_A$:

$$\frac{\partial^2 P_B}{\partial x^2} = \frac{\rho}{A_T - A_A} \frac{\partial^2 (A_T - A_A)}{\partial t^2} - \frac{1}{A_T - A_A} \left(\frac{\partial (A_T - A_A)}{\partial x} \right) \left(\frac{\partial P_B}{\partial x} \right)$$

From the last two equations, we can write (recalling that $\Delta P = P_A - P_B$):

$$\begin{aligned} \frac{\partial^2 \Delta P}{\partial x^2} = \frac{\partial^2 (P_A - P_B)}{\partial x^2} &= \left(\frac{\rho}{A_A} + \frac{\rho}{A_T - A_A} \right) \frac{\partial^2 A_A}{\partial t^2} - \left(\frac{A_T}{A_A (A_T - A_A)} \right) \frac{\partial A_A}{\partial x} \frac{\partial P_A}{\partial x} + \\ &\quad \frac{1}{A_T - A_A} \left(\frac{\partial A_A}{\partial x} \frac{\partial \Delta P}{\partial x} - \frac{\partial^2 A_T}{\partial t^2} + \frac{\partial A_T}{\partial x} \frac{\partial P_B}{\partial x} \right) \end{aligned}$$

We take the cross-sectional area A_A as a function of the pressure difference ΔP only, we therefore have:

$$\frac{\partial^2 A_A}{\partial t^2} = \frac{dA_A}{d\Delta P} \frac{\partial^2 \Delta P}{\partial t^2} \quad \text{and} \quad \frac{\partial^2 A_A}{\partial x^2} = \frac{dA_A}{d\Delta P} \frac{\partial^2 \Delta P}{\partial x^2}$$

With this consideration we can write that:

$$\begin{aligned} \frac{\partial^2 \Delta P}{\partial x^2} = \frac{\partial^2 (P_A - P_B)}{\partial x^2} = & \left(\frac{\rho}{A_A} + \frac{\rho}{A_T - A_A} \right) \frac{dA_A}{d\Delta P} \frac{\partial^2 \Delta P}{\partial t^2} - \left(\frac{A_T}{A_A(A_T - A_A)} \right) \frac{dA_A}{d\Delta P} \frac{\partial \Delta P}{\partial x} \frac{\partial P_A}{\partial x} + \\ & \frac{1}{A_T - A_A} \left(\frac{dA_A}{d\Delta P} \left(\frac{\partial \Delta P}{\partial x} \right)^2 - \frac{\partial^2 A_T}{\partial t^2} + \frac{\partial A_T}{\partial x} \frac{\partial P_B}{\partial x} \right) \end{aligned}$$

We consider propagation of small perturbations in ΔP . With $\Delta P = P_A - P_B$, we can consider that $\Delta P, P_A, P_B$ are of the same order so that we can neglect the product of two of these quantities. Therefore we obtain:

$$\frac{\partial^2 \Delta P}{\partial x^2} = \left(\frac{\rho}{A_A} + \frac{\rho}{A_T - A_A} \right) \frac{dA_A}{d\Delta P} \frac{\partial^2 \Delta P}{\partial t^2} + \frac{1}{A_T - A_A} \left(-\frac{\partial^2 A_T}{\partial t^2} + \frac{\partial A_T}{\partial x} \frac{\partial P_B}{\partial x} \right)$$

We assume that the total cross-sectional area is constant so that we can write:

$$\frac{\partial^2 \Delta P}{\partial x^2} = \left(\frac{\rho}{A_A} + \frac{\rho}{A_T - A_A} \right) \frac{dA_A}{d\Delta P} \frac{\partial^2 \Delta P}{\partial t^2} \quad (5.15)$$

Therefore, we can deduce the square of the wave speed in our model:

$$C^2 = \frac{1}{\rho \left(\frac{1}{A_A} + \frac{1}{A_T - A_A} \right) \frac{dA_A}{d\Delta P}} = \frac{A_A(A_T - A_A)}{\rho A_T \frac{dA_A}{d\Delta P}} \quad (5.16)$$

Lighthill (1978) has defined the distensibility in the theory for wave propagation in (single) elastic tubes in the linear case as (see section 5.2.2):

$$D = \frac{1}{A_0} \left. \frac{dA}{dP_e} \right|_{P_e=0}$$

By analogy we define the distensibility in our model as:

$$D = \frac{1}{A_r} \frac{dA_A}{d\Delta P} \quad (5.17)$$

If we insert the above distensibility definition into equation 5.16, we can write that the wave speed in the coaxial tube model is:

$$C = \sqrt{\frac{\alpha(1-\alpha)}{\rho D}} \quad (5.18)$$

where $\alpha = A_A / A_r$.

5.4 TUBE LAW (PRESSURE-AREA RELATION)

We have shown in the previous section and in chapter 4 (section 4.3), the importance of a tube law (pressure-area relation). It will provide us with the extra equation required in order to solve the problem. We will use a simple linear relation in order to develop a simple analysis for the small perturbation theory. We also cite two other tube laws (from the literature) for improvement of the theoretical model. These tube laws take the following forms:

$$(a) \quad \alpha = \alpha_o + D\Delta P \quad (5.19)$$

where $D = \frac{1}{A_r} \frac{dA_A}{d\Delta P}$ is the distensibility defined in section 5.3 (taken as constant) and

where $\Delta P = P_A - P_B$ is the pressure difference. Let us recall that $\alpha_o = A_{Ao} / A_r$.

$$(b) \quad P_A - P_B = K_p \frac{\alpha}{\alpha_o} \quad (\text{from Shapiro, 1977b}) \quad (5.20)$$

where $K_p \approx E(h/R)^3$, and E represents the elastic modulus, h is the wall thickness, R is the curvature radius of the elastic tube.

$$(c) \quad P_A - P_B = K \frac{(\alpha^2 - 1)}{\alpha} \quad (\text{from Oates, 1975}) \quad (5.21)$$

where $K \approx E(h / R)$.

In the next sections, we will only consider the tube law defined by equation (5.19).

5.5 ELASTIC JUMP PHENOMENON

5.5.1 Variations of the wave speed

The wave speed defined in equation 5.18 can be written as:

$$\frac{1}{C^2} = \frac{\rho D}{\alpha(1 - \alpha)} \quad (5.22)$$

where D is the distensibility defined in equation 5.17. It can be regarded as a known property of the system. In general it would be a function of ΔP . Another way to look at it is to consider equation 5.19:

$$\frac{A_A}{A_r} = \alpha = \alpha_o + D\Delta P \quad (5.23)$$

Here, we will assume that D is constant. The assumption that changes in cross-sectional area depend purely on local pressure difference implicitly ignores the effects of the diaphragm's inertia. This is acceptable for blood vessels since they are relatively thin. The spinal cord is plainly not a thin-walled tube so inertia effects could be more important in the present case. However, in order to depict the main parameters of our system, we need to make it simple. One can choose a more suitable distensibility by considering a more complex tube law (pressure-area relation).

For computational purposes, we need to estimate the value of the distensibility D . This can be done by recalling that we have evaluated the wave speed from Williams' data (1976). We found a value of 5 m/s. If we take $\alpha = 0.8$ and $\rho = 1000$ (density of water), we can obtain an estimate of the distensibility from equation 5.22:

$$D = \frac{\alpha(1-\alpha)}{\rho C^2} \approx 6.4 \cdot 10^{-6} (\text{Pa})^{-1}$$

Since we take D and ρ as constant, we consider that the variations of the wave speed are only due to the changes of the cross-sectional area A_A (or A_B).

In the next three sections, we consider a change in the outer cross-sectional area A_A , in different configurations: A_T is constant, gradually increasing or decreasing.

5.5.2 Non-linear effects on the wave speed: constant total cross-sectional area

Let us now discuss the variation of the wave speed with the cross-sectional area (since all the other quantities in equation 5.22 are taken as constant) for the case of a constant total cross-sectional area A_T .

It can be seen from equation 5.22 and figure 5.2 that small changes in α can lead to substantial change in wave speed, especially when $\alpha \rightarrow 1$.

We can thus determine the qualitative non-linear effects on the wave speed. Figure 5.2 depicts the variation of the wave speed with respect to the cross-sectional area. It shows that depending on whether α is superior or inferior to 0.5, an increase in the inner cross-sectional area will either increase or decrease the wave speed. That implies that either the wave is expansive in character (i.e. the leading edge of the wave is faster than the tailing

edge) or an elastic jump is created (the tailing edge of the wave is faster than the leading edge and tends to catch up the front wave).

Let us take an example to illustrate the above statement. Figure 5.3a depicts the propagation to the right of a pressure wave through which an increase of the outer tube cross-sectional area occurs. Figure 5.3b shows the variation of the outer tube cross-sectional area in that case.

At $x = x_0$, we have $\alpha = \alpha_0 > 0.5$, and $C = C_0$.

At $x = x_1$, we have $\alpha = \alpha_1 > \alpha_0$ which implies that $C_0 > C_1$ from figure 5.3d. Thus, in the (x,t) diagram of figure 5.3c (plain lines), the slope of the corresponding wave is such that

$\frac{1}{C_0} < \frac{1}{C_1}$. This implies that the wave at $x = x_0$ is propagating faster than the one at $x = x_1$,

so that an expansion wave develops.

If we use the same reasoning for the case $\alpha_0 < 0.5$, we can see in figure 5.3c (dashed lines) that the waves converge. They will ultimately join together to form an elastic jump or shock-like wave through which a discontinuity in the fluid properties occurs. So, depending on whether or not α_0 is superior to 0.5, we either have an expansion or an elastic jump.

If we now consider a decrease in the outer channel cross-sectional area A_A , we can develop the same kind of theory and reach the conclusion that an expansion wave develops when $\alpha_0 < 0.5$, whereas an elastic jump is created when $\alpha_0 > 0.5$.

Since we will focus our attention on the case where α_0 is greater than 0.5, let us emphasize that an expansion wave develops if the outer channel cross-sectional area

increases (i.e. $\Delta P_1 = P_{A1} - P_{B1} > 0$ with $\Delta P_0 = 0$), whereas an elastic jump is created if the outer channel cross-sectional area decreases ($\Delta P_1 < 0$).

In these cases, we have considered the total cross-sectional area A_T as constant. In the next section, we focus on the case where A_T can vary along the length of the tube.

5.5.3 Non-linear effects on the wave speed: gradual changes in the total cross-sectional area

In the next two cases, we will analyse the effects of the variation of the total cross-sectional area A_T . Following the same method, and only considering small variations of A_T with x , we will analyse the possibility of formation of elastic jump.

5.5.3.1 Increase of the total cross-sectional area

We assume that the variations in A_T are so small that it does not affect the shape of the graph plotted in figure 5.2. We can proceed in the same way as we did in the case of a constant total cross-sectional area. The main change is that an increase in A_B (see figure 5.4) does not necessarily imply a decrease in A_A as in the previous case. Indeed an increase or decrease in A_A will depend on whether or not the increase of the total cross-sectional area A_T compensates the increase in A_B . That is the reason why we will consider both situations (i.e. an increase and a decrease in A_A).

Let us consider an increase in A_B as it is shown in figure 5.4. We call A_{A1} , the case where A_A decreases (similar to the previous case where A_T is constant), and A_{A11} the case where A_A increases (see figure 5.5).

If we take the case $\alpha_o > 0.5$ and consider figure 5.6, we can deduce that depending on whether we deal with case A_{A1} or A_{A11} , we respectively have an elastic jump or an expansion.

If we now consider the case where $\alpha_o < 0.5$ and we keep the same notation, we obtain opposite results. Indeed we have an expansion wave for the A_{A1} case, and an elastic jump for the A_{A11} case.

We now consider a decrease in A_B . In this case, the effect of an increase in A_r is an intensification of the phenomenon seen in the section 5.5.2. Indeed, as A_r increases and A_B decreases, A_A will be even bigger than the case where A_r is constant, and so the elastic jump will be created more readily, and the expansion will also expand more rapidly. In fact an increase in A_r just emphasises the phenomenon.

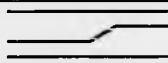

5.5.3.2 Decrease of the total cross-sectional area

We could apply exactly the same reasoning and we would find similar results.

Instead, we will summarize all the results, including those found for a decrease of the total cross-sectional area in the next section.



5.6 SUMMARY OF THE NON-LINEAR EFFECTS ON THE WAVE SPEED

* Case where A_T is constant



A_T is constant	$\alpha_o < 0.5$	$\alpha_o > 0.5$	Model sketch
A_B decreases	Shock	Expansion	
A_B increases	Expansion	Shock	

Note that the "model sketch" column in the above table represents one half of the longitudinal cross-section.

* Case where A_T increases.

A_T increases	$\alpha_o < 0.5$	$\alpha_o > 0.5$	Model sketch
A_B decreases	Shock (intensified)	Expansion (intensified)	
A_B increases	A_A increases: shock A_A decreases: expansion	A_A increases: expansion A_A decreases: shock	

* Case where A_T decreases.

A_T decreases	$\alpha_o < 0.5$	$\alpha_o > 0.5$	Model sketch
A_B decreases	A_A increases: shock A_A decreases: expansion	A_A increases: expansion A_A decreases: shock	
A_B increases	Expansion (intensified)	Shock (intensified)	

CHAPTER 6

SOLVING THE EQUATIONS

6.1 INTRODUCTION

The governing equations of the coaxial tube model have been derived in chapter 5. In this chapter, we will solve these equations. A *direct method* is developed in the first part of this chapter in order to understand the type of solution we are dealing with. Some examples will be given to explain some possible phenomena occurring in the model, especially when a blockage is placed in the outer channel. However, the disadvantage of this method is that we impose certain wave properties, such as the velocity or the pressure. Moreover, we will not be able to solve the full non-linear problem using the *direct method*. We will then opt for another technique to solve these non-linear equations namely, the method of characteristics. Therefore we will derive the characteristic lines and compatibility equations for the linear and non-linear cases. We will end this chapter by applying the method of characteristics to some particular examples.

6.2 DIRECT METHOD (LINEAR CASE)

6.2.1 Type of solution

We take a combination of the continuity and momentum equations (equations 5.7 and 5.9) to obtain the following relation:

$$\frac{\partial^2 P_A}{\partial x^2} = \frac{(1 - \alpha_a)}{C_o^2} \frac{\partial^2 \Delta P}{\partial t^2}$$

We do the same for the inner channel B (using equations 5.8 and 5.10) to obtain:

$$\frac{\partial^2 P_B}{\partial x^2} = \frac{-\alpha_o}{C_o^2} \frac{\partial^2 \Delta P}{\partial t^2}$$

We integrate these two equations twice with respect to x to obtain:

$$P_A = (1 - \alpha_o) \Delta P + \Phi_1(t)x + \Phi_2(t) \quad (6.1)$$

$$P_B = -\alpha_o \Delta P + \Phi_1(t)x + \Phi_2(t) \quad (6.2)$$

where $\Phi_{1,2}$ are some functions of integration which satisfy boundary conditions.

From the momentum equations in each tube, we can deduce the velocities of the fluid in both tubes:

$$U_A = \frac{\alpha_o - 1}{\rho C_o} (g(x - C_o t) - f(x + C_o t)) + \Psi_1(x) - \frac{1}{\rho} \int \Phi_1(t) dt \quad (6.3)$$

$$U_B = \frac{\alpha_o}{\rho C_o} (g(x - C_o t) - f(x + C_o t)) + \Psi_2(x) - \frac{1}{\rho} \int \Phi_1(t) dt \quad (6.4)$$

where $\Psi_{1,2}$ are some functions of integration which satisfy boundary conditions.

We have just shown that if the form of ΔP is known, one can deduce P_A, P_B, U_A, U_B .

In the next section, we give some examples of the use of the direct method.

6.2.2 Examples

6.2.2.1 Piston in simple harmonic motion (see figure 6.1)

We consider a piston driving the fluid in the outer channel only, and we analyse the propagation of disturbances in both channels, especially when they encounter a blockage in the upper chamber (A). We pay particular attention to the variations of the pressure difference ΔP .

Boundary conditions: at $x = 0$, $U_A = \bar{u}_o e^{i\omega t}$ and $U_B = 0$ (6.5)

with $\omega = \lambda C_o$ where ω is the period and λ is the wave length of the disturbance.

at $x = L$, $U_A = 0$ and $P_B = 0$

The boundary condition for P_B at $x = L$ is arguable. However if we consider that the cross-sectional area does not change at the blockage, the pressure should not vary there.

Let us consider that the function solution takes the following form:

$$\Delta P = f(x - C_o t) + g(x + C_o t) = C_1 e^{-i\lambda(x - C_o t)} + C_2 e^{i\lambda(x + C_o t)} \quad (6.6)$$

From the boundary conditions and the above equation, we can determine Φ_1, C_1, C_2 for

ΔP , and Φ_2 if P_A, P_B are required.

At $x = 0$:

We consider the momentum equation (5.9) and the boundary condition noted as equation 6.5:

$$\frac{\partial P_A}{\partial x} = -\rho \frac{\partial U_A}{\partial t} = -\rho(i\omega) \bar{u}_o e^{i\omega t}$$

From equation 6.1 and the boundary condition 6.5, we can deduce:

$$\frac{\partial P_A}{\partial x} = (1 - \alpha_o) \left. \frac{\partial \Delta P}{\partial x} \right|_{x=0} + \Phi_1(t) = -\rho i \omega \bar{u}_o e^{i\omega t}$$

In the same way, from equation 6.2 and the boundary condition $U_B = 0$ at $x = 0$:

$$\frac{\partial P_B}{\partial x} = -\alpha_o \left. \frac{\partial \Delta P}{\partial x} \right|_{x=0} + \Phi_1(t) = 0$$

We subtract these 2 equations in order to eliminate Φ_1 :

$$\left. \frac{\partial \Delta P}{\partial x} \right|_{x=0} = -\rho(i\omega) \bar{u}_o e^{i\omega t}$$

So that we can write that: $\Phi_1 = -\rho\alpha_o(i\omega)\bar{u}_o e^{i\omega x}$

We insert Φ_1 in equation 6.3, considering equation 6.6, the boundary condition 6.5 becomes:

$$U_A = \frac{\alpha_o - 1}{\rho C_o} (-C_1 e^{i\omega x} + C_2 e^{i\omega x}) + \alpha_o \bar{u}_o e^{i\omega x} = \bar{u}_o e^{i\omega x}$$

Note that we have set $\Psi_1(0) = 0$.

We now multiply this equation by $\frac{\rho C_o}{\alpha_o - 1} e^{-i\omega x}$ (considering that $\alpha_o \neq 1$ i.e. $A_{Ao} \neq A_T$) to

obtain:

$$(-C_1 + C_2) = -\rho C_o \bar{u}_o \quad (6.7)$$

At x = L: Boundary conditions are $U_A = 0$ and $P_B = 0$

Let us consider the first boundary condition:

$$U_A = \frac{\alpha_o - 1}{\rho C_o} (-C_1 e^{-i\omega L} e^{i\omega x} + C_2 e^{i\omega L} e^{i\omega x}) + \alpha_o \bar{u}_o e^{i\omega x} = 0$$

that we can simplify into:

$$(-C_1 e^{-i\omega L} + C_2 e^{i\omega L}) = -\frac{\alpha_o \rho C_o}{\alpha_o - 1} \bar{u}_o$$

Considering equations 6.7 and the above equation, we have two equations and two unknowns C_1 and C_2 . We can thus readily obtain:

$$C_1 = -\rho C_o \bar{u}_o \frac{1 + \frac{\alpha_o}{\alpha_o - 1} e^{-i\omega L}}{1 - e^{-2i\omega L}} \quad (6.8)$$

$$C_2 = -\rho C_o \bar{u}_o \frac{1 + \frac{\alpha_o}{\alpha_o - 1} e^{-i\omega L}}{1 - e^{-2i\omega L}} - \rho C_o \bar{u}_o$$

We have now found the expression of ΔP , but in order to find the other unknowns, we need to obtain Φ_2 . Evidently Φ_2 takes the following form: $\Phi_2(t) = C_3 e^{i\alpha t}$ where C_3 satisfies the boundary condition at $x = L$:

$$P_B = -\alpha_o (C_1 e^{-i\lambda(L-ct)} + C_2 e^{i\lambda(L+ct)}) - i\omega \alpha_o \rho L \bar{u}_o e^{i\alpha t} + C_3 e^{i\alpha t} = 0$$

whence we can deduce

$$C_3 = \rho C_o \alpha_o \bar{u}_o \left\{ -\frac{1 + \frac{\alpha_o e^{-i\lambda L}}{1 - \alpha_o}}{1 - e^{-2i\lambda L}} (e^{-i\lambda L} + e^{i\lambda L}) + e^{i\alpha L} + i\lambda L \right\}$$

In our case, we are interested in the pressure difference:

$$\Delta P = -\rho C_o \bar{u}_o \frac{1 + \frac{\alpha_o e^{-i\lambda L}}{1 - \alpha_o}}{1 - e^{-2i\lambda L}} \left\{ e^{-i\lambda(x-C_d)} + e^{i\lambda(x+C_d)} \right\} + \rho C_o \bar{u}_o e^{i\lambda(x+C_d)} \quad (6.9)$$

Notes:

- (1) The expression between brackets represents a standing wave.
- (2) If $2i\lambda L = 2n\pi$, i.e. $\lambda = n\pi / L$ ($n = 0, 1, 2 \dots$), the standing wave is greatly amplified: this can be thought of as *resonance*.
- (3) Note that when $\alpha_o \rightarrow 1$ (where $\alpha_o = A_{Ao} / A_T$), the standing wave is greatly amplified at any wave length λ .

6.2.2.2 Other case: with compliance, resistance (see figure 6.2)

In this case, we have the same boundary conditions at $x = 0$, and we add a new compartment C in order to model the compliance. Compliance is a quantity which relates pressure and volume.

$$\text{Compliance:} \quad \tilde{C} = \frac{dP_c}{dV_c} = \frac{dP_c/dt}{dV_c/dt} = \frac{dP_c/dt}{U_B A_B} \quad (6.10)$$

where V denotes the volume.

The amount of fluid passing from compartment B to compartment C can be described in the following way:

$$U_B A_B = \frac{P_B - P_c}{R_c} \quad (6.11)$$

where R_c is a resistance the value of which would need to be specified.

We can write this equation in a different way: $P_c = P_B - U_B A_B R_c$

We differentiate the above equation by t , we include the compliance definition (6.10) and equation 6.11:

$$\frac{dP_B}{dt} - A_B R_c \frac{dU_B}{dt} = \tilde{C} A_B U_B \quad (6.12)$$

For simplification, we call $\bar{R} = A_B R_c$ and $\bar{C} = \tilde{C} A_B$.

At $x = L$:

The main difference with the previous case is the boundary conditions at $x = L$. Thus, conditions that we found for C_1 and C_2 are the same. However we need to determine Φ_2 , i.e. to determine C_3 , using the new boundary condition at $x = L$ that we defined in equation 6.12:

$$\frac{dP_B}{dt} - \bar{R} \frac{dU_B}{dt} = \bar{C} U_B$$

Following similar reasoning as in the previous case, we can express each part of equation 6.12 at $x = L$:

$$\left. \frac{dP_B}{dt} \right|_{x=L} = -i\omega \alpha_o (C_1 e^{-i\omega L} + C_2 e^{i\omega L}) e^{i\omega t} + \omega^2 \alpha_o \rho \bar{u}_o e^{i\omega t} + i\omega C_3 e^{i\omega t}$$

$$U_B = \frac{\alpha_o}{\rho C_o} (-C_1 e^{-i\lambda l} + C_2 e^{i\lambda l}) e^{i\omega t} - \alpha_o \bar{u}_o e^{i\omega t}$$

$$\text{and } \frac{dU_B}{dt} = i\omega U_B$$

Replacing these quantities in equation (6.12), we find the expression of C_3 :

$$C_3 = \alpha_o (C_1 e^{-i\lambda l} + C_2 e^{i\lambda l}) + \frac{\alpha_o}{\rho C_o} \left(\bar{R} - i \frac{\bar{C}}{\omega} \right) (-C_1 e^{i\lambda l} + C_2 e^{-i\lambda l}) - \alpha_o \bar{u}_o \left(\bar{R} - i \frac{\bar{C}}{\omega} \right) + i\omega \alpha_o \rho \bar{u}_o$$

Because the capacitance/resistance end condition affects only C_3 rather than C_1 & C_2 , ΔP takes the same form as the previous case although the general pressure level may be raised through C_3 .

6.2.3 Analysis

We consider that the imposed velocity at $x=0$ is:

$$U_A = \bar{u}_o \cos(\omega t)$$

We apply equation 6.7 and 6.8 we respectively obtain:

$$C_2 - C_1 = -\rho C_o \bar{u}_o$$

$$C_1 = \rho C_o \alpha_o \bar{u}_o \frac{\frac{-\cos(\omega t)}{\alpha_o - 1} + \cos(\lambda l + \omega t)}{\cos(\lambda l + \omega t) - \cos(-\lambda l + \omega t)} \quad (6.13)$$

And we can deduce the pressure difference from equation 6.6 as:

$$\Delta P = C_1 \cos(-\lambda x + \omega t) + C_2 \cos(\lambda x + \omega t)$$

We can therefore write:

$$\Delta P = \rho C_o \alpha_o \bar{u}_o \frac{\frac{-\cos(\omega t)}{\alpha_o - 1} + \cos(\lambda l + \omega t)}{\cos(\lambda l + \omega t) - \cos(-\lambda l + \omega t)} (\cos(-\lambda x + \omega t) + \cos(\lambda x + \omega t)) - \rho C_o \bar{u}_o \cos(\lambda x + \omega t) \quad (6.14)$$

We can also determine pressures and velocities once we know that:

$$C_3 = \alpha_o \frac{C_1 \cos(-\lambda l + \alpha x) + C_2 \cos(\lambda l + \alpha x) - \rho \bar{u}_o \omega \sin(\alpha l)}{\cos(\alpha x)} \quad (6.15)$$

Figure 6.3 depicts what we called "resonance" in section 6.2.2. We have taken $L=1$ m, and $n = 1$. We have plotted the variations of the inner tube radius with the time. Note that the inner tube radius is related to the pressure difference through the relation $\alpha = \alpha_o + D\Delta P$, where D is the distensibility and is taken as a constant (see section 5.5.1). As $\lambda \rightarrow n\pi / l$, we can see that the denominator of the first term of the right hand side of equation 6.14 (representing the standing wave) tends to zero, making the pressure difference tending to infinity. In figure 6.3, the maximum value we gave for the wave length λ is 3.12 (not π). The picture 6.3 exhibits the resonance effect, which is the amplification of the standing wave for particular values of λ . In other word the natural frequency of the system is the same as the frequency of the impulse.

Another possibility to obtain an amplification of the standing wave from equation 6.14, is to have α_o close to 1. In this case, the numerator of the first term of equation 6.14 tends to infinity, amplifying the pressure difference at any λ (or frequency). Figure 6.4 depicts this phenomenon. We can see the variation of the inner tube radius for three different α_o , when λ is kept constant.

Figure 6.5 shows the variations of the inner tube radius with time at different locations along the tube. The pressure difference rise for $x = 0$ m (peak denoted 1 in figure 6.5) can be seen at a later time at $x = 0.8, 0.9, 0.99$ m., in peak denoted 2. Note that the pressure difference (or the inner tube radius) attenuates till it reaches the blockage. There, it grows

again. This implies that close to a blockage the pressure difference is higher (in amplitude) than anywhere else.

Figure 6.6 depicts the same feature as figure 6.5 with a longer time scale to show the attenuation of the peaks with time. This attenuation is due to the fact that the natural frequency of the system is no longer the same as the frequency of the system: no more resonance.

To conclude this chapter, we can say that this model is not suitable to analyse the propagation of a pressure pulse because the impulse is varying with time. However, it would be a reasonable model to represent the effects of heartbeats on the pressure in the spinal system. If for some reason the frequency of the heartbeat is the same or close to the natural frequency of the spinal system, we would obtain high increases in terms of pressure difference.

6.3 METHOD OF CHARACTERISTICS

6.3.1 Introduction

In chapter 5, we derived the governing equations and defined the wave speed for a model system. These governing equations are hyperbolic. The most suitable numerical technique for solving hyperbolic partial differential equations is the Method of Characteristics. Generally, the Method of Characteristics is a procedure for replacing a set of quasi-linear non-homogeneous partial differential equations by a set of compatibility equations (interior operator) that is valid only on surfaces called characteristic surfaces. For a problem in two independent dimensions (here one space dimension and time), the

characteristic surfaces are characteristic lines, called characteristics, and the compatibility equations are total differential relationships that are valid along the characteristics. Consequently, finite difference methods for solving the characteristic and compatibility equations are considerably simpler than methods for solving the original set of partial differential equations.

In this section we will first recall the governing equations using some new notation. Then we will derive the characteristics and compatibility equations for the linear case, after having linearized the equations by neglecting the second-order terms which appear as the product of two-first order terms. Afterwards, we will use the same general approach for the non-linear case. In the same section we will develop a weakly non-linear theory in order to discuss the possibility of the creation of elastic jumps, and compare it to the analysis made in the previous chapter (section 5.5). Finally, we will describe the numerical procedure used to solve the characteristics and compatibility equations, showing the unit process for both the linear and non-linear cases.

6.3.2 Governing equations (see figure 6.7)

If we insert equation 5.19 in the continuity equations 5.3 and 5.4, we obtain:

$$D \frac{\partial \Delta P}{\partial t} + D U_A \frac{\partial \Delta P}{\partial x} + \alpha \frac{\partial U_A}{\partial x} = 0 \quad (6.16)$$

$$-D \frac{\partial \Delta P}{\partial t} - D U_B \frac{\partial \Delta P}{\partial x} + (1 - \alpha) \frac{\partial U_B}{\partial x} = 0 \quad (6.17)$$

The momentum equations in both channels defined in equations 5.5 and 5.6 can be written as:

$$\frac{\partial U_A}{\partial t} + U_A \frac{\partial U_A}{\partial x} + \frac{1}{\rho} \frac{\partial P_A}{\partial x} = 0 \quad (6.18)$$

$$\frac{\partial U_B}{\partial t} + U_B \frac{\partial U_B}{\partial x} + \frac{1}{\rho} \frac{\partial P_B}{\partial x} = 0 \quad (6.19)$$

We now subtract equation (6.19) from (6.18) (momentum equations) considering that

$$\Delta P = P_A - P_B:$$

$$\frac{\partial U_A}{\partial t} - \frac{\partial U_B}{\partial t} + U_A \frac{\partial U_A}{\partial x} - U_B \frac{\partial U_B}{\partial x} + \frac{1}{\rho} \frac{\partial \Delta P}{\partial x} = 0 \quad (6.20)$$

Equations 6.16, 6.17, 6.20 are the governing equations.

6.3.3 Characteristic lines and compatibility equations

6.3.3.1 Linear case

Linearization

From equation 5.12, the wave speed in the linear case can be defined as:

$$C_o^2 = \frac{\alpha_o(1-\alpha_o)}{\rho D} \quad (6.21)$$

We now linearize equations (6.16, 6.17, 6.20) by neglecting products of small quantities:

$$\frac{\partial U_A}{\partial t} - \frac{\partial U_B}{\partial t} + \frac{1}{\rho} \frac{\partial \Delta P}{\partial x} = 0 \quad (6.22)$$

$$D \frac{\partial \Delta P}{\partial t} + \alpha_o \frac{\partial U_A}{\partial x} = 0 \quad (6.23)$$

$$-D \frac{\partial \Delta P}{\partial t} + (1-\alpha_o) \frac{\partial U_B}{\partial x} = 0 \quad (6.24)$$

Equations (6.22, 6.23, 6.24) become the governing equations for the linear case.

Characteristic lines and compatibility equations

It is shown in appendix A.1 (equations A.6 and A.7) that the characteristic lines are defined as:

$$\lambda_{\pm} = \pm C_o = \left(\frac{dx}{dt} \right)_{\pm} \quad (6.25, 6.26)$$

Equations (6.25, 6.26) are the characteristic lines. The upper sign stands for a discontinuity propagating in the positive direction of x , whereas the lower sign corresponds to a discontinuity propagating in the negative direction of x .

The compatibility equations have been found as (see appendix A.1, equations A.11 and A.12):

$$dU_A \pm \left(\frac{1 - \alpha_o}{\rho C_o} \right) d\Delta P = 0 \quad (6.27, 6.28)$$

Considering the inner tube, we similarly find (equations A.13 and A.14 in appendix A.1)

$$-dU_B \pm \left(\frac{\alpha_o}{\rho C_o} \right) d\Delta P = 0 \quad (6.29, 6.30)$$

Equations (6.27 to 6.30) are the compatibility equations for the linear case. They only hold along the characteristic lines defined above. The upper and lower sign respectively denotes the characteristic lines as the positive (C_+) and negative (C_-).

From a physical point of view, the characteristic lines are the path of propagation of physical disturbances (see figure 6.8). They can also be used to interpret the wave fronts. From a purely heuristic point of view, they are curves along which the governing partial differential equations can be manipulated into total differential equations. They are also curves across which the derivatives of a physical property may be discontinuous, while the property itself remains continuous. From a rigorous mathematical point of view, a

characteristic is defined as a curve along which the governing partial differential equations reduce to an interior operator, that is, a total differential equation.

Equations 6.27 to 6.30 link ΔP and U_A or U_B along the characteristic lines defined in equations 6.25 and 6.26. In order to have a complete solution of our problem, we need other relations to determine P_A or P_B , that are valid only along the characteristics.

When a perturbation is propagating along the characteristic lines defined in equations 6.25 and 6.26, we can find some fluid properties conserved across these lines. Indeed let us make a change of variables:

$$\xi_R = x - C_o t$$

$$\xi_L = x + C_o t$$

where $\xi_{R,L}$ are new variables which depend on x and t . The subscripts R and L respectively denote a right and left running wave.

From the above relation, we readily obtain the following expressions:

$$\frac{\partial \xi_{L,R}}{\partial x} = 1 \quad \text{and} \quad \frac{\partial \xi_{L,R}}{\partial t} = \pm C_o$$

Transforming the variables in the momentum equation (equation 6.18) for the linear case, we can write:

$$\frac{dU_A}{d\xi_{R,L}} \frac{\partial \xi_{R,L}}{\partial t} + \frac{1}{\rho} \frac{dP_A}{d\xi_{R,L}} \frac{\partial \xi_{R,L}}{\partial x} = 0$$

By integration of this relation, we can deduce:

$$-dP_A \pm \rho C_o dU_A = 0 \quad (6.31, 6.32)$$

Doing the same with the momentum equation in the inner tube (equation 6.19), we obtain:

$$-dP_B \pm \rho C_o dU_B = 0 \quad (6.33, 6.34)$$

Equations 6.31 to 6.32 are valid only along the characteristics defined by equations 6.25 and 6.26.

To obtain a complete solution of our problem we will need to consider equations 6.27 to 6.34 which are true only along the characteristic lines (equations 6.25 and 6.26). Note that equations 6.33 and 6.34 are not both necessary if we use an equation which relates the velocities in both tubes (equation A.10 in appendix A.1).

6.3.3.2 Non-linear case

Characteristic lines and compatibility equations

It is shown in appendix A.2 (equations A.19 and A.20) that the characteristic equations for the nonlinear case are:

$$\lambda_{\pm} = \frac{1}{1-\alpha} \left((1-2\alpha)U_A \pm C\sqrt{(1-\alpha)^2 - \rho DU_A^2} \right) \quad (6.35, 6.36)$$

Equations (6.35, 6.36) are the characteristic lines. The upper sign stands for a wave propagating in the positive direction of x , whereas the lower sign corresponds to a wave propagating in the negative direction of x . Note that these lines are no longer straight lines, unlike the linear case.

The compatibility equations become (equations A.24 and A.25 in appendix A.2):

$$dU_A + \frac{1}{\rho C} \left(\frac{\alpha U_A}{C} \pm \sqrt{(1-\alpha)^2 - \rho DU_A^2} \right) d\Delta P = 0 \quad (6.37, 6.38)$$

Equations (6.37, 6.38) are the compatibility equations in the non-linear case. They only hold along the characteristic lines defined above. The upper and lower sign respectively denotes the characteristic lines in the positive (C_+) and negative (C_-) direction.

Note that if we neglect the product of two small quantities in the characteristic and compatibility equations, we go back to the linear case.

6.3.3 Weakly non-linear case

Here we develop a weakly non-linear theory in order to be able to discuss the possibility of the creation of an elastic jump (or a shock-like wave). Indeed, since the characteristic lines are all of the same slope in the linear case these lines can never join together to form a discontinuity in the fluid properties. In the fully non-linear case, it is possible to see the lines coming together, but one has to obtain numerical results to do so. That is why we develop a weakly non-linear theory. We will be able to discuss qualitatively the creation of an elastic jump or the formation of an expansion wave. Indeed we will compare with the discussion already made in the previous chapter, in the case where the total cross-sectional area A_T is constant (see section 5.5.2).

By weakly non-linear we mean that we neglect terms which are the product of two small quantities like: $U_A \times \Delta P$, U_A^2 , $U_B \times \Delta P$, ...

Characteristic lines

In this case, the characteristic lines are (equations A.28 and A.29 in appendix A.3):

$$\lambda_{\pm} = \pm C_o \pm \frac{3}{2\rho C_o} (1 - 2\alpha_o) \Delta P \quad (6.39, 6.40)$$

If we consider a right-running characteristic (upper sign), we can write from equation 6.39:

$$\lambda_+ = C_o - C_o \frac{3(2\alpha_o - 1)}{2\rho C_o} \Delta P$$

Let us recall that α_o is always smaller than 1, so that $(2\alpha_o - 1) > 0$. Thus we can write that:

$$\lambda_+ = C_o - M\Delta P \quad \text{where } M \text{ is positive.}$$

In the undisturbed conditions (at equilibrium), we have $\Delta P = 0$, and hence $\lambda_o = C_o$. If we consider an increase $\Delta P_1 > 0$ in pressure difference (which means an increase in α), the new slope of the characteristic line will then be $\frac{1}{\lambda_1} = \frac{1}{C_o - M\Delta P_1}$ in the (x, t) diagram. Thus

we can deduce that $\frac{1}{\lambda_1} > \frac{1}{\lambda_o} = \frac{1}{C_o}$. Indeed, we have an expansion wave.

Using the same reasoning, we can show that a decrease in ΔP (which means a decrease in α) can create an elastic jump.

This analysis is consistent with the one obtained in the previous chapter in section 5.5.2.

Let us recall that this is a qualitative analysis and that the numerical results of the weakly non-linear theory will be taken with the characteristic lines defined in equations (6.39, 6.40). To do so, we need to define the compatibility equations, which is the focus of the next section.

Compatibility equations

The compatibility equations for the weakly non-linear theory take the following form (from appendix A.3, equations A.30, A.31):

$$dU_A + \frac{D}{\alpha_o} \left[\frac{\alpha_o}{1-\alpha_o} U_A \pm C_o \left(1 - \frac{\alpha - \alpha_o}{2\alpha_o(1-\alpha_o)} \right) \right] d\Delta P = 0 \quad (6.41, 6.42)$$

Interest of the weakly non-linear theory

The weakly non-linear equations are not of great use for obtaining numerical results because they require the same effort as the full non-linear case in terms of computing. Indeed, the characteristic lines and the compatibility equations are of the same form for both the weakly non-linear and the full non-linear theory. Its interest resides in the qualitative information that it provides. In fact, it shows that if the fluid is at equilibrium, an increase in pressure difference or in the outer tube cross-sectional area, will develop into an expansion wave, whereas a decrease in pressure difference or in the outer tube cross-sectional area will create an elastic jump. This is a very interesting point because the possibility of the occurrence of an elastic jump brings the possibility of large abrupt pressure rise. This will be the subject of chapter 7. In the next section, we will show the numerical procedure to solve our equations using the method of characteristics.

6.3.4 Numerical integration procedure

In section 6.3.3, we derived the characteristic and compatibility equations. We now develop a numerical procedure to solve these equations. In the linear case, equations (6.25, 6.26) define one C_+ and one C_- characteristic in the (x,t) plane, while the compatibility equations (equations 6.27, 6.28) provide a differential relationship between the pressure difference component ΔP and the velocity in the outer tube U_A that is valid only along each characteristic line. Since the set of equations (6.25, 6.26, 6.27, 6.28) and

(6.35, 6.36, 6.37, 6.38) are non-linear total differential equations, their solutions are usually obtained by applying finite difference techniques.

To obtain two independent relationships between ΔP and U_A at a point of the flow field, a network must be developed wherein two characteristics intersect at a common point. At the intersection point, there is one relationship between ΔP and U_A on each of the intersecting characteristics so that two relationships between ΔP and U_A are obtained at that point. The network used to integrate equations (6.25, 6.26, 6.27, 6.28) and (6.35, 6.36, 6.37, 6.38) is based on the direct marching method. In this method, continuous families of left and right running characteristics are followed throughout the flow field. By applying the unit processes directly from any two solution points (where all the flow properties are known) previously determined, the next point in the network may be determined (see figure 6.9).

6.3.4.1 Numerical procedure for the linear case

In fact, since the coefficients of the differential equations are constant (especially the wave speed which depends only on conditions at equilibrium) for the linear case, the numerical integration of the compatibility equations is very straightforward. Indeed, the integration of equations (6.27, 6.28) between an initial point (where the flow properties are known) and a final point (where the flow properties are unknown) along the characteristic lines gives:

$$U_{Af} \pm \frac{1-\alpha_o}{\rho C_o} \Delta P_f = U_{Ai} \pm \frac{1-\alpha_o}{\rho C_o} \Delta P_i \quad (6.43, 6.44)$$

Where the right hand side of these two equations is a known quantity. If we apply these equations from two different initial points (where the fluid properties are known) to a unique solution point, we will obtain a system of two equations with two unknowns ($U_{Af}, \Delta P_f$), that we can solve easily (see figure 6.9). Similar numerical equations can be found for equations 6.29 to 6.34.

$$-U_{Bf} \pm \frac{\alpha_o}{\rho C_o} \Delta P_f = -U_{Bi} \pm \frac{\alpha_o}{\rho C_o} \Delta P_i \quad (6.45, 6.46)$$

$$-P_{Af} \pm \rho C_o U_{Af} = -P_{Ai} \pm \rho C_o U_{Ai} \quad (6.47, 6.48)$$

$$-P_{Bf} \pm \rho C_o U_{Bf} = -P_{Bi} \pm \rho C_o U_{Bi} \quad (6.49, 6.50)$$

Note that the characteristic lines are straight lines ($\frac{dx}{dt} = \pm C_o$ where C_o is a constant).

We will give some results of this method in section 6.3.5.1.

6.3.4.2 Numerical procedure for the non-linear case

In the non-linear case, the characteristic lines are no longer straight and the wave speed varies according to the cross-sectional area. That implies that the coefficients of the differential equations are not constant. In fact we will use the modified Euler predictor-corrector method to integrate our equations, which is a second-order method of integrating total differential equations. The corrector algorithm used is based on the average coefficient method, wherein the numerical values of the coefficients of the differential equations are determined as the average of the values of the coefficients at the initial points and the solution point.

6.3.4.2.1 Finite difference equations

According to the Euler method, the finite difference equations are obtained from the characteristic and compatibility equations by replacing the differential $dx, dt, d\Delta P, dU_A$ by the differences $\Delta x, \Delta t, \Delta(\Delta P), \Delta U_A$. The coefficients λ_{\pm} and

$Q_{\pm} = \frac{1}{\rho C} \left(\frac{\alpha U_A}{C} \pm \sqrt{-\rho D U_A^2 + (1 - \alpha)^2} \right)$ are then determined at the initial points for the

predictor and in an average manner (average coefficient) for the corrector.

We can now write our finite difference equations:

$$\Delta t = \lambda_{\pm} \Delta x \quad (6.51, 6.52)$$

$$\Delta U_A + Q_{\pm} \Delta(\Delta P) = 0 \quad (6.53, 6.54)$$

where

$$\lambda_{\pm} = \frac{1}{1 - \alpha} \left((1 - 2\alpha) U_A \pm C \sqrt{-\rho D U_A^2 + (1 - \alpha)^2} \right) \quad (6.55, 6.56)$$

$$Q_{\pm} = \frac{1}{\rho C} \left(\frac{\alpha U_A}{C} \pm \sqrt{-\rho D U_A^2 + (1 - \alpha)^2} \right) \quad (6.57, 6.58)$$

and where the upper and lower signs denote a C_+ or C_- characteristic curve, respectively.

6.3.4.2.2 Numerical strategy

In order to find the fluid properties at any location of the flow field, we separate an interior point from a solid boundary point. In the former, both U_A and ΔP are unknowns.

Thus we have to consider two characteristics, a C_+ and a C_- passing through the final point (where the fluid properties are unknown) and passing through two different initial points where the properties of the fluid are known. In the latter, we will consider only one characteristic since only ΔP is unknown at the boundary ($U_A = 0$) (figure 6.10).

The unit process used in our computing program is well described by Zucrow and Hoffman (1977), and our approach will be similar. In the main program, we give the fluid properties at the initial points (two initial points for an interior point, and one initial point for a solid boundary point), we call the appropriate subroutine (interior point or solid boundary point) and we can obtain the fluid properties at any location of the flow field.

6.3.5 Numerical analysis

6.3.5.1 Linear case

In section 6.3.3.1, we have defined the equations of our problem for the linear case in terms of characteristic lines and compatibility equations. Section 6.3.4.1 was devoted to the numerical procedure to solve these equations. We now apply these theories to a particular example, and we discuss the results.

Pressure pulse propagation

Let us consider coaxial tubes with a blockage in the outer tube as seen in chapter 5. Both tubes are filled with water and are separated by a diaphragm (compliant wall). We consider the fluid at equilibrium, i.e. the pressure in the outer tube (part *A* in figure 6.7) is equal to the pressure in the inner tube (part *B*). We consider the flow to be in the conditions defined in section 5.2.1. In these conditions, we consider a sudden rise in pressure in the outer tube leading to a rise in ΔP . Immediately after the rise, the pressure drops back to the undisturbed pressure. Let us analyse the propagation of this pressure pulse, especially when it encounters a blockage in the outer tube.

Figure 6.11 represents the $(x-t)$ diagram in the outer tube. Region 0 represents the undisturbed conditions, i.e. the state of the fluid before the pressure pulse propagates. In region 1, the pressure in the outer tube has risen, whereas in region 3 the fluid properties go back to the same undisturbed conditions as region 0. In each region, the fluid properties are constant. The straight lines are the characteristics with a slope of $\pm 1/C_o$ (as found in equations 6.25 and 6.26), and separate two regions where the fluid properties change.

The blockage is placed at $x = L$ (in the outer tube only) so that the boundary conditions in the region adjoining it is $U_A = 0$.

To obtain the fluid properties in region 1, we use a C_- (i.e. a characteristic line with a negative slope: $-1/C_o$) from region 0. We impose the pressure rise (P_{A1} is known). The fluid properties in region 2 are found by using a C_+ from region 1 and by recalling the boundary condition determined by the blockage. Conditions in region 3 are found with a C_- from region 1, considering that the pressure of the outer tube goes back to its initial value. By using a combination of a C_- from region 2 and a C_+ from region 3, we can deduce the fluid properties in region 4. The fluid properties of region 5 are found in the same way as region 2, using a C_+ from region 4.

Table 6.1 shows the analytical results of the linear case (applying equations 6.43 to 6.48), whereas table 6.2 shows the numerical results. The subscripts denote the region and the pressure in the undisturbed flow is set to be: $P_{A0} = P_{B0} = \rho C_o \varepsilon_o$ (where ε_o is a known value). The pressure impulse takes the form $P_{A1} = \rho C_o \varepsilon$ where $\varepsilon < \varepsilon_o$ for a pressure drop.

Analysis of the results

We can see from these results that if the pressure rise in the outer tube ($P_{A1} > P_{A0}$), a large pressure difference is created in the vicinity of the blockage when the pressure wave reflects: $\Delta P_2 = -\frac{2\rho C_s}{1-\alpha_o}(\varepsilon_o - \varepsilon)$, which is negative. Moreover if the pressure decreases ($P_{A1} < P_{A0}$), we obtain a pressure difference at the blockage (in region 2) which can be extremely large depending on the expression of α_o . Indeed, as α_o tends to one, the pressure difference can reach very high values even if the pressure impulse is not very large.

If the pressure impulse is positive ($P_{A1} > P_{A0}$), we obtain the same magnitude for the pressure difference at the blockage, but with the opposite sign, i.e. positive. This means that the inner tube reduces at the blockage.

In the ($x-t$) diagram of figure 6.11, if we draw horizontal straight lines (time is constant), we can plot the pressure difference along the abscise at different times (figure 6.12). At time T1, the pressure pulse is propagating to the right. Time T2 represents the time when the leading edge of the wave has reflected and is traveling to the left, whereas the trailing edge of the wave is still propagating to the right. This is when the pressure difference doubles compared with the pressure difference before reflection (this high pressure difference is highlighted in figure 6.11). At time T3, both the leading and trailing edges have reflected, and the pressure pulse is propagating to the left.

If we plot the pressure difference variation at the blockage, which means that we set x near 1, and we follow the variations with the time (figure 6.13), we can see that there is a large pressure difference jump, larger than anywhere else (double). In this case we have the pressure at equilibrium which is 800 Pa, the cross-sectional area ratio α_o is 8/9 and

the outer tube pressure in region (1) is set as: $P_{A1} = 500 \text{ Pa}$. The pressure difference at the blockage is: $\Delta P_2 = -5400 \text{ Pa}$, which represents an increase of the inner tube radius of almost 1 mm.

Let us plot the equivalent of figure 6.12 in terms of radius of the inner tube in order to have a physical representation of the consequences of a pressure pulse propagation upon the inner tube (figure 6.14). This figure can be considered as a picture of the model at various times, when a pressure pulse propagates and reflects from a blockage. Indeed, if the outer tube radius is 3 cm whereas the inner tube radius is 1 cm, a pressure impulse of a magnitude double compared to the one existing in the undisturbed conditions (i.e. $P_{A1} = 2P_{Ao}$), creates a decrease or an increase (depending on whether the pressure impulse is a drop or a rise, respectively) of the inner tube radius of 3.1 mm, at the blockage.

Let us mention that the values of the radii are not important but their ratio is. Indeed α_o is a fundamental parameter. Figure 6.15 represents the variation of the pressure difference at the blockage for different cross-sectional area ratios in the undisturbed conditions (α_o). The pressure difference tends to be extremely large when α_o tends to 1.

The interest of the linear theory does not reside on the values of the fluid properties, but in their tendency. Indeed, the fact that the reflection of a pressure impulse can lead to very large pressure difference at the blockage is the main result of the linear theory. However the characteristic lines are straight in the linear case, which is obviously not the case in reality. That is the reason why we investigate the non-linear case in the next section and especially analyse the effect of the reflection of an expansion wave.

6.3.5.2 Full non-linear case

In section 6.3.3.3, we have shown that the characteristic lines could either coalesce or diverge, depending on whether the pressure difference across the wave was negative or positive (respectively). In the first part of the analysis we will consider both a compression wave and an expansion wave (a compression wave was defined as the characteristic lines coalescing and an expansion wave as the characteristic lines diverging). Since compression waves lead to the generation of an elastic jump, we will focus our attention in this section on the expansion wave.

Pressure increase analysis

By using equations 6.51 to 6.56 (section 6.3.4.2.1), we can define the fluid properties when the pressure suddenly increases. If we consider figure 6.16, we can distinguish certain regions. In this figure we have drawn 3 characteristic lines (in reality there will be an infinite number). Region 0 corresponds to the undisturbed conditions for the fluid. We consider a pressure increase in terms of ΔP . Moreover we know ΔP in region 6. Owing to approximating with a finite number (3) of characteristics, we have a step rise in ΔP in regions 1 and 3. Evidently the step rise depends on the number of characteristics that you have. The more characteristics the smoother the rise is. In our case (3 characteristics), if we set the pressure rise to be $\Delta P_6 = \varepsilon$, we have $\Delta P_1 = \varepsilon/3$ and $\Delta P_3 = 2\varepsilon/3$. Therefore, if we use a subroutine (called *chanlm*) that determines all the fluid properties through a C_+ when the pressure difference is predetermined in the unknown region, regions 1, 3 and 6 can be found. Regions adjacent to the blockage (regions 2, 5, 9) are determined using a

C_+ (from 1, 4, 8, respectively) and imposing the boundary condition in the unknown region: $U_A = 0$. A subroutine called *solid* does this task. The remaining regions (4, 8 for 3 characteristics) are determined through a combination of two characteristics: a C_+ (from 3 and 7 respectively) and a C_- (from 2 and 5). The subroutine *inter* will determine all the fluid properties in these regions. Note that regions 2, 4, 5 are non-simple regions because they are an intersection of both families of characteristics. Therefore in these regions, the fluid properties will no longer be constant.

Figure 6.17 shows the reflection of expansion waves from a blockage (5 characteristics). The coordinates of each point are recorded in table 6.3, whereas the fluid properties at these points are included in table 6.4.

With more characteristics, the (x,t) diagram looks like figure 6.18.

The pressure at the blockage ($x = L$) is plotted in figure 6.19, when 10 characteristics are used. If we compare the pressure difference after the expansion wave has reflected with the linear case, we notice that it has been attenuated but still is of the same order (about double the imposed pressure difference rise).

In figure 6.20, we plot the reflection of a compression wave. Although a compression wave will form an elastic jump, it can still be reflected from the blockage, if it is created close enough to the blockage.

Note that the reflection of an expansion wave is an expansion wave, and that of a compression wave is a compression wave.

CHAPTER 7

PROPAGATION OF PRESSURE PULSES IN A TWO- COAXIAL TUBE MODEL

7.1 INTRODUCTION

We have discussed in chapters 5 and 6 the possibility of the creation of a shock-like wave or elastic jump, analogous to a hydraulic jump. It is the shock-like behaviour that is most interesting for our purposes. It leads to the possibility of the reflection of an elastic jump at a blockage in the outer chamber A, leading to an intensification of pressure difference in the vicinity of the blockage.

In this section, we assume that an elastic jump exists, and we analyse the effects of such a phenomenon. We derive the governing equations. We will solve these equations using a small perturbation theory based on small pressure-difference jumps through the elastic jump, especially when a reflection occurs. This simple analysis will give us some valuable information about the system behaviour. We will then solve the equations using a numerical method based on a Laguerre polynomial without imposing any restriction on the size of the perturbation, and will compare the results to the small perturbation theory. In the meantime, we need to consider a pressure-area relationship: we will use a simple linear tube law.

We will finally analyze the propagation and reflection of a pressure pulse by using a combination of the method of characteristics and the elastic jump model.

7.2 GOVERNING EQUATIONS

We consider an elastic jump occurring in coaxial tubes, both filled with fluid (see figure 7.1). The outer tube is rigid, whereas the inner one is compliant. A previous study (Dardel, 1988) of elastic jumps in soft tubes shows that a one-dimensional analysis is satisfactory. The fluid is incompressible, and we neglect friction forces compared with the pressure forces. We consider the undisturbed flow to be quasi-stationary. The effects of wall inertia are neglected.

Conditions before the elastic jump (right side of the jump) are denoted by subscript (1), and those after the wave passes are denoted by (2). For the purposes of analysis, we will assume that the elastic jump is stationary. The true conditions can be recovered by carrying out a Galilean transformation using a reference frame attached to the elastic jump. Accordingly, in front of the elastic jump the fluid velocities in chambers (A) and (B) are the local velocities minus the wave speed for a right-running wave and plus the wave speed for a left-running wave. We are at equilibrium in region (1), so the pressure in the inner and in the outer tube is the same and equal to P_e .

7.2.1 Notation

In region 1: U_{A1}, P_{A1}, A_{A1} and U_{B1}, P_{B1}, A_{B1} are respectively the velocity, pressure, cross-sectional area in chambers (A) and (B).

In region 2: U_{A2}, P_{A2}, A_{A2} and U_{B2}, P_{B2}, A_{B2} are respectively the velocity, pressure, cross-sectional area in chambers (A) and (B).

$\Delta P_i = P_{Ai} - P_{Bi}$ is the pressure difference between the outer and the inner tubes ($i=1,2,\dots$).

$A_T = A_{A1} + A_{B1} = A_{A2} + A_{B2}$, is the total cross-sectional area, and is taken as a constant.

V_s is the shock-like wave speed.

In the undisturbed flow, we have: $P_e = P_{A1} = P_{B1}$, which is the pressure at equilibrium.

$\alpha_l = \frac{A_{A1}}{A_T}$ is a cross-sectional area ratio, and $\alpha_o = \frac{A_{A2}}{A_T}$ is the cross-sectional area ratio at

equilibrium.

7.2.2 Governing equations

Under the conditions noted above, the relations linking conditions downstream and upstream of the elastic jump become:

Conservation of mass applied to the control volume defined in figure (7.1):

$$A_{A1}(\pm V_s - U_{A1}) = A_{A2}(\pm V_s - U_{A2}) \quad (7.1)$$

$$A_{B1}(\pm V_s - U_{B1}) = A_{B2}(\pm V_s - U_{B2}) \quad (7.2)$$

where the upper and lower signs respectively refer to a right- and left-running elastic jump.

Momentum equations applied to the control volume defined in figure (7.1):

$$P_{A1}A_{A1} - P_{A2}A_{A2} = \rho A_{A1}(\pm V_s - U_{A1})(\pm V_s - U_{A2} - (\pm V_s - U_{A1})) \quad (7.3)$$

$$P_{B1}A_{B1} - P_{B2}A_{B2} = \rho A_{B1}(\pm V_s - U_{B1})(\pm V_s - U_{B2} - (\pm V_s - U_{B1})) \quad (7.4)$$

Rearranging equations 7.1 to 7.4, and inserting the notations defined in section 7.2.1, we can write that the fluid properties after the elastic jump are:

$$(7.1) \quad \Rightarrow U_{A2} = \pm \frac{\alpha_2 - \alpha_o}{\alpha_2} V_s + \frac{\alpha_o}{\alpha_2} U_{A1} \quad (7.5)$$

$$(7.2) \quad \Rightarrow U_{B2} = \pm \frac{\alpha_o - \alpha_2}{1 - \alpha_2} V_s + \frac{1 - \alpha_o}{1 - \alpha_2} U_{B1} \quad (7.6)$$

$$(7.3) \quad \Rightarrow P_e \alpha_o - P_{A2} \alpha_2 = \rho \alpha_o (\pm V_s - U_{A1})(U_{A1} - U_{A2}) \quad (7.7)$$

$$(7.4) \quad \Rightarrow P_e (1 - \alpha_o) - P_{B2} (1 - \alpha_2) = \rho (1 - \alpha_o) (\pm V_s - U_{B1})(U_{B1} - U_{B2}) \quad (7.8)$$

Equations 7.5 to 7.8 relate the fluid properties before and after an elastic jump running to the right (upper sign) or the left direction (lower sign). Let us recall that these relations do not consider any processes inside the elastic jump itself.

Considering that all the fluid properties are known before the elastic jump passes (zone 1 in figure 7.1), we have a set of 5 real unknowns (P_{A2} , P_{B2} , U_{A2} , U_{B2} , α_2) with only 4 equations (equations 7.5 to 7.8). The extra equation will be provided by the tube law, which is the subject of the next section.

7.3 TUBE LAW (PRESSURE-AREA RELATION)

We have shown in the previous section and in chapter 4 (section 4.3), the importance of a tube law (pressure-area relation). It will provide us with the extra equation required in order to solve the problem. We will use a simple linear relation in order to develop a simple analysis for the small perturbation theory. Other tube law relations are available in the literature (see section 5.4) to improve the theoretical model. Here we use:

$$\alpha = \alpha_o + D \Delta P \quad (7.9)$$

where $D = \frac{1}{A_T} \frac{dA_A}{d\Delta P}$ is the distensibility defined in section 5.3 (and is taken as constant),

and where $\Delta P = P_A - P_B$ is the pressure difference.

7.4 SMALL PERTURBATION THEORY FOR ELASTIC JUMP

We now consider small pressure difference changes through the elastic jump, i.e.

$\Delta P_2 = P_{A2} - P_{B2}$ is considered to be small and negative.

Since the undisturbed flow is considered to be stationary, we can write: $U_{A1} = U_{B1} = 0$.

Moreover, we consider that $P_e = 0$ (for simplification, but we can easily go back to the integral form).

Let us now consider a right-running elastic jump (upper sign in equations 7.5 to 7.8) propagating into an undisturbed flow (figure 7.2). Applying equations 7.5 to 7.8 to this case, we can readily write:

$$U_{A2} = -\frac{\alpha_o - \alpha_2}{\alpha_2} V_s \quad (7.10)$$

$$U_{B2} = -\frac{\alpha_2 - \alpha_o}{1 - \alpha_2} V_s \quad (7.11)$$

$$P_{A2} = \rho \frac{\alpha_o}{\alpha_2} V_s U_{A2} \quad (7.12)$$

$$P_{B2} = \rho \frac{1 - \alpha_o}{1 - \alpha_2} V_s U_{B2} \quad (7.13)$$

7.4.1 Estimate of the shock-like wave speed

We divide equation 7.9 applied to our case by α_o , and we obtain the relation:

$$\frac{\alpha_2}{\alpha_o} = 1 + \frac{D}{\alpha_o} \Delta P_2. \text{ Taking the inverse of this relation, we obtain: } \frac{\alpha_o}{\alpha_2} = \frac{1}{1 + (D / \alpha_o) \Delta P_2}.$$

Since we consider small pressure difference changes through the elastic jump, we can expand this ratio:

$$\frac{\alpha_o}{\alpha_2} = \frac{1}{1 + (D/\alpha_o)\Delta P_2} = 1 - \frac{D}{\alpha_o}\Delta P_2 + \left(\frac{D}{\alpha_o}\right)^2 (\Delta P_2)^2 - \left(\frac{D}{\alpha_o}\right)^3 (\Delta P_2)^3 + O((\Delta P_2)^4) \quad (7.14)$$

providing that $\Delta P_2 \ll \alpha_o / D$.

In the same way, we can write:

$$\begin{aligned} \frac{1 - \alpha_o}{1 - \alpha_2} &= \frac{1}{1 - D\Delta P_2 / (1 - \alpha_o)} \\ &= 1 + \frac{D}{1 - \alpha_o}\Delta P_2 + \left(\frac{D}{1 - \alpha_o}\right)^2 (\Delta P_2)^2 + \left(\frac{D}{1 - \alpha_o}\right)^3 (\Delta P_2)^3 + O((\Delta P_2)^4) \end{aligned} \quad (7.15)$$

providing that $|\Delta P_2| \ll (1 - \alpha_o) / D$.

Second order of approximation

In equations 7.14 and 7.15, we neglect the terms superior or equal to the order of $(\Delta P)^3$.

Therefore equations (7.10) and (7.11) can be approximated by:

$$U_{A2} \approx \left(\frac{D}{\alpha_o} \Delta P_2 - \left(\frac{D}{\alpha_o} \Delta P_2 \right)^2 \right) V_s = \frac{C_o D \Delta P_2}{\alpha_o} \left(1 - \frac{D \Delta P_2}{1 - \alpha_o} \right)$$

$$\text{and} \quad U_{B2} \approx - \left(\frac{D}{1 - \alpha_o} \Delta P_2 + \left(\frac{D}{1 - \alpha_o} \Delta P_2 \right)^2 \right) V_s = \frac{C_o D \Delta P_2}{1 - \alpha_o} \left(1 - \frac{D \Delta P_2}{\alpha_o} \right)$$

where we used a first order approximation for the elastic jump speed (see below).

We note that $|U_{A2}|$ and $|U_{B2}|$ are increased and reduced respectively compared with the constant wave-speed theory (equations 6.27 and 6.29).

In terms of pressure difference, we can substitute these approximations into equation (7.12) minus (7.13) in order to obtain the propagation speed:

$$V_s^{-2} = \rho D \left[\frac{1}{\alpha_o(1-\alpha_o)} - 2D\Delta P_2 \left(\frac{1}{\alpha_o^2} - \frac{1}{(1-\alpha_o)^2} \right) \right] + O((\Delta P_2)^2)$$

We can rewrite this equation in terms of the wave speed:

$$V_s^{-2} \approx C_o^{-2} - 2\rho D^2 \Delta P_2 \left(\frac{1-2\alpha_o}{\alpha_o^2(1-\alpha_o)^2} \right) \quad (7.16)$$

Equation (7.16) represents an approximation for the propagation speed. If we consider the case where the pressure difference after the elastic jump (ΔP_2) is negative, then as $\alpha_o > 0.5$, we can deduce that $V_s^2 > C_o^2$, and thus that the elastic jump propagates faster than the "normal" pressure wave.

Note: If we consider a first order approximation, we can readily obtain:

$$V_s^2 \approx \frac{\alpha_o(1-\alpha_o)}{\rho D} = C_o^2$$

Thus, for a small pressure difference jump across the wave, the propagation speed reduces to the wave speed, as expected. Indeed, the normal pressure wave speed is the limit of the shock-like wave speed.

7.4.2 Elastic jump reflection

We have seen in the chapter 6 that the reflection of a pressure wave from a solid boundary can create a region where the pressure difference ΔP in the vicinity of the blockage is approximately doubled. We now analyse the reflection of an elastic jump from a solid boundary. We still consider small pressure difference jumps across the elastic jump (second order of approximation).

Let us consider a right-running elastic jump running in an undisturbed flow, with a blockage in the outer tube only (figure 7.3). We denote by the subscript (1), all the flow properties before the incident elastic jump passes. After the passage of the incident elastic jump, and before it reflects, the fluid properties are denoted by subscript (2). When the reflection occurs, in general, transmitted and reflected waves propagate in the right and left directions, respectively. After the passage of the reflected wave running in the left direction, the flow properties are denoted by (R), whereas we will use the subscript (T) for the flow properties after the passage of the transmitted wave (see table 7.1).

7.4.2.1 Effects of the incident wave

The analysis of the effects of the incident elastic jump is the same as section 7.4.1, except that the shock-like wave speed and the pressure difference after the incident wave passes are denoted by $V_{s'}$ and ΔP_i instead of V_s and ΔP , respectively. Indeed, all the fluid properties in zone (2) can be found by means of equations 7.10 to 7.13, knowing the incident shock-like wave speed, as shown in table 7.2.

7.4.2.2 Effects of the reflected wave (figure 7.3)

After the passage of the reflected elastic jump, the boundary condition at the blockage in the outer chamber imposes the condition that: $U_{AR} = 0$.

If we carry out the same analysis as for the elastic jump, but considering a left-running wave propagation, we obtain:

Conservation of mass:

$$A_{AI}(U_{AI} + V_{SR}) = A_{AR}(U_{AR} + V_{SR}) \quad (7.17)$$

$$A_{BI}(U_{BI} + V_{SR}) = A_{BR}(U_{BR} + V_{SR}) \quad (7.18)$$

With $U_{AR} = 0$, and equations (7.5) and (7.10), we can deduce:

$$V_{SR} = -\frac{\alpha_I}{\alpha_I - \alpha_R} U_{AI} = \frac{\alpha_o - \alpha_I}{\alpha_I - \alpha_R} V_{SI} \quad (7.19)$$

We do the same for equation (7.6) to obtain

$$V_{SR} = -\frac{1 - \alpha_I}{\alpha_R - \alpha_I} U_{BI} + \frac{1 - \alpha_R}{\alpha_R - \alpha_I} U_{BR}$$

We note that if we use equation (7.11) to express U_{BI} into the above equation, we obtain:

$$V_{SR} = \frac{\alpha_o - \alpha_I}{\alpha_I - \alpha_R} V_{SI} + \frac{1 - \alpha_R}{\alpha_R - \alpha_I} U_{BR}$$

We have two different relations (equation 7.19 and the above one) linking V_{SR} and V_{SI} .

This can be possible only if $U_{BR} = 0$. We can thus write:

$$V_{SR} = -\frac{1 - \alpha_I}{\alpha_R - \alpha_I} U_{BI} = \frac{\alpha_o - \alpha_I}{\alpha_I - \alpha_R} V_{SI} \quad (7.20)$$

Momentum equations:

$$P_{AI}\alpha_I - P_{AR}\alpha_R = -\rho\alpha_I(U_{AI} + V_{SR})U_{AI} \quad (7.21)$$

$$P_{BI}(1 - \alpha_{2I}) - P_{BR}(1 - \alpha_R) = -\rho(1 - \alpha_I)(U_{BI} + V_{SR})U_{BI} \quad (7.22)$$

Let us write the outer tube cross-sectional area in another way:

$$\alpha_I = \alpha_o + \varepsilon \quad (7.23) \quad \text{where} \quad \varepsilon = D\Delta P_I \quad (7.24)$$

We can then deduce that the cross-sectional area after the reflected elastic jump is:

$$\alpha_R = \alpha_o + \varepsilon \frac{\Delta P_R}{\Delta P_I} \quad (7.25)$$

We have now a set of 4 independent equations (7.19, 7.21, 7.22, 7.25) with 4 unknowns (V_{SR} , P_{AR} , P_{BR} and α_R). We can thus manipulate these equations in order to obtain the values of the unknowns.

Using equation (7.19) to express U_{AI} , and inserting it in equation (7.21), we can obtain the pressure in the outer tube after the reflection of the elastic jump:

$$P_{AR} = \frac{\alpha_I}{\alpha_R} P_{AI} + \rho \frac{\alpha_I}{\alpha_R} \left(1 - \frac{\alpha_o}{\alpha_I}\right) V_{SI} \left(V_{SR} + \left(1 - \frac{\alpha_o}{\alpha_I}\right) V_{SI} \right) \quad (7.26)$$

We do the same to equation (7.22) using equation (7.20), and we obtain the pressure in the inner tube after reflection:

$$P_{BR} = + \frac{1 - \alpha_I}{1 - \alpha_R} P_{BI} + \rho \frac{1 - \alpha_I}{1 - \alpha_R} \left(1 - \frac{1 - \alpha_o}{1 - \alpha_I}\right) V_{SI} \left(V_{SR} + \left(1 - \frac{1 - \alpha_o}{1 - \alpha_I}\right) V_{SI} \right) \quad (7.27)$$

Let us now consider the form of the pressure differences ratio (reflected/incident):

$$\frac{\Delta P_R}{\Delta P_I} = 2 + \Lambda \varepsilon \quad (7.28)$$

where $\varepsilon = D\Delta P_I$ (7.24), and Λ is to be determined.

It is shown in appendix B.1 (equation B.2) that:

$$\Lambda = -\frac{1}{2} \left(\frac{1}{1 - \alpha_o} - \frac{1}{\alpha_o} \right) \quad (7.29)$$

And thus, with equation (7.28), we can evaluate the ratio of pressure difference of the reflected wave over the incident one:

$$\frac{\Delta P_R}{\Delta P_I} \approx 2 - \frac{1}{2} \left(\frac{1}{1 - \alpha_o} - \frac{1}{\alpha_o} \right) D\Delta P_I \quad (7.30)$$

Equation (7.30) predicts that the pressure difference after the passage of the reflected elastic jump can become extremely large for α_o near 1, which means that the inner tube can swell significantly as the cross-sectional area of the outer tube tends to the total cross-sectional.

Equation (7.30) is an approximation of the real pressure difference involved in the reflection of such a wave. However, after solving the same problem numerically (without assuming small perturbations), we will find that they are very good approximations, and that they can tell us important information about the behaviour of the system.

From equation 7.20, we can deduce the reflected wave speed:

$$V_{SR} = \frac{-1}{1 - \frac{\Delta P_R}{\Delta P_I}} V_{SI}$$

With equation 7.30, we can conclude that $V_{SR} < V_{SI}$.

7.4.2.3 Analysis of the transmitted wave (figure 7.3)

The transmitted wave propagates in the right direction, in an undisturbed flow. After the passage of the transmitted wave, we have $U_{AT} = 0$ due to the boundary condition.

Applying equations 7.1 and 7.2 to the transmitted wave, we obtain:

$$\begin{aligned}\alpha_o(U_{A1} - V_{ST}) &= \alpha_T(U_{AT} - V_{ST}) \\ (1 - \alpha_o)(U_{B1} - V_{ST}) &= (1 - \alpha_T)(U_{BT} - V_{ST})\end{aligned}$$

Recalling that $U_{A1} = U_{B1} = U_{AT} = 0$, we obtain from the first of these two equations that:

$$\alpha_T = \alpha_o.$$

Inserting this in the second relation, we obtain: $U_{BT} = 0$.

Applying equations 7.7 and 7.8 to the transmitted wave, we can write:

$$\alpha_T P_{AT} = \rho \alpha_o V_{ST} U_{AT}$$

$$(1 - \alpha_T) P_{BT} = \rho (1 - \alpha_o) V_{ST} U_{BT}$$

Including the above results into these two equations we find that

$$\Delta P_R = P_{AR} = P_{BR} = 0$$

These results mean that there is no transmitted wave. Since we have $U_{B1} = 0$ and no transmitted wave, it proves again that the velocity in the inner tube after reflection is zero ($U_{BR} = 0$), as it was shown in the reflected wave part.

Thus we will now consider in the following sections that there is no transmitted wave.

We have seen that the reflection of an elastic jump could more than double the pressure difference. Moreover Λ , in equation (7.29), could become very large and make the reflected pressure difference extremely large, regardless of the value of the incident pressure difference jump ΔP_I .

7.5 NUMERICAL SOLUTION

We have seen, in section 7.4, that we could solve equations 7.5 to 7.9 for the case of small pressure difference jumps across an elastic jump. We now consider pressure differences that are not so small, and we give a numerical solution to the problem set by equations 7.5 to 7.9 for the case of a reflection from a blockage placed in the outer chamber.

Note that we consider that there is no transmitted wave as it was shown in section 7.4.

7.5.1 Incident wave analysis

In this section, we consider a similar right-running elastic jump with the same notation. In these conditions, if we apply equations 7.5 to 7.9 in our particular case we readily obtain:

$$U_{A1} = -\frac{\alpha_o - \alpha_I}{\alpha_I} V_{S1} + \frac{\alpha_o}{\alpha_I} U_{A1} \quad (7.31)$$

$$U_{B1} = -\frac{\alpha_I - \alpha_o}{1 - \alpha_I} V_{S1} + \frac{1 - \alpha_o}{1 - \alpha_I} U_{B1} \quad (7.32)$$

$$P_e \alpha_o - P_{A1} \alpha_I = \rho \alpha_o (U_{A1} - V_{S1})(U_{A1} - U_{A1}) \quad (7.33)$$

$$P_e (1 - \alpha_o) - P_{B1} (1 - \alpha_I) = \rho (1 - \alpha_o) (U_{B1} - V_{S1})(U_{B1} - U_{B1}) \quad (7.34)$$

We isolate $P_{A1} - P_{B1}$ from equations (7.33) and (7.34), and using the tube law defined in equation (7.9) with equations (7.31) and (7.32) when appropriate, we have:

$$\begin{aligned} \Delta P_I = \frac{\alpha_I - \alpha_o}{D} = & \rho \alpha_o \frac{\alpha_I - \alpha_o}{\alpha_I^2} (U_{A1} - V_{S1})^2 - \rho (1 - \alpha_o) \frac{\alpha_o - \alpha_I}{(1 - \alpha_I)^2} (U_{B1} - V_{S1})^2 \\ & + \left(\frac{\alpha_o}{\alpha_I} - \frac{1 - \alpha_o}{1 - \alpha_I} \right) P_e \end{aligned}$$

There are two ways to consider this equation. Either we fix the pressure-difference jump across the elastic jump ΔP_I and directly deduce the rest of the unknowns through equations 7.31 to 7.346 and the tube law, or we fix the propagation speed and the only unknown is α_I . However, the latter needs more attention. Rearranging the above equations by multiplying by $\alpha_I^2 (1 - \alpha_I)^2$, we obtain an equation of the fifth degree in α_I :

$$\left\{\frac{1}{D}\right\}\alpha_i^5 + \left\{-\frac{2+\alpha_o}{D}\right\}\alpha_i^4 + \left\{\frac{1+2\alpha_o}{D} - \rho V_{si}^2 - P_e\right\}\alpha_i^3 + \left\{-\frac{\alpha_o}{D} + 3\rho V_{si}^2\alpha_o + (1+\alpha_i)P_e\right\}\alpha_i^2 + \left\{-\rho V_{si}^2(2\alpha_o^2 + \alpha_o) - \alpha_i P_e\right\}\alpha_i + \rho V_{si}^2\alpha_o^2 = 0 \quad (7.35)$$

For each equation we have 5 possible roots. When one has chosen a physically possible α_i (i.e. $0 < \alpha_i < 1$), then one can find the rest of the unknowns. Following this pattern (all the quantities before the jump are known):

$$A_{Ai} = A_T \alpha_i$$

$$A_{Bi} = A_T - A_{Ai}$$

$$U_{Ai} = -\frac{\alpha_o - \alpha_i}{\alpha_i} V_{si} + \frac{\alpha_o}{\alpha_i} U_{Ai}$$

$$V_{Bi} = -\frac{\alpha_i - \alpha_o}{1 - \alpha_i} V_{si} + \frac{1 - \alpha_o}{1 - \alpha_i} U_{Bi}$$

$$P_{Ai} - P_{Bi} = \frac{\alpha_i - \alpha_o}{D}$$

which is taken from equation (7.9).

7.5.2 Reflected wave analysis

The equations governing the reflected elastic jump are the same as the ones defined in section 7.4 for a reflected wave:

$$U_{Ai} = \frac{\alpha_R - \alpha_i}{\alpha_i} V_{SR} + \frac{\alpha_R}{\alpha_i} U_{AR}$$

With the velocity going back to its undisturbed state after the reflected elastic jump passes, we have, $U_{AR} = 0$. Thus the above equation yields

$$U_{AI} = \frac{\alpha_R - \alpha_I}{\alpha_I} V_{SR} \quad (7.36)$$

$$U_{BI} = \frac{\alpha_I - \alpha_R}{1 - \alpha_I} V_{SR} + \frac{1 - \alpha_R}{1 - \alpha_I} U_{BR}$$

In order to have a unique reflected propagation speed definition, we have seen in section 7.4.2.2 that the velocity in the inner tube has to be zero ($U_{BR} = 0$). Thus the above equation can be written as

$$U_{BI} = \frac{\alpha_I - \alpha_R}{1 - \alpha_I} V_{SR} \quad (7.37)$$

Note: If we insert equations (7.31) and (7.32) into equations (7.36) and (7.37) respectively, we obtain the same relation between the incident and reflected propagation speeds, as it should be.

The momentum equations give us:

$$P_{AI} \alpha_I - P_{AR} \alpha_R = \rho \alpha_I (U_{AI} + V_{SR}) (U_{AR} - U_{AI})$$

$$P_{BI} (1 - \alpha_I) - P_{BR} (1 - \alpha_R) = \rho (1 - \alpha_I) (U_{BI} + V_{SR}) (U_{BR} - U_{BI})$$

With $U_{AR} = U_{BR} = 0$, we can rearrange these two equations to give:

$$P_{AR} \alpha_R = P_{AI} \alpha_I + \rho \alpha_I U_{AI} (U_{AI} + V_{SR}) \quad (7.38)$$

$$P_{BR} (1 - \alpha_R) = P_{BI} (1 - \alpha_I) + \rho (1 - \alpha_I) U_{BI} (U_{BI} + V_{SR}) \quad (7.39)$$

Applying equation (7.9) after the passage of the reflected wave, we obtain

$$\Delta P_R = \frac{\alpha_R - \alpha_I}{D} \quad (7.40)$$

We combine equations (7.38) and (7.39) and equate it to equation (7.40), after having inserted the values of V_{SR} , U_{AI} , U_{BI} from equations (7.36), (7.37) and (7.31) respectively, to obtain:

$$\Delta P_R = \frac{\alpha_R - \alpha_o}{D} = \frac{\alpha_I}{\alpha_R} P_{AI} + \rho \frac{((\alpha_I - \alpha_o)V_{SI} + \alpha_o U_{AI})^2}{\alpha_I(\alpha_R - \alpha_I)} - \frac{1 - \alpha_I}{1 - \alpha_R} P_{BI} + \rho \frac{((\alpha_o - \alpha_I)V_{SI} + (1 - \alpha_o)U_{BI})^2}{(1 - \alpha_I)(\alpha_R - \alpha_I)}$$

Rearranging this equation by multiplying by $\alpha_R(1 - \alpha_R)(\alpha_R - \alpha_I)$, we have an equation of the 4th degree in α_R :

$$\left\{ -\frac{1}{D} \right\} \alpha_R^4 + \left\{ \frac{1 + \alpha_o + \alpha_I}{D} \right\} \alpha_R^3 + \left\{ -\frac{\alpha_o(1 - \alpha_I) + \alpha_I}{D} + \alpha_I P_{AI} + (1 - \alpha_I) P_{BI} + \frac{\rho}{\alpha_I} ((\alpha_I - \alpha_o)V_{SI} + \alpha_o U_{AI})^2 + \frac{\rho}{1 - \alpha_I} ((\alpha_o - \alpha_I)V_{SI} + (1 - \alpha_o)U_{BI})^2 \right\} \alpha_R^2 + \left\{ \frac{\alpha_o \alpha_I}{D} - \alpha_I(1 + \alpha_I) P_{AI} - \alpha_I(1 - \alpha_I) P_{BI} + \frac{\rho}{\alpha_I} ((\alpha_I - \alpha_o)V_{SI} + \alpha_o U_{AI})^2 + \frac{\rho}{1 - \alpha_I} ((\alpha_o - \alpha_I)V_{SI} + (1 - \alpha_o)U_{BI})^2 \right\} \alpha_R + \alpha_I^2 P_{AI} = 0 \quad (7.41)$$

Solving this equation for α_R , we can find the rest of the unknowns.

7.6 EXAMPLES

We have defined the governing equations for an elastic jump propagation in the previous sections. We now analyze the results by giving some examples. In the first part of this section, we analyze the properties of the fluid after the elastic jump has propagated, knowing the fluid properties before the elastic jump passes (undisturbed conditions). We then analyze the reflection of such a wave upon a blockage in the part A (see figure 7.2).

In the second part of the section, we compare the numerical results to the small perturbation theory developed in section 7.4 (and appendix *B.I*). This will enable us to confirm whether or not the approximations made are valid.

7.6.1 Relations before-after the elastic jump

Let us consider figure 7.1, where an elastic jump travels in the right direction. Before the elastic jump passes the fluid is in its undisturbed state. In order to create an elastic jump, we have shown in chapter 5 that the pressure difference disturbance between the outer and inner tube has to be negative (i.e. $\Delta P = P_A - P_B < 0$). Therefore, according to equation 7.16, the shock-like wave speed is greater than the pressure wave speed ($V_s > C_o$). Thus we will solve equation 7.35 for different shock-like wave speeds, always greater than the pressure wave speed. Table 7.3 shows the fluid properties before and after the elastic jump for various shock-like wave speeds. From this table, we can plot the velocities in part *A* and *B* (figure 7.4). The velocity in the outer tube is negative because the pressure in the outer tube after the shock is greater than the pressure before the shock (see table 7.3). This also confirms the estimate of the velocity that we made for the velocity in the outer tube (see section 7.4.1).

The undisturbed velocity in the outer tube has little effect on the pressure difference after the elastic jump. However the undisturbed pressure in each tube has a quite significant effect since the larger the undisturbed pressure is, the larger the pressure difference becomes.

7.6.2 Reflection of an elastic jump

We consider the same case as above, an elastic jump propagating to the right. We place a blockage in the outer tube, and we analyze the reflection of the elastic jump upon it. Solving equations 7.41, we can obtain all the fluid properties after the elastic jump reflects. Table 7.4 shows these fluid properties for different incident propagation speeds. It also includes the reflected propagation speed.

Figure 7.5 depicts schematically important practical outcomes of the theory. Figure 7.5a gives a plot of the wave-front positions in terms of time and space. The original (or incident) elastic jump corresponds to ab and the reflected wave to bc in figure 7.5a. At times before the incident wave reaches the blockage, the behavior is as depicted in figure 7.5b. Here we have the wave propagating at a speed $V_{sj} > C_o$ into the undisturbed conditions, denoted as O in figures 7.5a and 7.5b. As the elastic jump passes the pressure difference drops abruptly to ΔP_i and the radius of the inner chamber B undergoes a rapid jump in value. Since across the elastic jump we have $\alpha_i < \alpha_o$, we can deduce that the wave speed rises from C_o to C_i . Figure 7.5c depicts the state of affairs shortly after the elastic jump has reached the blockage. Now the reflected elastic jump is propagating back with a speed $V_{sr} > C_i$ into conditions I corresponding to those after the passage of the incident wave. Accordingly, as shown in figure 7.5c, there is a further drop in pressure difference from ΔP_i to ΔP_r and a jump in the radius of the inner chamber as the reflected shock passes. This is accompanied by a further rise in wave speed from C_i to C_r .

Figure 7.6 shows the pressure difference after the elastic jump has reflected for different incident propagation speeds. It is equivalent to imposing the incident pressure difference jump ΔP_i , and analyzing its effects on the incident propagation speeds V_{si} and reflected pressure difference ΔP_R . If we compare both pressure differences after the incident and reflected elastic jumps pass, we can see that the pressure difference after reflection is much larger. Indeed, recalling equation 7.30 for the estimate of the pressure difference after reflection, the results plotted in figure 7.6 strengthen the estimate (reflected pressure difference is about double the incident pressure difference). If we plot both pressure differences against various undisturbed cross-sectional area ratios (figure 7.7), we note that as α_o tends to 1, there is a substantial intensification of the elastic jump upon reflection and thus, the reflected pressure difference becomes larger and larger. Indeed, the inner chamber (part *B*) enlarges in diameter in the vicinity of the blockage.

7.6.3 Comparison between small perturbation theory and numerical results

In section 7.4, we made an estimate of the reflected pressure difference for the small perturbation theory. We now plot the numerical results and the estimate of the small perturbation theory for two different cases: for different pressure jumps across the incident elastic jump (figure 7.8) and for different α_o (figure 7.9). In both graphs, the curves have very similar shape. However, we recall the assumptions made for the small perturbation theory (see appendix *B.1*):

$$|\Delta P_i| \ll \alpha_o / D, \quad |\Delta P_i| \ll (1 - \alpha_o) / D$$

$$\text{and } |\Delta P_i| \ll 2 / (D(1 / (1 - \alpha_o) - 1 / \alpha_o))$$

We respectively call these assumptions *ap1*, *ap2* and *ap3*.

In table 7.5, we include these estimates for the case of figure 7.9. Indeed we observe that when the above assumptions are valid (we take ΔP_i as the tenth of the right hand expression), the estimate and the actual numerical results are very close. This shows us that the small perturbation theory can be trusted as long as the assumptions are justified.

This section concentrated on the effects of the reflection of an elastic jump alone. We have shown that the reflection of an elastic jump upon a blockage can lead to very high pressure differences in the vicinity of the blockage, especially when α_o tends to 1. To model a pressure pulse propagation, we have to combine the elastic jump with an expansion wave in order to obtain a rise followed by a drop in pressure difference, or vice versa. This will be the concern of the next sections.

7.7 PROPAGATION OF A PRESSURE PULSE

7.7.1 Introduction

In chapter 6, we have shown that a decrease in the inner tube created an expansion wave, and we analyzed the reflection of such a wave using the method of characteristics. In sections 7.1 to 7.6, we have shown that an increase in the inner tube could create an elastic jump, and we analyzed its reflection from an obstruction. Thus, using a

combination of both theories, we are able to analyze the effects of sudden pressure variations.

7.7.2 Propagation and reflection of a pulse with pressure difference drop

Let us consider figure 7.10, where a pressure pulse propagates so that the inner tube radius increases and decreases back to its undisturbed value. At the leading edge of the perturbation (right part of the bump), an elastic jump is created, whereas an expansion wave develops at the trailing edge, as predicted in chapter 6 (see figure 7.11). We now analyze the propagation of both waves in the rightward direction, especially when they reflect from a blockage placed in the outer tube.

Figure 7.12 represents the reflection of both waves in the outer tube in the space-time diagram. The bold lines represent the elastic jump, whereas the plain lines represent the characteristic lines of two families (right- and left-running families). In each region, denoted by a number, the flow properties are assumed constant. We now show how to obtain the flow properties in each of these regions.

Region (0) represents the fluid in undisturbed conditions, before any waves passes through it.

In region (10) (note that we have taken 3 characteristic lines for the expansion waves, but we can consider more lines if needed), we consider the flow after both waves passed but before any of them have reflected, so that we have again undisturbed conditions.

The fluid properties in region (1) are found through the analysis of a right-running elastic jump in an undisturbed flow (like in section 7.4).

Regions (3), (6), (10) are analyzed in the same way as in chapter 8, i.e. there is a drop in pressure difference of $\Delta P_1 / 3$ (since we consider 3 characteristics only) in each region going from region (1) to region (10), where ΔP_1 is the pressure difference in region (1) and 3 is the number of characteristics chosen.

The fluid properties in region (2) are found in the same way as in section 7.4, i.e. the analysis of a reflected wave.

In order to obtain the fluid properties in regions (4), (7), (11), we need to develop a method using a combination of both the theory for the elastic jump and the method of characteristics. Indeed, these regions are different from region (2) because the fluid velocity after the reflected elastic jump is no longer zero. Thus, we have one more unknown with the same number of equations. However regions (4), (7) and (11) are separated by right-running characteristics (C^+), so that knowing the fluid properties in the previous region, we can use a left-running characteristic (C^-) to get the extra equation needed. We use a subroutine called *Mix* to obtain the fluid properties in these regions. The method to obtain the fluid properties is well detailed in appendix B.2.

The fluid properties in the remaining regions 5, 8, 9, 12, 13 and 14 can be found in the same way as the reflection of an expansion wave, in section 6.3.5.2. Regions 5, 9 and 14 are found with the subroutine *Solid*, i.e. that the fluid velocity in the outer tube is zero in these regions.

For regions 8, 12 and 13, we use the subroutine *Inter*, which gives the intersection between characteristic lines of both families (a C_+ and a C_-).

7.7.3 Propagation and reflection of a pulse with pressure difference rise

We now consider the opposite case, i.e. the propagation and the reflection of a negative bump as described in figure 7.14. The pressure difference first rises and then falls to its undisturbed value. An expansion wave forms at the leading-edge of the pulse, whereas an elastic jump creates at the trailing edge. The analysis of such a case proceeds in a similar way as the case discussed in section 7.7.2. Figure 7.15 depicts schematically the state of affairs in this case.

In order to find the fluid properties in regions 0 to 9 (see figure 7.15), we apply the theory developed in the method of characteristics section (chapter 6) for the reflection of an expansion wave. In region 10, the fluid properties go back to its undisturbed conditions. To find the fluid properties in regions 11 to 13, we use a similar procedure developed in section 7.7.2 (subroutine *Mix*), the difference being that the shock-like wave (elastic jump) is a right-running wave and we use a C_+ from the previous region. The main equation to solve remains equation B.15 (in appendix B.2). The rest of the fluid properties can be found in a similar way.

The remaining region 14 is found as a reflected region from the incident region 13, as if the shock-like wave (elastic jump) was isolated.

We have shown how to analyse the propagation and reflection of a pressure pulse with pressure difference drop or increase. In chapter 9, we will apply this theory to a special case, and we will draw some conclusions for syrinx formation in syringomyelia.

CHAPTER 8

PHYSICAL MODEL OF THE SPINAL CSF SYSTEM

The idea of an experiment arose naturally in order to compare the theoretical predictions with reality. The design of the experimental rig was made to analyze the propagation of a pressure wave along a compliant wall which models the propagation of a sudden pressure rise in the spinal subarachnoid space. Particular attention is paid when the pressure pulse encounters a blockage in the outer channel (the subarachnoid space).

8.1 EXPERIMENTAL APPARATUS

8.1.1 Overview of the measurements

We have defined the wave speed in coaxial tubes in chapter 5 (equation 5.18). In the linear case, we obtained:

$$C_o = \sqrt{\frac{\alpha_o(1-\alpha_o)}{\rho D}} \quad (8.1)$$

where $\alpha_o = A_{Ao} / A_r$ is the undisturbed cross-sectional area ratio, ρ is the fluid density and D is the distensibility defined in equation 5.17 as:

$$D = \frac{1}{A_r} \frac{dA_r}{d\Delta P} \quad (8.2)$$

The first part of the experimental analysis consists of physically confirming equation 8.1. In chapters 5 to 7, we have seen that the pressure difference after reflection from a blockage in the upper channel was doubled compared with the pressure difference after the incident pressure wave passes. This means that the compliant tube enlarges more in

the vicinity of the blockage than anywhere else (when the pressure difference impulse is negative). The second part of the experiment is devoted to visualizing this phenomenon. Note that in both aspects of the experiment, we expect qualitative results, rather than quantitative ones.

8.1.2 Description of the apparatus

The apparatus consists of four parts (see figures 8.1 and 8.2 and appendix C): (1) an annular piston which creates the pressure impulses; (2) the coaxial tubes; (3) a water tank; and (4) the blockage.

(1) The piston is located between the two channels (see figure 8.2). It is driven by an exciter (see figures 8.2 and 8.3). The maximum displacement of the piston is 30 mm. However, the pressures driven by the exciter were absorbed by the rig through vibrations. We thus opt for a simpler way to create the pressure wave impulse which would not involve any energy dissipation. In fact, we blow inside the inner tube through one of the filling tubes on the top of the apparatus (see figure 8.4). This procedure enables us to visualize the wave propagation along the diaphragm, through deformations of the compliant tube.

(2) The two coaxial tubes are of the same length (80 cm). A rigid outer tube, made out of perspex, represents the vertebral column, and the diaphragm (compliant tube), made out of latex (translucent), corresponds to the spinal cord (channel B). The space between the two tubes corresponds to the subarachnoid space (channel A). The outer tube radius (R_T) is 10 cm, whereas the inner tube radius (R_s) is 5 cm. Both tubes are filled with water, which is a reasonable approximate of the CSF. The thickness of the compliant tube was

measured to be 0.1 mm and is taken as a constant along the tubes. At both ends of the tube the diaphragm is clamped around a perspex tube (see figures 8.2 and 8.4) of the same radius as the diaphragm. Some adhesive was used to fix the compliant tube and thereby preventing the water in both tubes from mixing.

(3) A water tank is placed above the two tubes for filling both tubes with water (see figure 8.4).

(4) A blockage was made to model the hindbrain related syringomyelia in particular. As we have seen in chapter 3, the hindbrain is driven down into the subarachnoid space (under some pressure gradients) thereby creating a blockage to the CSF circulation. In our physical model, the blockage is a circular ring (see figure 8.3). It is made of wood but a metal part is fixed on one side of the blockage to offer a better reflection and to allow the blockage to sink. The inner radius is 5.2 cm whereas the outer radius is 9 cm. The height of the blockage is 6 cm, which makes the first pressure tap to be exactly at the location of the blockage (see figure 8.3). It is located at the bottom of the apparatus, on the piston. Note that in appendix D and figure 8.2, the blockage represented by element 15 has been replaced in the actual experimental set-up by the circular ring shown in figure 8.3.

8.1.3 Measurement instruments

Some holes along the outer tubes were made in order to measure the pressure at different locations (see figures 8.1 and 8.2 and 8.5). There are five of them and the space separating two of them is 18.5 cm. They are connected to a *U* tube that had already been calibrated as: 1 cm of water column corresponds to a pressure of 100 Pa (1 cm = 1 mbar). The whole set up is recorded with a video camera. This allows us to use the slow motion

on the video in order to determine the exact pressure or to scale the time with a resolution of 0.02 s.

8.2 MEASUREMENT OF THE WAVE SPEED

The undisturbed cross-sectional ratio is:

$$\alpha_o = \frac{A_{Ao}}{A_r} = \frac{\pi(R_r^2 - R_b^2)}{\pi R_r^2} = 1 - \frac{R_b^2}{R_r^2} = 0.75 \quad (8.3)$$

Let us determine the theoretical wave speed for our experiment.

From Lighthill (1978), we have (see figure 8.6):

$$A_b - A_{bo} = \frac{2A_{bo}^2 \Delta P}{hE}$$

where h is the thickness of the elastic tube, E is the Young's modulus, and ΔP is the pressure difference applied to the compliant wall.

In our case we can write, with $A_b = A_r - A_A$, that:

$$-A_A + A_{Ao} = \frac{2(A_r - A_{Ao})^2 \Delta P}{hE}$$

From where we can deduce the distensibility D (equation 5.17):

$$D = \frac{1}{A_r} \frac{dA_A}{d\Delta P} = \frac{2A_r(1 - \alpha_o)^2}{hE}$$

We can now deduce the wave speed from equation 5.18:

$$C_o = \sqrt{\frac{\alpha_o(1 - \alpha_o)}{\rho D}} = \sqrt{\frac{hE\alpha_o}{2(1 - \alpha_o)\rho A_r}}$$

In our experiment, we have $\rho = 1000 \text{ kg/m}^3$, $E = 10^6 \text{ Pa}$ for latex rubber, $\alpha_o = 0.75$,

$A_r = 0.031416 \text{ m}^2$, and $h = 0.1 \text{ mm}$.

Thus we obtain an theoretical value of the wave speed for our experiment:

$$C_o = 2185 \text{ m / s} \quad (8.4)$$

We now estimate the experimental value of the wave speed.

In the undisturbed conditions, the level of water in the U tube is 246 cm (of water). When the pressure drops (until 243 cm of water), we start the stop watch. When the pressure wave reaches the bottom pressure tap (with a maximum of 249 cm of water), we stop the time. The time reading on the stop watch was 0.34 seconds. That means that it took 0.34 seconds for the pressure wave to travel 74 cm (the distance between the two pressure taps). This gives us a wave speed of 2.17 m/s.

We reran the experiment in the opposite case, i. e. when the pressure first rises and then drops. With a larger pressure amplitude, we obtain a wave speeds varying between 2.05 and 2.17 m/s. These variations on the experimental wave speed are due to the fact that we did not carefully control the stretching of the diaphragm. Therefore, the diaphragm being stretched stiffer in some cases than others, the wave speed will be bigger in these cases.

These experimental results confirm that the wave speed depends on the cross-sectional area ratio, and that the wave speed in coaxial tubes defined in equation 5.18 is in a good agreement with experiment.

8.3 REFLECTION OF A PRESSURE WAVE

We have seen that a pressure wave reflection from a blockage in the upper channel could raise the pressure pulse amplitude in the vicinity of the blockage. We now consider the experimental set-up in order to visualize this phenomenon. To achieve the reflection, we place a blockage (see figure 8.5) at the bottom of the outer channel. We drive a pressure

impulse and follow the propagation along the diaphragm, until it reaches the blockage. There a probe measures the pressure that we can compare with the pressure impulse at the initial part of the tubes.

We have been able to actually see that the pressure pulse reflection generates a larger pressure in the vicinity of the blockage. A video recorder shows the reflection of the pulse at the blockage. However, owing to the very elementary pressure sensors, we could not quantitatively confirm the theoretical predictions, i.e. the doubling of the pressure impulse at the blockage. We can however confirm that the pressure significantly rises at the blockage.

Note that it was easier to see the swallowing of the diaphragm at the blockage when the diaphragm remained clamped and stretched for a certain time. This tends to show that the weakening of the compliant wall could be the first step of the swallowing phenomenon. That would confirm the results of the end of chapter 9 where we will mention that the reflection of a pressure pulse could first act as a weakening of the spinal cord. Physically, it is linked with the fact that the distensibility D is not constant at the beginning of the experiment. It still varies after letting the diaphragm stretch for a certain period of time, but the range of variation is smaller. Note that after running the experiment the compliant tube has found to be about 7 cm longer than at the start of the experiment. This implies that the compliant tube properties have considerably changed during the running of the experiment, as its behavior does also.

Bearing in mind the above remarks, it would be best to be able to assess the distensibility during the experiment. To do so, one has to control the stretching of the compliant wall. Moreover a smaller apparatus would be better in order to keep the properties of the

compliant wall unchanged. Indeed, the force of gravity has a clear effect in our set-up. With a smaller scale apparatus gravitational effects would be reduced and thus a quantitative comparison with the theory would be feasible.

To conclude this chapter we will stress that more experimental work needs to be done in order to validate the theoretical model. However, the first results are encouraging and merely with better pressure transducers, we could confirm more theoretical results. In the conclusion (chapter 10), we will consider different ways to improve the experimental model.

CHAPTER 9

PRESSURE PULSE PROPAGATION IN THE SPINAL CSF SYSTEM: SYRINX FORMATION

9.1 INTRODUCTION

In chapters 2 and 3, we briefly described the spinal system and syringomyelia. We then developed a coaxial tube model (see figure 5.1) based on the collapsible tube theory in order to analyze the propagation of a pressure wave in the spinal system. We placed a blockage in the outer channel (see figure 6.7) and investigated the propagation and reflection of a pressure pulse. In the human spinal system, the pressure pulse represents any variation of pressure due to coughing, sneezing, changes in posture, etc. Therefore, the mechanical model we have developed, even though very crude, can be used to analyse the propagation and reflection of a pressure pulse (due to a cough for instance) in the spinal system. It will give us crucial information about the syrinx formation in syringomyelia.

In the first part of this chapter, we will analyse the effects of a pressure pulse reflection from a blockage placed in the subarachnoid space. Even though this analysis will give us valuable information like how high pressures are generated in the central canal (channel *B* in figure 5.1), it will not provide, at this stage, a full understanding of the syrinx formation. This is the reason why we will end this chapter by speculating on the effects of spinal cord porosity (that have been neglected in the model) on the syrinx formation. We will then suggest how a syrinx could expand, even though more investigation is also needed to understand this mechanism deeply.

9.2 ANALYSIS OF THE PROPAGATION AND REFLECTION OF A PULSE WITH PRESSURE DIFFERENCE DROP

We will now apply the procedure described in section 7.7.2. Let us consider the propagation of a pressure pulse (a simulated cough) down the two-chamber system, as depicted in figures 9.1a-d. Let us recall that the central canal cross-sectional area is much smaller than the subarachnoid one, i.e. $A_b \ll A_A$ (or $\alpha_o \rightarrow 1$). Table 9.1 shows the fluid properties in each region, defined in section 7.7.2. As in figure 7.5a of section 7.6.2, figure 9.1a plots the movement of the wave fronts. In this case it is assumed that there is a drop in pressure difference ΔP for a short period of time. This leads to a bump propagating down the system. Its leading edge generates a shock-like wave (elastic jump) ab and the trailing edge generates weaker 'expansion' waves ef , eg and eh (as illustrated in figure 9.1a), across which the pressure difference gradually increases.

Figure 9.1b depicts the situation before the pressure pulse reaches the blockage. The pressure pulse propagates into undisturbed conditions 0. The pressure difference drops to ΔP_1 across the shock-like wave (elastic jump) ab . Conditions after the passage of the wave ab being denoted by 1. As the trailing edge of the pulse is approached a gradual elevation in pressure difference back to undisturbed conditions occurs across waves ef to eh . When the shock-like wave (elastic jump) ab reaches the blockage, it reflects as wave bci .

Figure 9.1c corresponds to a time just after the leading-edge elastic jump has reflected from the blockage but before the leading expansion wave ef has reached the blockage. The conditions 2 in the region bci of space-time in figure 9.1a correspond precisely to

those after the reflection of the elastic jump in figure 7.6. Region 2 is highlighted in figure 9.1a because the magnitude of the pressure difference is at its greatest, which means that the inner tube radius is at its highest value.

Shortly after reflection, the elastic jump interferes with the incident expansion-like waves (between d and c in figure 9.1a). This weakens the elastic jump and reduces its propagation speed. Shortly after this time the expansion-like waves also reflect.

Figure 9.1d corresponds to the time T_3 , shortly after the trailing expansion-like wave has reflected from the blockage. Note that conditions after both waves have reflected are very close to the undisturbed conditions.

Figure 9.2 depicts the variations of the inner tube radius with time at the blockage for the same case as above. The inner tube enlarges considerably but for a short period of time only. It almost goes back to the undisturbed conditions after all the waves have reflected. We can deduce that when a pressure pulse (drop) propagates and encounters a blockage in the subarachnoid space, a sort of focusing effect occurs whereby the pressure difference is greatly intensified momentarily in the vicinity of the blockage.

In terms of velocity see table (9.1), the inner tube fluid speed is much larger than the outer one, as in the case of the reflection of an expansion wave (section 6).

In chapter 2 about syringomyelia, we described Williams' *suck* mechanism. At first sight, the large relative magnitude of U_b in the positive direction would appear to contradict William's theory. In fact, we have shown that there was no transmitted wave and therefore that there was no transmission to the 'spinal system' beyond the blockage.

9.3 ANALYSIS OF THE PROPAGATION AND REFLECTION OF A PULSE WITH PRESSURE DIFFERENCE RISE

Applying the procedure described in section 7.7.3, we can plot similar graphs as in section 9.2 (figure 9.1). This is depicted by figures 9.3 and 9.4. We distinguish two different cases:

(1) $U_{Ao} = 1 \text{ mm/s}$ (which is depicted in figure 9.3)

(2) $U_{Ao} = -5 \text{ mm/s}$ (figure 9.4)

Indeed we demarcate these two cases because in region 14 of figure 7.15, the pressure differences are of opposite signs, which means that the inner tube either enlarges or reduces. This comes from the fact that in region 11 of figure 7.15, the pressure difference is negative when the undisturbed inner chamber velocity is sufficiently negative. In regions 12, 13, 14 the pressure difference will increase since we cross the characteristic lines. However, if the absolute value of the pressure difference in region 11 is big enough, the following increases in ΔP until region 13 will not be enough in order to have a positive pressure difference in region 13. Then, the pressure difference in region 14 is approximately doubled compared with region 13.

However, the interesting feature of both cases is that the last region (region 14) has new fluid properties, which remain permanently. New equilibrium conditions are reached, unlike the previous case where we had an expansion wave following the shock-like wave (elastic jump) to go back to the undisturbed conditions.

Let us analyze the first case.

The analysis of this case is mainly the same as section 9.2 for figure 9.1. The main difference apart from having a positive pressure difference and thus a reduction of the

inner tube radius, is the fact that after both the expansion and elastic jumps have reflected, we do not have the undisturbed conditions anymore, or conditions very close to them. In fact, we obtain new equilibrium conditions. This implies that the inner tube is permanently reduced in cross-sectional area (figures 9.3d and 9.3e). This can be seen as an *overshooting effect*. Even if we do not actually get the increase of the inner tube cross-sectional area one would expect to be required to generate a syrinx, this phenomenon could lead to a weakening of the spinal cord thereby facilitating the formation of a syrinx.

In the second case, the pressure pulse propagates against the flow. If we impose a pressure difference rise, the pressure differences in regions 11 to 14 of figure 7.15 are all negative, which can be seen in figure 9.4c with the inner tube radius being larger than the undisturbed inner tube radius (1 mm). In this case we obtain an overshooting which stretches out the inner tube radius. This could be the beginning of the syrinx formation since the inner tube enlarges. Moreover, a combination of both cases could weaken the spinal cord.

Let us consider figure 9.5, which is the propagation and reflection of a small pressure difference pulse with a negative undisturbed upper chamber fluid velocity. It is qualitatively very similar to figure 9.4. We actually obtain a bigger enlargement of the spine with smaller amplitude of pressure difference impulses. This is due to the fact that along the characteristics, ΔP counter balances the effects of ρCU_{∞} , in magnitude. If ΔP is smaller, the effect of ρCU_{∞} will be more important and we obtain a negative pressure difference bigger in absolute value in region 11, and thus in region 14. With figures 9.4 and 9.5, we can conclude that pressure difference (rise) pulses (even of small amplitude) which propagate against the upper channel flow can

create an enlargement of the central canal of the spinal cord. This enlargement, which is due to the blockage in the upper channel, remains permanently.

Note that in figures 9.3 to 9.5, there is only one elastic jump propagating. The steep cross sectional area rise is a numerical artifact, which is due to the fact that we used 3 characteristics only, instead of an infinite number.

In figure 9.6, we plot the pressure difference in region 14 with respect to the undisturbed cross-sectional area ratios. The graph includes different cases of undisturbed upper channel velocities (U_{Ao}). We can see that the sign of the pressure difference depends on both α_o and U_{Ao} . As α_o tends to one (as is the case in the human spinal system), the pressure difference either increases or decreases. This is due to the fact that along the characteristics (equations 6.45 and 6.46), α_o intensifies the weight of term $\rho C U_{Ao}$. Let us consider the physical meaning of the effects of α_o . The smaller the inner tube radius is, there will be more fluid in the outer tube. That implies that for the same pressure difference pulse propagation, the effects in terms of pressure difference will be more important if one of the two tubes is much larger (in cross-sectional area) than the other. In our case the smaller the inner tube radius is, the bigger the pressure difference.

9.4 POSSIBLE MECHANISM FOR SYRINX FORMATION IN SYRINGOMYELIA.

We have seen that the reflection of a pressure pulse can either lead to a temporary enlargement of the spine close to the blockage (section 9.2) or to a permanent enlargement/reduction depending on whether the pressure bulge is positive or negative and on whether or not it travels with or against the main flow (section 9.3).

Table 9.1 summarizes these effects. Note that a recirculation phenomenon (flow separation) may occur as the pressure pulse propagates. Since flow separation is often associated with low pressure, a closer attention to this phenomenon should be paid.

In terms of syrinx formation, these results can be analysed in two ways that might be complementary. The first conclusion that can be drawn is the fact that repetitive applied large pressure differences ΔP at the blockage (i.e. enlargement and reduction of the spine at the blockage) can lead to a weakening of the spinal cord. This weakening could have tremendous effects on the wall properties (spinal cord) i.e. either on the tube law (circumferential and longitudinal bending, axial tension) or the wall porosity (that has been neglected in our model).

The second is the fact that we have neglected the porosity effect in our model.

9.4.1 Porosity effects on syrinx formation

At first sight the porosity effects did not seem important since pressure pulse propagation and reflection are transient phenomena. However, we have shown that some pressure pulse reflections could lead to more permanent states (overshooting for instance). Even though they are not fully permanent because of the restoring forces that we have neglected, they cannot be considered as transient. These quasi-permanent large pressure differences ΔP generated at the blockage could well lead to CSF flow across the spinal cord.

If we include porosity effects, a flow-resistance between part A and part B will appear.

If we call R_{AB} the flow resistance from A to B and R_{BA} the flow resistance from B to A, some simple conclusions can be drawn. If $R_{AB} = R_{BA}$, then the flow direction (from part A to part B or the other way around) will only depend on whether the pressure

difference ΔP is positive or negative. However, this assumption is not realistic as we could either have $R_{AB} < R_{BA}$ or $R_{AB} > R_{BA}$. The most interesting case for the syrinx formation is $R_{AB} < R_{BA}$. In this case, CSF would enter the central canal more easily than it would exit it. In other words, the CSF would enter the central canal and would be trapped within it. This would ultimately lead to the syrinx formation of syringomyelia. Note that the weakening of the spinal cord could have some effects on R_{AB} or R_{BA} and especially to reduce their strength.

9.4.2 Syrinx expansion

We have shown that pressure pulse reflection can be responsible for the syrinx formation. We can develop the theory to analyse the syrinx expansion. Indeed, patients who have syringomyelia have syringes of various lengths. However, most of them have a length of several segments (see figure 3.5). Let us consider that a syrinx has been created as explained in the previous section. We now consider a new pressure pulse propagating towards a syrinx (see figure 9.7). As the incident pressure pulse reaches the syrinx, a reflected wave and a transmitted wave will propagate in opposite directions (see figure 9.8). The transmitted wave will be weaker than the incident wave. The transmitted wave will then reflect from the blockage in the same way as in the theory developed in sections 9.2 and 9.3 (figure 9.9). However, the pressure difference, after the transmitted wave reflection (region BR in figure 9.9), will be much less than in the previous cases (i.e. without the syrinx). This is due to the fact that the transmitted wave is weaker than the incident wave and that the cross-sectional area α is smaller in this region (i.e. A_B is larger), due to the enlarged syrinx cross-sectional area. That means that the larger the syrinx is in cross-sectional area,

the smaller the reflected pressure difference will be. In other words, the size of the syrinx will regulate the expansion of the syrinx in the radial direction. At the same time, the larger the syrinx is, the larger the pressure difference at the beginning of the syrinx will be (region *ST* in figure 9.8). This implies that the syrinx will expand axially. In summary, once the syrinx is created, it expands radially until a certain limit and then expands only along the axis. This limit depends on the cross-sectional area of the syrinx which determines the reflected pressure difference. When the pressure difference at the blockage (region *BR* in figure 9.9) is a certain ratio of the pressure difference at the beginning of the syrinx (region *ST* in figure 9.8), then the syrinx expands.

We gave an explanation for the syrinx expansion. This reasoning is not rigorous since it is based on qualitative discussion rather than precise calculation. It was only mentioned to show that the theory developed in previous chapters has the potential to provide a fuller understanding of the syrinx formation and expansion.

Note that a partial blockage of the subarachnoid space could be treated by using a reasoning similar to the syrinx expansion one.

9.4.3 Conclusion

We have speculated on the effects of porosity in the syrinx formation. However, porosity should be included in a new model since it certainly plays a key role in the syrinx formation. In particular, attention should be paid to the microstructure of the spinal cord in order to analyse the connected pipes network which results in porosity. Only then, we will be able to draw more definite conclusions about syrinx formation.

We have shown a possible mechanism of syrinx formation with our simple model. We have also shown that with further investigation, we might be able to understand the syrinx expansion mechanisms. An implementation of this model (especially insertion of porosity) could lead to a fuller understanding of mechanisms of syrinx formation and expansion in syringomyelia.

CHAPTER 10

CONCLUSIONS AND RECOMMENDATIONS FOR FURTHER WORK

We have developed a new model for pressure pulse propagation in coaxial tubes system where the inner tube is compliant. In chapter 5, we have derived the governing equations from where we have extracted the definition of the wave speed. We solved these equations for the linear case in what we called the "direct method" (end of chapter 6). Results showed that a phenomenon of *resonance* happens if the wavelength of the impulse reaches a particular value ($\lambda = \pi / l$ in our particular case). In this case, the pressure difference $\Delta P = P_A - P_B$ is greatly amplified when there is a blockage in the upper channel (see figure 6.3). Moreover this phenomenon is intensified if the undisturbed cross-sectional area ratio α_0 tends to unity (see figure 6.4). However, this approach was unsatisfactory for modeling a pressure pulse propagation and reflection from a blockage because the driving impulse is oscillatory. Nevertheless, this model could constitute a basis for modeling the effects of the heartbeats on the spinal CSF fluid. The heartbeats are oscillatory and therefore this model has the potential to model it. To achieve it, one has to estimate the fluctuations of pressure or velocity at the entrance of the spinal system. Then, inserting this impulse function in our model, we could predict the effects of heartbeats in the vicinity of the blockage.

In the nonlinear case, the wave speed is no longer constant (chapter 5). It was assumed to vary mainly with the cross-sectional area ratio $\alpha = A_A / A_T$. Indeed the wave speed

increases when α decreases (when $\alpha_o > 0.5$, see figure 5.2). This implies the possibility of either having an elastic jump (or a shock-like wave) when α decreases or a fan of expansion waves when α increases. Because of the variation of the wave speed and the complexity of the governing equations in the nonlinear case, we could no longer use the direct method. Therefore, we developed a new model based on the method of characteristics. We derived the characteristic lines and compatibility equations in both the linear and nonlinear cases. The linear case showed that if a pressure disturbance propagates in the upper channel and encounters a blockage, the magnitude of the disturbance is doubled in the vicinity of the blockage. This was confirmed in the nonlinear case, even if it was slightly attenuated. It was shown in both cases that when α_o tends to unity the pressure difference ΔP at the blockage could become very large in magnitude. Moreover, in the nonlinear case, we confirmed that when α increases the characteristic lines diverge, and when α decreases, the characteristic lines converge and ultimately coalesce to form a discontinuity in the fluid flow: an elastic jump.

We analyzed the changes in the fluid properties through an elastic jump (chapter 7). We found that the pressure difference after an elastic jump could become large depending on its propagation speed. We then examined the reflection of an elastic jump from a blockage. We concluded that the pressure difference after reflection more than doubled compared to the pressure difference jump through the incident elastic jump. The reflected pressure difference becomes increasingly greater when α_o tends to unity. Using a combination of the method of characteristics and the reflection of an elastic jump, we were able to analyze the propagation and reflection from a blockage of a pressure pulse.

One could find various applications for this mechanical model. Indeed, the ability of generating very high pressures close to the blockage by simply reducing the inner tube cross-sectional area could have many engineering applications. However, in a final chapter, we applied this mechanical model to the human spinal system. We have shown that the propagation and reflection of a negative pulse (i. e. one with a drop in pressure difference) created a large negative pressure difference at the vicinity of the blockage. This means that the inner tube enlarges momentarily at the blockage. More interesting is the case of the propagation and reflection of a positive pulse with a pressure difference rise. It leads to new conditions remaining permanently (ignoring the restoring forces). We have seen that if the pressure pulse propagates in the same direction as the undisturbed fluid flow in the upper channel (U_{Ao}), a reduction of the inner tube happens. We called it the *overshooting effect*. Let us point out that, in reality, the overshooting effect should not be as important as in the theoretical model because of the restoring forces of the spinal cord which would push back the spinal cord to its undisturbed conditions. If the pressure pulse propagates against the undisturbed fluid flow in the upper channel, an enlargement of the inner tube occurs, remaining permanently. We also called it *overshooting*, but in order to distinguish the two cases, it would better to call it *positive overshooting* (and thus the former case would be called *negative overshooting*). This positive overshooting could be a possible explanation for the formation of syringes in syringomyelia. The combination of the positive and negative overshooting could weaken the spinal cord and help the formation of syringes. In that respect it would be interesting to compare the

compliance or distensibility of the spinal cord in both a normal patient and a patient with syringomyelia.

We then discussed a possible mechanism for the syrinx formation, especially by speculating on the porosity effects. We then develop the theory in an attempt to explain the syrinx expansion. Let us point out that the model has only demonstrated the generation of high pressure in the central canal when a pressure pulse reflects from a blockage. The discussion on the syrinx formation and expansion is purely speculative. Nevertheless, it constitutes a good basis for further investigation on the causes of syringomyelia.

As far as the experiment is concerned, we have been able to confirm the wave speed for one undisturbed cross-sectional area. It would be worthwhile to rerun the experiment with other undisturbed cross-sectional areas. However, we only required a rough estimate to confirm the theory. We have seen that the reflection of a pressure pulse from a blockage increased at the vicinity of the blockage, thereby confirming the theory. However, the rig is not entirely satisfactory. It was probably too complicated for an initial study. The design of the compliance of the cranial part was of no use. Because of its large dimensions, it was hard to find an exciter powerful enough to drive the piston, and therefore obtain pressures large enough to visualize the wave propagation. The tension of the compliant tube was not carefully controlled, and thus it makes it harder to quantitatively compare the experimental and theoretical results. However, the aim of the experiment was to produce qualitative results and this was achieved.

Recommendations for further work

As for a future physical model, it would be preferable to make it simpler and focus on some particular points only. The main points to keep in mind while designing it are the following ones.

- (1) Be able to stretch the membrane and control the tension.
- (2) Have an impulse driver powerful enough to readily visualize the wave propagation, and which will be able to deliver one pressure rise impulse as well as an oscillatory impulse. To achieve that, computer control of the piston driver might be a more suitable system. Note that it would be better to drive the impulse pressures from the inner tube.
- (3) A system which will allow us to locally measure the cross-sectional area of the compliant tube would be of much help. Some suitable instrumentation has been used for similar measurements (McClurken, 1978). If this system seems too complicated, one could go around the problem by first determining the tube law correctly. Then with pressure taps inside and outside the compliant tube (at the same level), one could obtain the pressure difference, and thus, through the tube law, obtain the cross-section area.
- (4) Adapt the rig for testing different undisturbed cross-sectional areas (i.e. different compliant tube diameters) because the theory shows that most of the predicted phenomena are amplified with smaller compliant tube diameters. If this is not possible, make the rig with a very small compliant tube diameter.

As far as the theoretical model is concerned, one could rightly argue that it is too simple for modeling the complex spinal system. However, the purpose of this work was to make it simple so that we would understand better which are the most influent parameters of

the system. In a certain extent, we applied Descartes' third rule of "Discours de la méthode" (1637). That rule mentions that we should start by understanding the easiest things, and then when we cannot doubt them, we should rise step by step to a more complicated degree and so on until we understand the most complex system. It seems that we may now be ready to progress to a more complex model. To see where more complexity may be required, we return to the main assumptions we have made, namely:

(1) We assumed inviscid flow but viscosity should play an important role in the spinal system owing to the low speed of the CSF flow. In terms of pressure pulse propagation, its effect should be less important. In order to include the viscous effect, we could use the following equations (based on Shapiro, 1977b):

$$\text{Conservation of mass (unchanged): } \frac{\partial A_{A,B}}{\partial t} + \frac{\partial (U_{A,B} A_{A,B})}{\partial x} = 0$$

$$\text{Conservation of momentum: } \frac{\partial U_A}{\partial t} + U_A \frac{\partial U_A}{\partial x} = -\frac{1}{\rho} \frac{dP_A}{dx} - \frac{R_A(A_A, U_A) U_A A_A}{\rho} \quad (\text{part A})$$

$$\frac{\partial U_B}{\partial t} + U_B \frac{\partial U_B}{\partial x} = -\frac{1}{\rho} \frac{dP_B}{dx} - \frac{R_B(A_B, U_B) U_B A_B}{\rho} \quad (\text{part B})$$

where the last term in the momentum equations represents the viscous forces. R is positive and increases rapidly as $A_{A,B}$ decreases. From Luo and Pedley (1995), we can suggest that:

$$R_A = \frac{8\pi \mu A_{Ao}^{1/2}}{A_A^{5/2}}$$

$$R_B = \frac{8\pi \mu A_{Bo}^{1/2}}{A_B^{5/2}}$$

where μ is the viscosity of the fluid.

Note that there might be a way to link these two expressions of R .

Another source of flow resistance are the trabeculae, arteries, veins, nerves. Their effects may be taken into account via a resistance to flow similar to R . At this point, their contribution to the flow resistance is not clear, but it would seem that a decrease in A_A would increase the flow resistance. Note that the flow resistance due to the trabeculae has to be taken into account only in channel A , since there is no trabeculae within the central canal.

(2) In our model, we have taken a very crude tube law which was defined as (equation 5.19):

$$\alpha = \alpha_0 + D\Delta P$$

This linear variation of the cross-sectional area with the pressure difference does not properly describe the reality. We suggest to use a more appropriate tube law:

$$\Delta P = K_p(\alpha^n - \alpha^{-3/2}) \quad \text{where } \alpha = A / A_0$$

Pedley made his calculations with $K_p = (E / 12(1 - \sigma^2))(h / r)^3 = 5 Pa$. The exponent n needs to be evaluated (it is equal to 10 for modeling veins and 20 for drain tubing). The interesting point concerning this tube law is that it is continuous and yet combines the properties of being very stiff when ($\alpha = A / A_0 > 1$) the tube is distended, compliant at intermediate α , and stiff again at very small α . It is particularly interesting for modeling the spinal cord where tube properties change along the spine due to different arrangements of the grey and white matter depending on the location (cervical, thoracic...).

Such a tube law is still not satisfactory if one wants to consider the circumferential and longitudinal bending, and axial tension. Then it should be better to use equation 5.9,

combined with the above tube law. However, this should be done for comparisons with experimental results only. For comparison with reality, a calibration of the tube law with empirical data should be satisfactory.

(3) One important aspect of the tube law that should be included is the wall inertia. It should play a more important role in our system than in blood-flow through veins and arteries because of the thickness of the spinal cord. This can be done by adapting the following term (which is for blood flow) to our case and add it to the tube law:

$$-m \frac{\partial^2 \alpha}{\partial t^2}$$

where $m = \rho_w w / \rho h_o$

and ρ_w, w are the density and thickness of the membrane, ρ is the fluid density and h_o is the undisturbed tube radius. In brief Luo and Pedley (1995) used $m=0.01$ when the flowing fluid is water and 0.1 (or greater) when it is air. Note that in some cases (especially air), Pedley has shown that the effect of the wall inertia could be very large.

(4) Porosity should be investigated (as suggested in chapter 9). It could be a path used by the CSF to enter the central canal under certain high negative pressure differences ΔP . Perhaps the easiest way to incorporate it is through the tube law.

(5) A partial blockage instead of a total blockage of the upper channel would also be an interesting point to investigate, especially for the cases of syringomyelia due to a trauma.

(6) Maybe a 3-chamber model should be developed in the future. The inner (central canal) and outer (subarachnoid space) tubes being of low viscosity, whereas the middle one (the spinal cord wall) would be of high viscosity. This would also be a way to incorporate wall inertia.

(7) Note that the one-dimensional analysis should be extended to a two-dimensional one. In blood-flow theory, the one-dimensional analysis fails to represent flow separation and the processes of energy loss/pressure recovery downstream of a constriction. The former case should not occur in our case since the fluid velocities are very small. However the second point should be investigated.

(8) Changes in the total cross-sectional area. We have shown in chapter 5 that a change in the total cross-sectional area A_T , could either intensify the effects of the wave speed (in terms of forming an elastic jump or developing a fan of expansion waves) or reverse its effects. Indeed, we have shown that if A_b decreases we do not have necessarily a fan of expansion waves, the creation of an elastic jump is still possible if A_T decreases and $\alpha_o > 0$ (see section 5.5). This point needs more investigation, in particular when rapid changes in total cross-sectional area occur.

We have enumerated the weaknesses of the theoretical model. A lot of work has still to be done in this field. Comparing definitions of syringomyelia in the Black's dictionary of medicine in 1946 and 1995, we realized that they were almost the same, in terms of understanding the causes. This is due to a lack of collaboration between the medical and engineering sides. We should have the tools to dramatically improve conditions of patients who have syringomyelia and other brain or spinal problems. Biotechnology and biomechanics are interacting fruitfully on a wide front. This interaction has proved to be fruitful in certain aspects of bio-fluid mechanics (blood-flows, air flows), but is still too little for cerebrospinal-fluid problems. Perhaps with the increased interest in the brain

being shown by physiologists, psychiatrists, and surgeons, specialists in fluid mechanics will devote more of their efforts to this interesting and challenging area.

REFERENCES

- ABBOT, M. B. 1966 *An introduction to the method of characteristics*, Elsevier, New York.
- AGARWAL, G. C., BERMAN, B. M. and STARK, L. 1969 A lumped parameter model of the cerebrospinal fluid system. *IEEE Trans., Biomed. Eng.*, Vol. 16, pp. 45-53.
- ALLEN, R. 1986 Intracranial pressure: a review of clinical problems, measurement techniques and monitoring methods. *J. of Medical Engineering & Technology*. Vol. 10 (6), pp. 299-320.
- BALL, M. J. and DAYAN, A. D. 1972 Pathogenesis of syringomyelia. *Lancet* ii: pp. 799-801.
- BARKOVICH, A. J., WIPPOLD, F. J., SHERMAN, J. L., CITRIN, C. M. 1986 Significance of cerebellar tonsillar position on magnetic resonance. *AJNR*, Vol. 7, pp. 795-799.
- BARNET, H. J. M., FOSTER J. B. and HUDGSON, P. 1973 *Syringomyelia*. Saunders, London Philadelphia Toronto.
- BEAM, R. M. 1968 Finite amplitude waves in fluid-filled elastic tubes: Wave distortion, shock waves, and Korotkoff sounds. NASA. Tech. Note D-480, Washington, D. C.
- BECKER, D. P., WILSON, J. A. and WATSON, G. W. 1972 The spinal cord central canal: response to experimental hydrocephalus and canal occlusion. *J. Neurosurgery*, Vol. 36, pp. 416-424.
- BERING, Jr., E. A. 1955 Choroid plexuses and arterial pulsation of cerebrospinal fluid: demonstration of the choroid plexuses as a cerebrospinal fluid pump. *AMA Archives of Neurology and Psychiatry*, Vol. 73, pp. 165-172.
- BERING, Jr., E. A. 1965 The cerebrospinal fluid circulation. In *Cerebrospinal Fluid and the Regulation of Ventilation*, edited by Brooks, C. McC., Kao, F. F. and Lloyd, B. B. (Blackwell scientific publications, Oxford), pp. 395-412.

- BERTRAM, C. D. and PEDLEY, T. J. 1982 A mathematical model of unsteady collapsible tube behavior. *J. Biomech.*, Vol. 15(1), pp. 39-50.
- BERTRAM, C. D. and PEDLEY, T. J. 1983 Steady and unsteady separation in an approximately two-dimensional indented channel. *J. Fluid Mech.*, Vol 130, pp. 315-345.
- BRADLEY, S. E. 1963 The hepatic circulation, in W. F. Hamilton and P. Dow (eds). *Handbook of Physiology*, Sec.2: Circulation, American Physiological Society, Washington, D. C., vol. 2., pp. 1387-1438.
- BRADLEY, K. C. 1970 Cerebrospinal fluid pressure. *Journal of Neurology, Neurosurgery and Psychiatry*, Vol. 33, pp. 387-397.
- BROWER, R. W. and NOORDERGRAAF, A. 1973 Pressure flow characteristics of collapsible tubes: A reconciliation of seemingly contradictory results. *Annals of Biomedical Engineering*, Vol.1, pp.333-335.
- BROWER, R. W. and SCHOLTEN, C. 1975 Experimental evidence on the mechanism for the instability of flow in collapsible vessels. *Med. Biol. Eng.*, Vol. 13, pp. 839-845.
- CANCELLI, C. and PEDLEY, T. J. 1985 Separated-flow model for collapsible-tube oscillations. *J. Fluid Mech.*, Vol. 157, pp. 375-404.
- CARPENTER, P. W., BERKOUK, K. and LUCEY, A. D. 1996 Progress in theoretical and physical modelling of pressure pulse propagation in the human spinal CSF system. Technical report. *Fluid Mechanics Research Centre*, University of Warwick.
- CHATEL, M., MENAULT, F. and PECKER, J. 1979 Argument in favor of the genetic origin of malformed syringohydromyelic pictures. *Neurochirurgie*, Vol. 25, pp. 160-165.
- COBEN, L. A. and SMITH, K. R. 1969 Iodide transfer at four cerebrospinal fluid sites in the dog: Evidence for spinal iodide carrier transport. *Exp. Neurol.*, Vol. 23, pp. 76-90.
- CONRAD, W. A. 1969 Pressure-flow relationships in collapsible tubes. *IEEE Trans. on Bio-Med. Eng.*, BME-16 (4), pp.284-295.
- CONRAD, W. A., COHEN, M. L. and MCQUEEN, D. M. 1978 Note on the oscillations of collapsible tubes. *Med. Biol. Eng. Comput.*, Vol. 16, pp. 211-214.

- COWLEY, S. J. 1982 Elastic jump on fluid-filled elastic tubes. *J. Fluid Mech.*, Vol 116, pp. 459-473.
- CSERR, H. F. 1971 Physiology of the choroid plexuses. *Physiology Review*, Vol. 51, pp. 273-311.
- CSERR, H. F. and JANG, D. T. 1975 Evidence for bulk flow of cerebral interstitial fluid and its possible contribution to cerebrospinal fluid production. In *Intracranial Pressure 2*. Eds Sundberg, N. Pontein, U., Brock, M.; Spring: Berlin, pp. 24-27.
- CUSHING, H. 1902 Some experimental and clinical observations concerning states of increased intracranial tension. *Amer. J. Med. Sci.*, Vol. 124, pp. 375-400.
- CUTLER, R. W. P., PAGE, L. GALICICH, J. and WATTERS, G. V. 1968 Formation and absorption of cerebrospinal fluid in man. *Brain*, Vol. 91, pp. 707-720.
- DARDEL, E. 1988 Wave propagation and flow velocity profiles in compliant tubes. *J. of Medical & Biological Engineering & Computing*, Vol. 26, pp. 46-49.
- DARDENNE, D., DEREYMAEKER, A. and LACHERON, J. M. 1969 Cerebrospinal fluid pressure and pulsatility: an experimental study of circulation and respiratory influences in normal and hydrocephalic dogs. *European Neurology*, Vol. 2, pp. 193-216.
- DAVSON, H. 1956 *Physiology of the Ocular and Cerebrospinal Fluids*. (Churchill Livingston, London).
- DAVSON, H. 1967 *Physiology of the Cerebrospinal Fluid*. (Churchill Livingston, London).
- DAVSON, H., HOLLINGSWORTH, G. and SEGAL, M. B. 1970 The mechanism of drainage of the cerebrospinal fluid. *Brain*, Vol. 93(4), pp. 665-678.
- DAWSON, S. V. and ELLIOTT, E. A. 1977b Wave-speed limitation on expiratory flow-A unifying concept. *J. Appl. Physiol.*, Vol. 43, pp. 498-515.
- DESCARTES, R. 1637 *Discours de la Méthode*. Librairie A. Hatier.

- DUDDY, M., WILLIAMS, B. 1991 Hindbrain migration after decompression for hindbrain hernia: a qualitative assessment using MRI. *Br J Neurosurg.*, Vol. 5, pp. 141-152.
- DUNBAR, H. S., GUTHRIE, T. C. and KARPELL, B. 1966 A study of the cerebrospinal fluid pulse wave. *Archives of Neurology*. Vol. 14, pp. 624-630.
- ELLIOTT, E. A. and DAWSON, S. V. 1979 Fluid velocity greater than wave speed and transition from supercritical to subcritical flow in elastic tubes. *Med. Biol. Eng. Comput.*, Vol. 17, pp.192-198.
- ENGLAND, M. A. and WAKELY, J. 1991 *A Colour Atlas of the Brain & Spinal Cord*. Wolfe Publishing Ltd, London.
- FLAHERTY, J. E., KELLER, J. B. and RUBINOW, S. I. 1972 Post buckling behavior of elastic tubes and rings with opposite sides in contact. *SIAM J. Appl. Math.*, Vol. 23 (4), pp. 446-455.
- FLUGGE, W. 1973 *Stresses in shells*. Springer.
- FRY, D. L., THOMAS L. J. and GREENFIELDS, J. C. 1980 Flow in collapsible tubes, in D. J. Patel and R. N. Vaishnav (eds.), *Basic Hemodynamics and Its Role in Disease Processes*, University Park Press, Baltimore.
- GARDNER, M. D. 1968 *Fundamentals of Neurology*. 5th edition. By W. B. Saunders Company, Philadelphia.
- GARDNER, W. J. 1973 The dysraphic states. *Excerpta Medica* (Amsterdam).
- GJERRIS, F. and BØRGESEN, S. E. 1992 Pathophysiology of the CSF circulation. In *Neurosurgery: the scientific basis of clinical practice*, Vol. 1, pp. 146-175. 2nd edition, Blackwell.
- GRANT, R., HADLEY, D. M., McPHERSON, P., *et al* 1987 Syringomelia: cyst measurement by magnetic resonance imaging and comparisons with symptoms, signs, and disability. *J. Neurol Neurosurg Psychiatry*, Vol. 50, pp. 1008-1014.

- GREENFIELD, J. G. 1963 Syringomyelia and syringobulbia. In: Blackwood W., McMenemy W. H., Myer A., et al (eds) *Greenfield's Neuropathology*, ed. 2. London: Edward Arnold.
- GRIFFITHS, D. J. 1971 Hydrodynamics of male micturition: 1. Theory of steady flow through elastic walled tubes. *Med. Biol. Eng. Comput.*, Vol. 9, pp. 581-588.
- GRIFFITHS, D. J. 1975 Negative resistance effects on flow through collapsible tubes: 1. Relaxation oscillations. *Med. Biol. Eng. Comput.*, Vol. 13, pp. 785-790.
- GRIFFITHS, D. J. 1977 Oscillations in the outflow from a collapsible tube. *Med. Biol. Eng. Comput.*, Vol. 15, pp. 357-362.
- GROTBERG, J. B. and DAVIS, S. H. 1980 Fluid-dynamic flapping of a collapsible channel: Sound generation and flow limitation. *J. Biomech.*, Vol. 13 (3), pp. 219-230
- GURR, K. R., TAYLOR, T. K. F. and STOBO, P. 1988 Syringomyelia and scoliosis in childhood adolescence. *J. Bone Joint Surg.*, Vol. 70 B, pp. 159.
- GUYTON, A. C. 1963: Venous return, in W. F. Hamilton and P. Dow (eds). *Handbook of Physiology*, Sec.2: Circulation, American Physiological Society, Washington, D. C., vol. 2.
- HAKIM, S., VENEGAS, J. G. and BURTON, J. D. 1976 The physics of the cranial cavities, hydrocephalus and normal pressure hydrocephalus: Mechanical interpretation and mathematical model. *Surgical Neurology*, Vol. 5, pp. 187-210.
- HAMIT, H. F., BEAL, A. C. and DEBAKEY, M. E. 1965 Hemodynamic influences upon brain and cerebrospinal fluid pulsations and pressures. *J. Trauma*, Vol. 5, pp. 174-184.
- HOFFMANN, O. 1987 Biomathematics of intracranial CSF and haemodynamics-Simulation and analysis with the aid of a mathematical model. *Acta Neurochirurgica Suppl.*, Vol. 40, pp. 117-130.
- HOLT, J. P. 1944 The collapse factor in the measurement of venous pressure; The flow of fluid through collapsible tubes. *American Journal of Physiology*, Vol. 134, pp 292-299.

HOLT, J. P. 1953 Flow of liquids through collapsible tubes. *American Heart Journal*, Vol. 46, pp. 715-725.

HOLT, J. P. 1959 Flow of liquids through collapsible tubes. *Circulation Research*, Vol. 7, pp. 342-353.

HOUSE, L. and PANSKY, B. 1967 *A Functional Approach to Neuroanatomy*. 2nd edition. By McGraw-Hill Inc, New York.

HULME, A. and COOPER, R. 1976 The effects of head position in jugular vein compression (JVC) on intracranial pressure (ICP). A clinical study. In *Intracranial Pressure III*, edited by Beks, J. W. F. Bosh, D. A. and Brock, M. (Springer-Verlag, Germany), pp. 259-263.

JACKSON, J. R. and WILLIAMS, B. 1979 Errors in velocity measurement by the pitot principle in fluids with slowly propagated pressure waves. *J. Biomed.*, Vol. 1, pp. 50-53.

JAN, D. L. 1980 Refilling of collapsible tubes. M. S. thesis, Massachusetts Institutes of Technology.

JAN, D. L., KAMM, R. D. and SHAPIRO, A. H. 1982 Filling of partially-collapsed compliant tubes. *J. Biomech. Eng.*, Vol. 105, pp. 12-19.

KATZ, A. I., CHEN, Y. and MORENO, A. H. 1969 Flow through a collapsible tube; Experimental analysis and mathematical model. *Biophysical Journal*, Vol. 9, pp. 1261-1279.

KAMM, R. D. And SHAPIRO, A. H. 1979 Unsteady flow in a collapsible tube subject to external pressure or body forces. *J. Fluid Mech.*, Vol. 95, pp. 1-78.

KAMM, R. D. 1982 Bioengineering studies of periodic external compression as prophylaxis against deep vein thrombosis: 1. Numerical studies. *J. Biomech. Eng.*, Vol 104, pp 87-95.

KAMM, R. D. 1987 Flow through collapsible tubes. *Handbook of Bioengineering*, Chapter 23. Co-editors: Skalak, R. and Shu Chien, M. D., by McGraw-Hill Book Company.

- KARNI, Z., BEAR, J., SOREK, S. and PINCZEWSKI, Z. 1987 Quasi-steady-state compartment model of intracranial fluid dynamics. *Medi. Biolog. Eng. Comput.*, Vol. 25, pp. 167-172.
- KECECIOGLU, I., McCLURKEN, M. E., KAMM, R.D. and SHAPIRO, A. H. 1981 Steady, supercritical flow in collapsible tubes: 1. Experimental observations. *J. Fluid Mech.*, vol. 109, pp. 367-389.
- KIVITY, Y. and COLLINS, R 1974 Nonlinear wave propagation in visco-elastic tubes: Application to aortic rupture. *J. Biomech.*, Vol. 7, pp. 67-76.
- KNOWLTON, F. P., and STARLING, E. H. 1912 The influence of variations in temperature and blood pressure on the performance of the isolated mammalian heart. *Journal of Physiology*, Vol.44, pp. 206-219.
- KRESH, E. 1979 Compliance of flexible tubes. *J. Biomech.*, Vol. 12, pp. 825-839.
- KRESH, E. and NOORDERGRAAF, A. 1972 Cross-shape of collapsible tubes. *Biophys. J.*, Vol. 12, pp. 274-294.
- LIGHTHILL, J. 1975 *Mathematical Biofluidynamics*. Philadelphia: SIAM.
- LIGHTHILL, J. 1978 *Waves in Fluids*. Cambridge University Press.
- LOCKEY, P., POOTS, G. and WILLIAMS, B. 1975 Theoretical aspects of the attenuation of pressure pulses within the cerebrospinal-fluid pathways. *Medi. and Biolog. Eng.*, Vol. 13, pp. 861-869.
- LUO, X. Y. and PEDLEY, T. J. 1995 A numerical simulation of steady flow in a 2-D collapsible channel. *J. Fluids & Structures*, Vol. 9, pp. 149-174.
- LUPS, S. and HAAN, A. M. F. H. 1954 *The Cerebrospinal Fluid*. (Elsevier, Amsterdam).
- McCLURKEN M. E. 1978 Shape-independent area measurement in collapsible tubes by an electrical impedance technique. *Proc. 31st Ann. Conf. Engng. Medicine & Biology, Atlanta, Georgia*, p. 95.

- McCLURKEN, M. E., KECECIOGLU, I., KAMM, R. D. and SHAPIRO, A. H. 1981 Steady, supercritical flow in collapsible tubes: 2. Theoretical studies. *J. Fluid Mech.*, Vol. 109, pp. 391-415.
- McDOWALL, D. G. 1974 Fluid dynamics of the cerebral circulation. In *Scientific Foundations of Anaesthesia*, edited by Scurr, C. and Feldman, S. (Heinemann Medical, London), pp. 146-152.
- McDOWALL, D. G. 1975 The influence of anaesthetic drugs and techniques on intracranial pressure. In *A Basis and Practice in Neuroanaesthesia*, edited by Gordon, E. (Elsevier, Amsterdam), Monographs in Anaesthesiology, Vol. 2, pp. 135-170.
- McMENEMY, W. H., MYER, A., NORMAN, R. and RUSSELL, D. S. (eds) *Greenfield's neuropathology, 2nd Ed.* Arnold, London.
- MASSERMAN, J. H. 1935 Correlations of the pressure of the cerebrospinal fluid with age, blood pressure and the pressure index. *Arch. Neurol. Psychiat.*, Vol. 34, pp. 564-566.
- MERRITT, H. H. and FREMONT-SMITH, F. 1937 *The Cerebrospinal Fluid*. Philadelphia: Saunders.
- MORTENSEN, O. A. and WEED, L. H. 1934 Absorption of isotonic fluids from the subarachnoid space. *Am. J. Physiol.*, Vol 108, pp. 458-468.
- NIGHTINGALE, S. and WILLIAMS, B. 1987 Hindbrain hernia headache. *Lancet i*: pp. 731-734.
- OATES, G. C. 1975 Fluid flow in soft walled tubes: 1. Steady flow. *Med. Biol. Eng.*, Vol. 13, pp. 773-778.
- O'CONNELL, J. E. A. 1943 The vascular factor in intracranial pressure and the maintenance of the cerebrospinal fluid circulation. *Brain*, Vol. 66, pp. 204-228.
- OLLIVIER, C. P. 1827 *Traité de la moelle épinière et de ses Maladies*. Crevot, Paris, p. 178.

- PARAICZ, E., SIMKOVIC, M. and KUTAS, V. 1972 Some peculiarities of the subarachnoid space at increased ICP investigated by radio-isotope methods. In Brock, M. Dietz, H. (eds), Springer: Berlin, *Intracranial Pressure*, pp. 33-36.
- PEDLEY, T. J. 1998 Flows and self-excited oscillations in collapsible tubes. Lecture Series 1998-04, *Von Karman Institute for Fluid Dynamics*, Brussels.
- POLLAY, M. and CURL, F. 1967 Secretion of cerebrospinal fluid by the ventricular ependyma of the rabbit. *Am. J. of Physiology*, Vol. 213, pp. 1031-1038.
- POLLAY, M. CURL, F. 1968 Transport of water and electrolytes between brain and ventricular fluid in the rabbit. *Exp. Neurol.*, Vol. 20(4), pp. 558-574.
- RALL, D. P., 1968 Transport through the ependyma linings. *Progr. Brain Res.*, Vol. 29, pp. 159-167.
- REXED, B. A. and WENNSTROM, K. G. 1959 Arachnoidal proliferation and cystic formation in the spinal nerve-root pouches of man. *J. Neurosurgery* Vol. 16, pp. 73-84.
- RISER, R. 1929 *Le Liquide Céphalo-rachidien*. Paris: Masson.
- RODBARD, S. 1952 Hydrodynamics illustrated in an artificial circulation model. *Journal of Applied Physiology*, Vol. 5, pp. 191-194.
- RODBARD, S. 1955 Flow through collapsible tubes; augmented flow produced by resistance at the outlet. *Circulation*, Vol. 11, pp. 280-287.
- RODBARD, S. 1966 A hydrodynamic mechanism for autoregulation. *Cardiologia*, Vol. 48, pp. 532-535.
- RODBARD, S. and SAIKI, H. 1953 Flow through collapsible tubes. *American Heart Journal*, Vol. 46, pp. 715-725.
- RODBARD, S. and TAKACS, L. 1966 Hydrodynamics of autoregulation. *Cardiologia*, Vol. 48, pp. 433-440.

- RUBIN, R. C. HENDERSON, E. S. OMAVA, A. K., WALKER, M. D. and RALL, D. P. 1966 The production of cerebrospinal fluid in man and its modification by acetazolamide. *J. Neurosurgery*, Vol. 25, pp. 430-436.
- SACHS, E., WILKINS, H. and SANS, C. F. 1930 Studies on cerebrospinal fluid circulation by a new method. *Arch. Neurol. and Psychiat.* (Chicago) Vol.33, pp. 130-151.
- SEPP, E. 1929 *Die dynamik der blutzirkulation*. Berlin: Springer.
- SGOUROS, S. and WILLIAMS, B. 1995 A critical appraisal of drainage in syringomyelia. *J. Neurosurg.*, Vol 82, pp. 1-10.
- SHADY, W., METCALFE, R. A. and BUTLER, P. 1987 The incidence of craniocervical bony anomalies in the adult Chiari malformation. *J. Neurol. Sci.*, Vol. 82, pp. 193-203.
- SHALTENBRAND, G and BAILEY, P 1928 Die perivaskuläre Piaamembran des Gehirns. *J. Physiol. Neurol. Lpz*, Vol. 35, pp. 199, 236.
- SHAPIRO, H. M. 1975 Intracranial hypertension: therapeutic and anaesthetic considerations. *Anaesthesiology*, Vol. 43, pp. 445-471.
- SHAPIRO, A. H. 1977a Physiological and medical aspects of flows in collapsible tubes. In *Proc. 6th Canadian Cong. Appl. Mech.*, Vancouver, pp. 883-906.
- SHAPIRO, A. H. 1977b Steady flow in collapsible tubes. *J. Biomech. Eng.*, Vol. 99, pp. 126-147.
- SHAPIRO, A. H., ELAD, D. AND KAMM, R. D. 1987 Choking phenomena in a lung-like model. *J. of Biomechanical Engineering*, Vol. 109, pp. 1-9.
- SHULMAN, K., YARNELL, P. and RANSOHOFF, J. 1964 Dural sinus pressure: in normal and hydrocephalic dogs. *Archives of Neurology*, Vol. 10, pp. 575-580.
- SMALL, J. D. and SHERIDAN, M. D. 1996 Research priorities for syringomyelia (A NINDS Workshop) 1994. *Neurology*, Vol. 46, pp. 577-582.
- SOREK, S., BEAR, J. and KARNI, Z. 1988a Intracranial compartment pulse-wave simulation. *Mathematical Biosciences*, Vol. 89, pp. 149-159.

SOREK, S., BEAR, J. and KARNI, Z. 1988b A non-steady compartmental flow model of the cerebrovascular system. *J Biomech.*, Vol. 21, pp. 695-704.

SOREK, S., BEAR, J. and KARNI, Z. 1989 Resistances and compliances of a compartmental model of the cerebrovascular system. *Annals of Biomed. Eng.*, Vol. 17, pp. 1-12.

STRONG, R. M., GREEN, L. D. and OLOVERIO, J. V. 1926 The lateral aperture of the fourth ventricle in man. *Anatomy Rec.*, Vol. 32, pp. 223.

WEED, L. H. 1935 Certain anatomic and physiological aspects of the meninges and cerebrospinal fluid. *Brain*, Vol. 58, pp. 383-397.

WELCH, K. and POLLAY, M. 1963 The spinal arachnoid villi of the monkeys. *Cercopithecus aethiops sabaeus and Macaca irus. Anat. Rec.*, Vol. 145, pp. 43-46.

WEST, R. J. and WILLIAMS, B. 1980 Radiographic studies of the ventricles in syringomyelia. *Neuroradiology*, Vol. 20, pp. 5-16.

WESTON, P. G. 1921 Phenole sulphonephthalein absorption from subarachnoid space in paresis. *Arch. Neurol. Psychiatr.* Chicago, Vol. 5, p. 58.

WHITHAM, G. B. 1974 *Linear and nonlinear waves*. Wiley, pp. 164-167.

WILLIAMS, B. 1974 A demonstration analogue for ventricular and intraspinal dynamics (DAVID). *J. Neurol. Sci.*, Vol. 23, pp. 445-461.

WILLIAMS, B. 1975 Cerebrospinal fluid pressure-gradients in spina bifida cystica, with special reference to the Arnold-Chiari malformation and aqueductal stenosis. *Dev. Med. Child Neurol.* (Suppl. 35) Vol. 17, pp. 138-150.

WILLIAMS, B. 1976 Cerebrospinal fluid pressure changes in response to coughing. *Brain*, Vol. 99, pp. 331-346.

WILLIAMS, B. 1977a Difficult labour as a cause of communicating syringomyelia. *Lancet* ii: pp. 51-53.

WILLIAMS, B. 1977b On the pathogenesis of Chiari malformation. *Z Kinderchir*, Vol. 22, pp. 533-553.

- WILLIAMS, B. 1979 Orthopaedic features in the presentation of syringomyelia. *J. Bone Joint Surg.*, Vol. 61 B, pp. 314-323.
- WILLIAMS, B. 1980 Cough headache due to craniospinal pressure dissociation. *Arch Neurol.* (Chicago), Vol. 37, pp. 226-230.
- WILLIAMS, B. 1981 Simultaneous cerebral and spinal fluid pressure recordings. 2. Cerebrospinal dissociation with lesions at the foramen magnum. *Acta Neurochir* (Wien), Vol. 59, pp. 123-142.
- WILLIAMS, B. 1986a Progress in syringomyelia. *Neurol. Res.*, Vol. 8, pp. 130-145.
- WILLIAMS, B. 1986b Surgery of arachnoid pouches. *Z Kinderchir*, Vol. 41, pp. 18-21.
- WILLIAMS, B. 1990a Post-traumatic syringomyelia. An update. *Paraplegia*, Vol. 28, pp. 296-313.
- WILLIAMS, B. 1990b Syringomyelia. *Neurosurgery Clinics of North America*, Vol. 1, No. 3, pp. 653-685.
- WILLIAMS, B. 1993 Surgery for hindbrain related syringomyelia. *Adv. and Tech. Standarts in Neurosurgery*, Vol. 20, pp. 107-164.
- WOOLAM, D. H. M. and MILLEN, J. W. 1954 Perivascular spaces of the mammalian central nervous system. *Biol. Rev*, Vol. 29, pp. 251-283.
- WOOLAM, D. H. M. and MILLEN, J. W. 1955 The perivascular spaces of the mammalian central nervous system and their relation to the peineuronal and subarachnoid spaces. *J. Anat. London*, Vol. 89, pp. 193-200.
- WOOLAM, D. H. M. and MILLEN, J. W. 1962 *The anatomy of the cerebrospinal fluid*. Oxford University Press, London.
- ZAKERI, A., GLASAUER, F. E. and EGNATCHIK J. G. 1995 Familial syringomyelia: case report and review of the literature. *Surg. Neurol.*, Vol. 44, pp. 48-53.
- ZUKROW, M. J. and HOFFMAN, J. D. 1976 *Gaz Dynamics*. Volumes 1 & 2. John Wiley and Sons, Inc.

A.1 TABLES OF CHAPTER 2

	CSF mg. per 100 ml.	Blood Plasma mg. per 100 ml.
Protein	16 to 38	6300 to 8500
Sugar	45 to 80	80 to 120
Amino acids	1.5 to 3	4.5 to 9
Creatinine	0.5 to 2.2	0.7 to 2
Uric acid	0.4 to 2.8	2.9 to 6.9
Urea	5 to 39	22 to 42
Cholesterol	trace	100 to 150
Chloride (NaCl)	700 to 750	560 to 630
Phosphate (inorganic)	1.2 to 2.1	2 to 5
Sodium	325	326
Potassium	12 to 17	12 to 20
Calcium	4.5 to 7	9 to 11
Magnesium	3 to 3.6	1 to 3
Lactic acid	8 to 25	10 to 32
Specific gravity	1.0075	1.025
Hydrogen ions (pH)	7.4	7.3 to 7.5

TABLE 2.1: Comparison of normal CSF and blood plasma (after Merritt and Fremont-Smith, 1937)

Fluid	Total Proteins mg. per 100 ml.	Globulin mg. per 100 ml.	Albumin mg. per 100 ml.	Glucose mg. per 100 ml.	Cells
Ventricles	10 to 16	1 to 4	8 to 14	50 to 90	0/3 to 2/3
Cisterna Magna	16 to 20	1 to 6	14 to 16	59 to 68	0/3 to 4/3
Lumbar Cistern	20 to 24	2 to 6	14 to 18	55 to 65	0/3 to 8/3

TABLE 2.2: Variations in composition of CSF withdrawn from different sites. (from Lups and Haan, 1954).

A.2 TABLES OF CHAPTER 3

Symptom grouping	Symptom	Number
Pain (82%)	headache	52
	nuchal pain	49
	limb pain	16
	trunk pain	8
	impulse related	44
Motor symptoms (70%)	weakness	52
	wasting	16
	spasticity	12
	clumsiness	22
	drop attacks	2
Sensory symptoms (65%)	numbness	42
	paraesthesiae	27
	dissociated loss	38
	posterior column	6
	other sensory	15
Stem symptoms (39%)	diplopia	5
	oscillopsia	4
	other visual	2
	trigeminal loss	4
	deafness	3
	tinnitus	9
	giddiness	19
	voice	9
	swallowing	9
Other symptoms (39%)	gait disturbance	30
	hyperhidrosis	4
	bladder symptoms	5
	syncope	4
	sexual problems	1

TABLE 3.1: Presenting symptoms in 100 cases of symptomatic hindbrain hernia (63 syringes) (from Williams, 1993).

Hindbrain related syringomyelia 71%
Hindbrain herniation
Idiopathic herniation (Chiari type 1) 32%
Secondary to birth injury 39%
Secondary to tumours 1-2%
Bony or meningeal tumours of the posterior fossa
Tumours forming the hindbrain hernia
Intrinsic brain tumours
Secondary to bony abnormality
Basilar invagination (idiopathic or birth injury) 10%
Sclerosteosis
Rickets
Acro-osteolysis
Osteogenesis imperfecta
Associated with hydrocephalus 10%
Intracranial arachnoid pouches 2%
Dandy-Walker cysts
Early onset hydrocephalus (aqueduct stenosis)
Secondary to spina bifida (Chiari type 2) 4%
Meningeal fibrosis
Birth injury related 9%
Post-inflammatory
Post-traumatic (post-natal) 1%
Infections
Unknown causes
Non-hindbrain related cases 19%
Spinal tumours 5%
Intramedullary 3%
Cysts wholly or partly within the tumour
Cysts outside the tumour
Extramedullary tumours, including disc disease
Meningeal fibrosis 15%
Post-inflammatory
Pyogenic meningitis
Epidural abscess
Post-traumatic 12%
Tuberculous meningitis
Myodil (pantopaque) 1%
Secondary to spinal body deformities
Post-traumatic 11%
Tuberculous bone disease
Idiopathic scoliosis

TABLE 3.2: Classification of syringomyelia according to presumed cause.
Percentages given in parentheses are from a database of syringomyelia and related disease. Diagnoses with no percentage given have an incidence of less than 1%. They do not add up to 100% because of intersections. Some factors such as peri-natal or post-natal head injury are difficult to interpret. Others such as a hydrocephalus or basilar impression are matters of degree. (from Williams, 1993).

A.3 TABLES OF CHAPTER 6

REGION	ΔP	P_A	P_B	U_A	U_B	$\alpha = A_A / A_T$
0	0	$\rho C_o \varepsilon_o$	$\rho C_o \varepsilon_o$	0	0	α_o
1	$\frac{-\rho C_o}{1-\alpha_o}(\varepsilon_o - \varepsilon)$	$\rho C_o \varepsilon$	$\frac{\rho C_o}{1-\alpha_o}(\varepsilon_o - \alpha_o \varepsilon)$	$-(\varepsilon_o - \varepsilon)$	$\frac{\alpha_o}{1-\alpha_o}(\varepsilon_o - \varepsilon)$	$\alpha_o + D\Delta P_1$
2	$\frac{-2\rho C_o}{1-\alpha_o}(\varepsilon_o - \varepsilon)$	$\rho C_o(2\varepsilon - \varepsilon_o)$	$\frac{\rho C_o}{1-\alpha_o}(\varepsilon_o(1+\alpha_o) - 2\alpha_o \varepsilon)$	0	0	$\alpha_o + 2D\Delta P_1$
3	0	$\rho C_o \varepsilon_o$	$\rho C_o \varepsilon_o$	0	0	α_o
4	$\frac{-\rho C_o}{1-\alpha_o}(\varepsilon_o - \varepsilon)$	$\rho C_o \varepsilon$	$\frac{\rho C_o}{1-\alpha_o}(\varepsilon_o - \alpha_o \varepsilon)$	$\varepsilon_o - \varepsilon$	$\frac{-\alpha_o}{1-\alpha_o}(\varepsilon_o - \varepsilon)$	$\alpha_o + D\Delta P_1$
5	0	$\rho C_o \varepsilon_o$	$\rho C_o \varepsilon_o$	0	0	α_o

TABLE 6.1: Analytical results for a pressure pulse reflection (note that $\varepsilon_o > \varepsilon$).

REGION	ΔP (Pa)	P_A (Pa)	P_B (Pa)	U_A (m/s)	U_B (m/s)	$\alpha = A_A / A_T$
0	0	8.00E+02	8.00E+02	0	0	8.89E-01
1	-2.70E+03	5.00E+02	3.20E+03	-6.00E-02	4.80E-01	8.78E-01
2	-5.40E+03	2.00E+02	5.60E+03	0	0	8.68E-01
3	0	8.00E+02	8.00E+02	0	0	8.89E-01
4	-2.70E+03	5.00E+02	3.20E+03	6.00E-02	-4.80E-01	8.78E-01
5	0	8.00E+02	8.00E+02	0	0	8.89E-01

TABLE 6.2: Numerical results for a pressure pulse reflection.

x (m)	t (s)
0.00E+00	0.00E+00
9.00E-01	1.77E-01
1.00E+00	1.97E-01
8.98E-01	1.78E-01
9.93E-01	1.98E-01
1.00E+00	2.00E-01
8.96E-01	1.78E-01
9.85E-01	2.00E-01
9.92E-01	2.02E-01
1.00E+00	2.03E-01
8.94E-01	1.78E-01
9.76E-01	2.01E-01
9.83E-01	2.03E-01
9.91E-01	2.05E-01
1.00E+00	2.08E-01
8.92E-01	1.79E-01
9.66E-01	2.03E-01
9.73E-01	2.05E-01
9.80E-01	2.08E-01
9.89E-01	2.10E-01
1.00E+00	2.14E-01
8.92E-01	1.97E-01
9.30E-01	2.10E-01
9.38E-01	2.12E-01
9.47E-01	2.15E-01
9.57E-01	2.18E-01

TABLE 6.3: Coordinates of the points in the (x,t) diagram (5 characteristics).

POINT	ΔP (m)	P_A (Pa)	P_B (Pa)	U_A (m/s)	U_B (m/s)	$\alpha = A_A / A_T$	C (m/s)
0	0.00E+00	4.00E+02	4.00E+02	0.00E+00	0.00E+00	9.72E-01	5.00E+00
1	1.60E+03	4.43E+02	-1.16E+03	-8.46E-03	3.16E-01	9.74E-01	4.85E+00
2	2.55E+00	4.00E+02	3.98E+02	0.00E+00	0.00E+00	9.72E-01	5.00E+00
3	3.20E+03	4.83E+02	-2.72E+03	2.59E-04	-1.04E-02	9.76E-01	4.69E+00
4	1.65E+03	4.44E+02	-1.21E+03	8.73E-03	-3.27E-01	9.74E-01	4.84E+00
5	3.25E+03	4.85E+02	-2.77E+03	0.00E+00	0.00E+00	9.76E-01	4.68E+00
6	4.80E+03	5.21E+02	-4.28E+03	8.09E-03	-3.50E-01	9.77E-01	4.52E+00
7	3.31E+03	4.86E+02	-2.82E+03	1.65E-02	-6.67E-01	9.76E-01	4.68E+00
8	4.85E+03	5.22E+02	-4.33E+03	7.84E-03	-3.40E-01	9.78E-01	4.52E+00
9	6.39E+03	5.55E+02	-5.83E+03	0.00E+00	0.00E+00	9.79E-01	4.35E+00
10	6.40E+03	5.55E+02	-5.85E+03	1.50E-02	-7.03E-01	9.79E-01	4.35E+00
11	4.96E+03	5.25E+02	-4.43E+03	2.34E-02	-1.02E+00	9.78E-01	4.50E+00
12	6.44E+03	5.56E+02	-5.89E+03	1.48E-02	-6.94E-01	9.79E-01	4.34E+00
13	7.92E+03	5.85E+02	-7.34E+03	6.94E-03	-3.54E-01	9.81E-01	4.18E+00
14	9.40E+03	6.12E+02	-8.78E+03	0.00E+00	0.00E+00	9.82E-01	4.00E+00
15	8.00E+03	5.86E+02	-7.41E+03	2.09E-02	-1.07E+00	9.81E-01	4.17E+00
16	6.62E+03	5.60E+02	-6.06E+03	2.93E-02	-1.39E+00	9.79E-01	4.33E+00
17	8.04E+03	5.86E+02	-7.45E+03	2.07E-02	-1.06E+00	9.81E-01	4.16E+00
18	9.45E+03	6.11E+02	-8.84E+03	1.29E-02	-7.24E-01	9.82E-01	4.00E+00
19	1.09E+04	6.34E+02	-1.02E+04	6.03E-03	-3.70E-01	9.84E-01	3.82E+00
20	1.23E+04	6.55E+02	-1.16E+04	0.00E+00	-1.07E+00	9.86E-01	3.64E+00
21	8.00E+03	5.86E+02	-7.41E+03	2.09E-02	0.00E+00	9.81E-01	4.17E+00
22	6.62E+03	5.60E+02	-6.06E+03	2.93E-02	-1.39E+00	9.79E-01	4.33E+00
23	8.04E+03	5.86E+02	-7.45E+03	2.07E-02	-1.06E+00	9.81E-01	4.16E+00
24	9.45E+03	6.11E+02	-8.84E+03	1.29E-02	-7.24E-01	9.82E-01	4.00E+00
25	1.09E+04	6.34E+02	-1.02E+04	6.03E-03	-3.70E-01	9.84E-01	3.82E+00

TABLE 6.4: Fluid properties at points defined in (x,t) diagram.

A.4 TABLES OF CHAPTER 7

ZONE: Flow state	1: Before incident wave	2: After incident and before reflected	R: After reflected wave	T: Transmitted wave
VELOCITY	$V_{A1} = V_{B1} = 0$	$U_{A2} = ?$ $U_{B2} = ?$	$U_{AR} = 0$ $U_{BR} = ?$	$U_{AT} = ?$ $U_{BT} = ?$
PRESSURE	$P_{A1} = P_{B1} = 0$	$P_{A2} = ?$ $P_{B2} = ?$	$P_{AR} = ?$ $P_{BR} = ?$	$P_{AT} = ?$ $P_{BT} = ?$
PRESSURE DIFFERENCE	$\Delta P_1 = 0$	$\Delta P_I = ?$	$\Delta P_R = ?$	$\Delta P_T = ?$
SHOCK-LIKE WAVE SPEED	$V_{SI} : \text{given}$		$V_{SR} = ?$	$V_{ST} = ?$

TABLE 7.1: Shock-like wave unknowns of the problem.

ZONE: Flow state	1: Before incident wave	2: After incident and before reflected	R: After reflected wave	T: Transmitted wave
VELOCITY	$V_{A1} = V_{B1} = 0$	$U_{A2} : \text{eq. 9.12}$ $U_{B2} : \text{eq. 9.13}$	$U_{AR} = 0$ $U_{BR} = 0$	$U_{AT} = U_{A1} = 0$ $U_{BT} = U_{B1} = 0$
PRESSURE	$P_{A1} = P_{B1} = 0$	$P_{A2} : \text{eq. 9.14}$ $P_{B2} : \text{eq. 9.15}$	$P_{AR} : \text{eq. 9.23}$ $P_{BR} : \text{eq. 9.24}$	$P_{AT} = P_{A1} = 0$ $P_{BT} = P_{B1} = 0$
PRESSURE DIFFERENCE	$\Delta P_1 = 0$	$\Delta P_I : \text{eq. 9.9}$	$\Delta P_R : \text{eq. 9.9}$	$\Delta P_T = \Delta P_1 = 0$
SHOCK-LIKE WAVE SPEED	$V_{SI} : \text{given}$		$V_{SR} : \text{eq. 9.21}$	$V_{ST} = 0$

TABLE 7.2: Shock-like wave relations.

v_s (m/s)	ΔP (Pa)	P_A (Pa)	P_B (Pa)	U_A (m/s)	U_B (m/s)	α
Before shock	0	400	400	0.001	0	0.88888
After shock						
5.10E+00	-7.31E+01	3.92E+02	4.66E+02	-6.58E-04	1.32E-02	8.89E-01
5.15E+00	-2.36E+02	3.73E+02	6.15E+02	-4.39E-03	4.28E-02	8.88E-01
5.20E+00	-3.99E+02	3.53E+02	7.67E+02	-8.23E-03	7.27E-02	8.87E-01
5.25E+00	-5.62E+02	3.32E+02	9.22E+02	-1.22E-02	1.03E-01	8.87E-01
5.30E+00	-7.27E+02	3.10E+02	1.08E+03	-1.62E-02	1.34E-01	8.86E-01
5.35E+00	-8.92E+02	2.87E+02	1.24E+03	-2.03E-02	1.65E-01	8.85E-01
5.40E+00	-1.06E+03	2.63E+02	1.41E+03	-2.45E-02	1.96E-01	8.85E-01
5.45E+00	-1.23E+03	2.39E+02	1.57E+03	-2.89E-02	2.28E-01	8.84E-01
5.50E+00	-1.40E+03	2.13E+02	1.74E+03	-3.33E-02	2.60E-01	8.83E-01
5.55E+00	-1.57E+03	1.86E+02	1.92E+03	-3.79E-02	2.93E-01	8.83E-01
5.60E+00	-1.73E+03	1.58E+02	2.09E+03	-4.25E-02	3.25E-01	8.82E-01
5.65E+00	-1.91E+03	1.28E+02	2.27E+03	-4.73E-02	3.59E-01	8.81E-01
5.70E+00	-2.08E+03	9.81E+01	2.45E+03	-5.21E-02	3.92E-01	8.81E-01
5.75E+00	-2.25E+03	6.65E+01	2.64E+03	-5.71E-02	4.26E-01	8.80E-01
5.80E+00	-2.43E+03	3.37E+01	2.83E+03	-6.22E-02	4.61E-01	8.79E-01
5.85E+00	-2.60E+03	-3.27E-01	3.02E+03	-6.74E-02	4.96E-01	8.79E-01
5.90E+00	-2.78E+03	-3.57E+01	3.21E+03	-7.28E-02	5.31E-01	8.78E-01
5.95E+00	-2.96E+03	-7.24E+01	3.41E+03	-7.83E-02	5.66E-01	8.77E-01
6.00E+00	-3.14E+03	-1.11E+02	3.61E+03	-8.38E-02	6.02E-01	8.77E-01
6.05E+00	-3.32E+03	-1.50E+02	3.81E+03	-8.95E-02	6.38E-01	8.76E-01
6.10E+00	-3.50E+03	-1.91E+02	4.02E+03	-9.54E-02	6.75E-01	8.75E-01
6.15E+00	-4.84E+03	-4.40E+02	5.08E+03	-1.34E-01	9.03E-01	8.70E-01
6.20E+00	-5.52E+03	-5.80E+02	5.60E+03	-1.55E-01	1.02E+00	8.67E-01
6.25E+00	-6.10E+03	-7.07E+02	6.05E+03	-1.73E-01	1.11E+00	8.65E-01
6.30E+00	-6.65E+03	-8.33E+02	6.46E+03	-1.91E-01	1.20E+00	8.63E-01
6.35E+00	-7.16E+03	-9.54E+02	6.84E+03	-2.08E-01	1.29E+00	8.61E-01
6.40E+00	-7.65E+03	-1.08E+03	7.20E+03	-2.24E-01	1.37E+00	8.59E-01
6.45E+00	-8.13E+03	-1.20E+03	7.55E+03	-2.41E-01	1.45E+00	8.57E-01

TABLE 7.3: Fluid properties after an elastic jump.

V_{si} (m/s)	V_{sr} (m/s)	ΔP_i (Pa)	ΔP_r (Pa)	P_A (Pa)	P_B (Pa)	α_R
5.05E+00	2.05E+00	-2.74E+02	-6.34E+02	3.89E+02	4.83E+02	8.88E-01
5.10E+00	3.50E+00	-3.22E+02	-7.82E+02	3.93E+02	4.51E+02	8.88E-01
5.15E+00	4.64E+00	-7.66E+02	-1.57E+03	3.99E+02	3.91E+02	8.86E-01
5.20E+00	4.70E+00	-1.07E+03	-2.16E+03	3.96E+02	3.92E+02	8.85E-01
5.25E+00	4.91E+00	-1.41E+03	-2.84E+03	3.98E+02	3.47E+02	8.83E-01
5.30E+00	5.02E+00	-1.71E+03	-3.47E+03	3.99E+02	3.13E+02	8.82E-01
5.35E+00	5.05E+00	-2.03E+03	-4.11E+03	3.96E+02	2.93E+02	8.81E-01
5.40E+00	5.06E+00	-2.37E+03	-4.86E+03	3.91E+02	2.75E+02	8.80E-01
5.45E+00	5.15E+00	-2.69E+03	-5.51E+03	3.91E+02	2.22E+02	8.78E-01
5.50E+00	5.17E+00	-3.04E+03	-6.22E+03	3.86E+02	1.94E+02	8.77E-01
5.55E+00	5.17E+00	-3.37E+03	-6.95E+03	3.79E+02	1.73E+02	8.76E-01
5.60E+00	5.19E+00	-3.73E+03	-7.69E+03	3.71E+02	1.40E+02	8.74E-01
5.65E+00	5.20E+00	-4.06E+03	-8.42E+03	3.63E+02	1.11E+02	8.73E-01
5.70E+00	5.22E+00	-4.40E+03	-9.15E+03	3.54E+02	7.45E+01	8.72E-01
5.75E+00	5.23E+00	-4.75E+03	-9.93E+03	3.43E+02	3.97E+01	8.70E-01
5.80E+00	5.25E+00	-5.09E+03	-1.07E+04	3.31E+02	1.32E+00	8.69E-01
5.85E+00	5.27E+00	-5.45E+03	-1.15E+04	3.19E+02	-4.24E+01	8.67E-01
5.90E+00	5.27E+00	-5.81E+03	-1.23E+04	3.02E+02	-7.14E+01	8.66E-01
5.95E+00	5.29E+00	-6.16E+03	-1.31E+04	2.87E+02	-1.20E+02	8.65E-01
6.00E+00	5.29E+00	-6.52E+03	-1.39E+04	2.68E+02	-1.55E+02	8.63E-01
6.05E+00	5.30E+00	-6.88E+03	-1.47E+04	2.48E+02	-1.92E+02	8.62E-01
6.10E+00	5.31E+00	-7.25E+03	-1.55E+04	2.26E+02	-2.33E+02	8.60E-01
6.15E+00	5.32E+00	-7.61E+03	-1.64E+04	2.03E+02	-2.77E+02	8.59E-01
6.20E+00	5.33E+00	-7.99E+03	-1.72E+04	1.77E+02	-3.19E+02	8.57E-01
6.25E+00	5.33E+00	-8.37E+03	-1.81E+04	1.49E+02	-3.62E+02	8.56E-01
6.30E+00	5.34E+00	-8.73E+03	-1.90E+04	1.18E+02	-4.02E+02	8.54E-01
6.35E+00	5.34E+00	-9.11E+03	-1.99E+04	8.56E+01	-4.50E+02	8.53E-01
6.40E+00	5.35E+00	-9.50E+03	-2.08E+04	4.97E+01	-4.90E+02	8.51E-01
6.45E+00	5.35E+00	-9.88E+03	-2.18E+04	1.24E+01	-5.39E+02	8.50E-01
6.50E+00	5.36E+00	-1.03E+04	-2.27E+04	-2.85E+01	-5.83E+02	8.48E-01

TABLE 7.4: Fluid properties after the reflected elastic jump ($\alpha_o = 0.93$).

α_s	ap1	ap2	ap3
5.40E-01	-1.85E-02	-2.17E-02	-1.61E-03
5.50E-01	-1.82E-02	-2.22E-02	-2.02E-03
5.60E-01	-1.79E-02	-2.27E-02	-2.43E-03
5.70E-01	-1.75E-02	-2.33E-02	-2.86E-03
5.80E-01	-1.72E-02	-2.38E-02	-3.28E-03
5.90E-01	-1.69E-02	-2.44E-02	-3.72E-03
6.00E-01	-1.67E-02	-2.50E-02	-4.17E-03
6.10E-01	-1.64E-02	-2.56E-02	-4.62E-03
6.20E-01	-1.61E-02	-2.63E-02	-5.09E-03
6.30E-01	-1.59E-02	-2.70E-02	-5.58E-03
6.40E-01	-1.56E-02	-2.78E-02	-6.07E-03
6.50E-01	-1.54E-02	-2.86E-02	-6.59E-03
6.60E-01	-1.52E-02	-2.94E-02	-7.13E-03
6.70E-01	-1.49E-02	-3.03E-02	-7.69E-03
6.80E-01	-1.47E-02	-3.12E-02	-8.27E-03
6.90E-01	-1.45E-02	-3.23E-02	-8.88E-03
7.00E-01	-1.43E-02	-3.33E-02	-9.52E-03
7.10E-01	-1.41E-02	-3.45E-02	-1.02E-02
7.20E-01	-1.39E-02	-3.57E-02	-1.09E-02
7.30E-01	-1.37E-02	-3.70E-02	-1.17E-02
7.40E-01	-1.35E-02	-3.85E-02	-1.25E-02
7.50E-01	-1.33E-02	-4.00E-02	-1.33E-02
7.60E-01	-1.32E-02	-4.17E-02	-1.43E-02
7.70E-01	-1.30E-02	-4.35E-02	-1.52E-02
7.80E-01	-1.28E-02	-4.54E-02	-1.63E-02
7.90E-01	-1.27E-02	-4.76E-02	-1.75E-02
8.00E-01	-1.25E-02	-5.00E-02	-1.87E-02
8.10E-01	-1.23E-02	-5.26E-02	-2.01E-02
8.20E-01	-1.22E-02	-5.55E-02	-2.17E-02
8.30E-01	-1.20E-02	-5.88E-02	-2.34E-02
8.40E-01	-1.19E-02	-6.25E-02	-2.53E-02
8.50E-01	-1.18E-02	-6.66E-02	-2.74E-02
8.60E-01	-1.16E-02	-7.14E-02	-2.99E-02
8.70E-01	-1.15E-02	-7.69E-02	-3.27E-02
8.80E-01	-1.14E-02	-8.33E-02	-3.60E-02
8.90E-01	-1.12E-02	-9.09E-02	-3.98E-02
9.00E-01	-1.11E-02	-1.00E-01	-4.44E-02
9.10E-01	-1.10E-02	-1.11E-01	-5.00E-02
9.20E-01	-1.09E-02	-1.25E-01	-5.70E-02
9.30E-01	-1.08E-02	-1.43E-01	-6.60E-02
9.40E-01	-1.06E-02	-1.67E-01	-7.80E-02
9.50E-01	-1.05E-02	-2.00E-01	-9.47E-02
9.60E-01	-1.04E-02	-2.50E-01	-1.20E-01
9.70E-01	-1.03E-02	-3.33E-01	-1.61E-01
9.80E-01	-1.02E-02	-5.00E-01	-2.45E-01
9.90E-01	-1.01E-02	-1.00E+00	-4.95E-01

TABLE 7.5: Validity of the small perturbation theory.

A.5 TABLE OF CHAPTER 9

Region	ΔP (Pa)	P_A (Pa)	P_B (Pa)	U_A (m/s)	U_B (m/s)	α	C (m/s)	V_s (m/s)
0	0	500	500	0	0	0.9100	5.0000	0
1	-1862	308.8	2171	-0.0361	0.3397	0.9039	5.1490	5.3520
2	-3781	501.1	4282	0	0	0.8976	5.2970	-5.1930
3	-1241	367.6	1609	-0.0240	0.2308	0.9059	5.1000	0
4	-3112	171.4	3284	0.0127	-0.1141	0.8998	5.2460	-5.4070
5	-2450	237	2687	0	0	0.9020	5.1950	0
6	-620.7	425.3	1046	-0.0122	0.1203	0.9080	5.0510	0
7	-2485	231	2716	0.0242	-0.2227	0.9019	5.1980	-5.3890
8	-1829	294.6	2124	0.0115	-0.1086	0.9040	5.1470	0
9	-1214	353	1567	0	0	0.9060	5.0980	0
10	0	481.8	481.8	-0.0008	0.0081	0.9100	5.0000	0
11	-1859	289.4	2148	0.0354	-0.3327	0.9039	5.1490	-5.3710
12	-1209	351	1560	0.0227	-0.2186	0.9060	5.0980	0
13	-599.6	407.5	1007	0.0111	-0.1100	0.9080	5.0490	0
14	9.14	462.9	453	0	0	0.9100	4.9990	0

TABLE 9.1: Fluid properties in each region for a pressure pulse reflection.

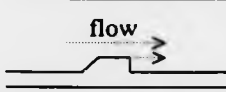
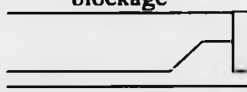
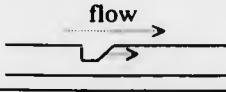
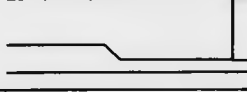
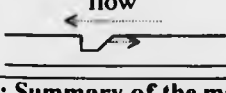
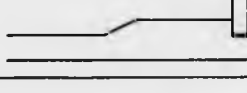
<p>positive bulge propagating with flow</p> 	<p>⇒ Temporary high positive bulge at blockage</p> 
<p>negative bulge propagating with flow</p> 	<p>⇒ Permanent negative overshooting</p> 
<p>negative bulge propagating against flow</p> 	<p>⇒ Permanent positive overshooting</p> 

TABLE 9.2: Summary of the main results

B.1 FIGURES OF CHAPTER 2

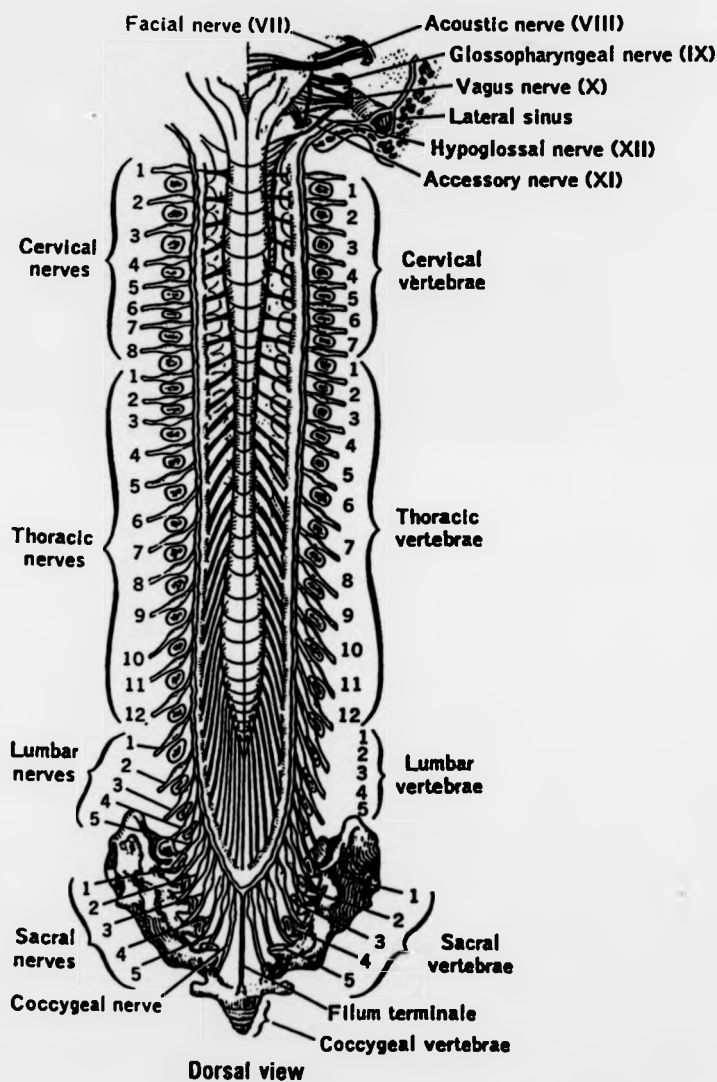


FIGURE 2.1: Gross aspect of the spinal cord and lower brain stem viewed from the dorsal side with bone and meninges removed (from House and Pansky, 1967, p. 57).

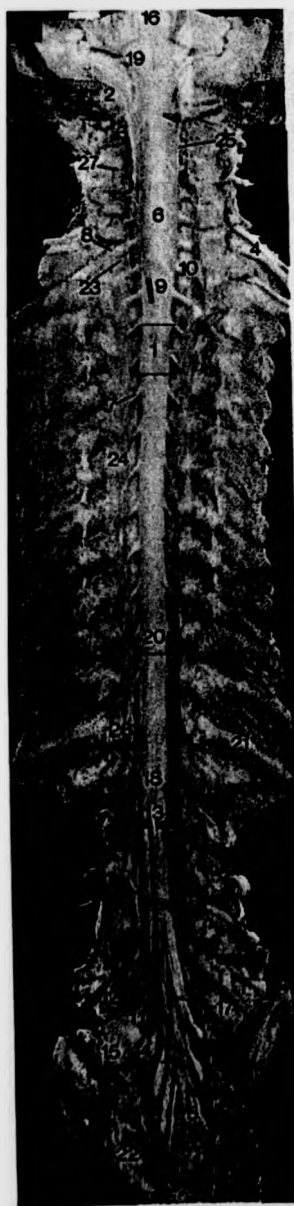
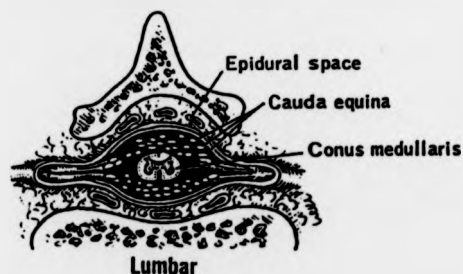
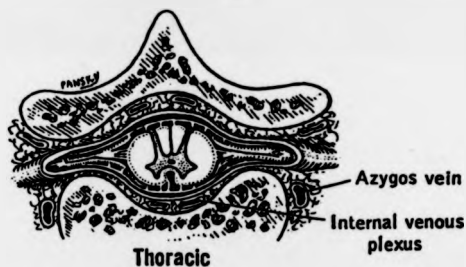
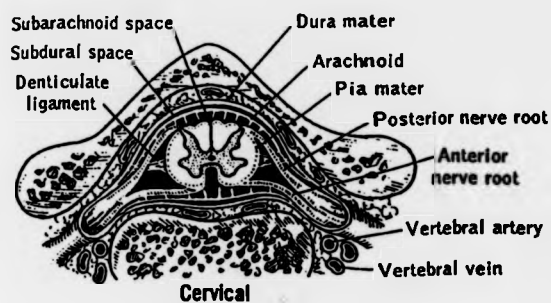
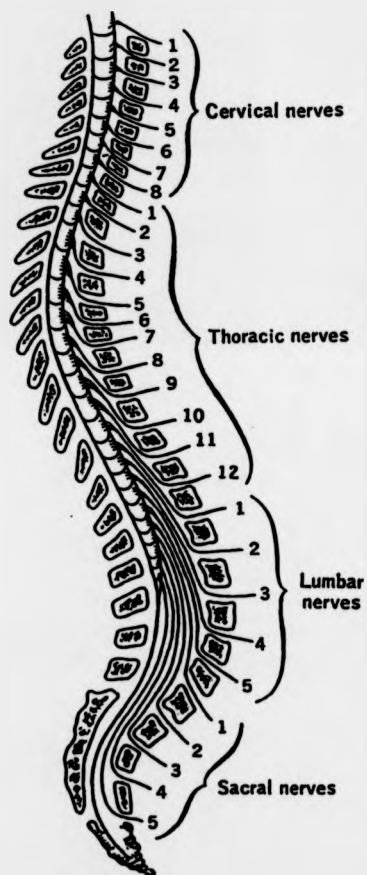


FIGURE 2.2: Dissection of the adult spinal cord. $\times 28$ (from England and Wakely, 1991, p. 173). (1-Arachnoid mater; 5-Caudal equina; 6- Cervical enlargement; 9- Dura mater; 13-Filum terminale; 16-Fourth ventricle; 18-Lumbar enlargement; 19- Medulla oblongata; 20-Pia mater; 22-Sacrum).



CROSS SECTIONS



Lateral view

FIGURE 23: Gross aspect of the spinal cord and nerves as related to vertebral levels seen in the sagittal plane. The relations of the cord and nerves to the meninges together with variations in size and shape of the cord at different levels is shown in a series of three cross-sections. (from House and Pansky, 1967, p. 58).

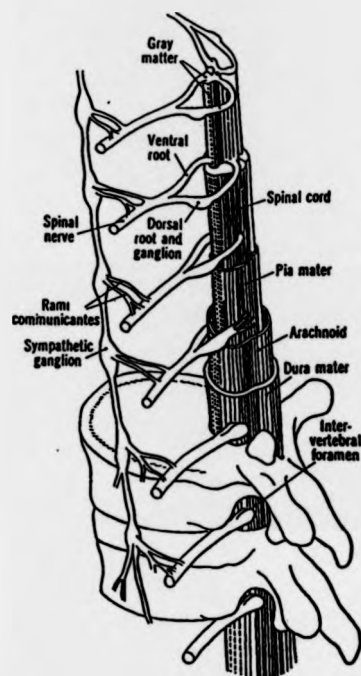


FIGURE 2.4: The spinal cord and meninges within the vertebral canal. (from Gardner, 1968, p. 32).



FIGURE 2.5: Layered dissection of the scalp, showing the meninges and the cranial vault. $\times 54$ (from England and Wakely, 1991, p. 42). (1 to 5: Five layers of scalp; 7-Cranial vault bone; 9-Dura mater; 10-Pia-arachnoid mater).

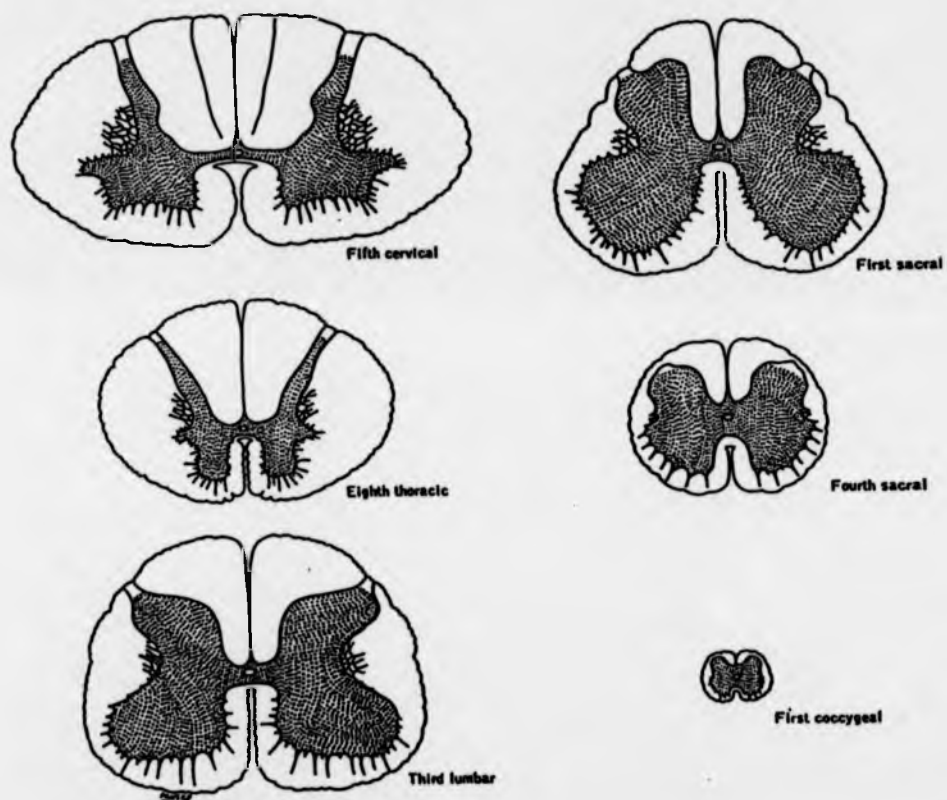


FIGURE 2.6: Transverse section of the spinal cord at different levels to show the variations in amount and configuration of the white and grey matter. (from House and Pansky, 1967, p. 60).

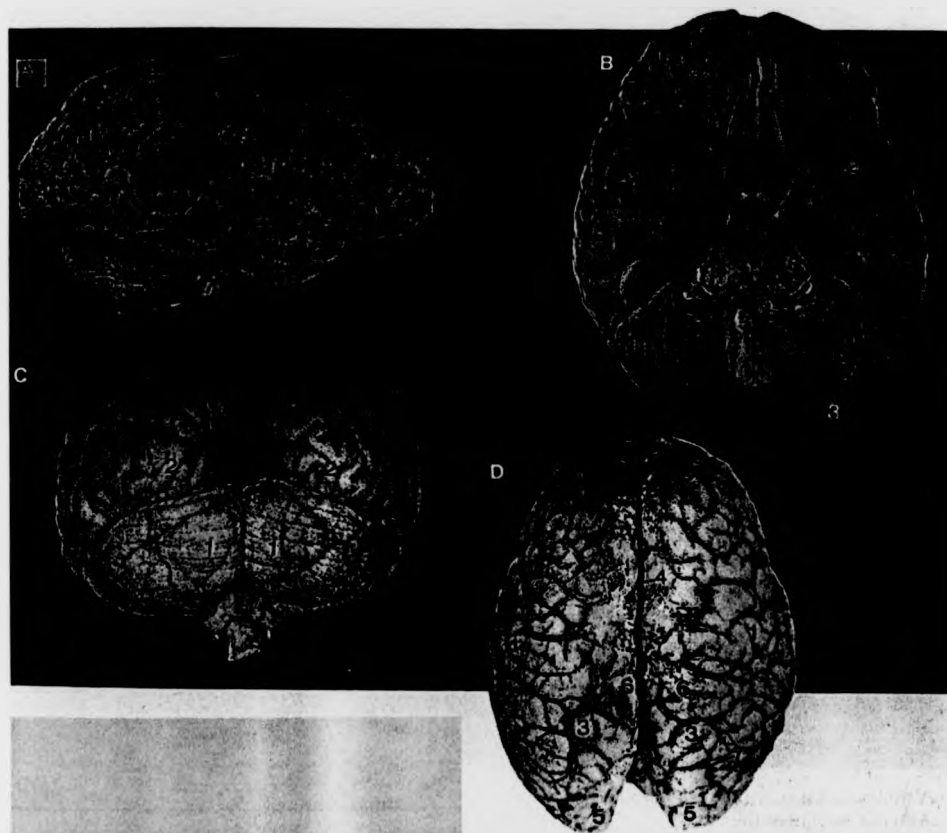


FIGURE 2.7: The brain viewed from the right (A) $\times 42$ (cerebral hemisphere: 1, 2, 3, 4), from the base (B) $\times 5$ (cerebral hemisphere: '1, 2, 3), from the back (C) $\times 42$ (occipital lobe of cerebral hemisphere: 2) and from above (D) $\times 5$ (cerebral hemisphere: 1, 2, 5, 6), to show the cerebral hemispheres. (from England and Wakely, 1991, p. 39).

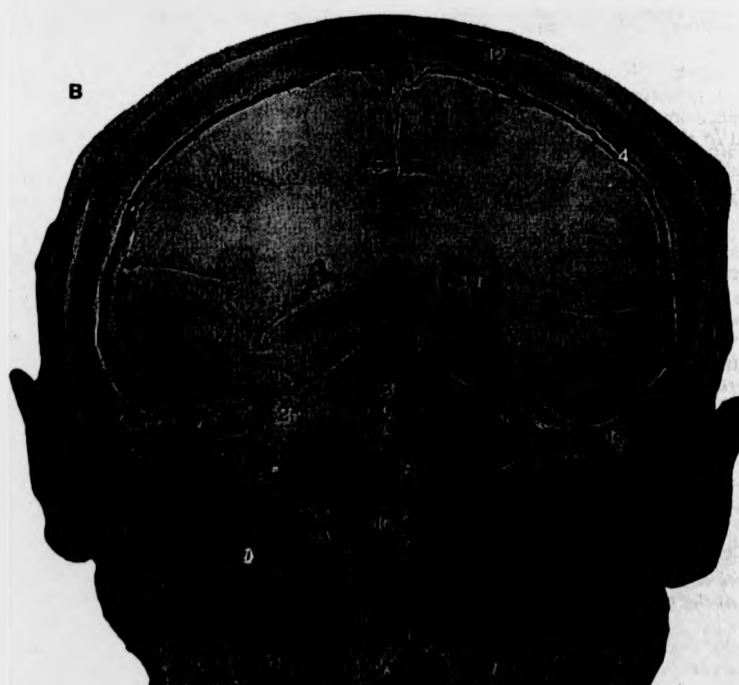
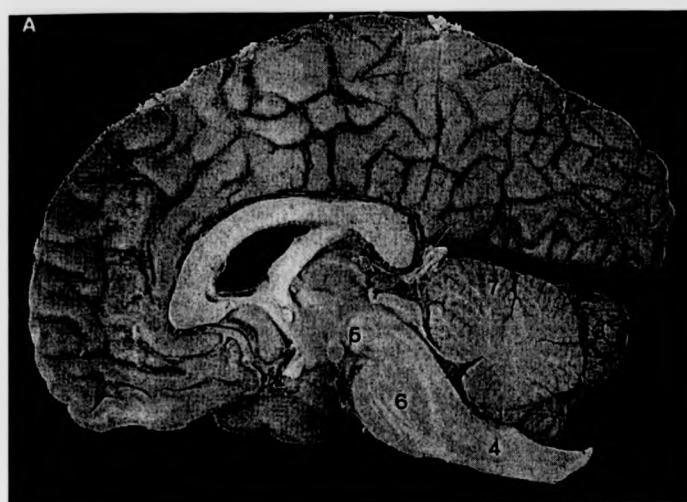


FIGURE 2.8: The cerebellum viewed in midsagittal section (A) $\times 59$ (3-Hemisphere of cerebellum, 7- Vermis of cerebellum), and coronal section (B) $\times 7$ (2-cerebellar hemisphere) (from England and Wakely, 1991, p. 162).

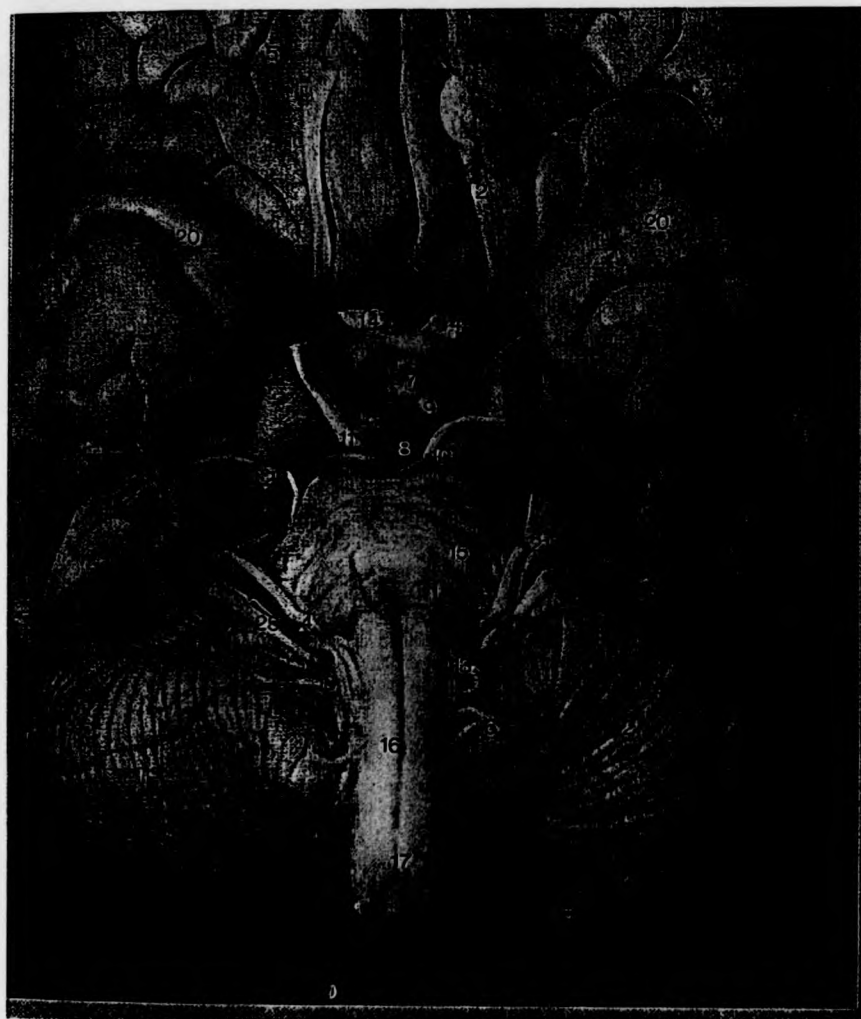


FIGURE 2.9: The brain viewed from the basal aspect to show the brainstem, $\times 1.2$ (from England and Wakely, 1991, p. 135) (15-Pons; 17-Medulla oblongata).

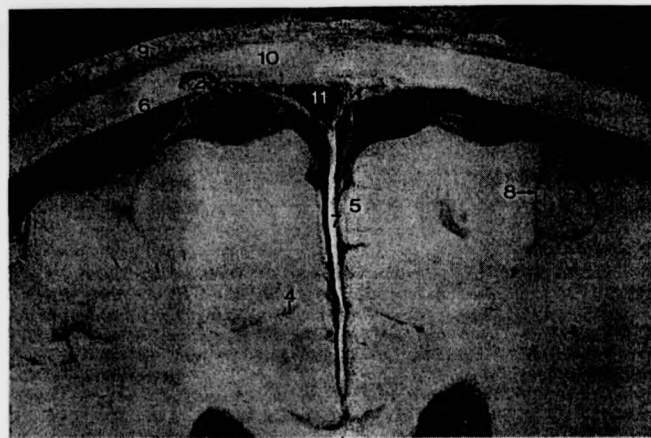


FIGURE 2.10: A coronal section of the falx cerebri, $\times 135$ (from England and Wakely, 1991, p. 42) (7-Falx cerebri).

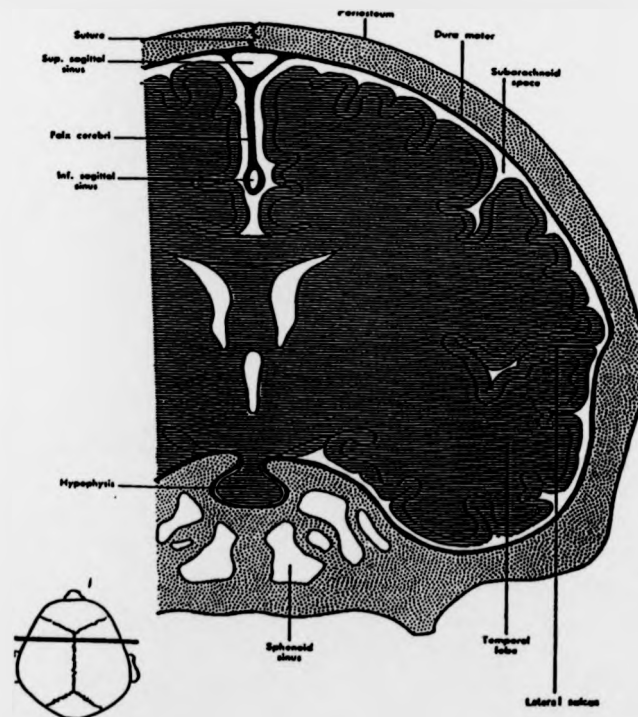


FIGURE 2.11: Diagram of a coronal section of skull and brain to show the falx cerebri. (from Gardner, 1968, p. 11).

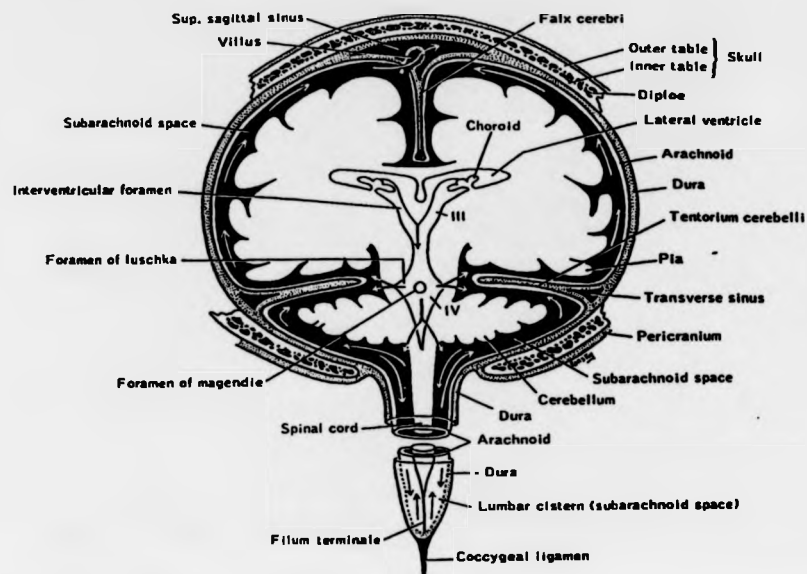


FIGURE 2.12: Diagram to illustrate the essential points relating to the production, course, and absorption of CSF. Meningeal layers are also shown. (from House and Pansky, 1967, p. 72).

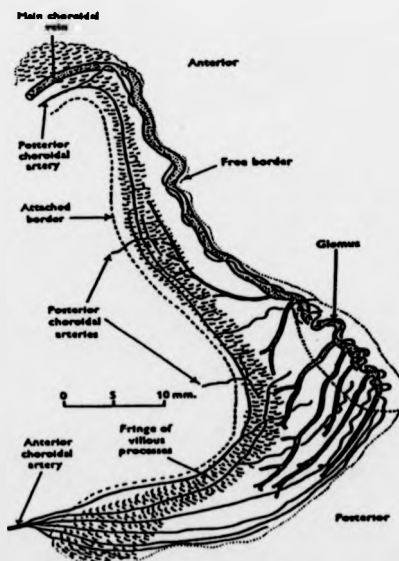


FIGURE 2.13: Diagram to illustrate the choroid plexus (from Woollam and Millen, 1962)

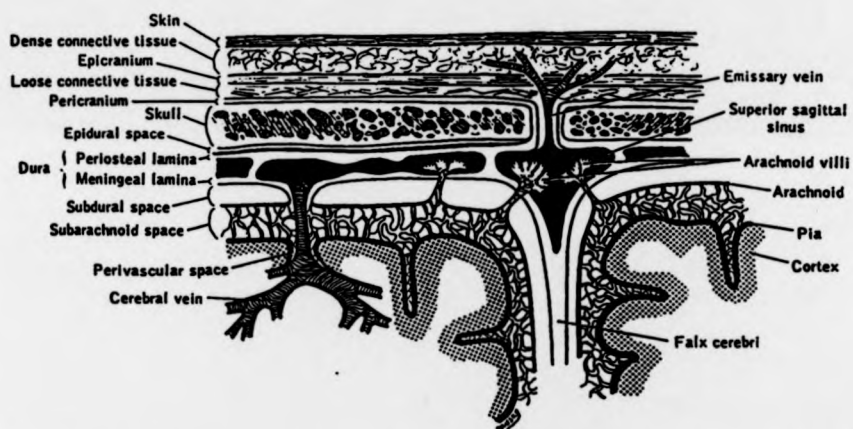


FIGURE 2.14: Diagrammatic coronal section through the head to show the relations of the arachnoid villi to the dural sinus. (from House and Pansky, 1967, p. 72).

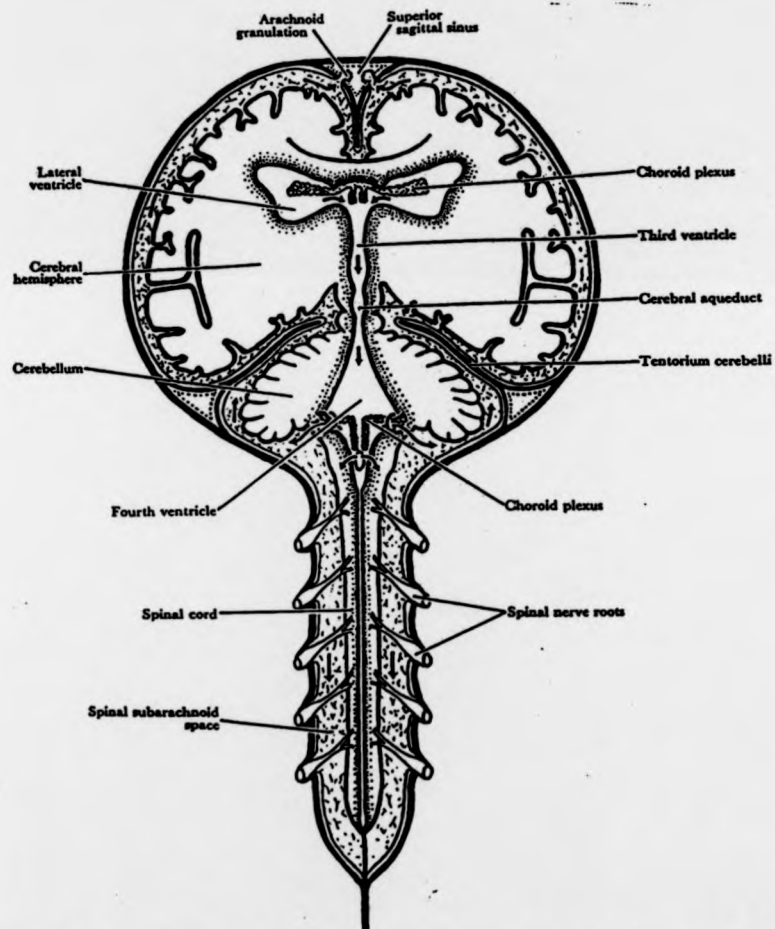


FIGURE 2.15: Diagram showing the locations of structures related with formation, route and absorption of CSF. (from Woollam and Millen, 1962)



FIGURE 2.16: A sagittal section of the head to illustrate the cisternae. $\times 56$ (from England and Wakely, 1991, p. 79) (6-Interpeduncular cisterna; 7-Lateral ventricle; 12-Pontine cisterna; 14-Spinal cord).

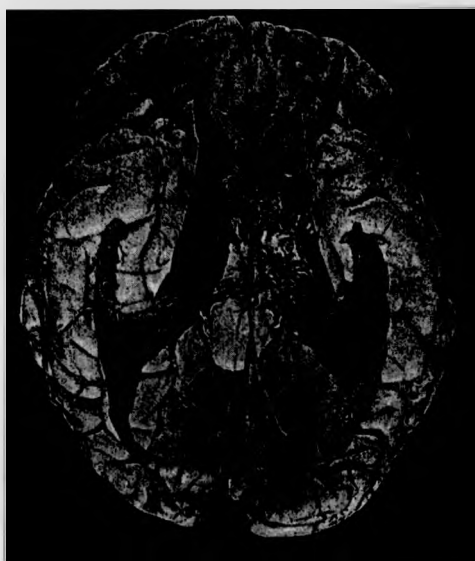


FIGURE 2.17: A cast of the ventricles to illustrate their position internally. $\times 65$ (from England and Wakely, 1991, p. 71) (1 to 5-Lateral ventricle; 6-Third ventricle; 7-Fourth ventricle).

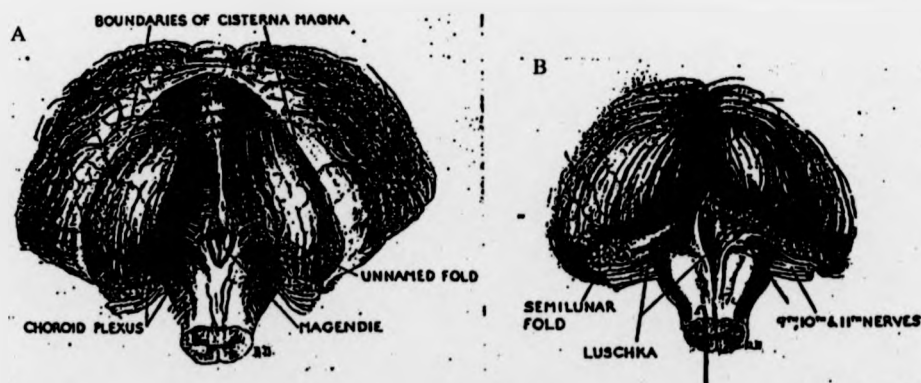


FIGURE 2.18: Dissection to illustrate the median foramen (of Magendie) in figure 18a; and the lateral foramen (of Lushka) in figure 18b. (from Woollam and Millen, 1962)

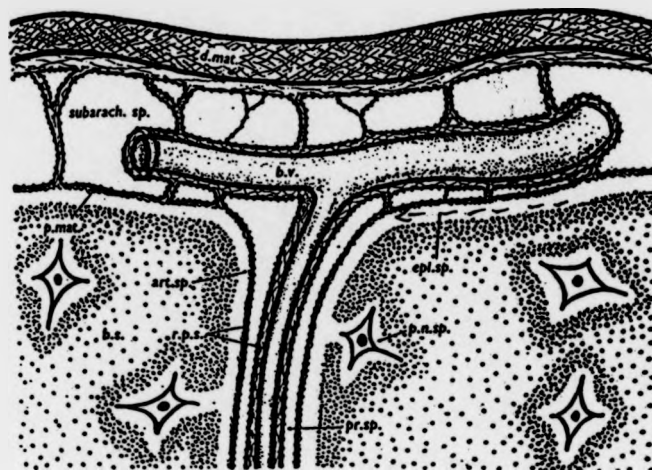


FIGURE 2.19: Diagram illustrating the perivascular space. *art.sp.*, artifact space; *b.s.*, brain substance; *b.v.*, blood vessel; *d.m.*, dura mater; *epi.sp.*, epispinal space of His; *p.n.sp.*, perineuronal space; *pr.sp.*, perivascular space; *p.mat.*, pia mater; *r.p.s.*, reticular perivascular sheath; *subarach.sp.*, subarachnoid space (from Woollam and Millen, 1962)

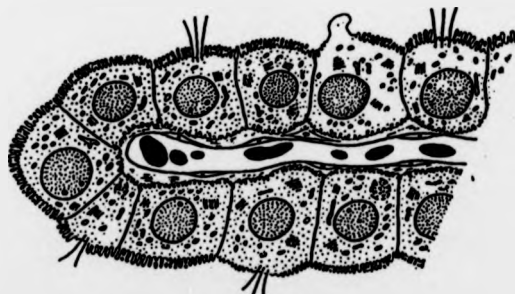


FIGURE 2.20: Diagram illustrating the general appearance of choroidal villus. (from Woollam and Millen, 1962)

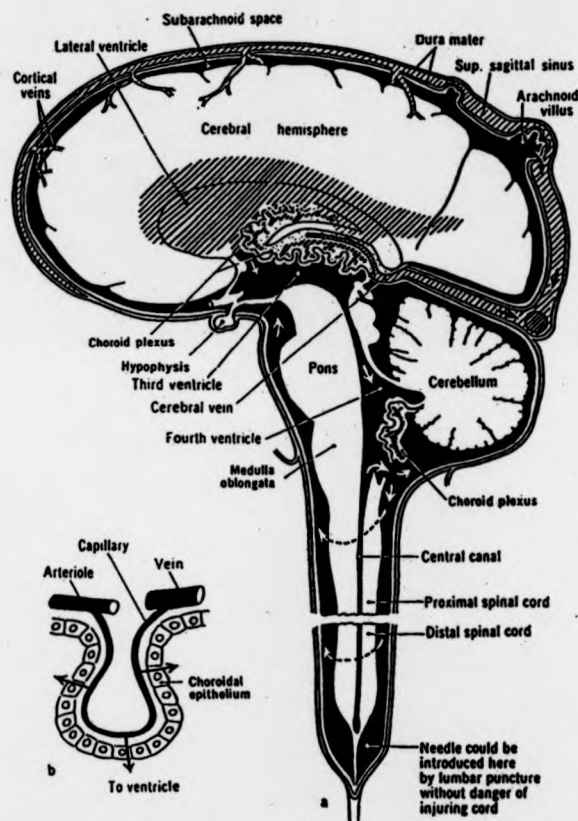


FIGURE 2.21: Circulation of CSF (in black). The arrows indicate the direction of circulation. (from Gardner, 1968, p. 53)



FIGURE 2.22: Sagittal section of the head to illustrate the circulation of CSF through the ventricles and subarachnoid space and its return to blood circulation. $\times 64$. Black arrows: circulation of CSF; Shaded arrows: return of CSF to blood circulation. (from England and Wakely, 1991, p. 76).

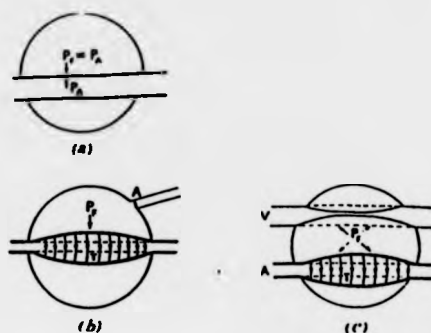


FIGURE 2.23: Effect of artery on Csf pressure (2.23a). Valve action and its effect (2.23b). Effect of veins on CSF pressure (2.23c). (from Davson, 1967)

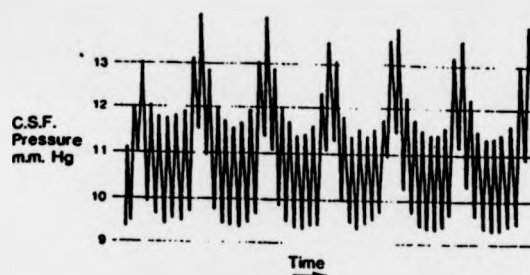


FIGURE 2.24: Recording of CSF pressure from the lateral ventricle. (from Allen, 1986, adapted from McDowall, 1969)

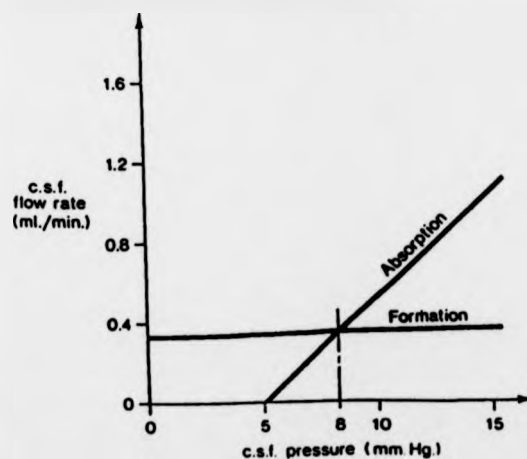


FIGURE 2.25: Relationship between pressure and rate of formation and absorption of CSF. (from Allen, 1986 adapted from Cutler et al, 1968)



FIGURE 2.26: Vertical section through the midline body. During coughing the areas shaded in dots, up to the larynx, is subjected to sudden high pressure. This pressure is transmitted to the central canal whence it travels upwards. (from Lockey et al, 1975).

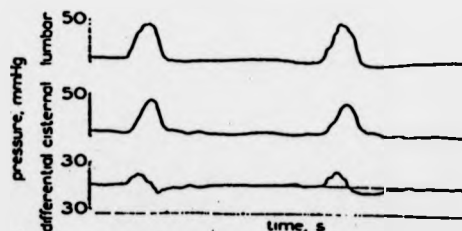


FIGURE 2.27: Two normal coughs in the erect position. The top trace is lumbar from the bottom of the spine. The middle trace is cisternal, from the base of the skull, the bottom trace is differential, lumbar minus cisternal. The mean attenuation factor is 91.5%. The pressure given is the pressure above the manubrium sterni, which is the top of the breast bone. (from Lockey et al, 1975).

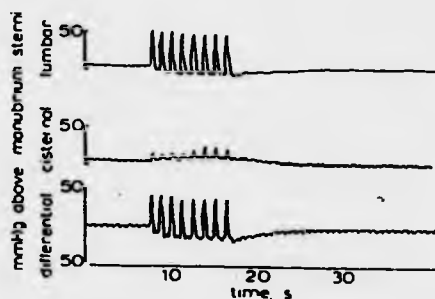


FIGURE 2.28: Eight coughs in presence of spinal block. The impulses are greatly attenuated by the time they reach the cistern. The mean attenuation factor is 23.5%. Note the change in time scale from figure 2.27. (from Lockey et al, 1975).

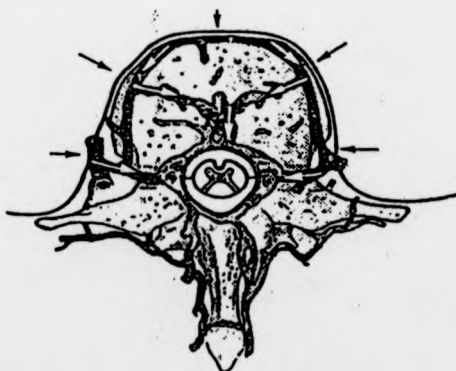


FIGURE 2.29: Transverse section through the spine. The abdominal pressure (black arrows) is transmitted along the veins (white arrows) and is reflected in the CSF which is represented as a clear, unshaded area around the cord (from Lockey et al, 1975).

B.2 FIGURES OF CHAPTER 3

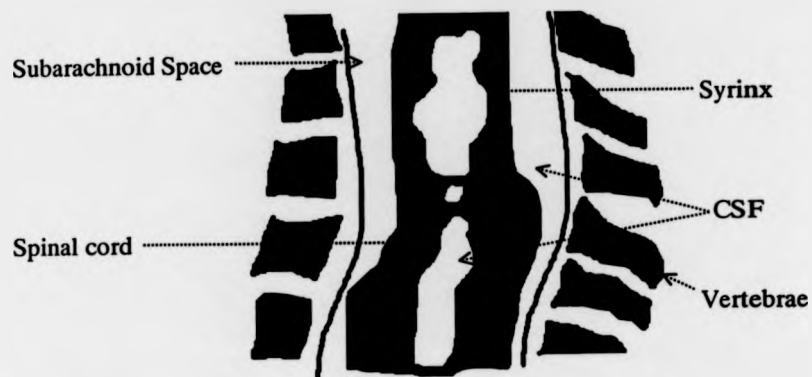


FIGURE 3.1: Diagram to demonstrate syrinxes in syringomyelia.

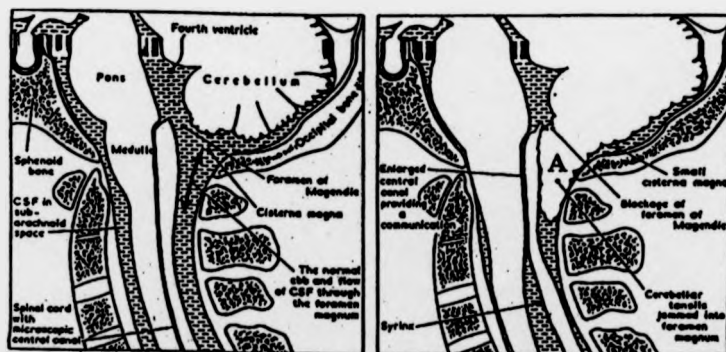


FIGURE 3.2: Midline section through an unaffected case on the left. Hindbrain hernia (A) and syringomyelia on the right. (from Williams, 1986, p132)



FIGURE 3.3: Magnetic resonance image to show syringes in hindbrain-related syringomyelia. (from Williams, 1993, p. 120)



FIGURE 3.4: Magnetic resonance image to show syringes (severe case). (from Williams, 1990b, p. 667)

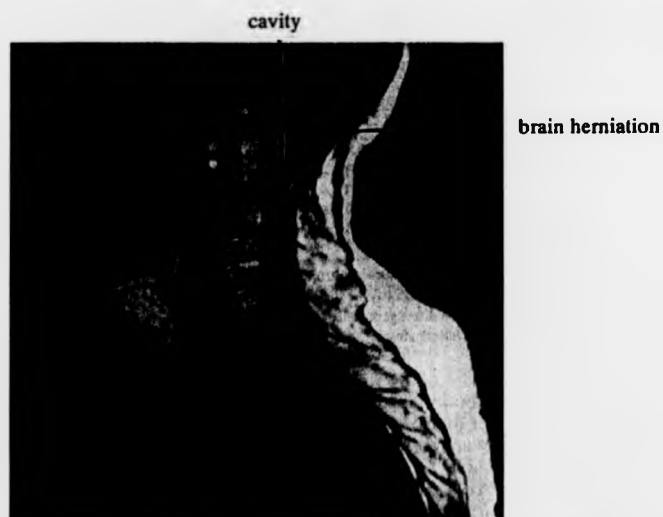


FIGURE 3.5: Magnetic resonance image demonstrating the appearance of a syrinx after craniocervical decompression. (Sgouros & Williams, 1995, p. 4)

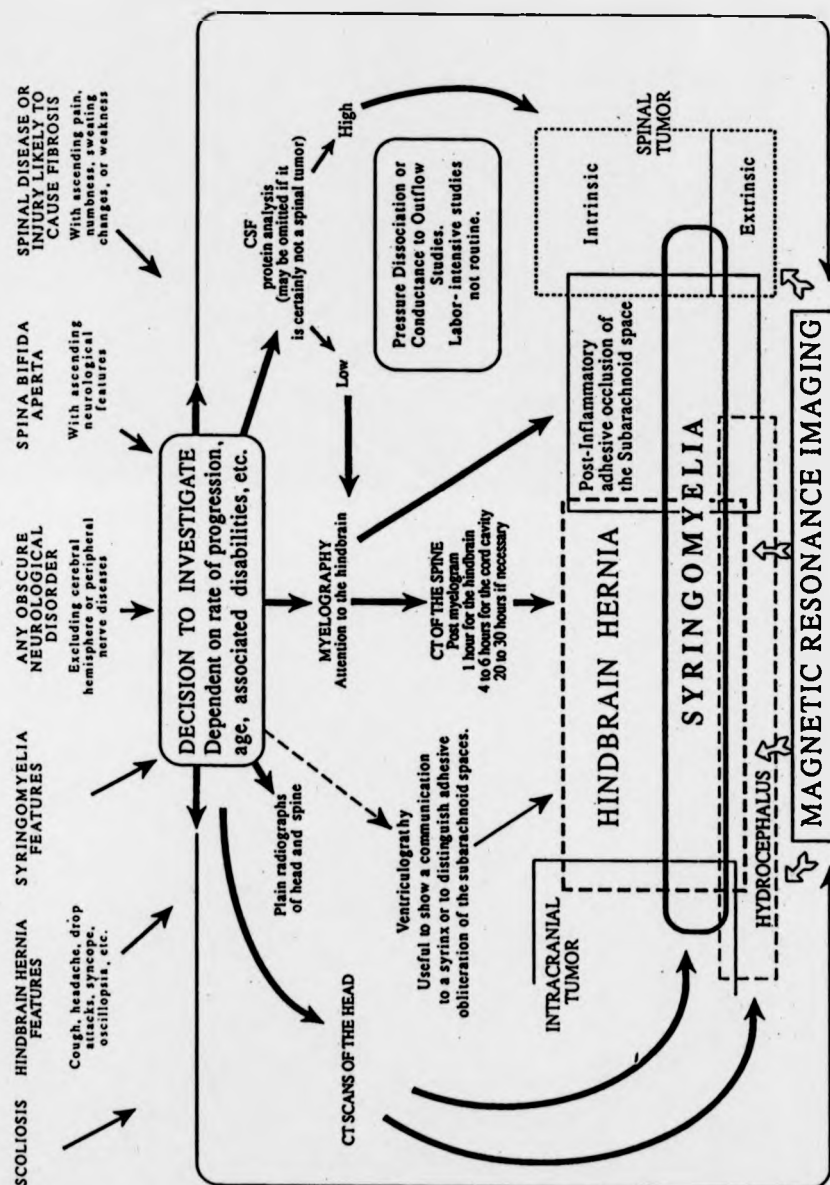


FIGURE 3.6: Suggestions for syringomyelia investigation. (Williams, 1990b, p. 671)



FIGURE 3.7: Postmyelographic CT reconstructions of the lower end of the hindbrain. (Williams, 1990b, p. 665)

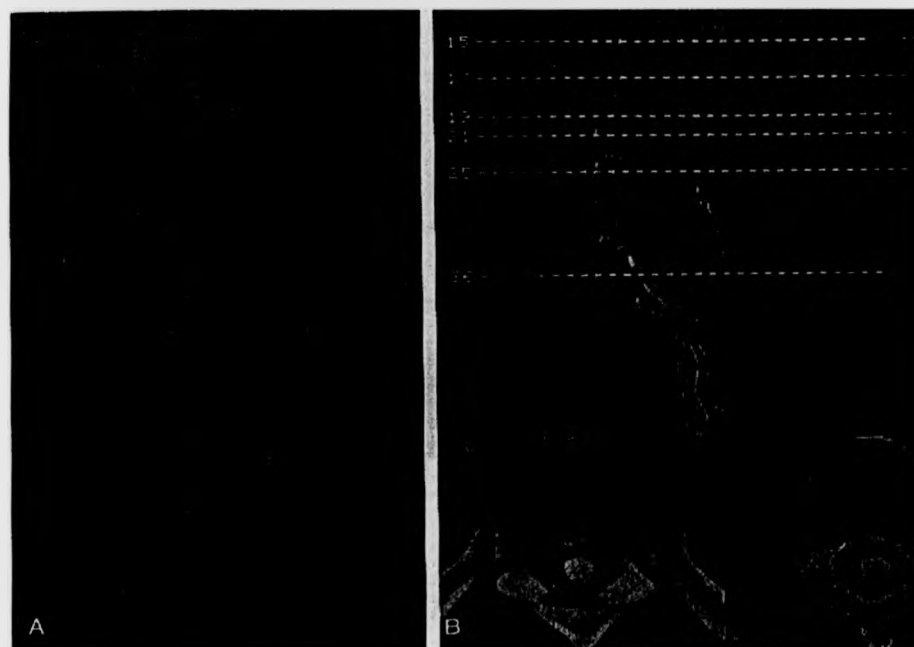


FIGURE 3.8: (A) A myelography in post-traumatic syringomyelia. (B) Computed tomography scan about 1 hour after myelography. (Williams, 1990b, p. 673)



FIGURE 3.9: Magnetic resonance image of a sagittal midline cut through the hindbrain and upper cord in the most common case of syringomyelia: hindbrain related. (Williams, 1990b, p 658)



FIGURE 3.10: Same case as figure 3.9 after decompression, the patient experienced motor and sensory clinical improvement. Note the bottom of the tonsils now assume a more rounded shape, the midline outlet of the fourth ventricle has opened up, there is a large artificial cisterna magna, and the syrinx has almost entirely disappeared. (Williams, 1990b, p. 658)

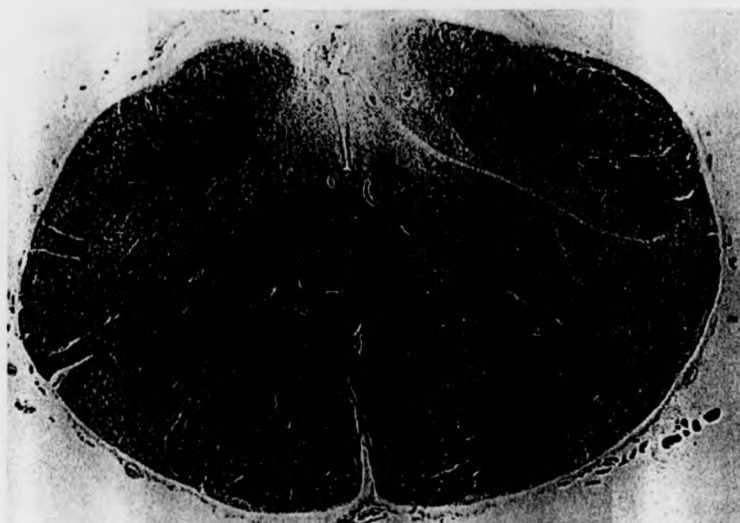


FIGURE 3.11: Histological preparation of syringobulbia. (from Williams, 1993, p. 113)



FIGURE 3.12: Flow void in a T_2 -weighted magnetic resonance. (from Williams, 1990b, p. 662)

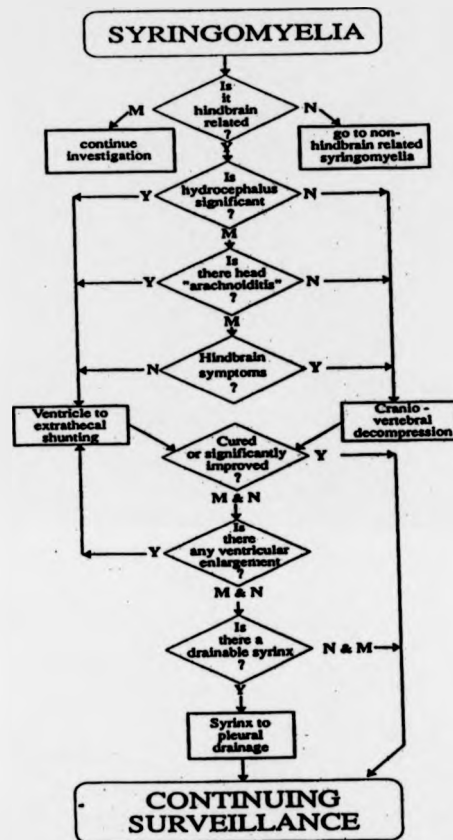


FIGURE 3.13: Decision tree for syringomyelia surgery. *Y*: Yes; *N*: No; *M*: May be. (from Williams, 1990b, p. 674)

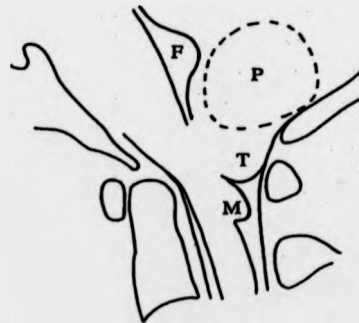


FIGURE 3.14: Diagram of Hindbrain hernia. *F* fourth ventricle; *P* pouch; *T* tonsils; *M* medullary deformity. (from Williams, 1993, p.115)

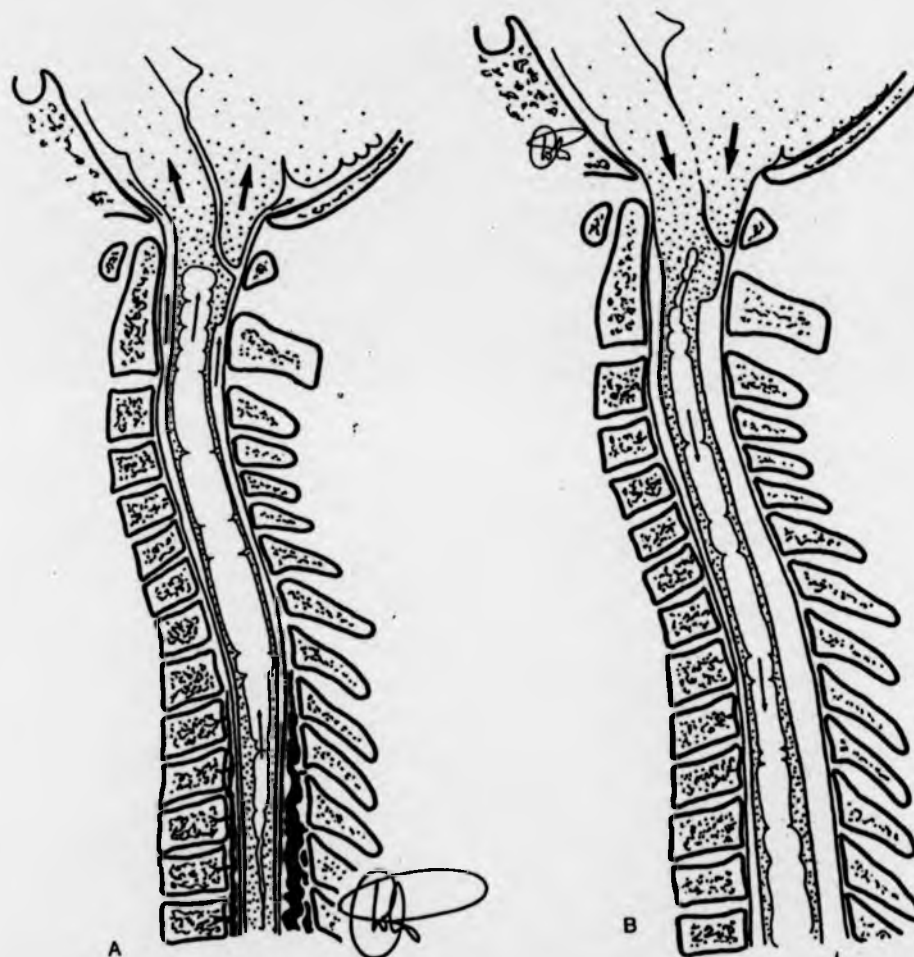


FIGURE 3.15: (A), Upward movement of the CSF lifts the hindbrain out of the foramen magnum, separates the close approximation of the tonsils to each other and to the back of the medulla, and allows the CSF to enter the head freely. (B), During the rebound, the intracranial pressure carries the hindbrain tightly into position and moulds it firmly. (from Williams, 1990b, p. 660)



FIGURE 3.16: Magnetic resonance in a patient with a spinal lipoma. There is a hindbrain hernia in this patient. (from Williams, 1990b, p. 663)

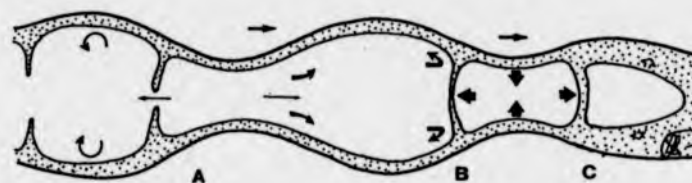


FIGURE 3.17: If the fluid is forced up and down the cord it probably almost always displays wave phenomena. (from Williams, 1993, p. 122)

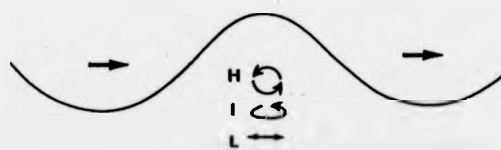


FIGURE 3.18: Wave motion above a flat surface produces horizontal movement (*L*) close to the bottom, sinusoidal movement (*H*) close to the surface and ellipsoidal movement (*I*) between. (from Williams, 1993, p. 122)

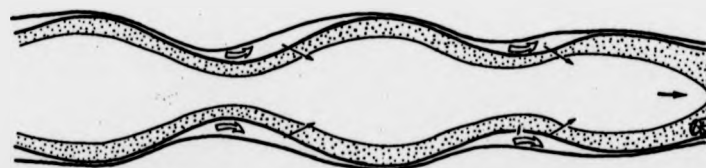


FIGURE 3.19: The easy passage of fluid up the centre of the cord compared with the difficulty in movement within the subarachnoid space. (from Williams, 1993, p. 123)

B.3 FIGURES OF CHAPTER 4

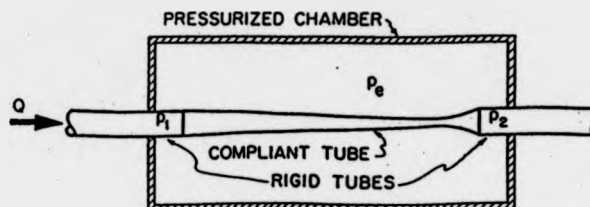


FIGURE 4.1: Diagram of the Starling resistor.

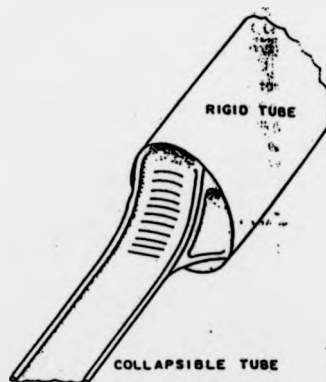


FIGURE 4.2: Adjustment zone of a highly collapsed compliant tube mounted on a circular rigid tube (from Shapiro, 1977b).

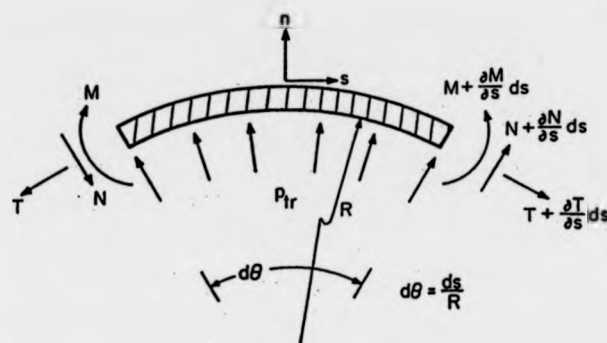


FIGURE 4.3: Free-body diagram for a small segment of tube wall (from Kamm, 1987).

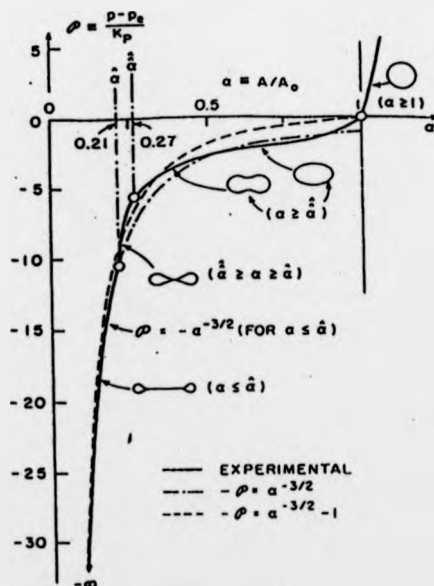


FIGURE 4.4: Comparison of the tube law model (Eq. 4.10) with experimental measurements. Taken from Shapiro (1977b).

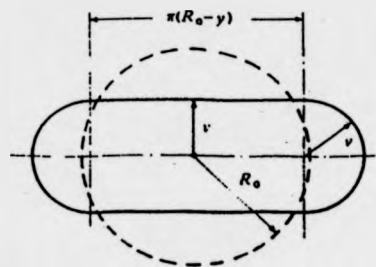


FIGURE 4.5: Geometric model used to estimate stiffness due to longitudinal tension and bending (from McClurken et al, 1981).

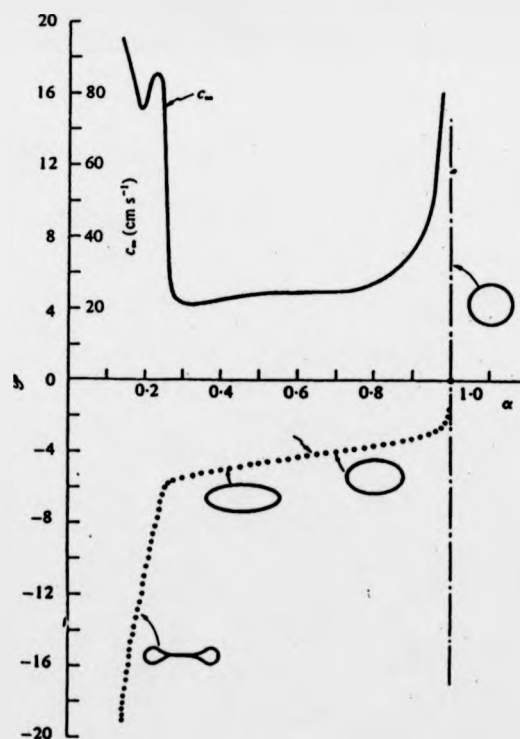


FIGURE 4.6: Local tube law with the tube mounted as in figure 4.8. Lower curve: experimental data $P(\alpha)$. Upper curve: $C_\infty(\alpha)$ from smoothed curve of $P(\alpha)$ (from Kececioğlu et al, 1981).

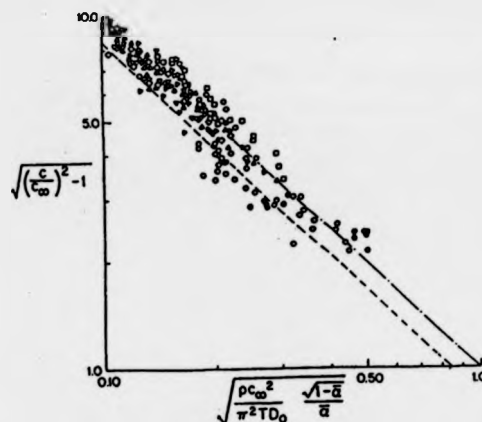


FIGURE 4.7: Comparison of measured and theoretical wavelengths in a compliant tube mounted as in figure 4.8. Dash-dot line: based on equation 4.12, neglecting the longitudinal bending. Dashed line: reduced by 30 percent. Open symbols: steady-flow experiments as in figure 4.8; closed symbols: unsteady-flow experiments from Jan, 1980 (from McClurken et al, 1981).



FIGURE 4.8: Photograph of an elastic jump in a compliant tube suspended in water. Flow from left to right. (a-b) Supercritical region with precursor waves emanating from jump. (b-c) Elastic jump. (c-end) Subcritical region. (from Kececiloglu et al, 1981).

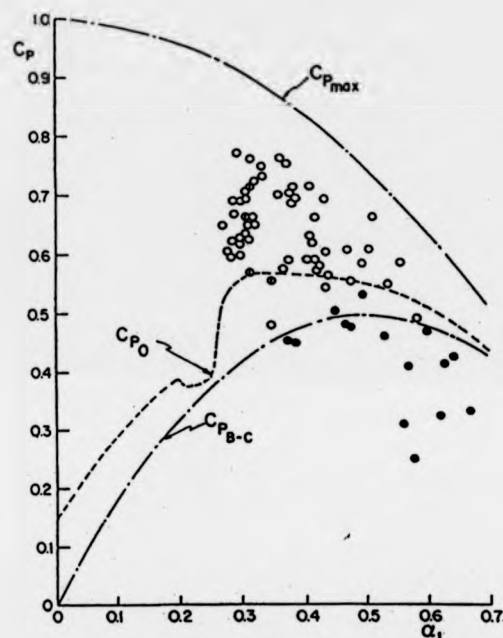


FIGURE 4.9: Experimental values for the jump pressure recovery coefficient ($C_p = 2(P_c - P_b) / \rho u_b^2$) compared to various calculated values: $C_{p_{max}}$ based on the assumption of no loss of kinetic head; $C_{p_{B-C}}$ based on the Borda-Carnot solution; C_{p_0} based on the prediction of equation 4.16. • = long shocks, o = intermediate shocks, others = short shocks. (from Kececioğlu et al, 1981).

B.4 FIGURES OF CHAPTER 5

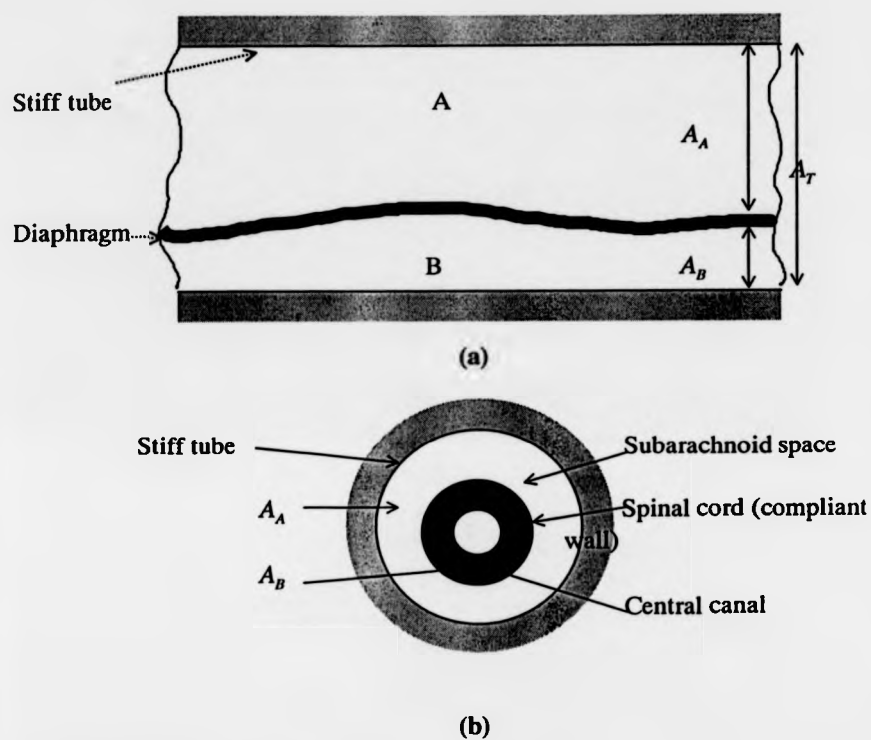


FIGURE 5.1: Schematic sketch of theoretical model.

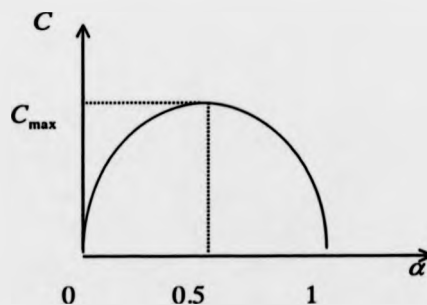


FIGURE 5.2: Shape of the wave speed against the outer cross-section area ratio.



FIGURE 5.3a: Increase of the outer cross-sectional area.

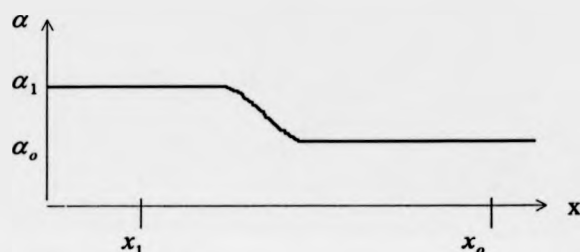


FIGURE 5.3b: Outer cross-sectional area against the length.

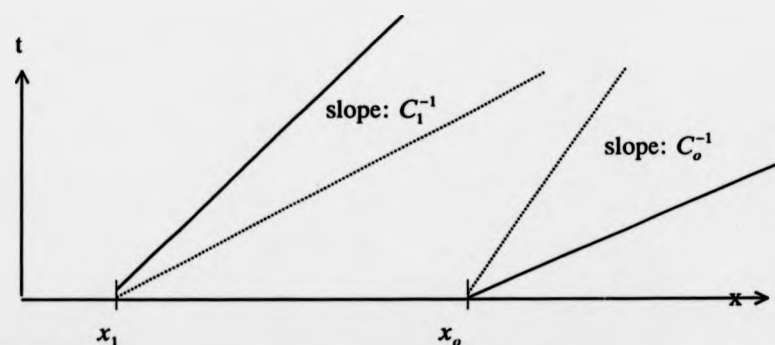


FIGURE 5.3c: Pressure waves propagation.

lines: — case $\alpha_0 > 0.5$; case $\alpha_0 < 0.5$

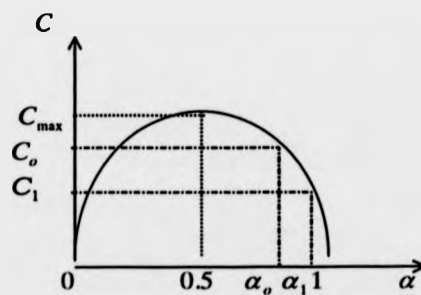


FIGURE 5.3d: Wave speed against the outer cross-sectional area.
FIGURE 5.3: Non linear effect on the wave speed.

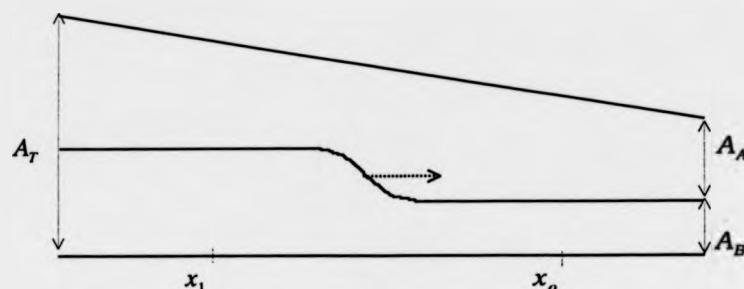


FIGURE 5.4: Total cross-sectional area increase.

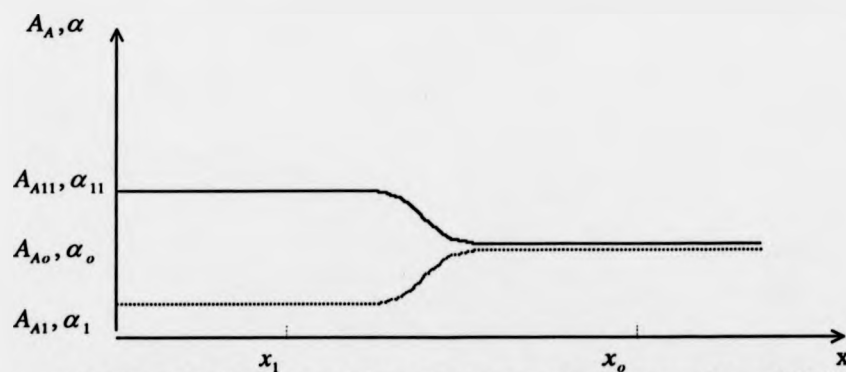


FIGURE 5.5: Variation of the outer cross-sectional area: 2 possibilities.

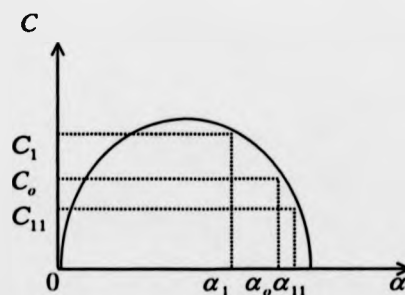


FIGURE 5.6: Wave speed against the outer cross-sectional area.

B.5 FIGURES OF CHAPTER 6

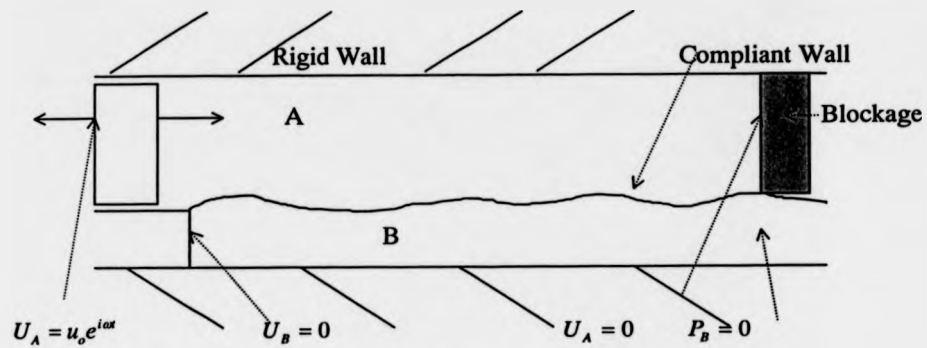


FIGURE 6.1: Piston in simple harmonic motion.

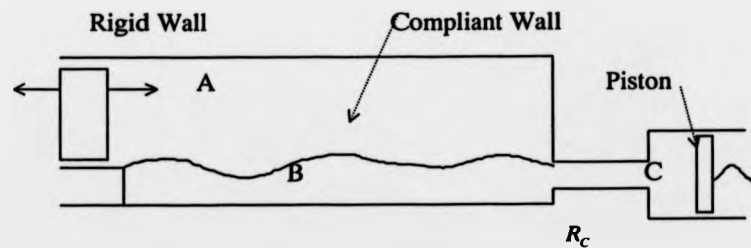


FIGURE 6.2: Piston in simple harmonic motion with compliance and resistance.

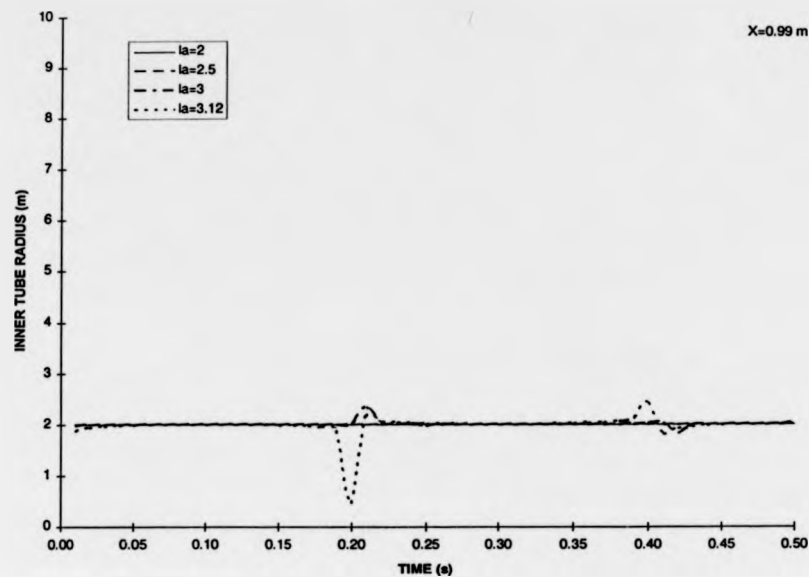


FIGURE 6.3: Effects of the period impulse on inner tube radius: resonance ($l_a = \lambda$).

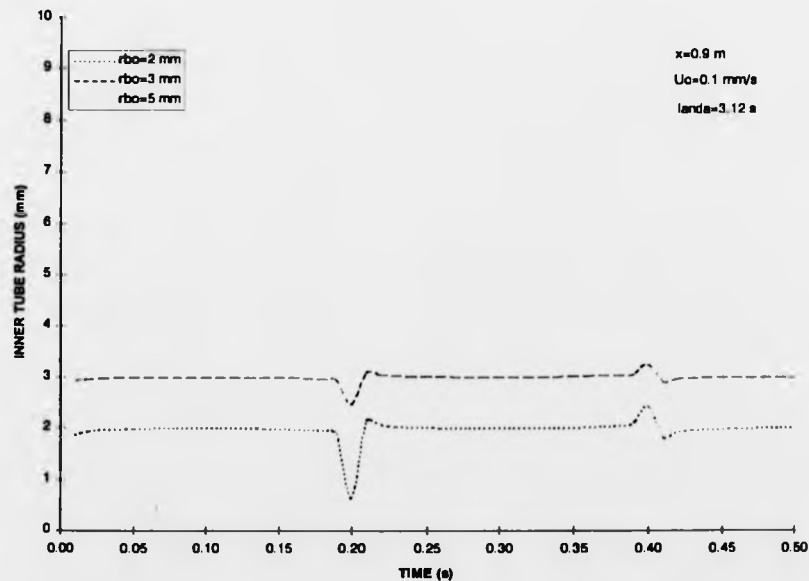


FIGURE 6.4: Variation of the pressure-difference with respect to the inner tube radius.

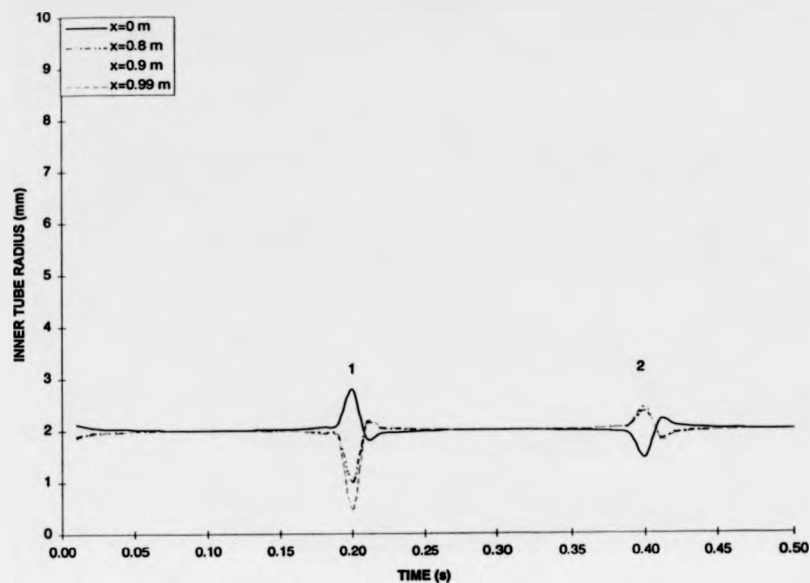


FIGURE 6.5: Variation of the inner tube radius with time.

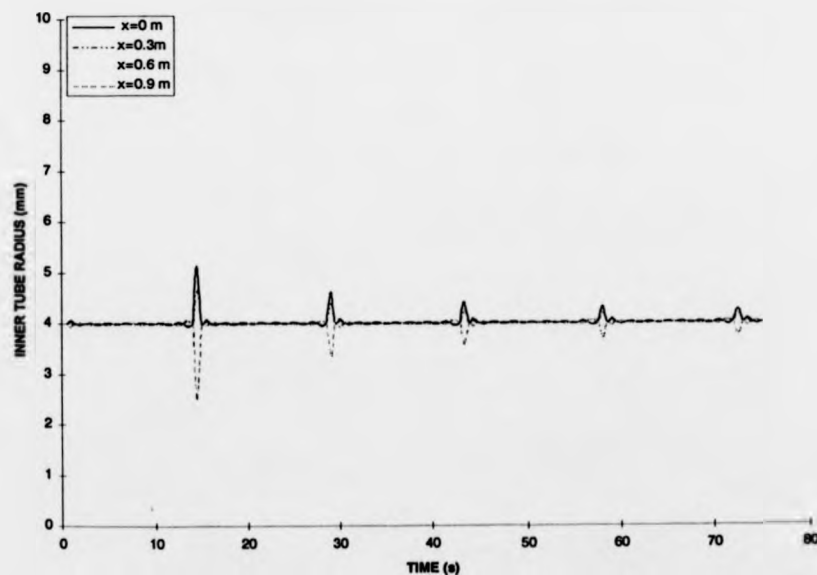


FIGURE 6.6: Attenuation of the peaks with time.

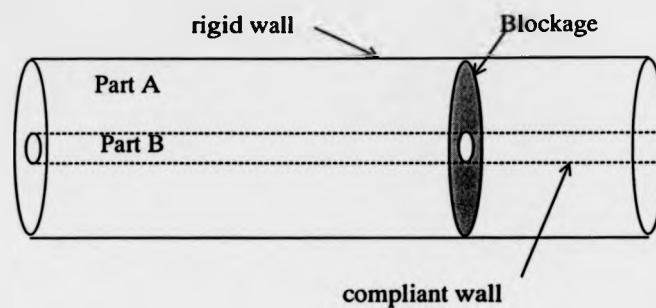


FIGURE 6.7: Coaxial tubes model with blockage.

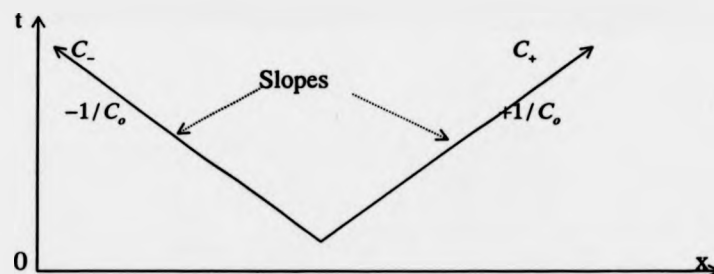


FIGURE 6.8: Characteristic lines.

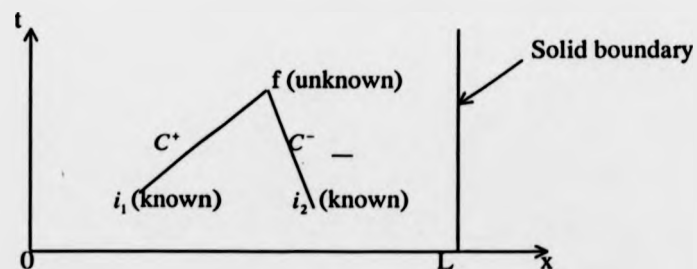


FIGURE 6.9: Interior point.

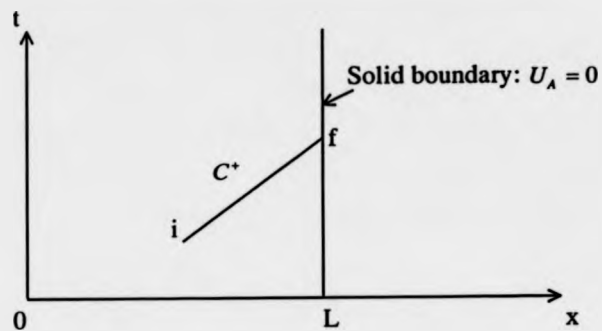


FIGURE 6.10: Solid boundary point.

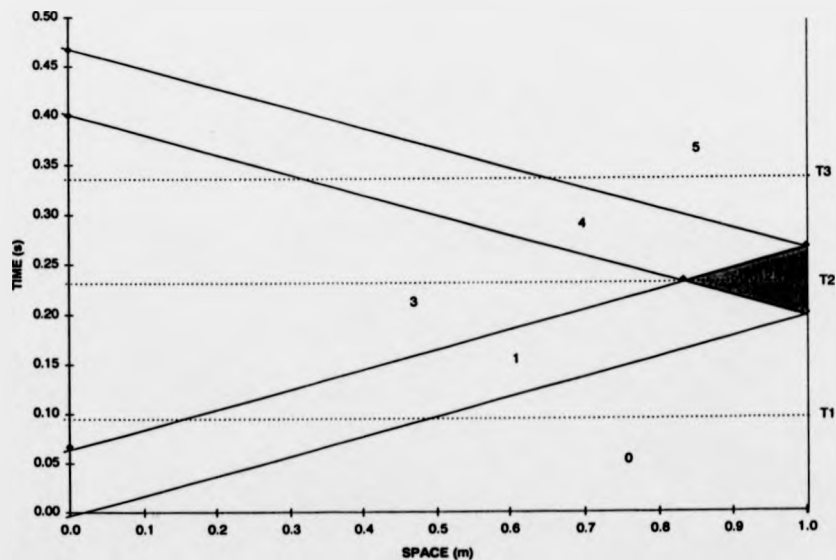


FIGURE 6.11: (x-t) diagram for a pressure pulse propagation.
(Impulse: $P_{A0} = 800 \text{ Pa}$ and $P_{A1} = 500 \text{ Pa}$)

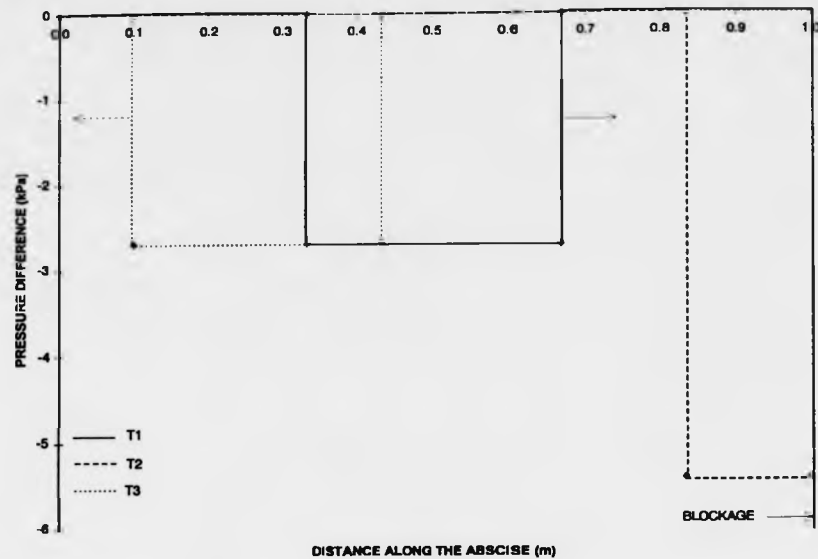


FIGURE 6.12: Pressure pulse propagation (different times).
(Impulse: $P_{Ao} = 800 Pa$ and $P_{A1} = 500 Pa$)

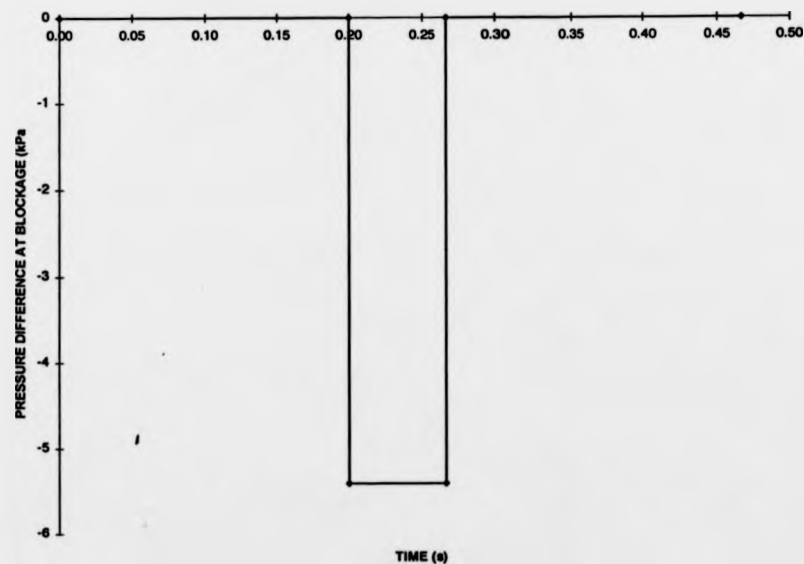


FIGURE 6.13: Pressure difference at blockage.
(Impulse: $P_{Ao} = 800 Pa$ and $P_{A1} = 500 Pa$)

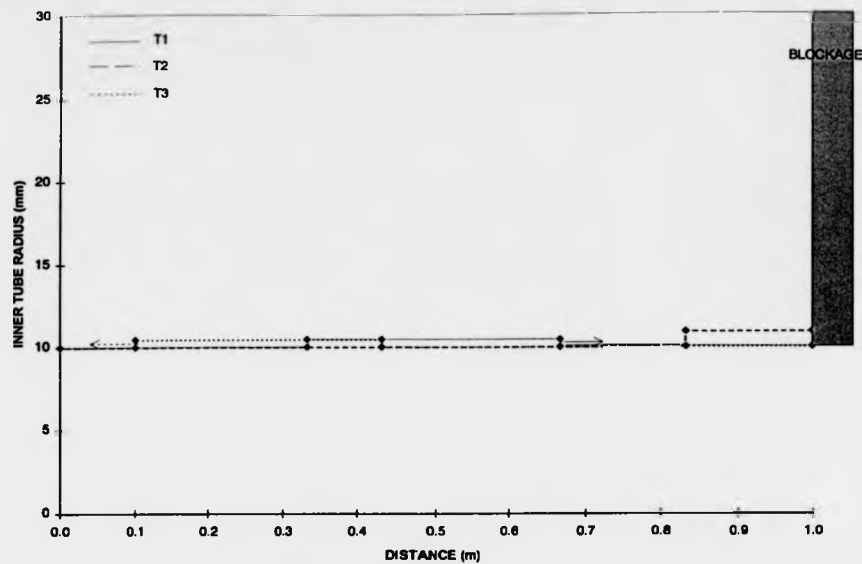


FIGURE 6.14: Inner tube radius variation with a pressure pulse reflection.
(Impulse: $P_{A0} = 800 Pa$ and $P_{A1} = 500 Pa$)

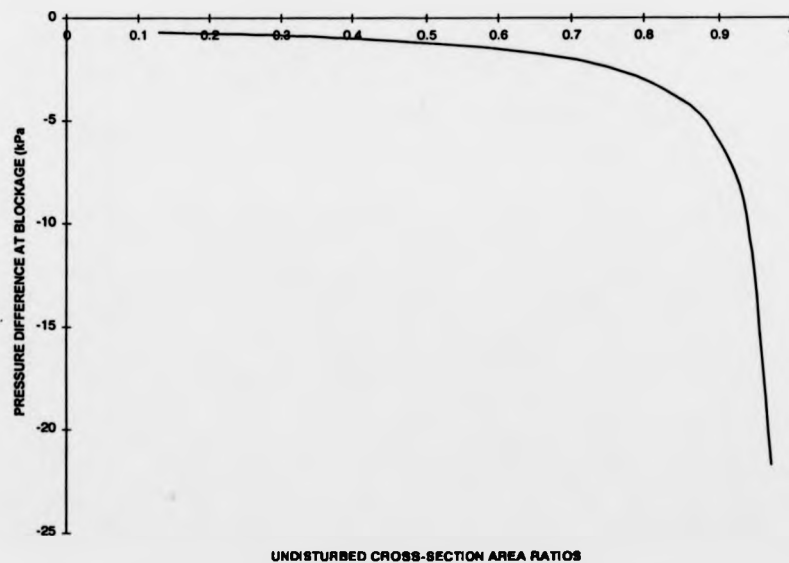


FIGURE 6.15: Variation of the pressure difference at blockage for different undisturbed cross-section areas. (Impulse: $P_{A0} = 800 Pa$ and $P_{A1} = 500 Pa$)

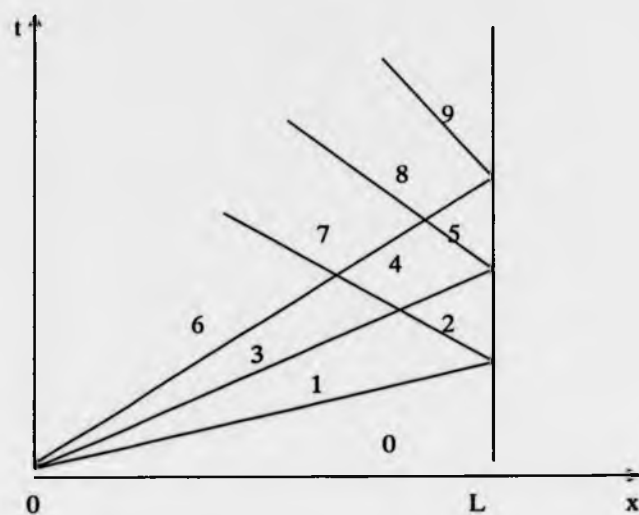


FIGURE 6.16: Sketch for the reflection of an expansion wave.

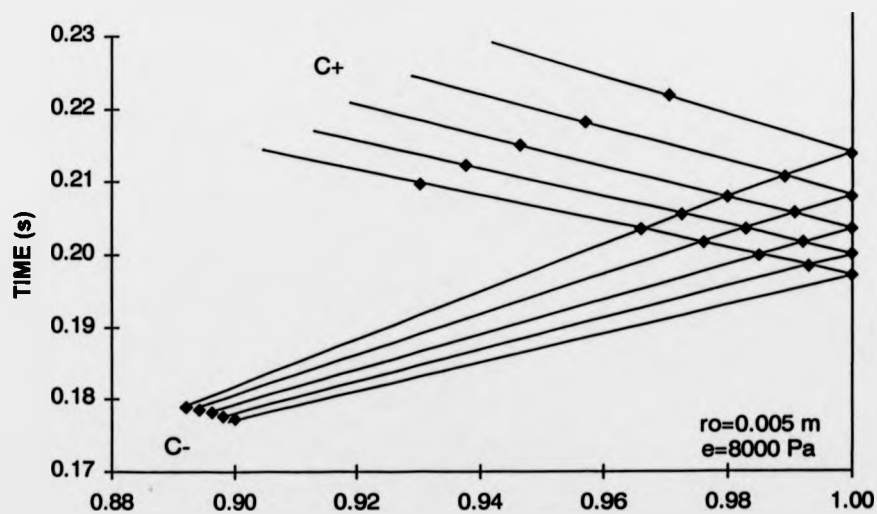


FIGURE 6.17: Numerical results for an expansion wave reflection.
(e is the pressure difference impulse)

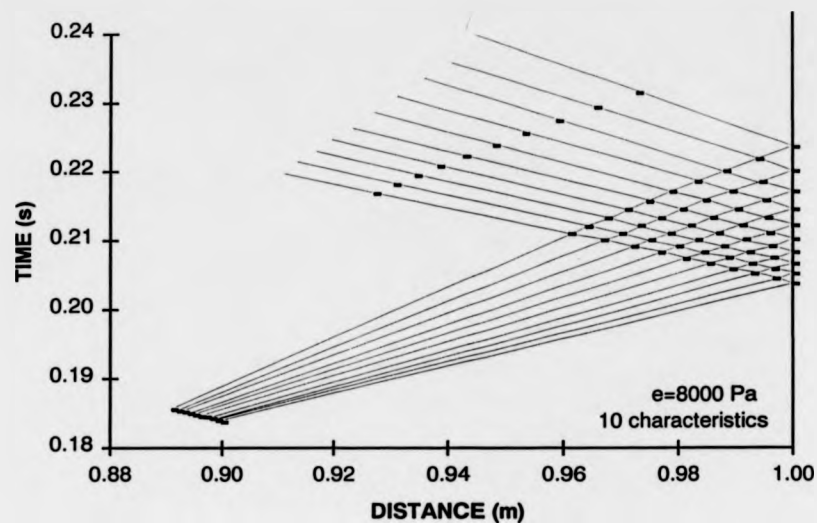


FIGURE 6.18: Expansion wave reflection for 10 characteristics.
(e is the pressure difference impulse)

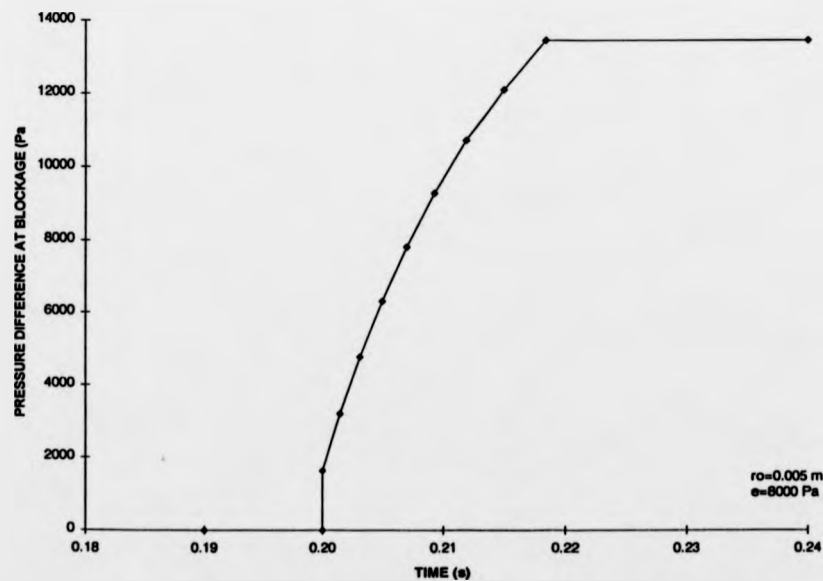


FIGURE 6.19: Pressure difference at blockage for an expansion wave reflection.
(e is the pressure difference impulse)

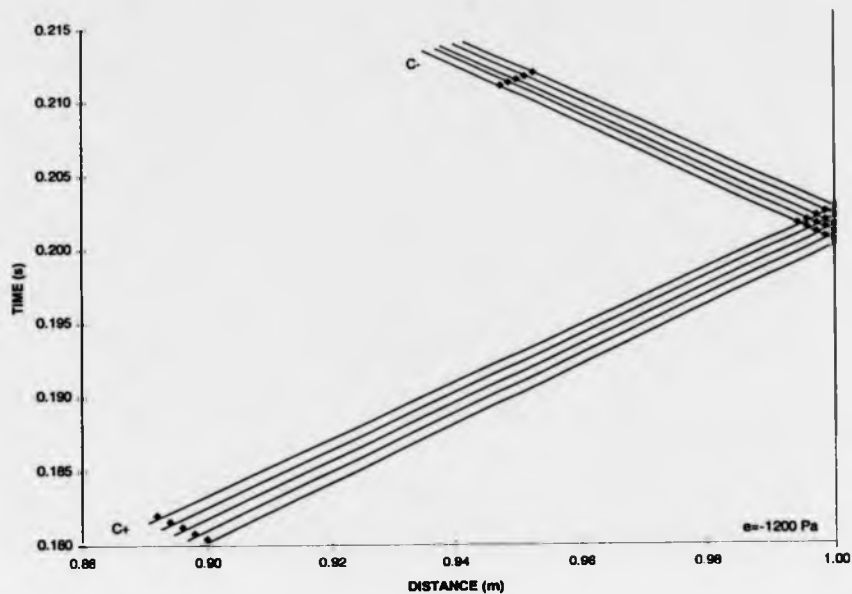


FIGURE 6.20: Reflection of a compression wave.
 (e is the pressure difference impulse)

B.6 FIGURES OF CHAPTER 7

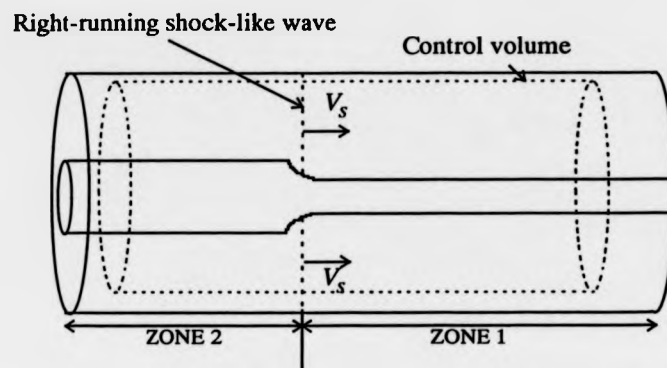


FIGURE 7.1: Propagation of an elastic jump in a two-chamber channel.

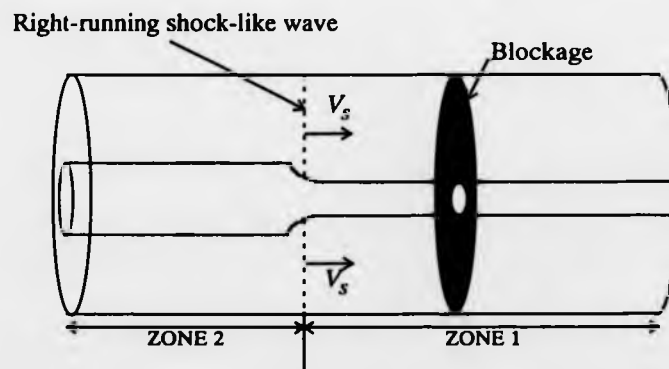


FIGURE 7.2: Incident elastic jump approaching a blockage in the upper chamber.

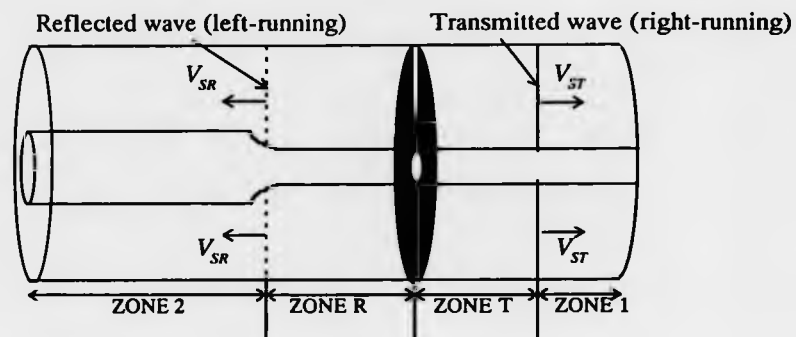


FIGURE 7.3: Reflected and transmitted elastic jumps.

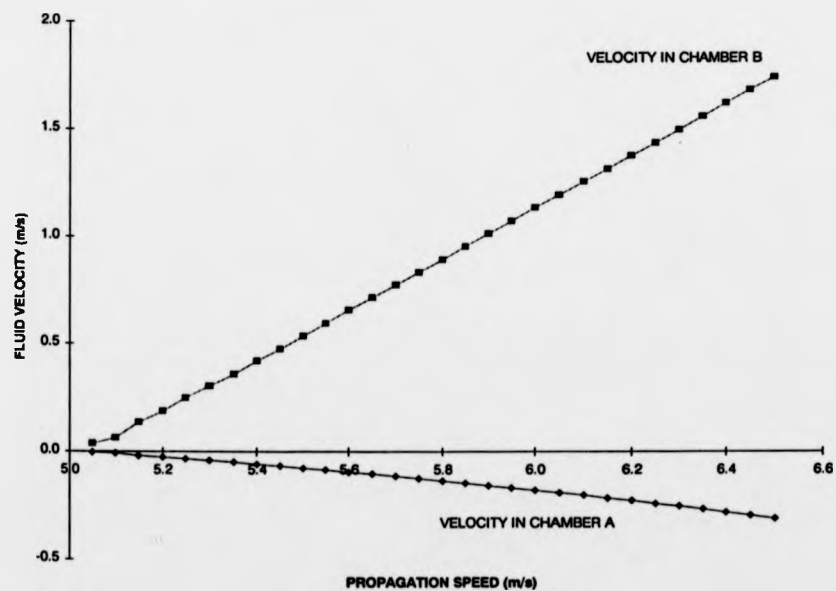


FIGURE 7.4: Velocity in both chambers after the passage of an elastic jump.

FIGURE 7.5: Reflection of an elastic jump from a blockage in the upper channel.

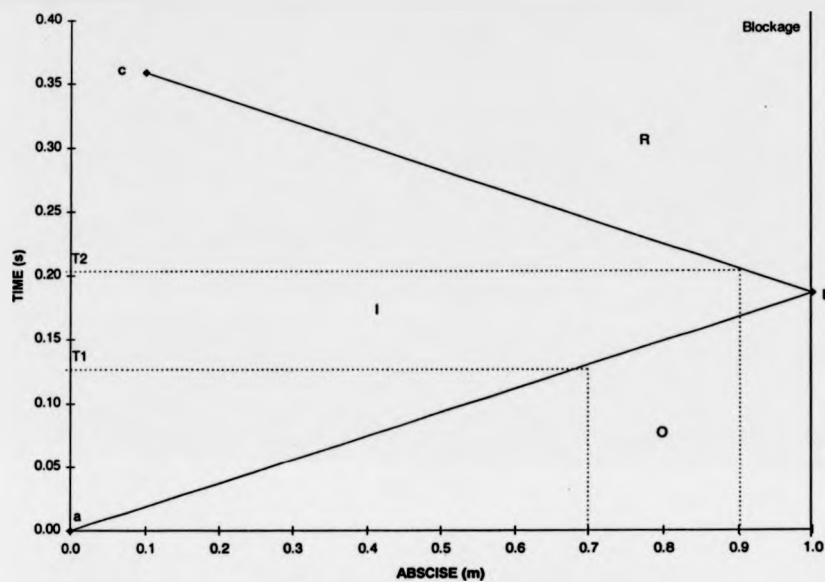


FIGURE 7.5a: Variation of wave fronts with time and distance.

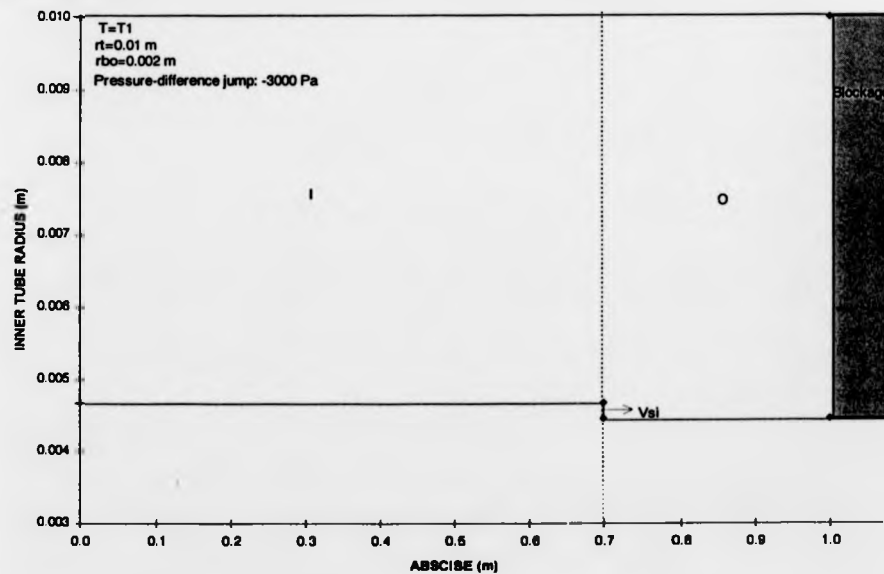


FIGURE 7.5b: Elastic jump approaching the blockage.

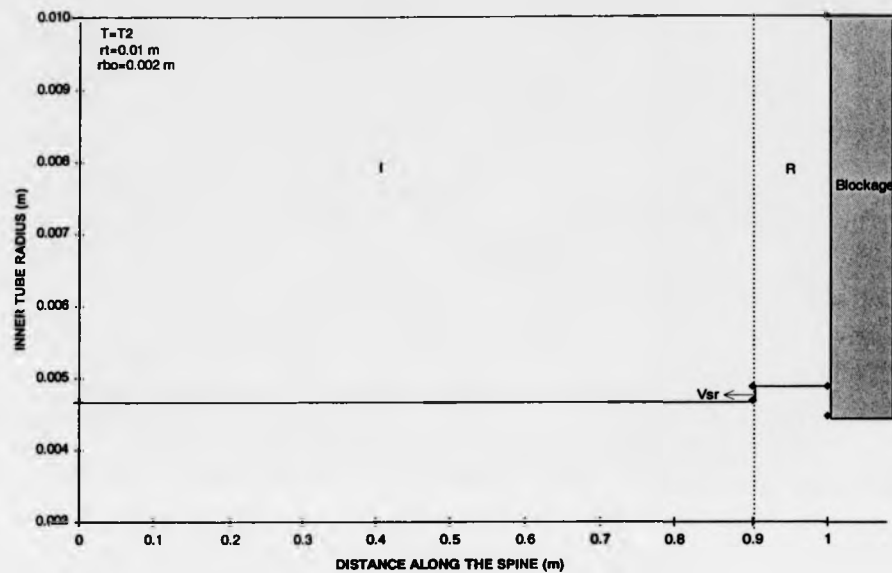


FIGURE 7.5c: After elastic jump reflects from blockage.

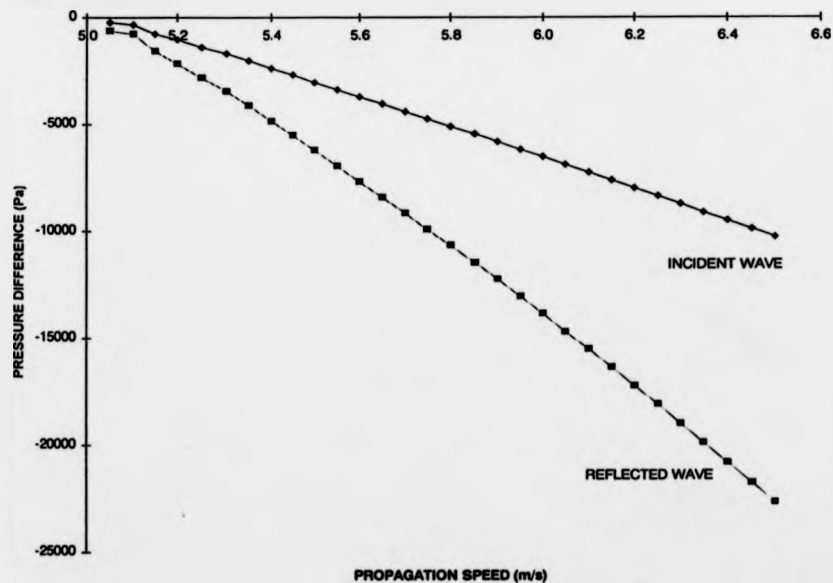


FIGURE 7.6: Comparison between the incident and reflected pressure-differences for different propagation speeds ($\alpha_o = 0.93$).

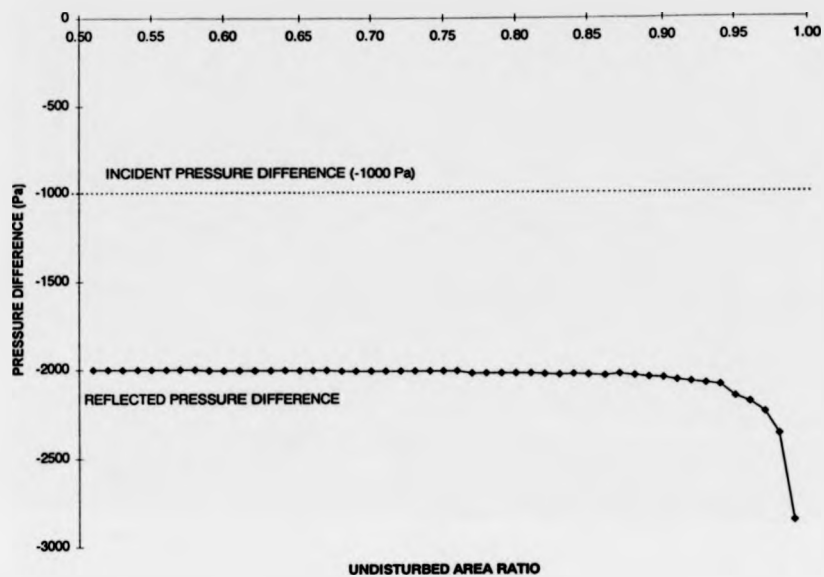


FIGURE 7.7: Effects of the undisturbed cross-sectional area ratio on the reflected pressure-difference.

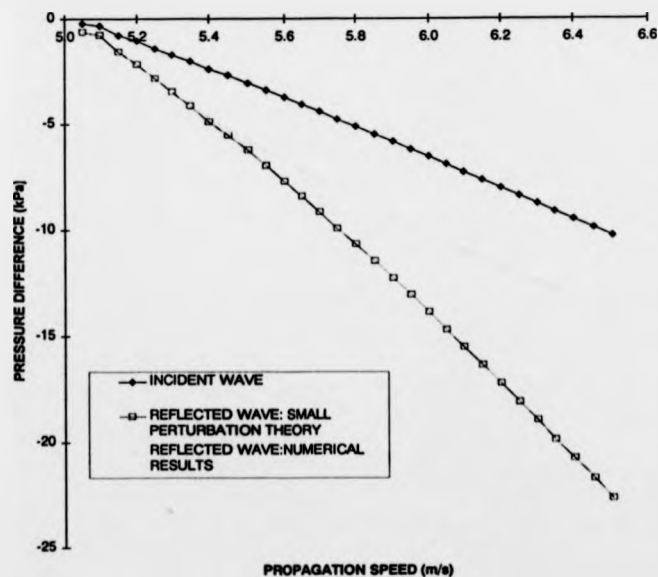


FIGURE 7.8: Comparison between the numerical procedure and the small perturbation theories for different incident pressure-difference jumps.

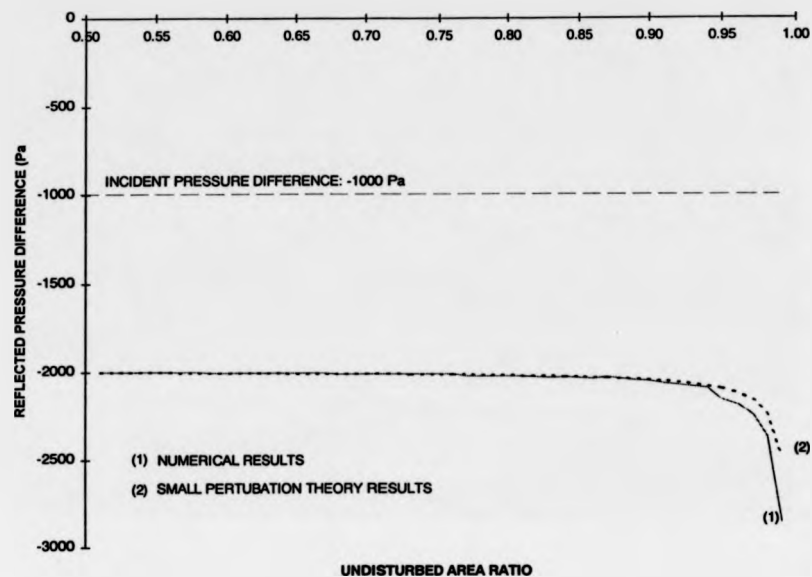


FIGURE 7.9: Comparison between the numerical procedure and the small perturbation theory for different undisturbed cross-sectional area ratios.

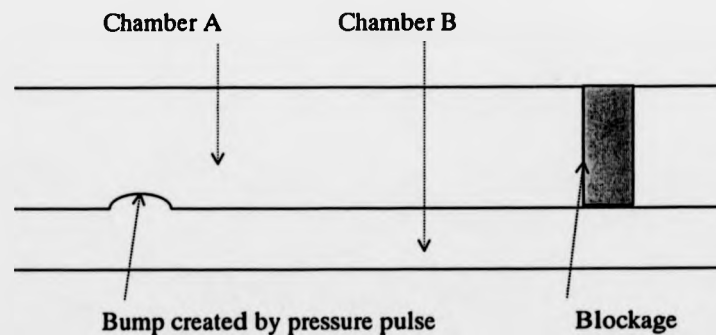


FIGURE 7.10: Pressure pulse propagating to the right.

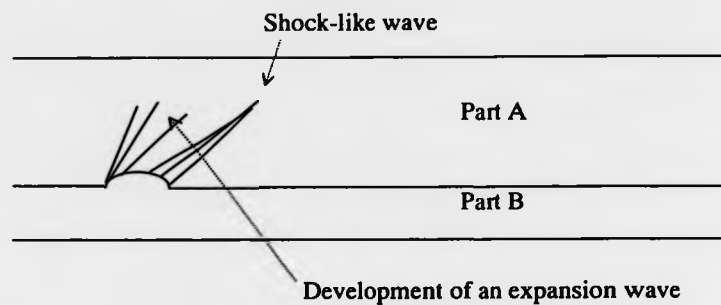


FIGURE 7.11: Creation of an elastic jump and expansion wave.

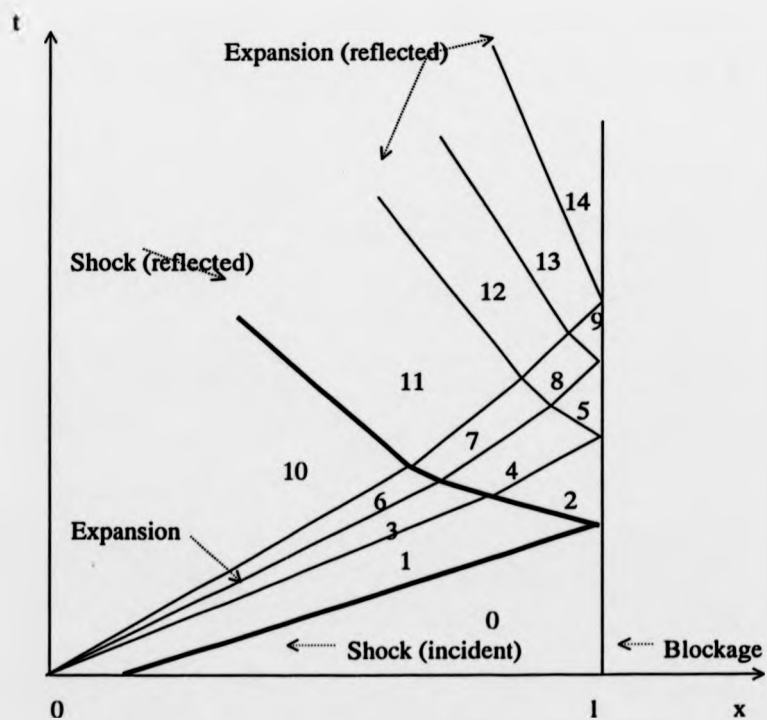


FIGURE 7.12: Intersection between an elastic jump and an expansion.

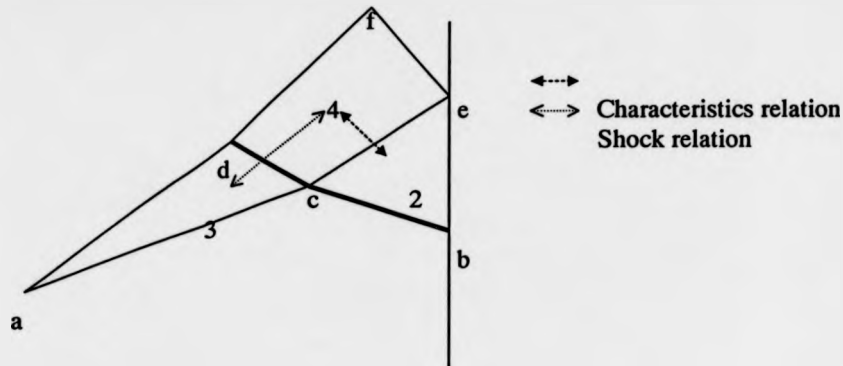


FIGURE 7.13: Determination of fluid properties in region 6.

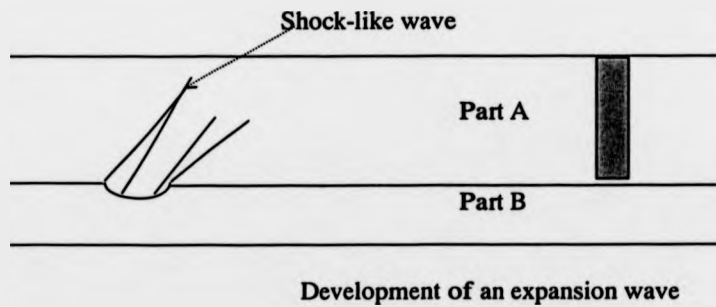


FIGURE 7.14: Creation of an elastic jump and expansion wave.

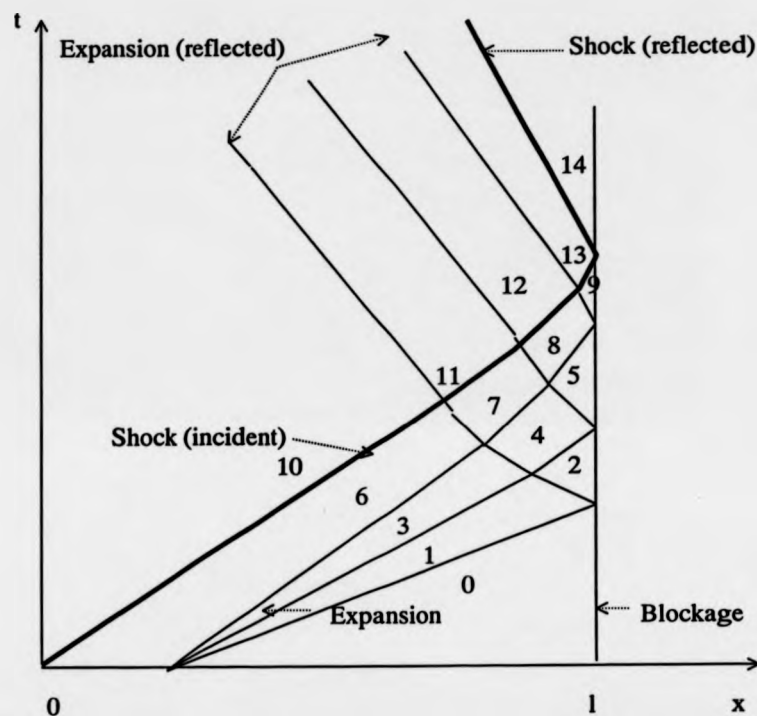


FIGURE 7.15: Intersection between an expansion and an elastic jump.

B.7 FIGURES OF CHAPTER 8

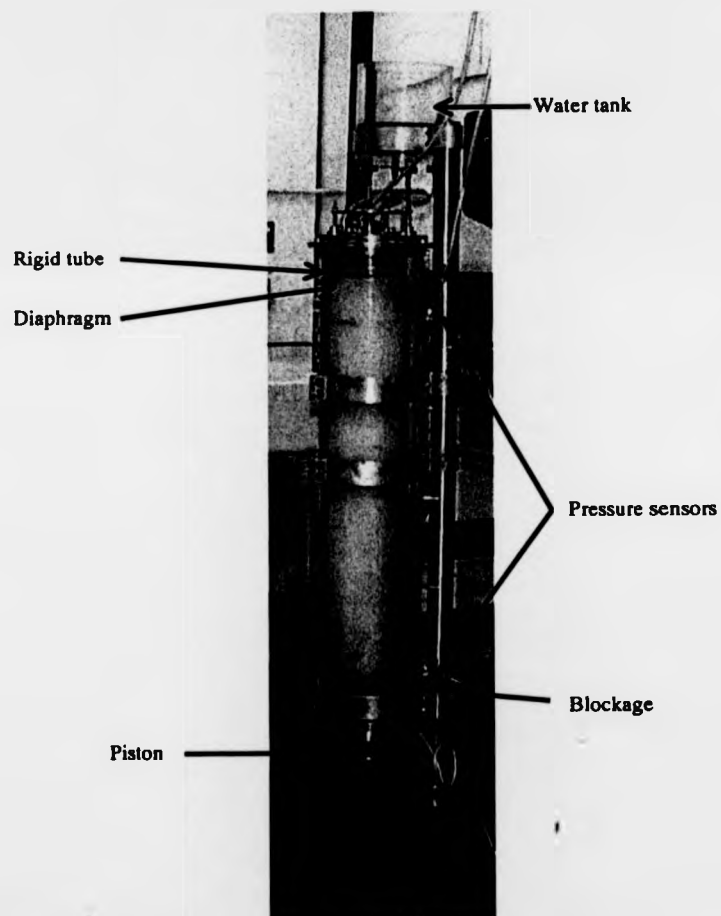


FIGURE 8.1: Picture of the physical model of the spinal system.

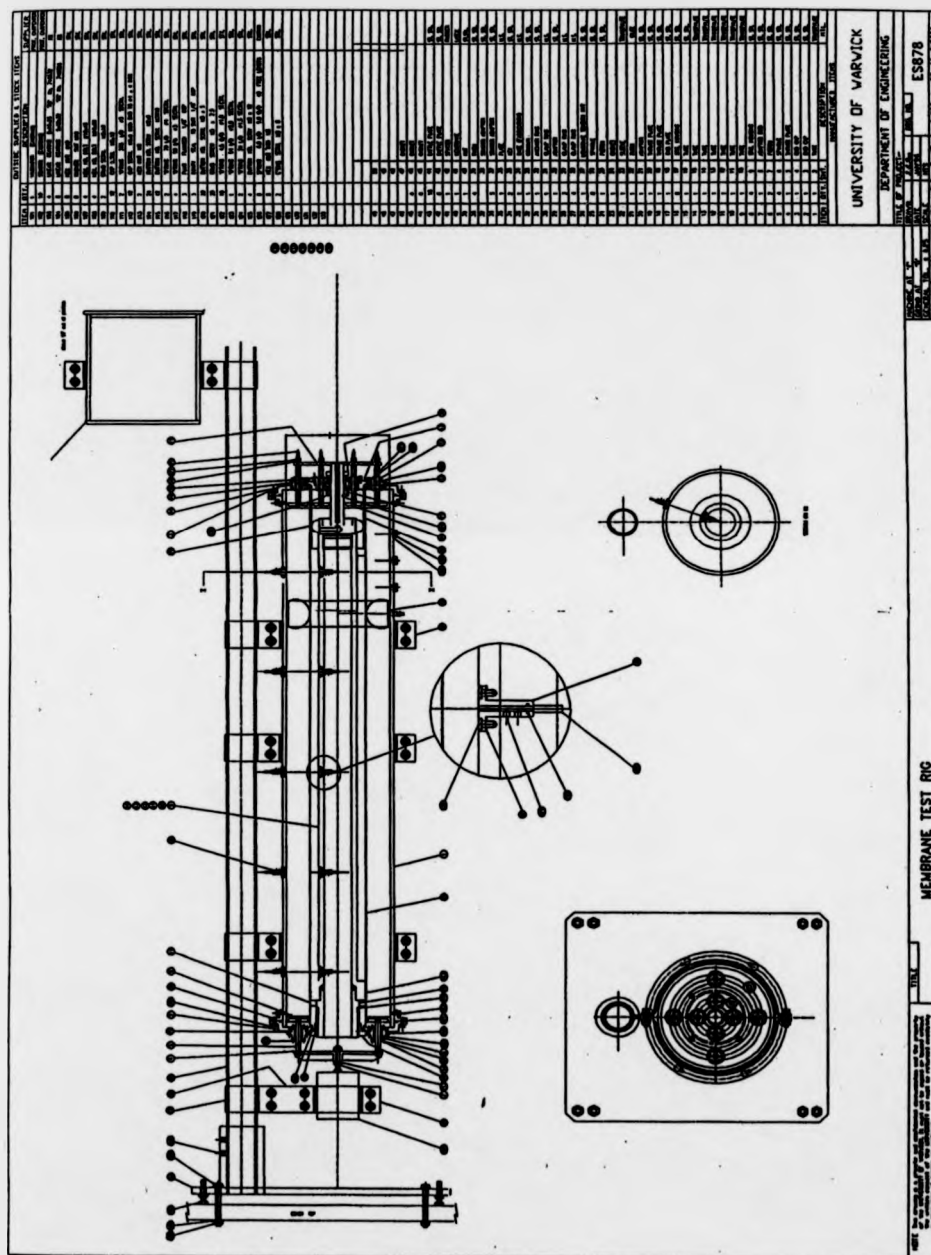


FIGURE 8.2: Diagram of the experimental rig (appendix *D* shows the same figure in format A3).

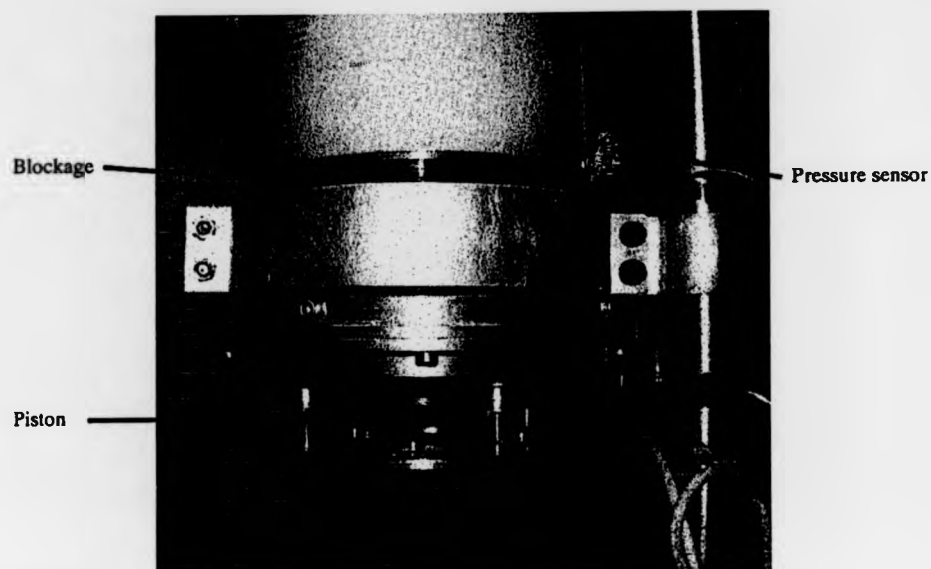


FIGURE 8.3: Picture showing the piston, blockage and pressure sensor.

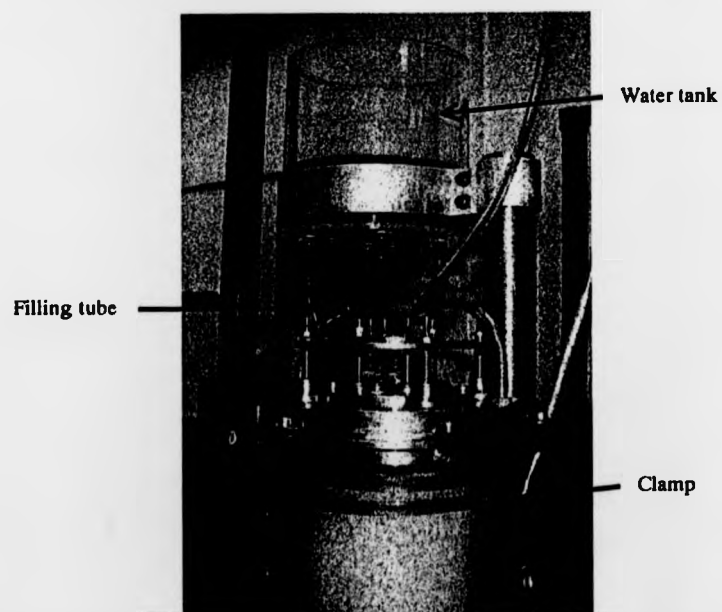


FIGURE 8.4: Picture of the top of the apparatus showing the water tank and the clamp of the diaphragm.

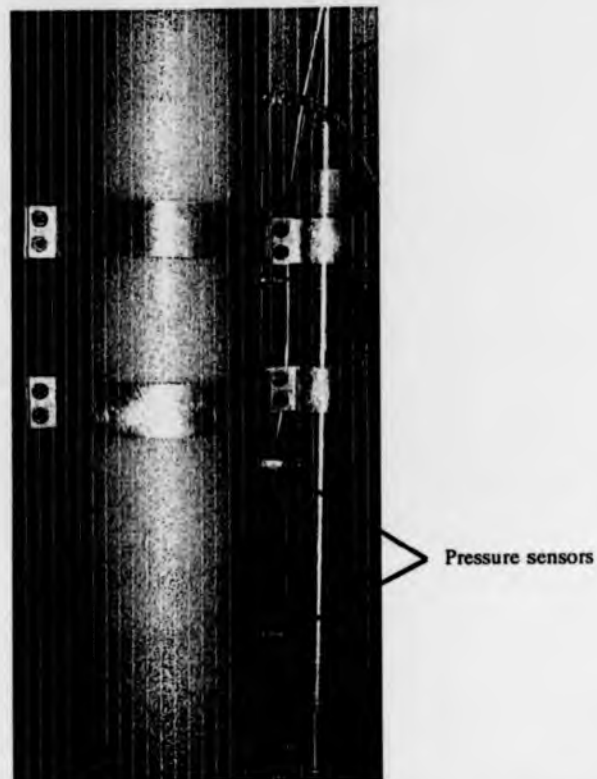


FIGURE 8.5: Picture of the middle part of the apparatus showing the pressure sensors.

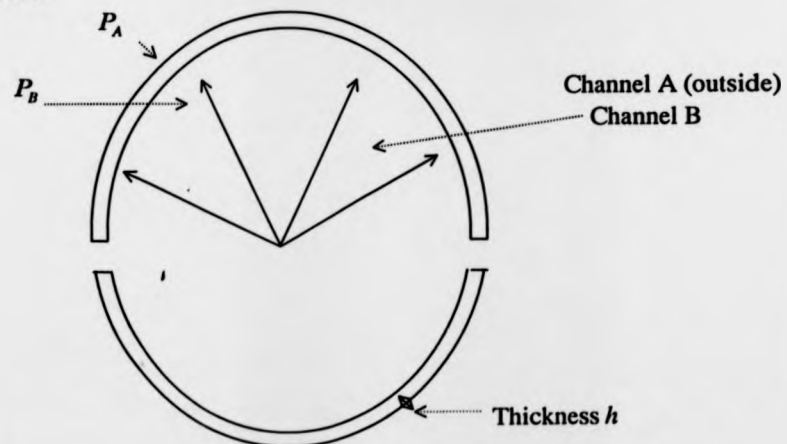


Figure 8.6: Diagram to determine the theoretical wave speed.

B.8 FIGURES OF CHAPTER 9

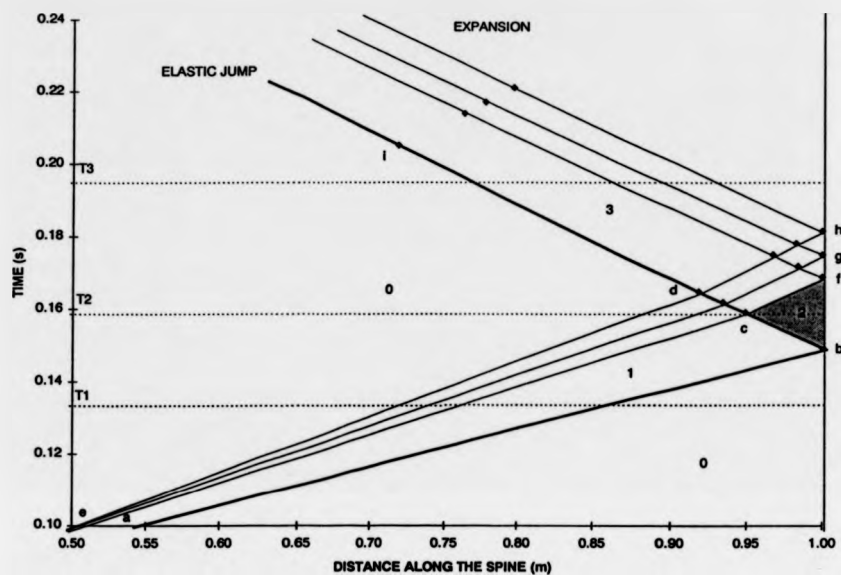


FIGURE 9.1a: Variation of wave fronts with time and distance.

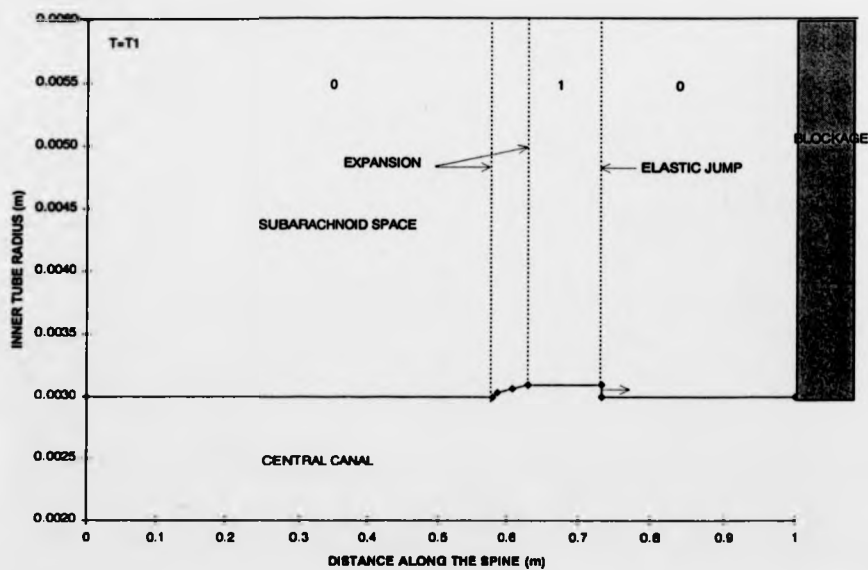


FIGURE 9.1b: Pulse of pressure difference drop approaching the blockage.

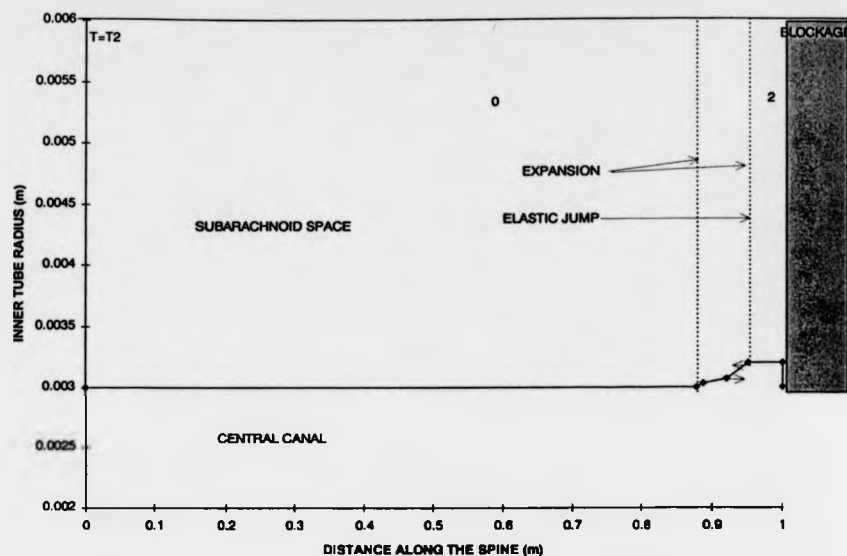


FIGURE 9.1c: Immediately after leading-edge elastic jump reflects from blockage.

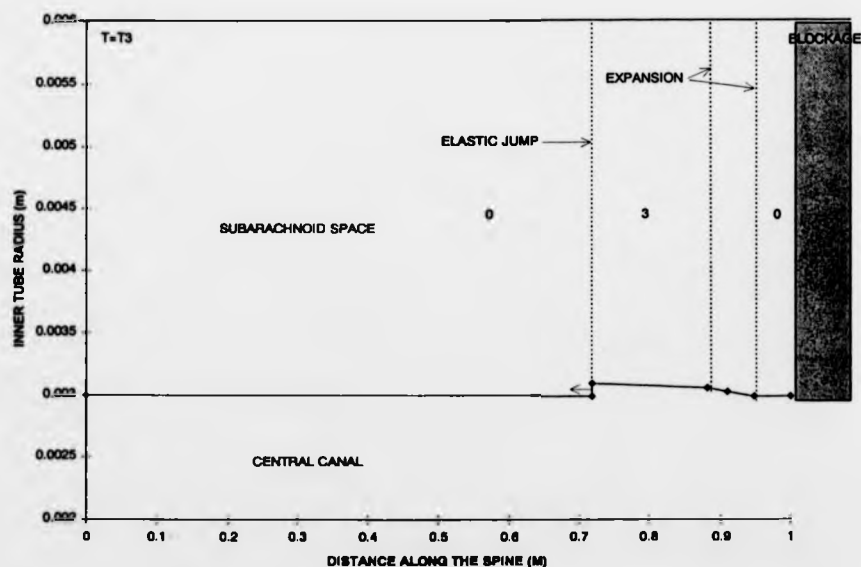


FIGURE 9.1d: Shortly after whole pressure pulse has reflected from blockage.

FIGURE 9.1: Propagation of a pulse of finite pressure difference drop along the two-chamber channel and reflection from a blockage in the upper channel.

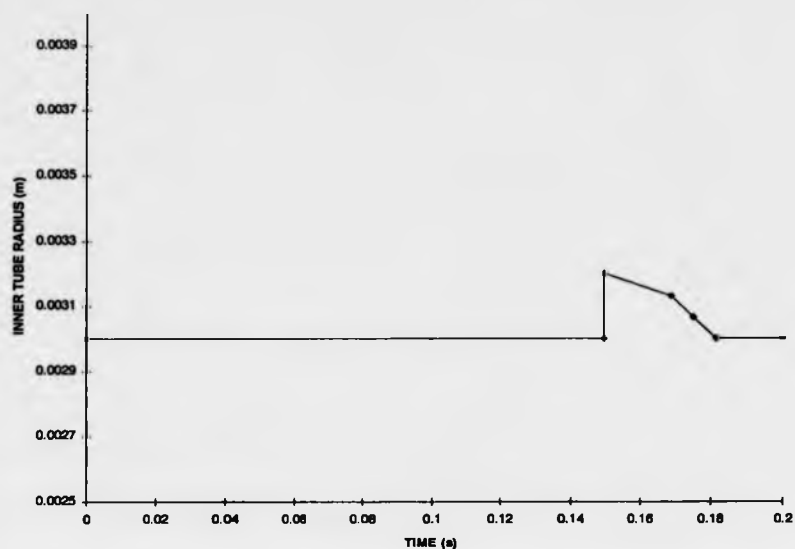


FIGURE 9.2: Inner tube radius variations with time at the blockage.

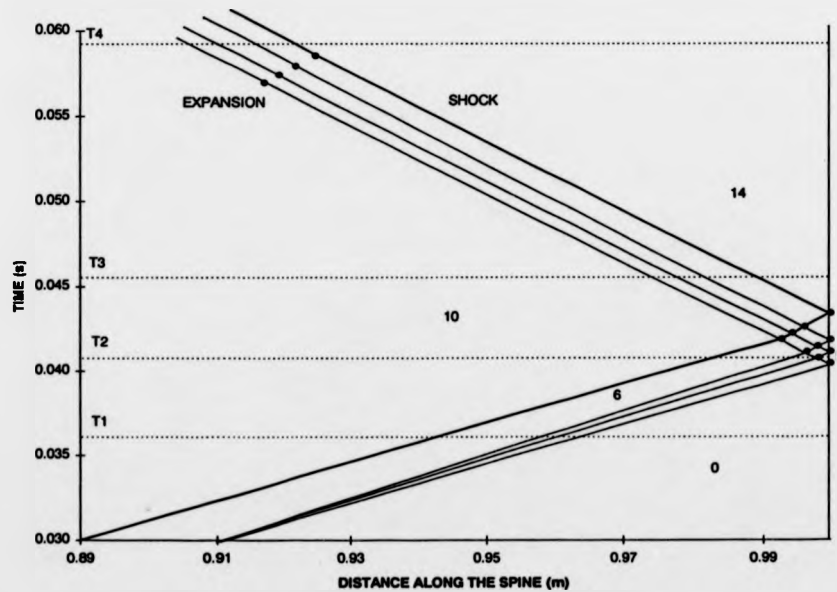


FIGURE 9.3a: Variation of wave fronts with time and distance.

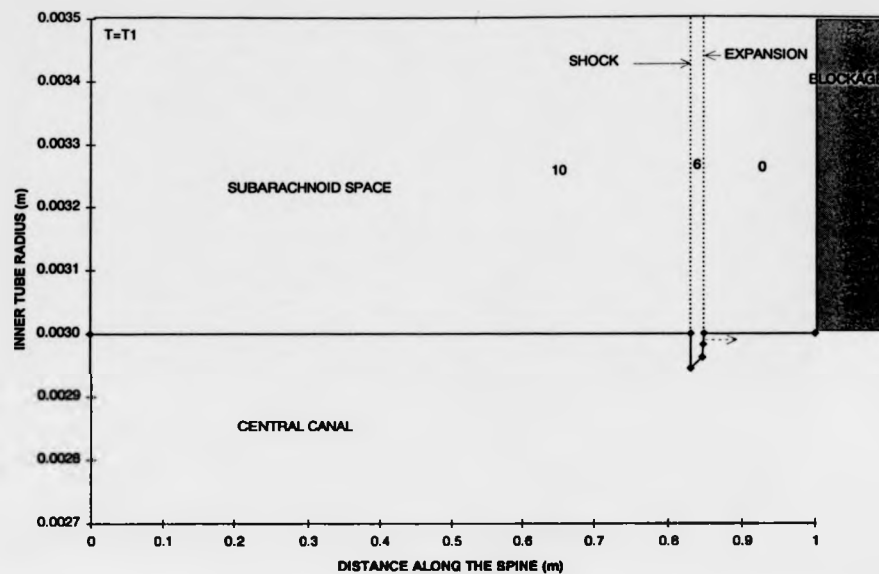


FIGURE 9.3b: Pulse of pressure difference rise approaching the blockage.

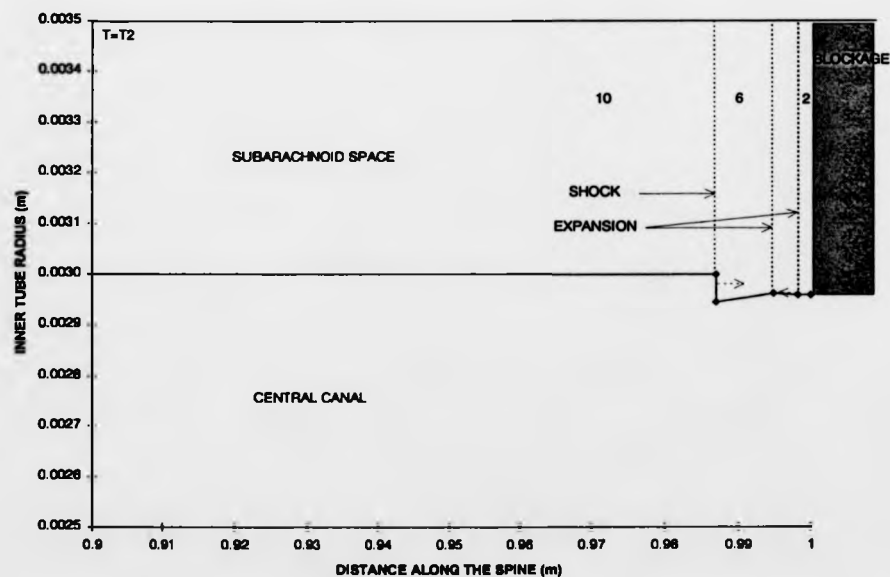


FIGURE 9.3c: Immediately after the first characteristic wave reflects from blockage.

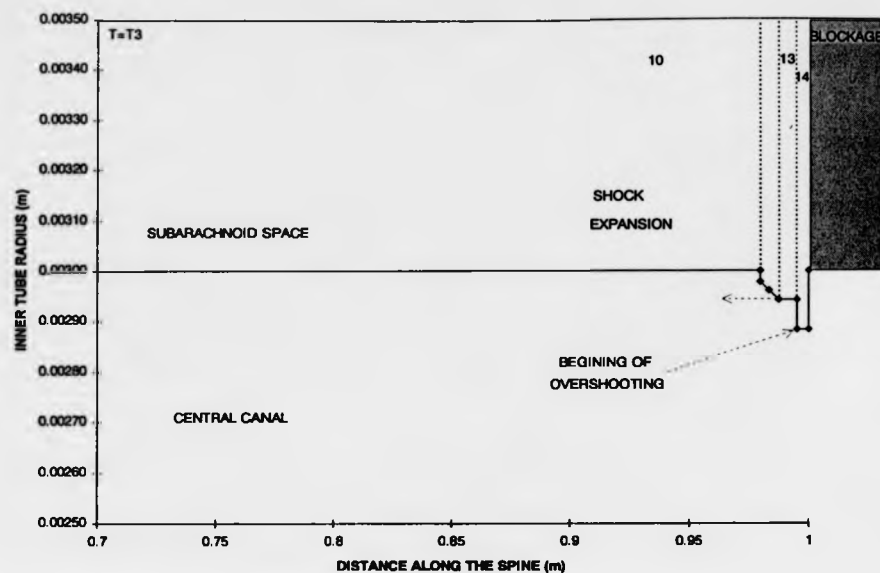


FIGURE 9.3d: Shortly after the whole pressure pulse has reflected: the overshooting effect.

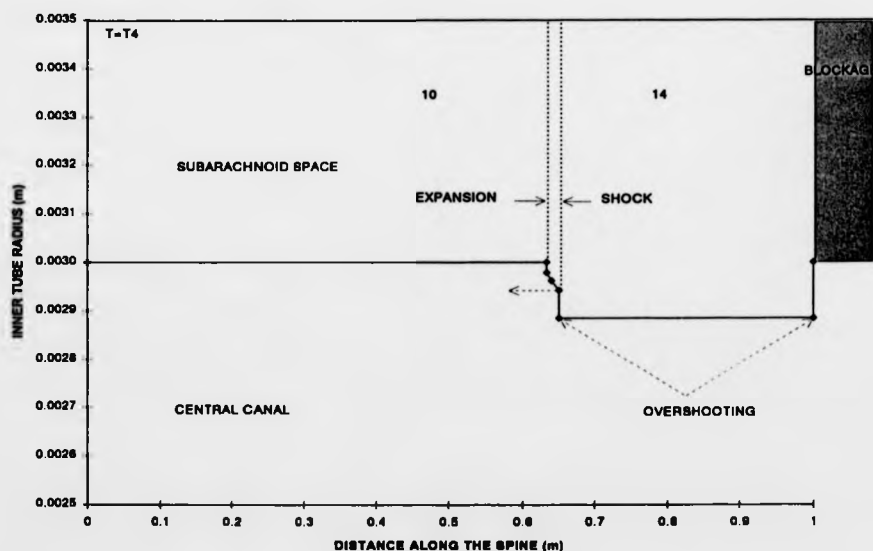


FIGURE 9.3e: Some time after the whole pressure pulse has reflected: the overshooting effect.

FIGURE 9.3: Propagation of a finite pulse of a pressure difference rise along the two-chamber channel and reflection in the upper ($U_{Au} = 1 \text{ mm/s}$).

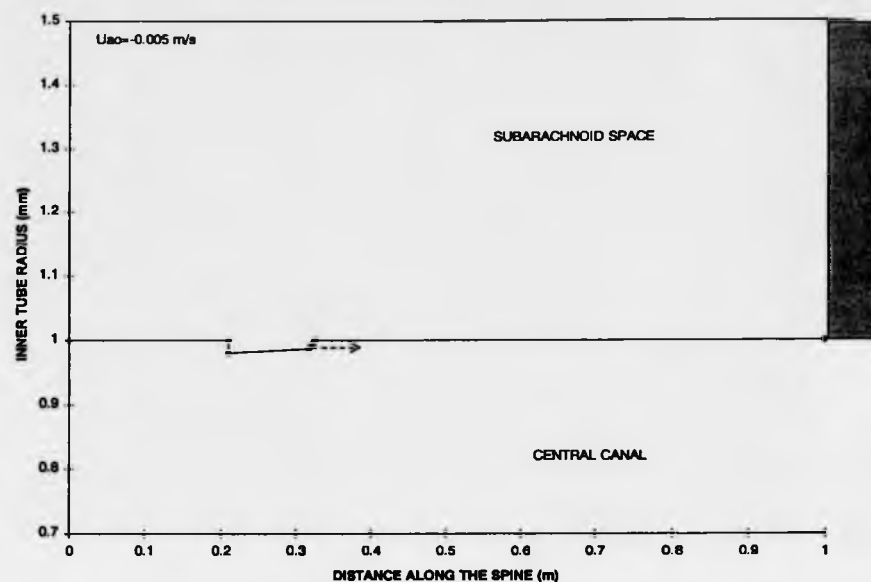


FIGURE 9.4a: Pulse of pressure difference rise approaching the blockage.

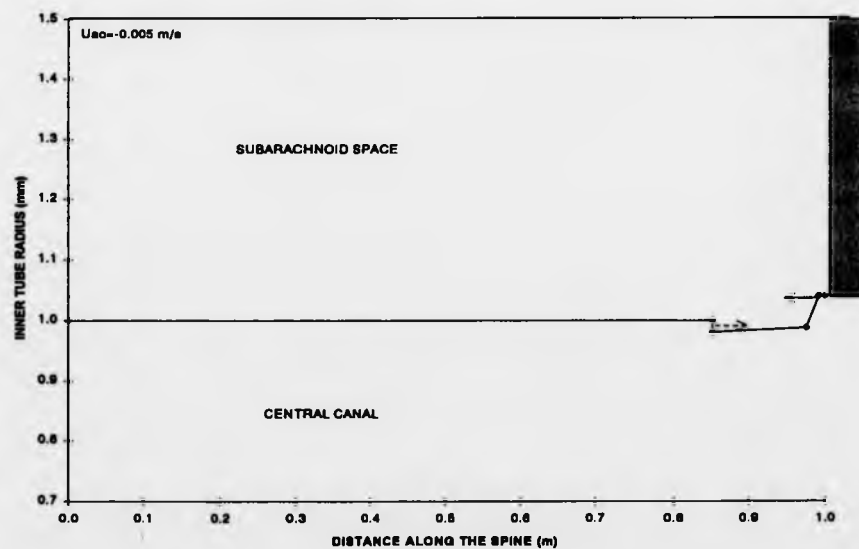


FIGURE 9.4b: Immediately after the first characteristic wave reflects from blockage.

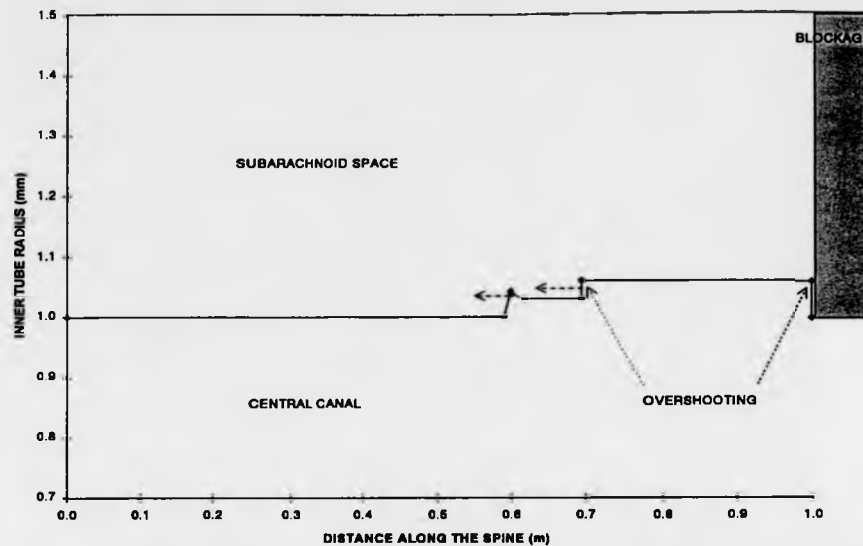


FIGURE 9.4c: Shortly after the whole pressure pulse has reflected: the overshooting effect.

FIGURE 9.4: Propagation of a finite pulse having a pressure difference rise along the two-chamber channel and reflection in the upper channel when the undisturbed velocity in the upper chamber is negative. (Pressure difference impulse: 1000 Pa and $U_{Ao} = -5 \text{ mm/s}$).

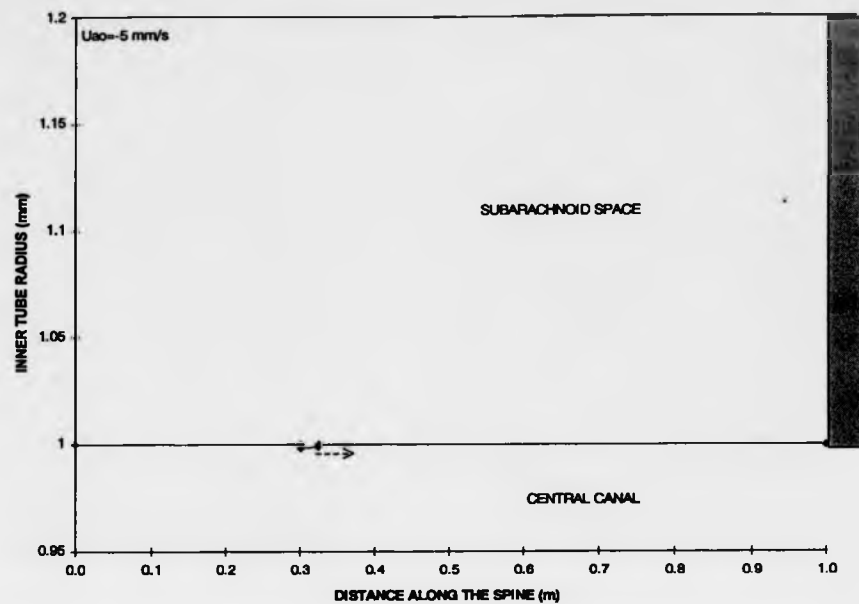


FIGURE 9.5a: Pulse of pressure difference rise approaching the blockage.

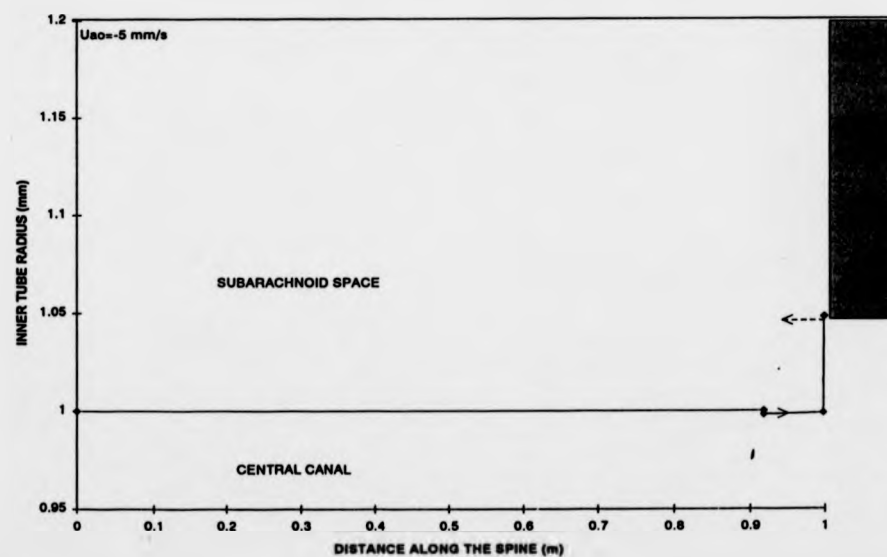


FIGURE 9.5b: Immediately after the first characteristic wave reflects from blockage.

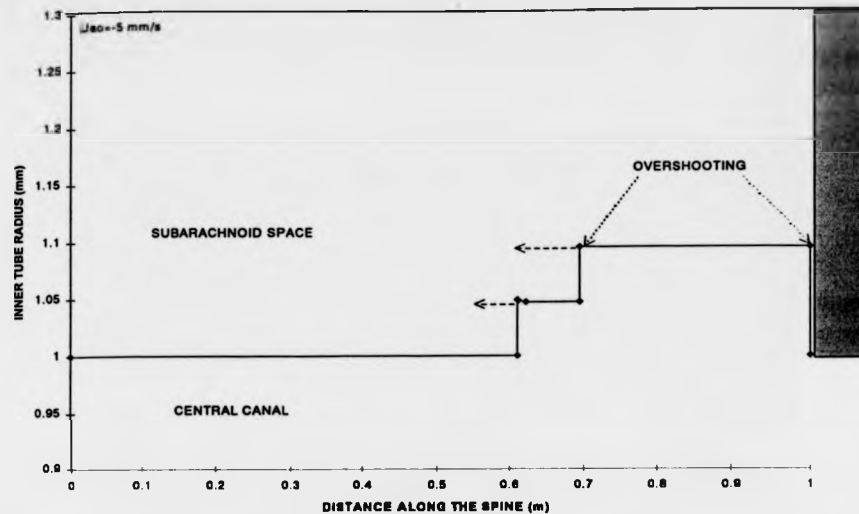


FIGURE 9.5c: Shortly after the whole pressure pulse has reflected: the overshooting effect.

FIGURE 9.5: Propagation of a finite pulse having a small pressure difference rise along the two-chamber channel and reflection in the upper channel when the undisturbed velocity in the upper chamber is negative. (Pressure difference impulse: 100 Pa and $U_{Ao} = -5 \text{ mm/s}$)

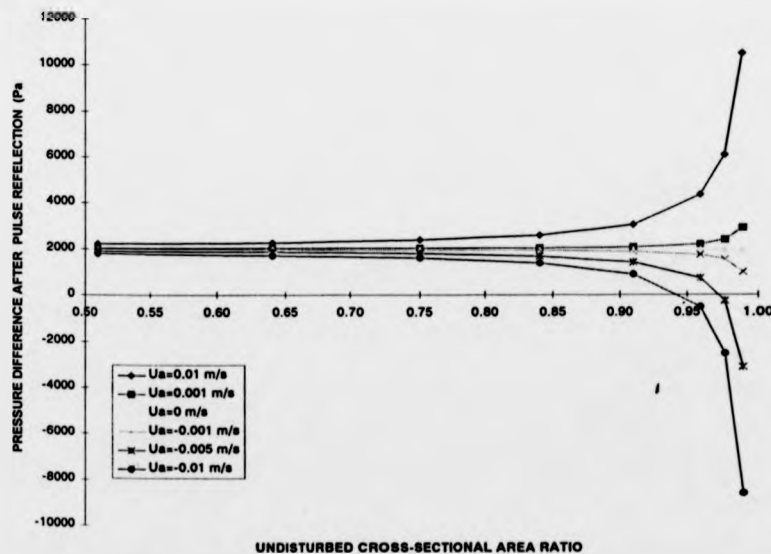


FIGURE 9.6: Effect of the undisturbed inner chamber velocity on the pressure difference after the whole pulse has reflected (region 14) for various undisturbed cross-sectional area ratios (Pressure impulse: 1000 Pa).

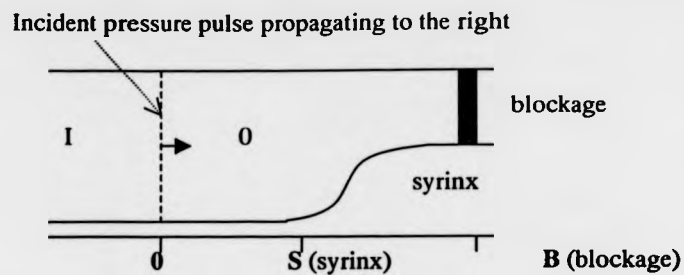


FIGURE 9.7: Diagram for an incident pressure pulse reaching a syringe.

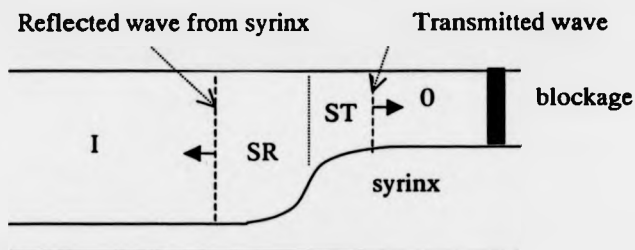


FIGURE 9.8: Diagram for the reflected and transmitted pressure waves from the beginning of the syringe.

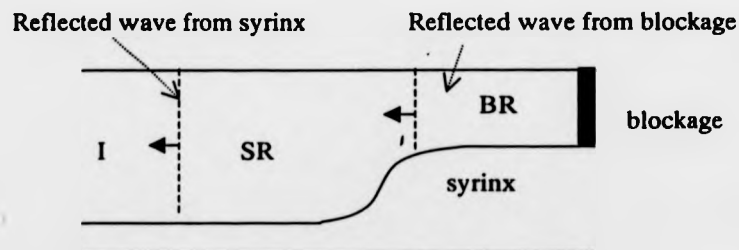


FIGURE 9.9: Diagram after the transmitted wave has reflected from the blockage.

APPENDIX A

METHOD OF CHARACTERISTICS

INTRODUCTION

In this section, we will derive the characteristic lines and compatibility equations for the linear, fully non-linear and weakly non-linear cases. A standard way of obtaining the characteristic lines and the compatibility equations is described in many books (Zucrow & Hoffman, 1977, for instance). We follow the technique step by step.

Let us recall the governing equations of our model (equations 6.16, 6.17 and 6.20 in section 6.3.2):

$$D \frac{\partial \Delta P}{\partial t} + D U_A \frac{\partial \Delta P}{\partial x} + \alpha \frac{\partial U_A}{\partial x} = 0 \quad (6.16)$$

$$-D \frac{\partial \Delta P}{\partial t} - D U_B \frac{\partial \Delta P}{\partial x} + (1 - \alpha) \frac{\partial U_B}{\partial x} = 0 \quad (6.17)$$

$$\frac{\partial U_A}{\partial t} - \frac{\partial U_B}{\partial t} + U_A \frac{\partial U_A}{\partial x} - U_B \frac{\partial U_B}{\partial x} + \frac{1}{\rho} \frac{\partial \Delta P}{\partial x} = 0 \quad (6.20)$$

Note: Relation between the fluid velocity in parts A and B.

If we add equations (5.3) and (5.4) we can write:

$$\frac{\partial (\alpha U_A' + (1 - \alpha) U_B)}{\partial x} = 0$$

We integrate this equation with respect to x :

$$U_B = \frac{-\alpha}{1 - \alpha} U_A + E(t)$$

Where $E(t)$ is a function of integration depending on the time only. We will show later that $E(t)$ has to be zero and we obtain the following relation:

$$U_B = \frac{-\alpha}{1-\alpha} U_A \quad (\text{A.1})$$

A.1 LINEAR CASE

If we linearize the above equations (see section 6.3.3.1), we obtain:

$$\frac{\partial U_A}{\partial t} - \frac{\partial U_B}{\partial t} + \frac{1}{\rho} \frac{\partial \Delta P}{\partial x} = 0 \quad (6.22)$$

$$D \frac{\partial \Delta P}{\partial t} + \alpha_o \frac{\partial U_A}{\partial x} = 0 \quad (6.23)$$

$$-D \frac{\partial \Delta P}{\partial t} + (1 - \alpha_o) \frac{\partial U_B}{\partial x} = 0 \quad (6.24)$$

A.1.1 Characteristic lines

We take a linear combination of our governing equations (6.22, 6.23, 6.24):

$$\sigma_1(6.22) + \sigma_2(6.23) + \sigma_3(6.24) = 0$$

We develop this equation and rearrange it to obtain:

$$\begin{aligned} & \sigma_1 \left[\frac{\partial U_A}{\partial t} + \frac{\sigma_2 \alpha_o}{\sigma_1} \frac{\partial U_A}{\partial x} \right] - \sigma_1 \left[\frac{\partial U_B}{\partial t} + \frac{\sigma_3 (1 - \alpha_o)}{-\sigma_1} \frac{\partial U_B}{\partial x} \right] + \\ & D(\sigma_2 - \sigma_3) \left[\frac{\partial \Delta P}{\partial t} + \frac{\sigma_1}{\rho D(\sigma_2 - \sigma_3)} \frac{\partial \Delta P}{\partial x} \right] = 0 \end{aligned} \quad (\text{A.2})$$

If we set $\lambda = \frac{dx}{dt}$ (i.e. the slope of a characteristic line), then we can write:

$$\lambda = \frac{\alpha_o \sigma_2}{\sigma_1} = \frac{(1 - \alpha_o) \sigma_3}{-\sigma_1} = \frac{\sigma_1}{\rho D(\sigma_2 - \sigma_3)} \quad (\text{A.3})$$

We can then write $dU_A = \frac{\partial U_A}{\partial t} + \lambda \frac{\partial U_A}{\partial x}$. Doing the same for dU_B and $d\Delta P$, equation

(A.2) becomes:

$$\sigma_1 dU_A - \sigma_1 dU_B + D(\sigma_2 - \sigma_3) d\Delta P = 0 \quad (\text{A.4})$$

We can write the set of equations (A.3) in their matrix form:

$$\begin{bmatrix} \lambda & -\alpha_o & 0 \\ \lambda & 0 & 1 - \alpha_o \\ -1 & \rho D \lambda & -\rho D \lambda \end{bmatrix} \begin{bmatrix} \sigma_1 \\ \sigma_2 \\ \sigma_3 \end{bmatrix} = \begin{bmatrix} 0 \\ 0 \\ 0 \end{bmatrix} \quad (\text{A.5})$$

For equation (A.5) to have a solution for $\sigma_1, \sigma_2, \sigma_3$ other than the trivial one $\sigma_1 = \sigma_2 = \sigma_3 = 0$, the determinant of the coefficients of σ_i must be zero. Developing this determinant, and setting it equal to zero, we obtain:

$$\lambda^2 = \frac{\alpha_o (1 - \alpha_o)}{\rho D}$$

Note: we can show here that the type of partial differential equation is hyperbolic since the expression of λ^2 is strictly positive.

Comparing this equation of λ to equation (6.21), we have:

$$\lambda_{\pm} = \pm C_o = \left(\frac{dx}{dt} \right)_{\pm} \quad (\text{A.6, A.7})$$

Equations (A.6, A.7) are the characteristic lines. The upper sign stands for a wave propagating in the positive direction of x , whereas the lower sign corresponds to a wave propagating in the negative direction of x .

A.1.2 Compatibility equations

Equation (A.4) corresponds to the compatibility equations. In order to use it we need to find the values of the σ_i along the characteristic lines (A.6, A.7).

From the equation (A.5) (matrix form), we can easily obtain the following relations:

$$\sigma_2 = \frac{\lambda}{\alpha_o} \sigma_1 \quad (\text{A.8})$$

$$\sigma_3 = \frac{-\lambda}{1 - \alpha_o} \sigma_1 \quad (\text{A.9})$$

We insert equations (A.8, A.9) into the remaining equation of (A.5) to get:

$$\sigma_1 \left(\lambda^2 \frac{\rho D}{\alpha_o (1 - \alpha_o)} - 1 \right) = 0$$

If we take into account the expression of λ^2 along the characteristic lines, the expression between parentheses is zero, whatever the value of σ_1 . This implies that σ_1 is arbitrary.

Expression of dU_B for equation (A.4).

We derive equation (A.1) applied to the linear case and we obtain:

$$dU_B = \frac{-\alpha_o}{1 - \alpha_o} dU_A \quad (\text{A.10})$$

We insert equations (A.8, A.9, A.10) into equation (A.4), and we rearrange to find that:

$$\sigma_1 \left(dU_A + \frac{D\lambda}{\alpha_o} d\Delta P \right) = 0$$

We showed that σ_1 is arbitrary, so that the expression between parentheses is zero. We also consider the expressions of λ from the characteristic lines (equations A.6, A.7) to finally obtain:

$$dU_A \pm \left(\frac{1 - \alpha_o}{\rho C_o} \right) d\Delta P = 0 \quad (\text{A.11, A.12})$$

If we insert equation (A.10) into equations (A.11) and (A.12), we can get similar compatibility equations linking U_B and ΔP :

$$-dU_B \pm \left(\frac{\alpha_o}{\rho C_o} \right) d\Delta P = 0 \quad (\text{A.13, A.14})$$

A.2 FULLY NON-LINEAR CASE

We follow exactly the same general approach as in the linear case in determining the characteristic and compatibility equations.

A.2.1 Characteristic lines

We take a linear combination of our governing equations (6.16, 6.17, 6.20):

$$\sigma_1(6.20) + \sigma_2(6.16) + \sigma_3(6.17) = 0$$

We develop this equation and we rearrange to obtain:

$$\begin{aligned} & \sigma_1 \left[\frac{\partial U_A}{\partial t} + \frac{\sigma_1 U_A + \sigma_2 \alpha}{\sigma_1} \frac{\partial U_A}{\partial x} \right] - \sigma_1 \left[\frac{\partial U_B}{\partial t} + \frac{-\sigma_1 U_B + \sigma_3(1 - \alpha)}{-\sigma_1} \frac{\partial U_B}{\partial x} \right] + \\ & D(\sigma_2 - \sigma_3) \left[\frac{\partial \Delta P}{\partial t} + \frac{\frac{\sigma_1}{\rho} + DU_A \sigma_2 - DU_B \sigma_3}{D(\sigma_2 - \sigma_3)} \frac{\partial \Delta P}{\partial x} \right] = 0 \end{aligned} \quad (\text{A.15})$$

If we set $\lambda = \frac{dx}{dt}$ then we can write:

$$\lambda = \frac{\sigma_1 U_A + \alpha \sigma_2}{\sigma_1} = \frac{-\sigma_1 U_B + (1 - \alpha) \sigma_3}{-\sigma_1} = \frac{\frac{\sigma_1}{\rho} + DU_A \sigma_2 - DU_B \sigma_3}{D(\sigma_2 - \sigma_3)} \quad (\text{A.16})$$

We can then write $dU_A = \frac{\partial U_A}{\partial t} + \lambda \frac{\partial U_A}{\partial x}$. Doing the same for dU_B and $d\Delta P$, so

equation (A.15) becomes:

$$\sigma_1 dU_A - \sigma_1 dU_B + D(\sigma_2 - \sigma_3) d\Delta P = 0 \quad (\text{A.17})$$

so that we can write equation (A.16) in its matrix form:

$$\begin{bmatrix} \lambda - U_A & -\alpha & 0 \\ \lambda - U_B & 0 & 1 - \alpha \\ -\frac{1}{\rho} & D(\lambda - U_A) & -D(\lambda - U_B) \end{bmatrix} \begin{bmatrix} \sigma_1 \\ \sigma_2 \\ \sigma_3 \end{bmatrix} = \begin{bmatrix} 0 \\ 0 \\ 0 \end{bmatrix} \quad (\text{A.18})$$

The above determinant of the (3×3) matrix has to be zero. Developing this determinant, and setting it equal to zero, we obtain the following quadratic equation (substituting the expressions of U_B and C^2 defined before):

$$\lambda^2 - 2U_A \frac{1-2\alpha}{1-\alpha} \lambda + U_A^2 \frac{1-3\alpha+3\alpha^2}{(1-\alpha)^2} - C^2 = 0$$

We solve this quadratic equation to find:

$$\lambda_{\pm} = \frac{1}{1-\alpha} \left((1-2\alpha)U_A \pm C\sqrt{(1-\alpha)^2 - \rho DU_A^2} \right)$$

We have seen that $(1-\alpha)$ is always positive. This implies that the expression within the absolute value is always positive. We can therefore write the characteristic lines as:

$$\lambda_{\pm} = \frac{1}{1-\alpha} \left((1-2\alpha)U_A \pm C\sqrt{(1-\alpha)^2 - \rho DU_A^2} \right) \quad (\text{A.19, A.20})$$

Equations (A.19, A.20) are the characteristic lines. The upper sign stands for a discontinuity propagating in the positive direction of x , whereas the lower sign

corresponds to a discontinuity propagating in the negative direction of x . Note that these lines are no longer straight lines unlike in the linear case.

A.2.2 Compatibility equations

Equation (A.17) corresponds to the compatibility equations. In order to use it we need to find the values of the σ_i along the characteristic lines (A.19, A.20).

From the equation (A.18) (matrix form), we can easily obtain:

$$\sigma_2 = \frac{\lambda - U_A}{\alpha} \sigma_1 \quad (\text{A.21})$$

$$\sigma_3 = -\frac{\lambda - U_B}{1 - \alpha} \sigma_1 \quad (\text{A.22})$$

We insert equations (A.21, A.22) into the remaining equation of (A.18) to get:

$$\sigma_1 \left(-\frac{\alpha(1-\alpha)}{\rho D} + (1-\alpha)(\lambda - U_A)^2 + \alpha(\lambda - U_B)^2 \right) = 0$$

The expression in parentheses is equivalent to zero (this follows from setting the determinant of the set of equations A.18 to zero). This implies that σ_1 is arbitrary.

We differentiate equation (A.1) to obtain:

$$dU_B = \frac{-\alpha}{1-\alpha} dU_A - \frac{DU_A}{(1-\alpha)^2} d\Delta P \quad (\text{A.23})$$

We insert equations (A.21, A.22, A.23) into equation (A.17), and we rearrange to get:

$$\sigma_1 \left(dU_A + \frac{D}{\alpha} \left(\lambda + U_A \frac{3\alpha-1}{1-\alpha} \right) d\Delta P \right) = 0$$

We showed that σ_1 is arbitrary, so that the expression between parenthesis is zero. We also use the expression for λ from the characteristic lines (equations A.19, A.20) and the wave speed equation (5.18) to finally obtain:

$$dU_A + \frac{1}{\rho C} \left(\frac{\alpha U_A}{C} \pm \sqrt{(1-\alpha)^2 - \rho D U_A^2} \right) d\Delta P = 0 \quad (\text{A.24, A.25})$$

Equations (A.24, A.25) are the compatibility equations in the non-linear case. They only hold along the characteristic lines defined above. The upper and lower sign respectively denotes the characteristic lines in the positive (C_+) and negative (C_-) direction.

A.3 WEAKLY NON-LINEAR CASE

Here we develop a weakly non-linear theory in order to be able to discuss the possibility of the creation of an elastic jump (or a shock-like wave). Indeed, since the characteristic lines are all of the same slope in the linear case these lines can never join together to form a discontinuity in the fluid properties. In the fully non-linear case, it is possible to see the lines coming together, but one has to obtain numerical results to do so. That is why we develop a weakly non-linear theory. We will be able to discuss qualitatively the creation of an elastic jump or the formation of an expansion wave. Indeed we will compare with the discussion already made in the previous chapter, in the case where the total cross-sectional area A_T is constant (see section 5.5.2).

By weakly non-linear we mean that we neglect terms which are the product of two small quantities like: $U_A \times \Delta P$, U_A^2 , $U_n \times \Delta P$, ...

A3.1 Characteristic lines

Let us recall the quadratic equation in λ that we found in section A.2.1 by expanding the determinant of the matrix (A.18):

$$\lambda^2 - 2U_A \frac{1-2\alpha}{1-\alpha} \lambda + U_A^2 \frac{1-3\alpha+3\alpha^2}{(1-\alpha)^2} - C^2 = 0$$

Neglecting the third term on the left hand side of this equation and solving the equation for λ we can obtain (recalling equation 5.23):

$$\lambda_{\pm} = \frac{1-2\alpha_o}{1-\alpha_o} U_A \pm C_o \sqrt{1 + \frac{1-2\alpha_o}{\alpha_o(1-\alpha_o)} D\Delta P} \quad (\text{A.26, A.27})$$

Expanding the square roots yields:

$$\lambda_{\pm} \approx \frac{1-2\alpha_o}{1-\alpha_o} U_A \pm C_o \left(1 + \frac{1-2\alpha_o}{2\alpha_o(1-\alpha_o)} D\Delta P \right)$$

Note that if we set $U_A = \Delta P = 0$ in these characteristic lines, we go back to the linear case.

Across the characteristic lines, we have seen in the linear case that we have the following relation (equations A.11, A.12):

$$U_A = \pm \frac{1-\alpha_o}{\rho C_o} \Delta P$$

Note that we have considered that the undisturbed conditions were: $U_{Ao} = \Delta P_o = 0$.

We can now insert this relation in the weakly non-linear characteristic lines to write that:

$$\lambda_{\pm} = \pm C_o \pm C_o \frac{1-2\alpha_o}{2\alpha_o(1-\alpha_o)} D\Delta P \pm \frac{1}{\rho C_o} (1-2\alpha_o) \Delta P$$

where the upper and lower signs respectively stand for a right and left running characteristics.

The second term on the left hand side of the above equation is purely due to cross-sectional area change. The third term is due to induced fluid velocity.

Using equation 6.21, we can write the distensibility D as:

$$D = \frac{\alpha_o(1-\alpha_o)}{\rho C_o^2}$$

Using the above expression for the distensibility, the characteristic lines become:

$$\lambda_{\pm} = \pm C_o \pm \frac{3}{2\rho C_o}(1-2\alpha_o)\Delta P \quad (\text{A.28, A.29})$$

A.3.2 Compatibility equations

Applying the same reasoning as in section A.2.2, and recalling the simplifications for the weakly non-linear theory (section A.3.1), the compatibility equations for the weakly non-linear theory take the following form:

$$dU_{\lambda} + \frac{D}{\alpha_o} \left[\frac{\alpha_o}{1-\alpha_o} U_{\lambda} \pm C_o \left(1 - \frac{\alpha - \alpha_o}{2\alpha_o(1-\alpha_o)} \right) \right] d\Delta P = 0 \quad (\text{A.30, A.31})$$

APPENDIX B

ABOUT THE ELASTIC JUMP

B.1 ESTIMATE OF THE REFLECTED PRESSURE DIFFERENCE (SECTION 7.4.2.2)

Let us consider the form of the pressure differences ratio (reflected/incident):

$$\frac{\Delta P_r}{\Delta P_i} = 2 + \Lambda \varepsilon \quad (7.28)$$

where $\varepsilon = D\Delta P_i$ (7.24), and Λ is to be determined.

With equations (7.23), (7.25) and (7.28), we can write the following relations:

$$\frac{\alpha_o}{\alpha_i} = 1 - \frac{1}{\alpha_o} \varepsilon + \frac{1}{\alpha_o^2} \varepsilon^2 + O(\varepsilon^3)$$

$$\frac{\alpha_o}{\alpha_r} = 1 - \frac{2}{\alpha_o} \varepsilon + \left(\frac{4}{\alpha_o^2} - \frac{\Lambda}{\alpha_o} \right) \varepsilon^2 + O(\varepsilon^3)$$

$$\frac{\alpha_i}{\alpha_r} = 1 - \frac{1}{\alpha_o} \varepsilon + \left(\frac{2}{\alpha_o^2} - \frac{\Lambda}{\alpha_o} \right) \varepsilon^2 + O(\varepsilon^3)$$

$$\frac{1 - \alpha_o}{1 - \alpha_i} = 1 + \frac{1}{1 - \alpha_o} \varepsilon + \frac{1}{(1 - \alpha_o)^2} \varepsilon^2 + O(\varepsilon^3)$$

$$\frac{1 - \alpha_o}{1 - \alpha_r} = 1 + \frac{2}{1 - \alpha_o} \varepsilon + \left(\frac{4}{(1 - \alpha_o)^2} + \frac{\Lambda}{1 - \alpha_o} \right) \varepsilon^2 + O(\varepsilon^3)$$

$$\frac{1 - \alpha_i}{1 - \alpha_r} = 1 + \frac{1}{1 - \alpha_o} \varepsilon + \left(\frac{2}{(1 - \alpha_o)^2} + \frac{\Lambda}{1 - \alpha_o} \right) \varepsilon^2 + O(\varepsilon^3)$$

$$\frac{\alpha_o - \alpha_i}{\alpha_i - \alpha_r} = 1 - \Lambda \varepsilon + \Lambda^2 \varepsilon^2 + O(\varepsilon^3)$$

In these relations we have assumed that $|\Delta P_i| \ll \frac{\alpha_o}{D}$, $|\Delta P_i| \ll \frac{1 - \alpha_o}{D}$, and that

$|\Delta P_i| \ll \frac{1}{D\Lambda}$. These assumptions are validated in section 7.6.3.

First order approximations

In the above relations, we only keep the terms in ε . Moreover, we do not keep the term in Λ in equation (7.28). We also make the approximation that the shock-like wave speeds before and after the reflection are the same and equal to the wave speed in the undisturbed conditions: $V_{Si} = V_{SR} = C_0$.

In these conditions, using the appropriate approximations in equation (7.26) and recalling equations (7.10) and (7.12) for P_{A2} and U_A , we can deduce the pressure in the outer tube after the reflection of the elastic jump:

$$P_{AR} \approx \frac{2\rho C_0^2}{\alpha_o} \varepsilon$$

We do the same with equations (7.27), (7.11) and (7.13) to obtain the pressure in the inner tube after the reflection of the elastic jump:

$$P_{BR} \approx -\frac{2\rho C_0^2}{1 - \alpha_i} \varepsilon$$

Thus, we can readily write:

$$\Delta P_R = P_{AR} - P_{BR} \approx \frac{2\rho C_0^2 \varepsilon}{\alpha_o(1 - \alpha_o)}$$

If we recall the wave speed definition, we notice that the above equation is equivalent to:

$$\Delta P_R = 2\Delta P_I$$

which is equivalent to equation 7.28.

Second order approximations

We now keep the terms of order ε^2 , and we consider the whole of equation (7.28).

From equation (7.20), we can write:

$$V_{SR} \approx (1 - \Lambda\varepsilon + \Lambda^2\varepsilon^2)V_{SI} \quad (\text{B.1})$$

Using equations (7.12) and (7.10), we can deduce that:

$$\frac{\alpha_I}{\alpha_R} P_{AI} \approx \rho V_{SI}^2 \left(\frac{1}{\alpha_o} - \frac{3}{\alpha_o^2} \varepsilon \right)$$

We insert the above relations for V_{SR} and $\frac{\alpha_I}{\alpha_R} P_{AI}$ in equation (7.26), and we use the

appropriate approximations to obtain:

$$P_{AR} \approx \rho V_{SI}^2 \varepsilon \left(\frac{2}{\alpha_o} - \left(\frac{4}{\alpha_o^2} + \frac{\Lambda}{\alpha_o} \right) \varepsilon \right)$$

Proceeding exactly in the same way for P_{BR} by the mean of equations (7.11), (7.13), (7.27) and (7.29), we find that:

$$P_{BR} \approx \rho V_{SI}^2 \varepsilon \left(-\frac{2}{1-\alpha_o} + \left(-\frac{4}{(1-\alpha_o)^2} + \frac{\Lambda}{1-\alpha_o} \right) \varepsilon \right)$$

We can then deduce the relation for the pressure difference after reflection:

$$\Delta P_R \approx \frac{\rho V_{SI}^2 \varepsilon}{\alpha_o(1-\alpha_o)} \left(2 + \left(4 \left(\frac{1}{\alpha_o} - \frac{1}{1-\alpha_o} \right) - \Lambda \right) \varepsilon \right)$$

Recalling equations (7.24), (7.28) and considering the propagation speed of the elastic jump as the wave speed, we can find Λ :

$$\Lambda = -\frac{1}{2} \left(\frac{1}{1-\alpha_o} - \frac{1}{\alpha_o} \right) \quad (\text{B.2})$$

And thus, with equation (7.28), we can evaluate the ratio of pressure difference of the reflected wave over the incident one:

$$\frac{\Delta P_R}{\Delta P_I} \approx 2 - \frac{1}{2} \left(\frac{1}{1-\alpha_o} - \frac{1}{\alpha_o} \right) D \Delta P_I \quad (\text{B.3})$$

B.2 OBTAINMENT OF THE FLUID PROPERTIES IN REGION 4 FOR THE COMBINED METHOD (section 7.7.2)

Let us obtain the fluid properties for the case of region (4), as depicted in figure 7.13 (see section 7.7.2). We can see that a left-running elastic jump (reflected jump) separates regions (3) and (4), whereas a C^* separates (2) from (4). At this stage of the calculations, all the properties in regions (2) and (3) are known.

Applying equations (7.1 to 7.4) to a left-running elastic jump (line cd in figure 7.13), yields:

$$U_{A4} = -\frac{\alpha_4 - \alpha_3}{\alpha_4} V_{S2} + \frac{\alpha_3}{\alpha_4} U_{A3} \quad (\text{B.4})$$

where the subscript numbers denote the region and V_{S2} is the reflected shock-like wave speed from c to d in figure 7.13.

$$U_{B4} = \frac{\alpha_4 - \alpha_3}{1 - \alpha_4} V_{S2} + \frac{1 - \alpha_3}{1 - \alpha_4} U_{B3} \quad (\text{B.5})$$

$$P_{A4} = \frac{\alpha_3}{\alpha_4} P_{A3} - \rho \frac{\alpha_3}{\alpha_4} (U_{A3} + V_{S2})(U_{A4} - U_{A3}) \quad (\text{B.6})$$

$$P_{B4} = \frac{1-\alpha_3}{1-\alpha_4} P_{B3} - \rho \frac{1-\alpha_3}{1-\alpha_4} (U_{B3} + V_{S2})(U_{B4} - U_{B3}) \quad (\text{B.7})$$

The tube-law, in this case, can be written as:

$$\alpha_4 = \alpha_o + D(P_{A4} - P_{B4}) \quad (\text{B.8})$$

So far, we have 5 equations and 6 unknowns, namely $P_{A4}, P_{B4}, U_{A4}, U_{B4}, V_{S2}, \alpha_4$.

However, using a characteristic line (C^-), we can write the compatibility equation which is valid only on this line (see section 6.3):

$$U_{A4} + Q_- \Delta P_4 = U_{A2} + Q_- \Delta P_2 = K_- \quad (\text{B.9})$$

$$\text{where} \quad Q_- = \frac{1}{\rho C} \left(\frac{\alpha U_A}{C} - \sqrt{-\rho D U_A^2 + (1-\alpha)^2} \right) \quad (\text{B.10})$$

and K_- is constant along the characteristic line.

Note that Q_- is first determined in region (2) in a predictor step and is then evaluated in an average manner between region (2) and (4) for the corrector step.

We now have a set of 6 equations with 6 unknowns, and thus we can find all the fluid properties in region (4).

We isolate V_{S2} from equations B.4 and B.5 in order to obtain the inner tube fluid velocity in region (4):

$$U_{B4} = -\frac{\alpha_4}{1-\alpha_4} U_{A4} + \frac{\alpha_3}{1-\alpha_4} U_{A3} + \frac{1-\alpha_3}{1-\alpha_4} U_{B3} \quad (\text{B.11})$$

From equation B.4, we can also express the shock-like wave speed V_{s2} in terms of U_{A4} to obtain:

$$V_{s2} = \frac{\alpha_4}{\alpha_3 - \alpha_4} U_{A4} - \frac{\alpha_3}{\alpha_3 - \alpha_4} U_{A3} \quad (\text{B.12})$$

We insert equation B.12 in equation B.6 in order to obtain the outer tube fluid pressure in region (4):

$$P_{A4} = \frac{\alpha_3}{\alpha_4} P_{A3} - \rho \frac{\alpha_3}{\alpha_3 - \alpha_4} (U_{A4} - U_{A3})^2 \quad (\text{B.13})$$

We insert equations B.11 and B.12 in equation B.7 to obtain the inner tube fluid pressure in region (4):

$$P_{B4} = \frac{1 - \alpha_3}{1 - \alpha_4} P_{B3} + \rho \frac{1 - \alpha_3}{(1 - \alpha_4)^2 (\alpha_3 - \alpha_4)} (\alpha_4 U_{A4} - \alpha_3 U_{A3} + (\alpha_3 - \alpha_4) U_{B3})^2 \quad (\text{B.14})$$

If we now express α_4 and U_{A4} in terms of pressure difference ΔP_4 in the expression between brackets (using equations B.8 and B.9 respectively), we can write for equations B.13 and B.14:

$$P_{A4} = \frac{\alpha_3}{\alpha_4} P_{A3} - \rho \frac{\alpha_3}{\alpha_3 - \alpha_4} (Q_- \Delta P_3 - K_- + U_{A3})^2$$

$$P_{B4} = \frac{1 - \alpha_3}{1 - \alpha_4} P_{B3} + \rho \frac{1 - \alpha_3}{(1 - \alpha_4)^2 (\alpha_3 - \alpha_4)} (-DK_- \Delta P_4^2 + (DK_- - \alpha_o Q_- - DU_{B3}) \Delta P_4 + \alpha_o K_- - \alpha_3 U_{A3} + (\alpha_3 - \alpha_o) U_{B3})^2$$

In order to obtain an expression only in terms of ΔP_4 , we expand the ratios where α_4 appears in the denominator:

$$\frac{\alpha_3}{\alpha_4} = \frac{\alpha_3}{\alpha_o} \left(1 - \frac{D}{\alpha_o} \Delta P_4 + \left(\frac{D}{\alpha_o} \Delta P_4 \right)^2 + O(\Delta P_4^3) \right)$$

$$\frac{1}{1-\alpha_4} = \frac{1}{1-\alpha_o} \left(1 + \frac{D}{1-\alpha_o} \Delta P_4 + \left(\frac{D}{1-\alpha_o} \Delta P_4 \right)^2 + O(\Delta P_4^3) \right)$$

We now form the expression ΔP_4 by subtracting P_{A4} and P_{B4} : $P_{A4} - P_{B4} = \Delta P_4$.

In this equation, we replace the expressions of P_{A4} and P_{B4} developed above using the expansions for the ratios in α_4 . We multiply both sides by $(\alpha_3 - \alpha_4)$ and we obtain, after some simple manipulations, an equation of the fifth degree in ΔP_4 :

$$\begin{aligned} & \left\{ -2\rho A^2 \frac{1-\alpha_3}{(1-\alpha_o)^3} \right\} \Delta P_4^5 + \left\{ -\rho \frac{1-\alpha_3}{D(1-\alpha_o)^2} \left(A^2 + 4 \frac{ABD}{1-\alpha_o} \right) \right\} \Delta P_4^4 + \\ & \left\{ -\rho \frac{1-\alpha_3}{D(1-\alpha_o)^2} \left(2AB + 2 \frac{D(AC+B^2)}{1-\alpha_o} \right) \right\} \Delta P_4^3 + \\ & \left\{ 1 + \frac{\alpha_3}{\alpha_o^2} DP_{A3} + \frac{1-\alpha_3}{(1-\alpha_o)^2} DP_{B3} - \frac{\rho}{D} \left(\alpha_3 Q^2 + \frac{1-\alpha_3}{(1-\alpha_o)^2} \left(2AC + B^2 + 4 \frac{BCD}{1-\alpha_o} \right) \right) \right\} \Delta P_4^2 \\ & + \left\{ -\Delta P_3 - \frac{\alpha_3}{\alpha_o^2} DP_{A3} \Delta P_3 - \frac{\alpha_3}{\alpha_o} P_{A3} - \frac{1-\alpha_3}{(1-\alpha_o)^2} DP_{B3} \Delta P_3 + \frac{1-\alpha_3}{1-\alpha_o} P_{B3} + \right. \\ & \left. \frac{\rho}{D} \left(\frac{1-\alpha_3}{(1-\alpha_o)^2} \left(-2\alpha_3 Q_- (K_- - U_{A3}) + 2BC + 2 \frac{C^2 D}{1-\alpha_o} \right) \right) \right\} \Delta P_4 + \\ & \left\{ \frac{\alpha_3}{\alpha_o} P_{A3} \Delta P_3 - \frac{1-\alpha_3}{1-\alpha_o} P_{B3} \Delta P_3 + \alpha_3 (K_- - U_{A3})^2 + \frac{1-\alpha_3}{(1-\alpha_o)^2} C^2 \right\} = 0 \end{aligned} \quad (B.15)$$

where $A = -Q_- D$

$$B = DK_- - \alpha_o Q_- - DU_{B3}$$

$$\text{and } C = \alpha_o K_- + (\alpha_3 - \alpha_o) U_{B3} - U_{A3}$$

Equation B.15 has 5 roots. After keeping the most suitable one (i.e. physically meaningful), we can find the rest of the fluid properties, following the procedure given immediately below.

From equation B.8 we can write that the cross-sectional areas ratio is:

$$\alpha_4 = \alpha_o + D\Delta P_4.$$

From equation B.9 we can obtain the fluid velocity in the outer tube:

$$U_{A4} = -Q_- \Delta P_4 + K_-.$$

We can then find the velocity in the inner tube and the propagation speed of the elastic jump respectively through equations B.11 and B.12:

$$U_{B4} = -\frac{\alpha_4}{1-\alpha_4} U_{A4} + \frac{\alpha_3}{1-\alpha_4} U_{A3} + \frac{1-\alpha_3}{1-\alpha_4} U_{B3}$$

$$V_{s2} = \frac{\alpha_4}{\alpha_3 - \alpha_4} U_{A4} - \frac{\alpha_3}{\alpha_3 - \alpha_4} U_{A3}$$

Finally we obtain the pressure in the inner and outer tube, using equations B.13 and B.14:

$$P_{A4} = \frac{\alpha_3}{\alpha_4} P_{A3} - \rho \frac{\alpha_3}{\alpha_3 - \alpha_4} (U_{A4} - U_{A3})^2$$

$$P_{B4} = \frac{1-\alpha_3}{1-\alpha_4} P_{B3} + \rho \frac{1-\alpha_3}{(1-\alpha_4)^2 (\alpha_3 - \alpha_4)} (\alpha_4 U_{A4} - \alpha_3 U_{A3} + (\alpha_3 - \alpha_4) U_{B3})^2$$

Note that only a simple verification is needed to check if the difference of the two above equations is equal to ΔP_4 , the root of equation B.15.

These calculations are made by a subroutine named *Mix*.

C- GLOSSARY

Definitions were taken from:

- (1) *International dictionary of medicine and biology* (three volumes) 1986. By Wiley Medical, S. I. Landau.
- (2) *The Oxford Companion to Medicine* (two volumes) 1986. By Walton, Beeson and Bodley Scott, Oxford University press, New York.
- (3) England M. A. and Wakely, J. 1991 *A Color Atlas of the Brain & Spinal Cord*. Wolfe Publishing Ltd, London.

Acro-osteolysis: The loss of terminal digits, with bone resorption.

Aetiology: The cause or causes of a particular disease.

Afferent: Towards (sensory if towards the central nervous system).

Albumen: is a soluble protein of high molecular weight which is the most abundant protein constituent of blood serum in vertebrates.

Anastomose: To create a communication between two separate structures.

Anencephalus: A fetus or newborn infant with anencephaly.

Anencephaly: is a congenital abnormality in which the osseous vault of the cranium is defective and the underlying cerebral hemispheres are either undeveloped or absent altogether.

Anterior: Pertaining to the foreparts of a body or part. In human anatomy, it corresponds roughly to 'ventral'.

Anteroposterior: Pertaining to both front and back, usually when referring to a direction or distance from front to back of the body or part.

Arachnoid mater: Middle layer of meninges.

Arachnoid villi: Main site of CSF reabsorption to the venous blood. (see also section 2.4.1)

Arachnoiditis: Inflammation of the arachnoid .

Arnold-Chiari Malformation: is a developmental anomaly which results in congenital downwards displacement of the cerebellum and medulla oblongata through the foramen magnum . There is usually obstruction to the circulation of cerebrospinal fluid with consequent hydrocephalus, and other congenital defects may be present.

Arthropathy: Any pathological condition affecting one or more joints.

Atlas: In human, a unique vertebra that lacks a body and spinous process.

Basilar invagination: See platybasia.

Bifid(a): split into two parts.

Bilateral: Having, affecting or pertaining to the two sides of an organ or the body.

Blue dextran: is a polysaccharide of high molecular weight which takes several weeks to undergo metabolic degradation. It has the capacity to expand blood volume.

Brainstem: Medulla, pons and midbrain. Some authors include the diencephalon. (see also section 2.3)

Bulbar: Pertaining to a bulb or denoting the medulla oblongata.

Calamus scriptorius: The tapering inferior extremity of the fourth ventricle.

Capillary: The smallest subdivision of the vessels forming the blood circulatory system (a hair or minute tube).

Caudal: Toward the tail or posterior end (in man, inferior).

Central canal (of spinal cord): A tenuous canal extending throughout the length of the spinal cord and continuing above into the medulla oblongata, where it enlarges to merge with the fourth ventricle. It is located centrally within the grey matter, is lined by ependyma, and contains a minute amount of CSF. (see also section 2.2.2)

Cerebellar hemisphere: One of two lateral component of the cerebellum. (see also section 2.3)

Cerebellum: "little brain", a dorsal outgrowth from the embryonic hindbrain. (see also section 2.3)

Cerebral cortex: The grey matter which forms the outmost layer of the two cerebral hemispheres .

Cerebral aqueduct (of Sylvius): Passage through midbrain, part of ventricular system. (see also section 2.4.2)

Cerebral hemisphere: One half of cerebrum. (see also section 2.3)

Cerebrospinal fluid (CSF): A clear, colorless fluid that circulates within the four ventricles of the brain and the subarachnoid spaces surrounding the brain and the cord. An ultrafiltrate of the blood secreted by the choroid plexus in the lateral, third and fourth ventricles, it is largely resorbed into the venous system via the arachnoid villi. (see also section 2.5)

Cerebrum: Largest part of the brain, consists of two hemispheres. (see also section 2.3)

Cervical: refering to the neck region.

Charcot's joint: Neuropathic arthropathy.

Chiasmatic (cistern): is an anatomical term denoting an intersection or decussation (crossing in the form of the letter x).

Choroidal: pertaining to the choroid .

Choroid plexus: Vascular structure secreting CSF into ventricles. (see also section 2.4.1)

Ciliary: Pertaining to or resembling the eyelashes or any cilia or hairlike processes.

Cisterna: expanded portion of subarachnoid space

Cisterna magna (cerebellomedullaris):

Cisterna venae magnae cerebri:

Cisternography: the demonstration of the anatomical spaces occupied by the CSF and of the circulation of kinetics of CSF by means of intrathecally administred radioactive tracers or contrast agents.

Coccygeal: Relating to the os coccygis.

Colloid (osmotic): A substance which disperses into particles much larger than atoms or molecules.

Conus medullaris: The tapering caudal extremity of the spinal cord proper.

Coronal: Pertaining to the crown of the head or any corona (a partially or completely encircling structure). Directed or located in the side-to-side plane of the coronal suture or in a vertical plane parallel to it.

Corpus callosum: The great longitudinal arched commissure which connects the cortices of the cerebral hemispheres .

Cortex: Superficial layer of grey matter covering the cerebrum, midbrain, and cerebellum.

Cuff: A wide encircling band containing a balloon which can be inflated to control the flow of a fluid passing through it by constricting or sealing the conveying vessel.

Dandy Walker cyst: injection of air into the cerebral ventricles or into the spinal subarachnoid space for localising tumours.

Denticulate: Having small, toothlike projections.

Diencephalon: The between-brain.

Diplopia: The seeing of a single object as double.

Dorsal: Pertaining to the back of the body or to the dorsum of any part. In human anatomy, it is commonly equivalent to 'posterior'.

Dorsum: The back. Any locus, surface or part corresponding in position to the back; the posterior.

Dura mater: Outermost layer of meninges. (see also section 2.2.2)

Dysplasia (osseous): is disordered development or growth.

Efferent: Away from (motor if away from the central nervous system).

Embryogenesis:

Endothelium: the layer of cells lining the interior of the blood vascular system, the lymphatic system, and the serous membranes.

Ependyma: The membrane lining the ventricles of the brain and the central canal of the spinal cord.

Epilepsy: is a periodic disorder characterised by outbursts of excessive activity in part of the brain.

Epithelial: Of or relating to epithelium.

Epithelium: is the general name given to the firmly adherent sheet of cells of epidermal origin which covers the body surface, both external and internal, comprising the skin and the mucous membrane lining tubes and cavities.

Erect position: Upright position.

Eustachian (tube): An osseocartilaginous tube through which air passes.

Falx cerebelli: Fold of dura mater between cerebellar hemispheres.

Falx cerebri: Fold of dura mater between cerebral hemispheres. (see also section 2.3)

Fasciculation: Spontaneous twitching of small groups of muscle fibres (each group representing a fasciculus, or bundle, of muscle fibres).

Filum terminale: The slender, threadlike prolongation of the conus medullaris of the spinal cord.

Flocculonodular: Denoting the flocculonodular lobe of the cerebellum .

Foramen: An anatomical feature consisting of a passage or opening.

Foramen of Magendie: median aperture of fourth ventricle. (see also section 2.4.2)

Foramen magnum: The largest cranial foramen, the middle opening of the occipital bones through which emerges the medulla oblongata extending caudally into the vertebral canal. (see also section 2.4.2)

Forebrain: Cerebrum and diencephalon of adult.

Fossa: An anatomical term for a depression or hollow in a bone or in other tissues.

Fossacerebri lateralis: A slight depression that appears at the beginning of the fourth fetal month in the lateral surface of the cerebrum anterior and superior to the temporal lobe.

Froin's syndrome: The changes in the spinal fluid which result from a complete block in the spinal subarachnoid space. The CSF obtained by lumbar puncture below the block is xanthochromic (yellow in colour), has a very high protein content, and often coagulates on standing.

Frontal: Pertaining to the front of the body (to the frontal bone or to the forehead).

Funiculus (plural: funiculi): A large aggregation of white mater in the spinal cord.

Gait: The way in which an individual walks.

Giddiness: is synonymous with dizziness.

Glia: is a synonymous with neuroglia.

Glosis: is a scar inside the spinal cord.

Glottis: The opening of the larynx, comprising the vocal cords and the space between them.

Grey matter: Nervous tissue, mainly nerve cell bodies. (see also section 2.2.2)

Gyrus (Plural: gyri): One of the convoluted ridges of the cerebral cortex.

Haustrae: Any one of the pouches in the wall of the colon.

Hemiatrophy: is unilateral atrophy (of the whole body or of a part).

Hemorrhage: The escape of blood from blood vessels. Such bleeding continues until external pressure exceeds that within the blood vessel.

Hernia: Protrusion of any organ or part of an organ, into or through the wall of the cavity which contains it.

Hindbrain: Pons, medulla oblongata and cerebellum of adult.

Hydrocephalus: It is the condition in which there is abnormal accumulation of cerebrospinal fluid within the skull.

Hyperhidrosis: Characterized by increased sweating.

Idiopathic: Having no known cause.

Iniencephalus: An embryo, fetus or newborn infant with iniencephaly.

Iniencephaly: A developmental defect in which the occipital part of the cranium and upper spinal regions fail to close about the neural tube, thus permitting exposure of brain and cord tissue.

Interpeduncular fossa: Situated between paired peduncles, like the fossa separating the cerebral peduncles from the nucleus interpeduncularis.

Interventricular foramen (of Monro): Opening from the lateral to 3rd ventricle. (see also section 2.4.2)

Intracerebellar: Within the cerebellum.

Jerk: A momentary, involuntary movement. (tendon jerk= tendon reflex).

Jugular (veins): are the veins responsible for drainage of the head and neck.

Korotkoff (sound):

Lacunae: Irregularly-shaped venous "lakes" or channels draining into the superior sagittal sinus.

Lateral: Of, at or toward the side (right or left).

Ligature: A suture that is tied around a tissue or vessel in order to obliterate the lumen.

Lipoma: A benign growth of mature adipose tissue cells showing no evidence of cellular atypia.

Lobe: A rounded projection or subdivision of an organ or structure demarcated by fissures, sulci, constrictions, or connective tissue septa.

Lumbar: referring to the lower back region.

Lumen (plural: lumina): The cavity within a tubular structure, either natural or artificial.

Median vermis: The central portion of the cerebellum.

Medulla: The innermost or middle part of an organ or structure. Also called marrow.

Medulla oblongata: The lowermost part of the brain, connecting the spinal cord with the pons.

Menigeal: Related to meninges.

Meninges: The three membranes enveloping the brain and spinal cord known as the pia mater, the arachnoid mater and the dura mater. (see also section 2.2.2)

Meningitis: is inflammation of the meninges.

Mesothelium: The epithelium of the serous membranes, i.e. pleura, peritoneum, pericardium.

Midbrain: the middle division of the embryonic brain, also part of the adult brainstem.

Myelin: An insulating, multilaminar sheath around axons.

Myelinated: Having a myelin sheath.

Myelography: is radiographic visualisation of the spinal cord after injection of a contrast medium into the subarachnoid space.

Neuraxis: The straight longitudinal axis of the embryonic or primitive neural tube, bent in later evolution and development.

Neurites: A long process of a neuron.

Neurofibromatosis: is a genetically determined disorder, inherited as an autosomal dominant characteristic, of which the major manifestations are multiple tumours attached to peripheral nerves (neurofibromas) and pigmented skin patches.

Neuroglia: is the supportive tissue of the central nervous system, analogous to connective tissue elsewhere.

Neuron: A nerve cell, comprising a cell body with several short processes (dendrites) and one long one (the axon) which together its sheaths forms a nerve fibre. They are responsible for receiving and transmitting nervous impulses.

Nuchal: Pertaining to nucha (back of the neck).

Nuclei (plural: nucleus): The cell nucleus is a membrane-bounded body found within the cytoplasm of most biological cells. It contains the chromosomes.

Occipital: Of or relating to the occiput.

Occiput: the posterior projection of the head (or skull).

Oscillopsia: A condition in which the visual image is seen to move rapidly from side to side or vertically.

Osmosis: is the flow of water (or other solvent) through a semipermeable membrane, that is one which will permit passage of the solvent but not of the substance dissolved.

Osmotic: Of or relating to osmosis.

Osteogenesis imperfecta: Any of the several heritable disorders of connective tissue that are marked by bone fragility.

Paraesthesiae: Any sensation, such as pins and needles, burning, prickling, etc., which occurs spontaneously without external cause in certain diseases of the central or peripheral nervous system.

Paraplegia: Paralysis of the lower half of the body.

Parenchyma: is the distinctive tissue characteristic of an organ and responsible for its functioning.

Parietal: Pertaining to the wall or of any cavity or organ.

Pathogenesis: The mode of production or development of a disease; the developing pathological process.

Peduncle: A stalk or stem; any stem-like structure serving as attachment, for example of a tumour.

Peri-natal: Pertaining to the period extending from the 28th week of gestation to the 28th day after birth.

Perineuronal: Surrounding a neuron.

Perivascular space: The space around a blood or lymph vessel. (see also section 2.4.2)

Pia mater: Innermost layer of meninges. (see also section 2.2.2)

Platybasia: A development defect of the skull in which the floor of the posterior fossa is elevated in the region around the foramen magnum so that the entire cranial base appears somewhat flatter than usual. Also called basilar invagination.

Plexoctomy: An operation to remove the plexus.

Plexus: Any network of vessels or nerves.

Pons: That part of the brainstem which connects the mid-brain above with the medulla oblongata below and lies in front of the cerebellum.

Pontine cisterna: Pertaining to the pons cisterna.

Posterior: Pertaining to the hind parts of a body or to the back surface of a body or part. In human anatomy, it refers to 'dorsal'.

Posterior fossa: Pertaining to the hind part (dorsal) of the fossa.

Pott's disease: tuberculosis of spine.

Prophylaxis: The prevention of disease.

Prosthetic: Substituting for or replacing a missing part of the body.

Pyogenic: Able to cause formation of purulent lesions in tissue.

Recess: A small hollow or space.

Ricket: A disease, primarily of infants or children, that is brought on by a deficiency of vitamin D. It results in a softening of the bones with deformities, fractures and tenderness.

Rostral: Towards the nose, or the most anterior of the neuraxis.

Sacral: Referring to the pelvic region.

Sagittal: Of or pertaining to the sagittal or midline suture of the skull and any plane parallel to this suture.

Scintigram: A representation on paper or film of the distribution in a patient or in an organ of a radioactive substance.

Sclerosteosis: It is a condition associated with digital abnormalities and, frequently, with sensorineural deafness and facial paralysis.

Scoliosis: a spinal deformity due to curvature in a lateral direction.

Septum (plural: septa): A partition or a dividing wall.

Serous: Of, pertaining to, or containing serum.

Serum: It's the clear slightly yellow fluid which separates from blood when it clots.

Sheath: A tubular structure enveloping a muscle, tendon, nerve, blood vessel, or other organ.

Sinus: In the anatomical sense, it's a term which is applied to a variety of channels or cavities; in the pathological sense, it denotes a blind channel opening on to the surface of the body.

Spasticity: That type of hypertonia with hyperreflexia which results from a lesion of the corticospinal tract.

Sphygmomanometer: is the measurement of arterial blood pressure.

Spinospinal: Shaped like a spine.

Splenium: a thickened, bandlike structure.

Sulcus (plural sulci): a groove or furrow.

Subarachnoid space: Space between arachnoid and pia mater. (see also section 2.4.2)

Subdural space: Space between the dura and arachnoid mater. (see also section 2.4.2)

Supratentorial: Situated or occurring superior to the tentorium cerebelli.

Sympathetic: Indicating, expressing, or characterized by sympathy.

Sympathy: A state of mutual relation or coordination existing between two body parts or structures such that a change in one is likely to produce a change in the other.

Syncope: is a sudden temporary loss of consciousness due to transient cerebral anoxia; it is synonymous with faint.

Syringobulbia: A congenital cavitation in the medulla oblongata almost invariably the result of an upward extension of syringomyelia.

Systole: The contraction phase of the atria or ventricles in the cardiac cycle.

Systolic: Relating to or occurring during systole.

Tela choroidea: A duplicated fold of pia mater that forms in the choroid .

Temporal: Of or relating to the region of the temple.

Tentorial: Relating or pertaining to a tentorium, especially the tentorium cerebelli.

Tentorium cerebelli: fold of dura mater overlying cerebellum.

Theca: An enclosing sheath, particularly the dura mater of the spinal cord.

Thoracic: Referring to the chest region.

Thrombosis: The formation of clot or thrombus (a semisolid aggregate of blood cell) within a blood vessel.

Tinnitus: Any form of adventitious noise arising within the ears or head and audible to the subject.

Tomography: is a radiographic technique which, by altering the geometrical relationship between the X-ray tube and the film during exposure, allows the visualisation of structures in a single plane (or 'cut') and blurs images in other planes.

Trabeculation: The process of developing trabeculae (small beam or rib) in a organ or structure.

Transverse: to turn or direct across.

Trophic: Having to do with nutrition.

Ulceration: is the formation of an ulcer (a breach or discontinuity in skin or mucous membrane, usually one that is persistent), or the ulcer itself.

Unilateral: On or affecting one side only.

Valsalva manoeuvre (rebound): Forced expiration against a closed glottis, a simple bedside test of circulatory function.

Ventricle: Cerebrospinal fluid-filled cavities: lateral, third, fourth and fifth (terminal) ventricles. (see also section 2.4.2)

Ventriculogram: A technique to show the ventricles of the brain or the heart with the use of contrast medium (air in the brain, radiopaque in the heart).

Vermis: Unpaired midline portion of cerebellum between hemispheres .

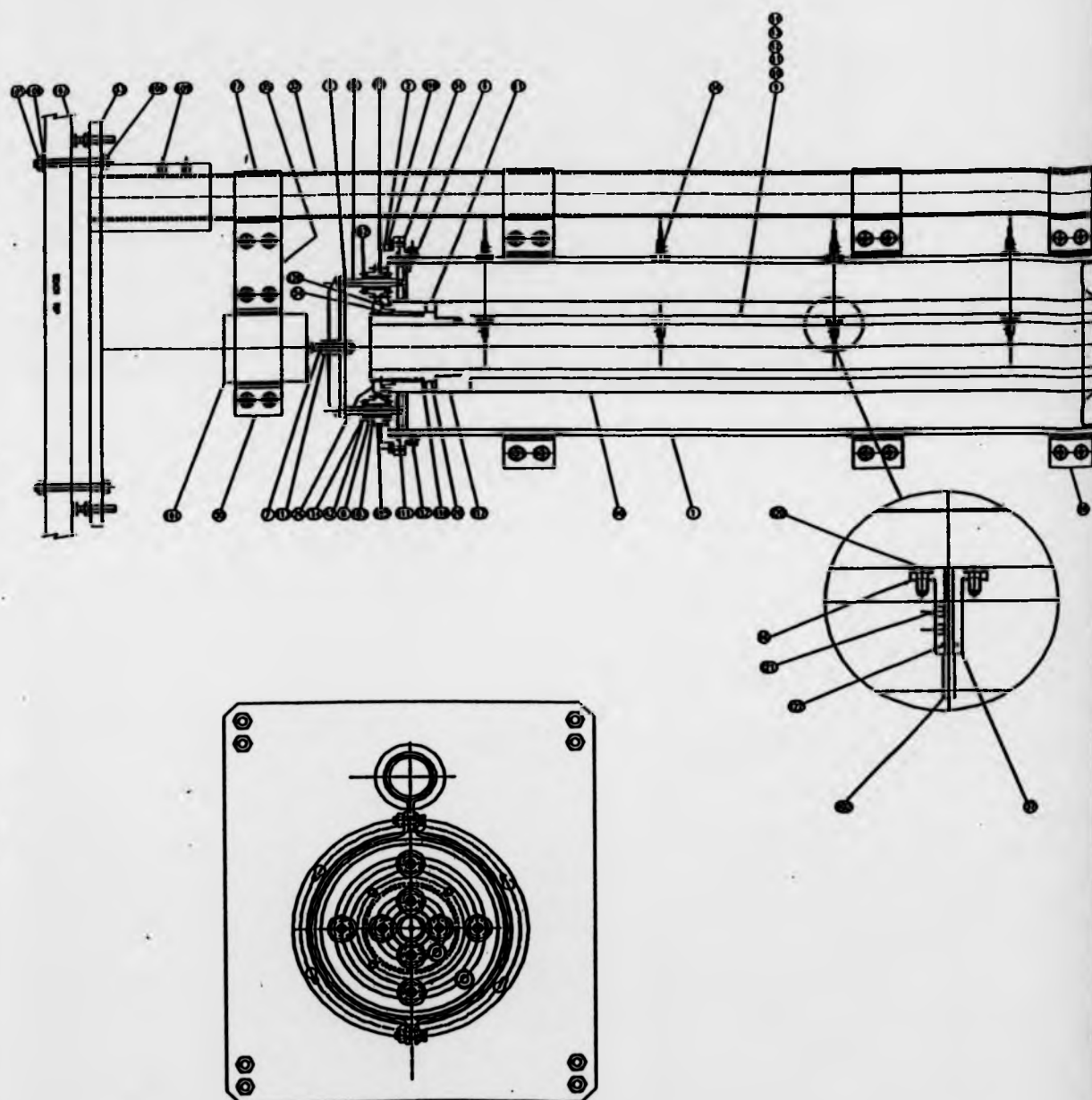
Vertex: An apex, especially a highest point in a vertical axis of a body or structure.

Villi(us): A projection from a membrane, usually with a rich blood supply.

White matter: Nervous tissue made up mainly of nerve fibres. (see also section 2.2.2).

D. Diagram of the experimental apparatus: format A3
(see next page)

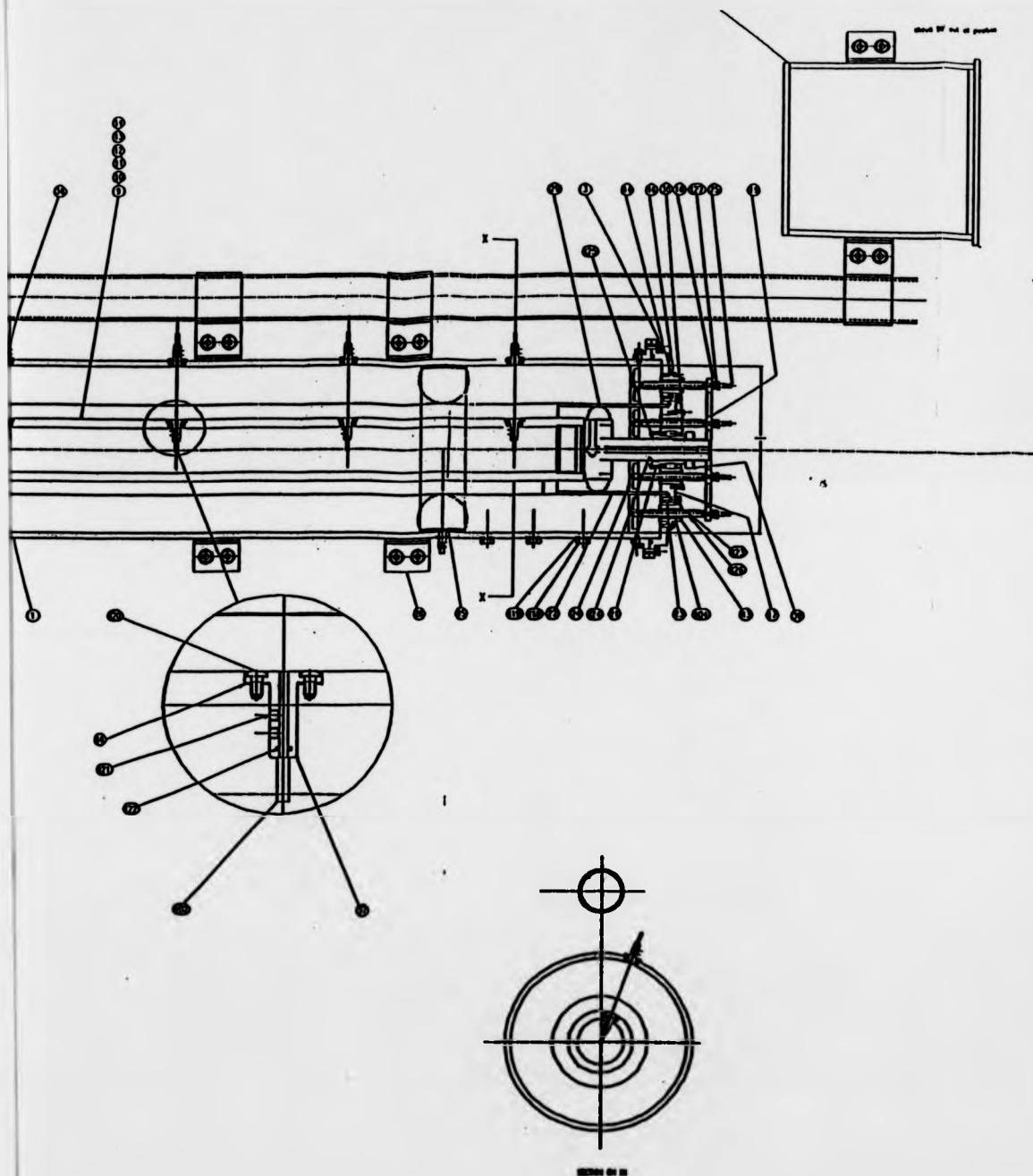
Original
Contains
Pullouts



NOTE: The drawing is a property and confidential communication and the property of the UNIVERSITY of Waterloo. It must not be copied or loaned without the written consent of the UNIVERSITY and must be returned immediately on completion of order or contract.

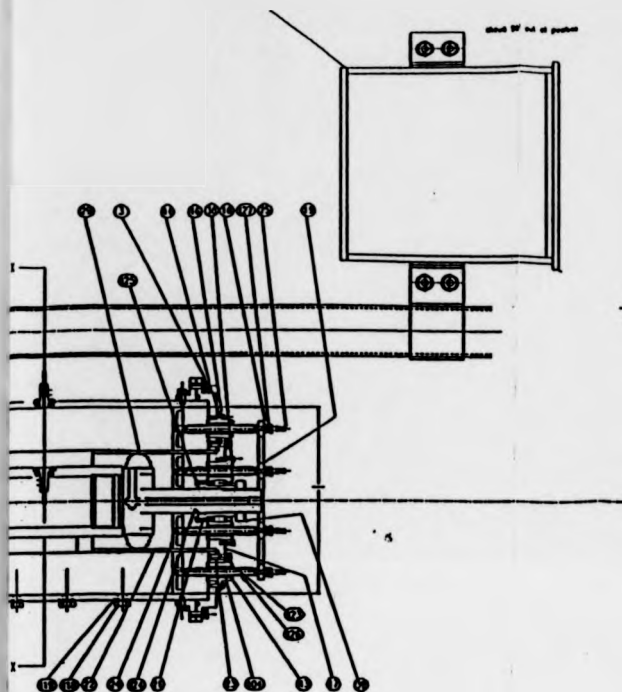
TITLE

MEMBRANE TEST RIG



CRANE TEST RIG

DRAWN AT 1/2"
 SCALE AT 1/2"
 GENERAL ENG. & DES.
 THE UNIVERSITY



1
2
3
4
5
6
7
8
9
10
11
12
13
14
15
16
17
18
19
20
21
22
23
24
25
26
27
28
29
30

ITEM	REF.	DESCRIPTION	SUPPLIER
1	1	COVER PLATE	W. H.
2	2	COVER PLATE	W. H.
3	3	COVER PLATE	W. H.
4	4	COVER PLATE	W. H.
5	5	COVER PLATE	W. H.
6	6	COVER PLATE	W. H.
7	7	COVER PLATE	W. H.
8	8	COVER PLATE	W. H.
9	9	COVER PLATE	W. H.
10	10	COVER PLATE	W. H.
11	11	COVER PLATE	W. H.
12	12	COVER PLATE	W. H.
13	13	COVER PLATE	W. H.
14	14	COVER PLATE	W. H.
15	15	COVER PLATE	W. H.
16	16	COVER PLATE	W. H.
17	17	COVER PLATE	W. H.
18	18	COVER PLATE	W. H.
19	19	COVER PLATE	W. H.
20	20	COVER PLATE	W. H.
21	21	COVER PLATE	W. H.
22	22	COVER PLATE	W. H.
23	23	COVER PLATE	W. H.
24	24	COVER PLATE	W. H.
25	25	COVER PLATE	W. H.
26	26	COVER PLATE	W. H.
27	27	COVER PLATE	W. H.
28	28	COVER PLATE	W. H.
29	29	COVER PLATE	W. H.
30	30	COVER PLATE	W. H.
31	31	COVER PLATE	W. H.
32	32	COVER PLATE	W. H.
33	33	COVER PLATE	W. H.
34	34	COVER PLATE	W. H.
35	35	COVER PLATE	W. H.
36	36	COVER PLATE	W. H.
37	37	COVER PLATE	W. H.
38	38	COVER PLATE	W. H.
39	39	COVER PLATE	W. H.
40	40	COVER PLATE	W. H.
41	41	COVER PLATE	W. H.
42	42	COVER PLATE	W. H.
43	43	COVER PLATE	W. H.
44	44	COVER PLATE	W. H.
45	45	COVER PLATE	W. H.
46	46	COVER PLATE	W. H.
47	47	COVER PLATE	W. H.
48	48	COVER PLATE	W. H.
49	49	COVER PLATE	W. H.
50	50	COVER PLATE	W. H.
51	51	COVER PLATE	W. H.
52	52	COVER PLATE	W. H.
53	53	COVER PLATE	W. H.
54	54	COVER PLATE	W. H.
55	55	COVER PLATE	W. H.
56	56	COVER PLATE	W. H.
57	57	COVER PLATE	W. H.
58	58	COVER PLATE	W. H.
59	59	COVER PLATE	W. H.
60	60	COVER PLATE	W. H.
61	61	COVER PLATE	W. H.
62	62	COVER PLATE	W. H.
63	63	COVER PLATE	W. H.
64	64	COVER PLATE	W. H.
65	65	COVER PLATE	W. H.
66	66	COVER PLATE	W. H.
67	67	COVER PLATE	W. H.
68	68	COVER PLATE	W. H.
69	69	COVER PLATE	W. H.
70	70	COVER PLATE	W. H.
71	71	COVER PLATE	W. H.
72	72	COVER PLATE	W. H.
73	73	COVER PLATE	W. H.
74	74	COVER PLATE	W. H.
75	75	COVER PLATE	W. H.
76	76	COVER PLATE	W. H.
77	77	COVER PLATE	W. H.
78	78	COVER PLATE	W. H.
79	79	COVER PLATE	W. H.
80	80	COVER PLATE	W. H.
81	81	COVER PLATE	W. H.
82	82	COVER PLATE	W. H.
83	83	COVER PLATE	W. H.
84	84	COVER PLATE	W. H.
85	85	COVER PLATE	W. H.
86	86	COVER PLATE	W. H.
87	87	COVER PLATE	W. H.
88	88	COVER PLATE	W. H.
89	89	COVER PLATE	W. H.
90	90	COVER PLATE	W. H.
91	91	COVER PLATE	W. H.
92	92	COVER PLATE	W. H.
93	93	COVER PLATE	W. H.
94	94	COVER PLATE	W. H.
95	95	COVER PLATE	W. H.
96	96	COVER PLATE	W. H.
97	97	COVER PLATE	W. H.
98	98	COVER PLATE	W. H.
99	99	COVER PLATE	W. H.
100	100	COVER PLATE	W. H.

UNIVERSITY OF WARWICK

DEPARTMENT OF ENGINEERING

TITLE OF PROJECT:-

DESIGN

REF. NO.

ES878

DATE

DATE

DESIGNER

DATE

DESIGNER

DATE

DESIGNER

DATE

DESIGNER

DATE

DESIGNER

DATE

DESIGNER

DATE

DESIGNER

DATE

DESIGNER

DATE